NASA Contractor Report 185129

Users Manual for the NASA Lewis Ice Accretion Prediction Code (LEWICE)

Gary A. Ruff and Brian M. Berkowitz

Sverdrup Technology, Inc.
Lewis Research Center Group
Brook Park, Ohio

May 1990

NASA

National Aeronautics and
Space Administration

TABLE OF CONTENTS

i

ACKNOWLEDGEMENTS

List Of Symbols

A	Characteristic area
A_c	Accumulation parameter
$\overline{A}_c$	Modified accumulation parameter
ΔB	Mass transfer driving potential
c	Characteristic length
c_d	Drag coefficient
c_f	Skin friction coefficient
c_l	Lift coefficient
c_m	Pitching moment coefficient
c_p	Pressure coefficient, also specific heat, J/kg
C_f	Cunningham correction factor
CVF	Control volume fraction
d_i	Ice thickness, m
$\overline{d}_m$	Mass median droplet diameter, μm
D	Drag force, N
E_m	Total collection efficiency
f	Freezing fraction
FRL	Flight reference line
g	Mass transfer coefficient, kg-K/J
H	Projected height, m
h_c	Convective heat transfer coefficient, $W/m^2/K$
i	Enthalpy, J/kg
I_{zz}	Moment of inertia relative to z axis
k_s	Equivalent sand-grain roughness, m
L	Lift force, N
L_f	Heat of fusion, J/kg
L_v	Heat of vaporization, J/kg
LWC	Liquid water content, g/m^3
M	Mach number; moment of aerodynamic forces
m	Mass, kg
m''	Mass per unit area, kg/m^2
$\dot{m}$	Mass flow rate, kg/sec
$\dot{m}''$	Mass flux, kg/m^2 /sec
n_i	Mass fraction of liquid water for droplet diameter i

N	Number of droplet sizes defining a droplet distribution
	Number of points describing geometry
P	Pressure, Pa
Pr	Prandtl number
q_c	Convective heat flux, W/m^2
q_k	Conductive heat flux, W/m^2
r_c	Recovery factor
Re	Freestream Reynolds number
Re_k	Laminar/turbulent transition Reynolds number
Re_p	Droplet Reynolds number based on V_p
s	Surface length, m; surface length increment, m
Sc	Schmidt number
St	Stanton number
St_k	Roughness Stanton number
T	Temperature, ^oK
t	Icing time, sec
Δt	Icing time increment, sec
V	Velocity, m/s
V_f	Volume fraction of LWC
V_k	Velocity at $y = k_s, m/s$
x	x-coordinate
y	y-coordinate
α	Angle of attack, degrees
β	Local collection efficiency
θ	Pitch angle, degrees; momenteum thickness, m
ν	Viscosity, Ns/m^2
ρ	Density, g/m^3
σ	Shear stress, N/m^2
ϵ	Particle trajectory convergence criteria
δ	Boundary layer thickness, m
λ	Thermal conductivity of air, $W/m -^o K$

Subscripts

a	Air
aw	Adiabatic wall
c	Critical; convection
d	Droplet

e	Evaporation; condition at the edge of the boundary layer
i	Ice
(i)	Control volume
(i-1)	Preceding control volume
l	Lower surface; laminar
L	Local condition; condition at the edge of the boundary layer
p	Particle
r	Runback water
r_{in}	Runback into control volume
r_{out}	Runback out of control volume
s	Static condition
sur	Surface condition
T	Total condition
t	Turbulent
tr	Laminar to turbulent transition
u	Upper surface
v	Vapor
w	Liquid water
x	Magnitude of the vector in the x-direction
y	Magnitude of the vector in the y-direction
o	Initial
∞	Freestream conditions
σ	Shear

Superscripts

$\rightarrow$	Vector quantity
$\cdot$	Derivative with respect to time
$\prime$	Non-dimensionalized parameter

SUMMARY

LEWICE is an ice accretion prediction code that applies a time-stepping procedure to calculate the shape of an ice accretion. The potential flow field is calculated in LEWICE using the Douglas Hess-Smith 2-D panel code (S24Y). This potential flow field is then used to calculate the trajectories of particles and the impingment points on the body. These calculations are performed to determine the distribution of liquid water impinging on the body, which then serves as input to the icing thermodynamic code. The icing thermodynamic model is based on the work of Messinger, but contains several major modifications and improvements. This model is used to calculate the ice growth rate at each point on the surface of the geometry. By specifying an icing time increment, the ice growth rate can be interpreted as an ice thickness which is added to the body, resulting in the generation of new coordinates. This procedure is repeated, beginning with the potential flow calculations, until the desired icing time is reached.

The operation of LEWICE is illustrated through the use of five examples. These examples are representative of the types of applications expected for LEWICE. All input and output is discussed, along with many of the diagnostic messages contained in the code. Several error conditions that may occur in the code for certain icing conditions are identified, and a course of action is recommended.

LEWICE has been used to calculate a variety of ice shapes, but should still be considered a research code. The code should be exercised further to identify any shortcomings and inadequacies. Any modifications identified as a result of these cases, or of additional experimental results, should be incorporated into the model. Using it as a test bed for improvements to the ice accretion model is one important application of LEWICE.

Chapter 1

BACKGROUND

The evaluation of both commercial and military flight systems in icing conditions has become important in the design and certification phases of system development. These systems have been evaluated in flight in natural icing, in a simulated cloud produced by a leading aircraft, and in ground test facilities. All icing testing is relatively expensive, and each test technique, i.e., flight or ground testing, has operational limitations which limit the range of icing conditions that can be evaluated. It would benefit the aircraft or flight system manufacturer to be able to analytically predict the performance of the system for a range of icing conditions.

This first step in the prediction of the performance characteristics is the determination of the location, size, and shape of the ice that will form. An analytical ice accretion model would allow the evaluation of a wide range of proposed test conditions to identify those that will be most critical to the flight system. This could substantially reduce the amount of test time required to adequately evaluate a system and increase the quality and confidence level of the final evaluation. The analytically predicted ice accretion could also serve as the input to an advanced aerodynamic or system performance code to allow more complete evaluation in the design phases of the system. For these reasons, several analytical ice accretion prediction methods have been developed by various investigators.

The most well-known are those of Ackley and Templeton[1], Lowzowski[2], Hankey and Kirchner[3], and Cansdale and Gent[4]. All apply essentially the same physical model of the ice accretion process but differ in the manner that the surface properties, for example, the local collection efficiency and convective heat transfer coefficient, are calculated and allowed to vary over the surface. Also, several of these models were restricted to the simulation of the icing of a cylinder. One of the major inadequacies of these models is that they do not account for any of the time-dependent aspects of the ice accretion process. In general, the ice accretion rate is calculated as a function of position on the airfoil and projected at a constant rate to approximate a finite growth over a prescribed period of time. Therefore,

any sensitivity of the ice accretion process to the changing iced airfoil shape is not included.

The purpose of the current study was to develop a time-dependent, analytical model of the ice accretion process that could be used to predict the shape of the ice accretion that would form on an arbitrary two-dimensional geometry when exposed to icing conditions. The development of the computer code (LEWICE) was begun by the University of Dayton Research Institute (UDRI) under contract to NASA Lewis Research Center. The results of this study are described in Reference 5. Development of the code was then continued at the NASA Lewis Research Center under NASA funding until October 1984 when funding by the Federal Aviation Administration (FAA) was begun. This document describes the results of the current development effort and contains the information necessary to apply the ice accretion prediction method to practical icing problems.

Chapter 2

INTRODUCTION

The computer code, LEWICE, embodies an analytical ice accretion model that evaluates the thermodynamics of the freezing process that occurs when supercooled droplets impinge on a body. The atmospheric parameters of temperature, pressure, and velocity, and the meteorological parameters of liquid water content (LWC), droplet diameter, and relative humidity are specified and used to determine the shape of the ice accretion. The surface of the clean (uniced) geometry is defined by segments joining a set of discrete body coordinates (Fig. 2.1). The code consists of three major modules. They are 1) the flow field calculation, 2) the particle trajectory and impingement calculation, and 3) the thermodynamic and ice accretion calculation. Each of these modules will be discussed in detail in following sections.

LEWICE differs from other ice accretion prediction codes[1-4] because it applies a time-stepping procedure to "grow" the ice accretion. Initially, the flow field and droplet impingement characteristics are determined for the clean geometry. The ice growth rate on each segment defining the surface is then determined by applying the thermodynamic model. When a time increment is specified, this growth rate can be interpreted as an ice thickness and the body coordinates are adjusted to account for the accreted ice. This procedure is repeated, beginning with the calculation of the flow field about the iced geometry, then continued until the desired icing time has been reached. The application of this time-stepping procedure to the prediction of an ice accretion shape will be discussed in greater detail in following chapters.

Ice accretion shapes for cylinders and several single-element airfoils have been calculated using this computer code. The calculated results have been compared to experimental ice accretion shapes obtained both in flight and in the Icing Research Tunnel at NASA Lewis Research Center. In general, the comparisons have been encouraging but inconsistent. Ice shapes for some conditions are well predicted, while for others there is little similarity between the predicted accretion and that obtained by experiment. Unfor-

tunately, the poorer predictions do not consistently occur in only one type of icing condition such as glaze or rime icing, on a specific type of airfoil, or in comparisons with results from a specific facility. There are many possible explanations for this behavior including inaccurate modeling of the accretion process, occasional errors in setting test conditions, and overextending the computer code into conditions where the assumptions, such as potential flow, do not apply. The known limitations will be addressed throughout this user's manual.

The manual begins with a discussion of the ice accretion process to identify the requirements of an ice accretion prediction methodology. The major components of the code and the mathematical models applied in each are then discussed. The input and output to the code are described, followed by the presentation of several sample cases, which illustrate various aspects of the code. The manual concludes with a summary of the current results and shortcomings of the method.

Areas requiring additional development are identified and discussed in the Appendices (A through F).
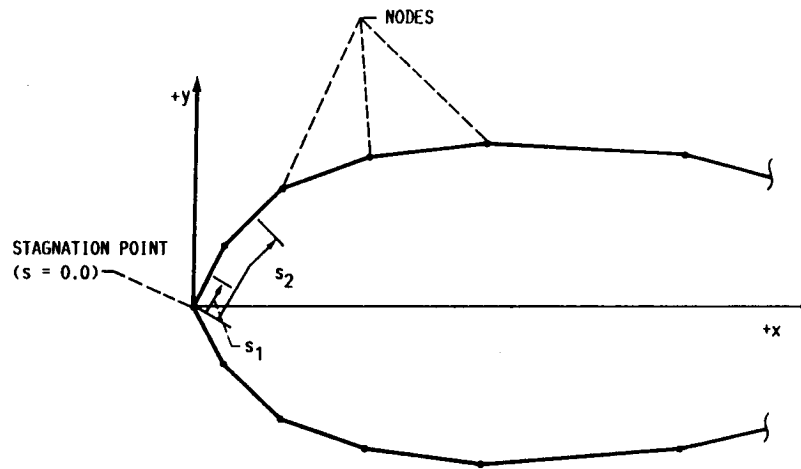
Figure 2.1: Geometry defined by segments joining body coordinates

Chapter 3

DICUSSION OF THE ICE ACCRETION PROCESS

The model of the ice accretion process applied in LEWICE is presented in this chapter, beginning with a discussion of some of the general characteristics of ice accretion shapes, and followed by a description of the physical model of the ice accretion process from which a mathematical model must be formulated.

3.1   Ice Accretion Characteristics

Before discussing the physical model of the ice accretion process, it is necessary to define some of the terms used in such a discussion.

Ice may form on the forward facing surfaces of an aircraft flying through clouds composed of supercooled water droplets. The type and shape of ice that forms are functions of the atmospheric parameters of velocity, pressure, and temperature, and the meteorological parameters of liquid water content, droplet diameter, and icing time.

Ice shapes are generally classified as glaze, mixed, and rime accretions. Rime ice is milky white and opaque, and will be denoted in the ice accretion profiles in this report by shading as shown in Figure 3.1a. Glaze ice is generally clear and is characterized by the presence of larger protuberances, commonly known as glaze horns, as shown in Figure 3.1b. A mixed ice accretion will have some of the characteristics of both glaze and rime ice accretions. As shown in Figure 3.1c, the center portion of a mixed ice accretion will have the characteristics of glaze ice accretion. This glaze center will be surrounded by rime ice accretions, commonly called rime feathers because of their thin, feather-like shape and delicate structure.

The type of ice that will be formed is dependent on the atmospheric and meteorological conditions identified in the preceding paragraph. Predicting the type and shape of the ice accretion that will be formed for a specified set of icing conditions is difficult because of the complex interactions between the atmospheric and meteorological parameters. Typically, rime ice is formed at lower temperatures, velocities, and LWC than glaze

ice. An example of the transition from glaze to rime ice as the total temperature is lowered is shown in Figure 3.2. At the warmest total temperature, $T_T = -2.0C$, the accretion is composed exclusively of glaze ice. As the temperature decreases, areas of rime ice begin to form near the impingement limits. As the temperature decreases further, these rime portions increase in size until the accretion is composed solely of rime ice. The extent of icing and the locations at which ice forms on a surface are largely dictated by the size of the droplets impinging on the surface. For a given icing condition, and in the absence of ice shedding, the size of the accretion depends on the length of time ice is allowed to accrete. The general effects of temperature, droplet size, LWC, and angle of attack on ice shapes formed on a NACA 0012 airfoil in the NASA Lewis Icing Research Tunnel (IRT) are documented in Reference 6.

3.2   Description of the Physical Model

An understanding of the interactions between these parameters is required to predict the shape of an ice accretion that will be formed at a specified set of icing conditions. To develop this fundamental understanding, it is necessary to examine the physical model of the ice accretion process.

A model of the ice accretion process was first presented by Tribus[7] and developed further by Messinger[8]. While many studies have been done to understand various aspects of the ice accretion process, the original physical model has been applied relatively unchanged. Recent close-up movies and photographs of the ice accretion process made at the NASA Lewis Research Center[9] have increased our understanding of the process and indicated that modifications to the physical model may be necessary. Conclusions drawn from the observations are included in the following discussion of the ice accretion process, and differences from the previous model are highlighted.

The ice accretion process is characterized by the presence of supercooled droplets entrained in the flow about a body. These droplets follow trajectories that will cause them to either be carried past or impinge upon a body. Upon impact with a clean surface, the droplets coalesce into larger surface drops under the effects of surface tension and flow along the surface as dictated by the airflow along the surface of the body. These surface drops will then either freeze on the surface or be shed from the surface because of the

aerodynamic forces on the drop. The ice accretions formed by this initial freezing form a rough surface which enhances the convective heat transfer and local collection efficiency of the surface, and therefore allows the ice accretion process to continue.

The type of ice that will form for a given set of conditions is determined primarily by the rate at which the freezing process occurs. For example, if the conditions are such that the droplets freeze rapidly, there is essentially no initial coalescing and flowing of the droplets. Instead, they freeze on impact and form the characteristic rime ice accretions. These accretions are opaque and milky white in color because of the presence of air bubbles that are trapped in the structure during the rapid freezing process. As the rate of the freezing process decreases, the droplets begin to coalesce and flow on the surface. Upon freezing, these larger surface droplets form surface roughness elements which tend to enhance the convective heat transfer and local collection efficiency characteristics, which, in turn, enhance the continuing growth of the ice accretion in this region. These local areas of enhanced ice growth are, therefore, the beginnings of the characteristic horns found on mixed and glaze ice accretions. As the freezing rate decreases further, the drops flow further along the surface of the body before freezing, thus moving the regions of enhanced ice growth away from the stagnation point. This, in turn, causes the horns of the accretion to move further apart and forms the familiar glaze ice accretions. As the rate of the freezing process decreases, less air is trapped within the ice structure and the ice gradually becomes clearer until it is essentially transparent, as in glaze ice.

This description of the ice accretion process has identified four basic areas or processes that must be modeled in order to predict the shape of an ice accretion that will form on a body for a specified set of icing conditions. These areas are 1) the flow field about the body, 2) the droplet trajectory and impingement characteristics on the body, 3) the thermodynamics of the freezing process, and 4) the accumulation of ice on the surface of the body. To analytically predict an ice accretion shape, a mathematical model of each of these physical processes must be developed. Each of these areas will be discussed in subsequent sections to identify the methods used in the ice accretion prediction code, LEWICE.

8

ICING CONDITIONS

	A	B	C
CYLINDER DIAM. IN.	1.0	2.0	1.0
P_s, PSIA	14.2	12.2	14.2
T_s, °F	-5.0	21.1	5
V, fps	200	367	400
d_m, µm	20	22	15
LWC, g/m³	0.6	0.35	0.53
T, MIN	8.0	30.6	6.8

SHADED PORTIONS DENOTE RIME ICE
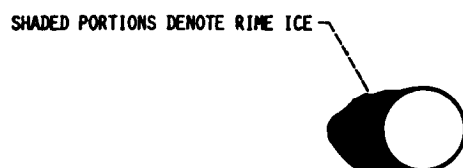
a. Rime ice accretion, f = 1.0

GLAZE HORNS

b. Glaze ice accretion, f = 0.15

RIME FEATHERS

GLAZE CENTER
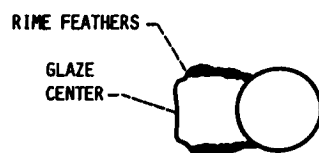
c. Mixed ice accretion, f = 0.53

Figure 3.1: Examples of ice accretions formed at various atmospheric and meteorological conditions

9

(A) TOTAL TEMPERATURE, -2 °C
(STAGNATION FREEZING FRACTION, 0.22).

(B) TOTAL TEMPERATURE, -8 °C
(STAGNATION FREEZING FRACTION, 0.32).

(C) TOTAL TEMPERATURE, -15 °C
(STAGNATION FREEZING FRACTION, 0.55).

(D) TOTAL TEMPERATURE, -18 °C
(STAGNATION FREEZING FRACTION, 0.65).

(E) TOTAL TEMPERATURE, -20 °C
(STAGNATION FREEZING FRACTION,   )

(F) TOTAL TEMPERATURE, -26 °C
(STAGNATION FREEZING FRACTION, 0.9).
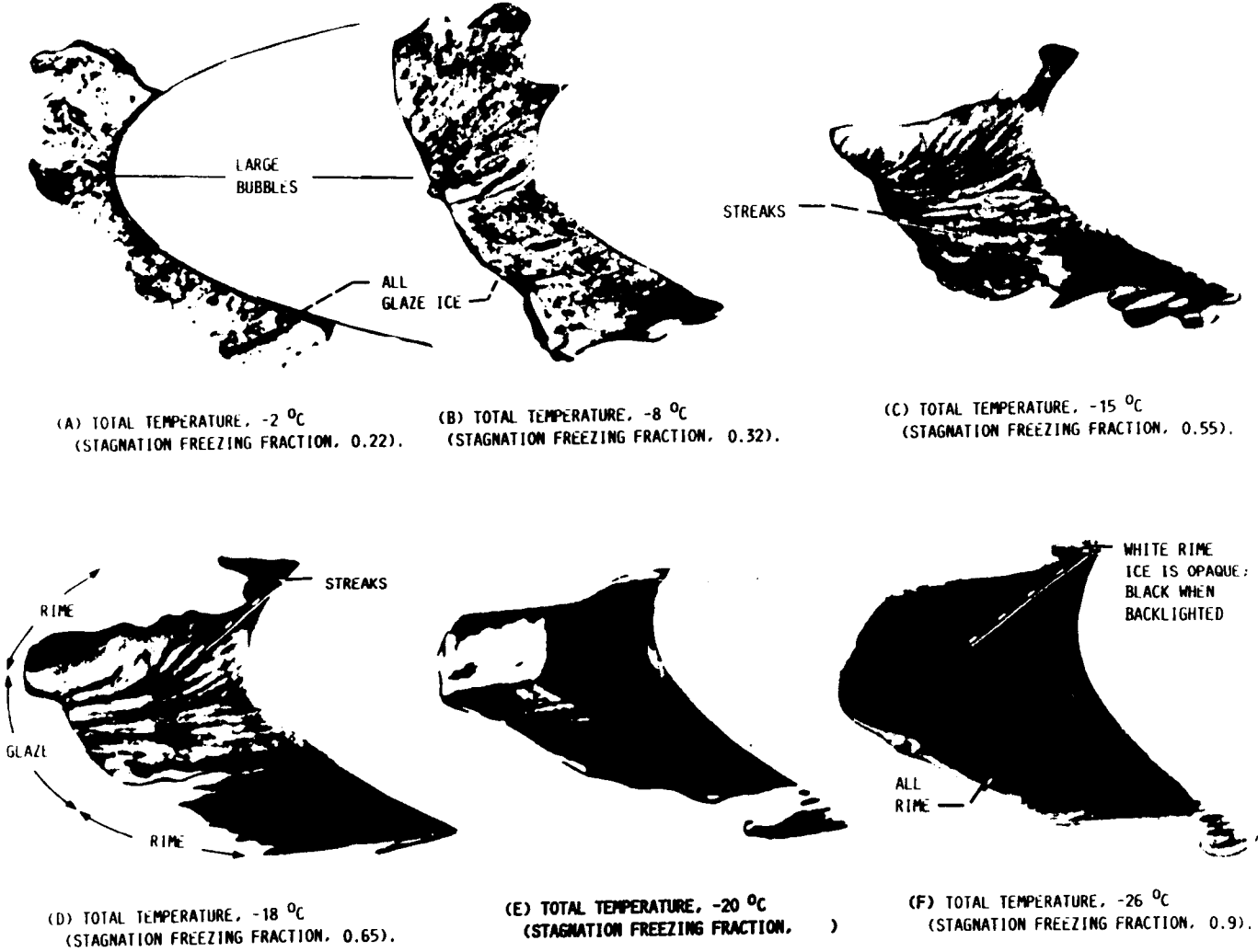
Figure 3.2: Effect of temperature on the ice accretion shape. Thin ice samples removed from the airfoil and backlighted; Airspeed, 209km/hr; LWC, $1.3g/m^3$; DVM, 20m; Time, 8min; Airfoil, 0.53m chord 0012 airfoil at 4° angle.

Chapter 4

METHODOLOGY

The phenomena that make up the ice accretion process have been identified and now must be investigated in order to accurately predict the shape of an ice accretion that will form on a body. These include the evaluation of

1) the flow field about the body,

2) the droplet trajectory and impingement characteristics,

3) the thermodynamics of the freezing process, and

4) the accumulation of the ice on the surface.

The computational methodology used to evaluate each of the above areas is discussed in the following sections.

4.1   Calculation of the Flow Field

The application of a flow field calculation method to an ice accretion prediction code requires that the method not only be able to calculate accurate flow fields about clean geometries, but also around the irregular, convoluted ice shapes that occur for many icing conditions. It is also desirable that the computational time and memory requirements of the method be as small as possible so that the use of the code is not limited to icing researchers with large computer facilities.

The Douglas two-dimensional potential flow program developed by Hess and Smith, described in Reference 10, meets these requirements, and is used in the present study for calculating the flow field about the body. This program uses a distribution of sources, sinks, and/or vortices along the body surface to calculate the potential flow field. The body surface is represented by an arbitrary number of straight line segments. In calculating the flow field, contributions from all the sources, sinks, and/or vortices are summed. The accuracy of this method was tested by comparing its predicted velocities and surface pressure coefficients with both analytical solutions and

experimental data[10]. Excellent agreement was found. Similar comparisons were performed at NASA Lewis and compared with pressure coefficient data found in Reference 11. These comparisons, shown in Figures 4.1a-j, show that the surface pressure coefficient is well predicted by the potential flow method for angles of attack up to approximately 11.0 degrees and Mach numbers up to 0.50. These flow field limitations must be considered when predicting ice accretion shapes at high Mach numbers or high angles of attack.

Only limited details of the methodology applied in the potential flow program are provided in this manual since the purpose of this study was to develop an analytical ice accretion prediction program. However, sufficient description of the input as well as subroutines are supplied to allow the user to become familiar with the primary aspects and limitations of the code.

4.2 Calculation of the Droplet Impingement Characteristics

The algorithm applied in the current ice accretion model to calculate the droplet trajectory and impingement characteristics was originally developed by Frost, Chang, Shieh, and Kimble of FWG Associates under contract to NASA Lewis[12-13].

This code was developed to calculate the trajectories and impingement characteristics of arbitrarily-shaped particles, and although water droplets are of primary concern when evaluating the ice accretion process, the generality has been retained in LEWICE. While much of this code has been applied in its original form in the current study, there are significant changes in many areas and, therefore, the current version of the code is discussed in detail in this report.

4.2.1 Definitions

The primary droplet impingement characteristics that must be evaluated by an ice accretion prediction code are the regions of droplet impingement and the distribution of the mass of liquid on the surface of the body within this impingement region.

The equations of particle motion, to be discussed in the following section, are used to calculate droplet trajectories from far upstream to impinge-

ment on the body and, if it occurs, the total and local collection efficiencies. The total collection efficiency is defined as the ratio of the actual mass of impinging water to the maximum value that would occur if the droplets followed straight-line trajectories. Figure 4.2 illustrates that this definition can be given in equation form as

$$E_m = \frac{y_0}{H} \tag{1}$$

where y_0 is the vertical distance between the droplet release points of the upper and lower surface tangent trajectories. The local collection efficiency, β, is also defined in Figure 4.2 and can be written in differential form as

$$\beta = \frac{dy_0}{ds} \tag{2}$$

It is related to the total collection efficiency by the equation

$$E_m = \frac{1}{H} \int_{s_l}^{s_u} \beta \, ds \tag{3}$$

where s_u and s_l are the upper and lower surface impingement limits, respectively. The following sections will cover the methods applied to calculate the variables discussed above.

4.2.2 Equations of Particle Motion

The motion of a particle is analyzed as a point mass particle that is acted on by the potential flow field but which itself does not affect the flow. The forces acting on the particle are considered to be those of lift, drag, pitching moment, and gravity. Figure 4.3 shows the forces acting on the particle and the velocity vectors relative to the motion of the particle. The flight reference line (FRL) is not significant for a spherical particle; however, for arbitrarily shaped particles, i.e., a snow flake, the FRL must be defined relative to the lift, drag, and moment coefficient data available. The equations of motion of an arbitrarily shaped particle are derived from a force balance on a point mass, as shown in Figure 4.3, and are as follows:

$$m\ddot{x} = -\vec{D}\cos\gamma - \vec{L}\sin\gamma + mg\sin\alpha$$
$$m\ddot{y} = -\vec{D}\sin\gamma + \vec{L}\cos\gamma - mg\cos\alpha \tag{4}$$

13

where

$$\gamma = tan^{-1} \frac{\dot{y}_p - V_y}{\dot{x}_p - V_x} \qquad (5)$$

In Figure 4.3, note that the coordinate system used in LEWICE is fixed to the leading edge of the clean airfoil.

For an airfoil at an angle of attack α, the coordinate system is at an angle to the gravitational coordinate system. Therefore, the effect of gravity must be accounted for in the equations for both lift and drag.

The flow field velocity components in the x and y directions, i.e., V_x and V_y, respectively, are obtained from the potential flow program. The aerodynamic drag and lift forces are defined as

$$\vec{D} = c_d \frac{\rho_a V^2}{2} A_p$$

$$\vec{L} = c_l \frac{\rho_a V^2}{2} A_p \qquad (6)$$

where A_p is a characteristic area of the particle, ρ_a is the density of air at the position of the particle, and V is the particle velocity relative to the flow field and defined as

$$V = \sqrt{\left(\dot{x}_p - V_x\right)^2 + \left(\dot{y}_p - V_y\right)^2} \qquad (7)$$

For arbitrarily shaped particles, the pitch angle, θ_p, is required to evaluate the angle of attack α_p, using the following equation

$$\alpha_p = \theta_p - \gamma \qquad (8)$$

This motion is governed by the following equation

$$\ddot{\theta} = \frac{M}{I_{zz}} \qquad (9)$$

where I_{zz} is the moment of inertia of mass relative to the z axis. The moment of aerodynamic forces acting on the particle is

$$M = c_m \frac{\rho_a V^2}{2} A_p d_p \qquad (10)$$

where c_m is the pitching moment coefficient which must also be specified by the user.

The lift, drag, and pitching moment coefficients, c_l, c_d, and c_m respectively, must be provided by the user for arbitrarily shaped particles. The coefficient data is input to the program through subroutine COEFF and should be functions of the particle angle of attack, as defined by Equation 8, and the particle Reynolds number based on the particle diameter, given by the following equations:

$$R_{e_p} = \frac{V\,d_p}{\nu} \tag{11}$$

The diameter of the particle, d, and the kinematic viscosity of air, ν, are assumed constant along the trajectory of the particle.

Since water droplets are usually assumed to be rigid spheres in icing studies, the only forces considered to be acting on the particle are those of drag and gravity. The governing equations can therefore be simplified as follows:

$$m\ddot{x} = -\vec{D}\cos\gamma + mg\,\sin\alpha$$

$$m\ddot{y} = -\vec{D}\sin\gamma - mg\,\cos\alpha \tag{12}$$

In this case, the drag force, D, is determined using a steady-state drag coefficient for a sphere which is a function of the droplet Reynolds number, Re_p. Approximating droplets as rigid spheres is valid for drop radii less than 500.0 microns[14]. A valid drag law for spherical particles is built into the computer program in subroutine COEFF.

For particles with diameters of less than 10 microns, the ratio of particle diameter to the mean distance between air molecules is small enough so that molecular slip phenomena result in drag forces lower than those calculated by the drag law used in LEWICE. The Cunningham correction factor, C_f, Reference 15, is therefore applied to correct the drag coefficient using the following equation:

$$c_d|slip = \frac{c_d}{C_f} \tag{13}$$

The values of C_f are input by the user when necessary and are given in Table 4.1. As shown in Table 4.1, this effect is small for particles with diameters greater than 1.0 micron. Droplets this small would be included

Table 4.1: Cunningham Correction Factor for Standard Air

d(u)	C	d(u)	C
0.001	221.600	0.1	2.911
0.002	111.100	0.2	1.890
0.003	74.250	0.3	1.574
0.004	55.830	0.4	1.424
0.005	44.780	0.5	1.337
0.006	37.410	0.6	1.280
0.007	32.150	0.7	1.240
0.008	28.200	0.8	1.210
0.009	25.140	0.9	1.186
0.010	22.680	1.0	1.168
0.020	11.650	2.0	1.084
0.030	7.978	3.0	1.056
0.040	6.151	4.0	1.042
0.050	5.060	5.0	1.034
0.060	4.337	6.0	1.028
0.070	3.823	7.0	1.024
0.080	3.441	8.0	1.021
0.090	3.145	9.0	1.019
		10.0	1.017

in an ice accretion prediction only in exceptional circumstances, such as testing the limiting capabilities of an ice accretion code.

4.2.3 Method of Integration

The equations governing the motion of arbitrarily-shaped particles are as follows:

$$\dot{x} = \frac{dx}{dt} \qquad \dot{y} = \frac{dy}{dt} \qquad \dot{\theta} = d\frac{\theta}{dt} \qquad (14a - c)$$

$$\frac{d\dot{x}}{dt} = -\frac{\vec{D}}{m}\cos\gamma - \frac{\vec{L}}{m}\sin\gamma + g\sin\alpha$$

$$\frac{d\dot{y}}{dt} = -\frac{\vec{D}}{m}\sin\gamma + \frac{\vec{L}}{m}\cos\gamma - g\cos\alpha$$

$$\frac{d\theta}{dt} = \frac{M}{I_{zz}}$$

$$(14d - f)$$

For spherical water droplets, Equations 14c and 14f are not applicable and Equations 14d and 14e are simplified to result in the following four equations:

$$\dot{x} = \frac{dx}{dt}$$

$$\dot{y} = \frac{dy}{dt}$$

$$\frac{d\dot{x}}{dt} = -\frac{\vec{D}}{m}\cos\gamma + g\sin\alpha$$

$$\frac{d\dot{y}}{dt} = -\frac{\vec{D}}{m}\sin\gamma - g\sin\alpha \qquad (15)$$

These equations are integrated using the method of Gear developed for stiff equations[16-17]. The details of the subroutines that make up the integration method, i.e., DIFSUB, DECOMP, SOLVE, and PEDERV, can be found in Reference 16 and in COMMENT statements in the computer code. The integration routine also requires that the equations to be integrated be located in a subroutine named DIFFUN. This subroutine currently contains Equations 14 - 15.

4.2.4 Determination of Droplet Impingement

The calculation of the droplet trajectories is continued until the droplets impinge upon the body or move out of range. This section describes the procedure used to determine whether or not a droplet impacts the body and, if so, the location of impingement. These calculations are controlled by subroutine MODE.

As previously discussed, the geometry is defined by segments joining a discrete set of body coordinates as shown in Figure 2.1. A droplet is considered to impact the body when its trajectory intersects one of these body segments. The current model does not take account of grazing collisions or droplets that may impact the body so that they are re-introduced into the flow by bouncing, splashing, etc. The impact algorithm, found in subroutine INTRST, sequentially sums the angles between lines drawn from the particle position to adjacent points describing the closed curve of the geometry, as shown in Figure 4.4. The summation starts with the angle between lines drawn to the first and second points, continuing with the angle between the lines to the second and third points, and so on, all the way to the angle between lines drawn to the next to last and last points. If the particle is outside the body, the sum of these angles will always be zero. If the particle has crossed one of the body segments and lies inside the body, the sum of the angles is 2π. If the particle lies directly on one of the body segments, the summed angle will equal π.

A particle trajectory is calculated until the summed angles total π or 2π, which indicates that the particle has impinged upon the body, or until the particle passes outside of the pre-specified boundaries. The impact point results from the intersection of the particle trajectory and the line connecting the adjacent ice shape points through which the particle trajectory passed (Figure 4.5). The particular line segment through which the particle passed is determined by first calculating the intersection of the line joining the present and previous particle positions and the line formed by each of the adjacent points that describe the body geometry, as shown in Figure 4.5. If the particle passed through a particular segment, the distance from the intersection (impingement) point to the endpoints of the segments will be less than the length of either the trajectory or body segments. Once the body segment through which the particle passed and the intersection (impingement) point have been determined, the surface distance, s, from the stagnation point to the impingement point is determined by interpolation.

4.2.5 Calculation of the Local Collection Efficiency

The particle trajectories and impingement points, calculated as previously described, are used to establish the relations between the particle's initial position (x_0, y_0) and the position where it impinges on the body surface,

18

specified by the surface distance, s, which is the length along the body surface measured from the stagnation point. The value of s is defined as negative on the lower surface and positive on the upper surface.

The local collection efficiency is calculated by first calculating droplet trajectories and producing a plot of particle release point, y_0, vs. surface impact distance, s, as shown in Figure 4.6. As was indicated by Equation 2, the local collection efficiency is a function of the surface distance and can be determined by differentiating the curve shown in Figure 4.6 with respect to s.

The derivative at the center of each body segment is calculated by first determining the four y_0 vs. s points whose s values are closest to the s value of the body segment at which the local collection efficiency is desired, as shown in Figure 4.6. These four points are then fit with a quadratic polynomial using the method of least squares. The local collection efficiency at the desired s location is determined by differentiating the polynomial. The local collection efficiency is calculated in subroutine EFFICY, while the curve fitting/differentiation procedure is found in subroutine TERP.

4.2.5.1 Local Collection Efficiency Calculation for Multidispersed Particle Distributions

The previous section described how the local collection efficiency was calculated for a single droplet diameter. In icing applications, the mass median droplet diameter of the droplet size distribution is used to characterize the size of the droplets. A feature of the particle trajectory portion of the trajectory program is that it allows the user to analyze the local collection efficiency for a multidispersed particle distribution.

To perform this calculation, the user must input the droplet diameter and the associated mass fraction and Cunningham correction factor for each specified droplet size. A maximum of 10 droplet sizes can be used to characterize a droplet distribution. For example, the required input for a Langmuir D distribution with a mass median of 20.0 microns is shown in Table 4.2.

The solution procedure is begun by calculating the local collection efficiency distribution for each droplet size characterizing the distribution. The

Table 4.2: Langmuir D droplet size distribution with a mass median of 20 microns

Percentage LWC	Ratio of Diameters	Droplet Diameter (μm)	Cunningham Correction Factor
0.05	0.31	6.2	1.0272
0.10	0.52	10.4	1.00
0.20	0.71	14.2	1.00
0.30	1.00	20.0	1.00
0.20	1.37	27.4	1.00
0.10	1.74	34.8	1.00
0.05	2.22	44.4	1.00

local collection efficiency for the distribution is determined by summing the contributions of each of the droplet sizes using the following equation:

$$\beta\left(s\right) = \sum_{i=1}^{N} n_i\, \beta_i\left(s\right) \tag{16}$$

where n_i is the mass fraction of liquid water associated with droplet diameter i and N is the number of droplet sizes used to characterize the distribution. The local collection efficiency for a droplet size distribution is also calculated in subroutine EFFICY.

4.2.6 Computational Procedure

The previous sections described various aspects of the calculation of the particle impingement characteristics. The purpose of this section is to describe how these calculations work together to yield the desired local collection efficiency information.

After calculating the flow field about the body, the program enters the particle trajectory main subroutine, TRAJ. First, the initial particle location x_0, y_0 and velocity V_{x_p}, V_{y_p} must be determined, either by the computer program or from information input by the user. A particle should be released at a location upstream of the airfoil where the flowfield is essentially

the same as the free stream conditions. The program will select an initial upstream x-coordinate, x_0, by searching for a position where the local velocity V_L and the freestream velocity V_∞ satisfy the following inequality:

$$\left|1 - \frac{V_L}{V_\infty}\right|_{y_0|_{min}}^{y_0|_{max}} \le \epsilon \tag{17}$$

where ϵ (VEPS in the computer program) is specified by the user. Equation (17) is tested over a specified range, $y_0|_{min} < y_0 < y_0|_{max}$, where $y_0|_{min}$ and $y_0|_{max}$, illustrated in Figure 4.7, are also input by the user.

With the initial upstream x-coordinate known, the next step is to locate two trajectories, one that passes above the body and one that passes below the body. The vertical distances from which these particles are released, $y_0|_{max}$ and $y_0|_{min}$, respectively, are specified by the user. The calculation of these particle trajectories is controlled by subroutine RANGE. Using these upper and lower trajectories as boundaries, the upper and lower impingement limits, y_{0u} and y_{0l}, are determined in subroutine IMPLIM (Figure 4.7b). This subroutine uses a Newton iteration scheme to determine the release points for particles with trajectories that impinge upon the body tangent to the surface. For example, when searching for the upper impingement limit, the trajectory of a particle released from $y_0|_1 = \frac{(y_0|_{min} + y_0|_{max})}{2}$ is computed. If the particle passes under or hits the body, the next trajectory is computed from $y_0|_2 = \frac{(y_0|_1 + y_0|_{max})}{2}$. If it passes over the body, the next trajectory is calculated from $y_0|_2 = \frac{(y_0|_1 + y_0|_{min})}{2}$. Successive halving of the range $y_0|_{min}$ to $y_0|_{max}$ continues until the upper impingement limit is found. Convergence of this iterative procedure is assumed when the difference between the y_0 values of two trajectories, i.e., one that hit the body and one that missed, is less than a small value specified by the user (YOLIM). This procedure is then repeated for the lower surface to determine the lower surface impingement limit. Any particle released between the upper and lower impingement limits will strike the body and any particle released from outside this range will miss the body.

With the limiting release points known, the program enters subroutine COLLEC where the range of vertical position, y_{0u} to y_{0l}, is divided into a number (NPL) of equally-spaced increments prescribed by the user. The trajectory of particles leaving each of these vertical positions is calculated,

and the impingement position of the particle on the body surface is determined using the method previously described. The y_0 vs. surface distance, s, information obtained in this calculation is then differentiated in subroutine EFFICY to determine the local collection efficiency at the midpoint of each of the body segments.

4.3   Calculation of the Thermodynamic Characteristics

The thermodynamic analysis of an icing surface was first developed by Tribus[7] from the physical model of the ice accretion process previously discussed. This model was used to calculate the heating requirements for icing protection and proposed LWC measurement systems. Messinger[8] developed the thermodynamic model further to include an analysis of the temperature of an unheated surface in icing conditions for three surface temperature regimes, i.e., less than 273.15 K, equal to 273.15 K, and above 273.15 K, and the concept of the freezing fraction, f, to be discussed later. These early formulations have been used in various icing applications.

As discussed in Section 3.2, microscopic movies of the ice accretion process made at NASA Lewis Research Center[9] indicate that the process may be more accurately modeled by modifying the equations used in past icing studies. The observations reveal that, after the initial flow of the coalesced droplets on the surface, the liquid does not flow but is caught and frozen in the grooves between the individual surface roughness elements. Incorporating this observation into a mathematical model would probably require modeling the individual roughness elements and the freezing of pools of water surrounded on all sides by ice. A microscopic and possibly three-dimensional analysis of the icing surface would be required to mathematically apply this model to an ice accretion prediction method. The mathematical model used in this and previous studies is more macroscopic in nature because the roughness elements do not directly effect the freezing process except to enhance the convective heat transfer coefficient.

The equations that model the thermodynamics of the freezing process on a body undergoing icing are formulated by performing a First Law of Thermodynamic mass and energy balance on a control volume located on the surface. The control volume to be analyzed is located on the surface of the body and extends from outside the boundary layer to the surface of the

body, as shown in Figure 4.8a. The lower boundary of the control volume is initially on the surface of the clean geometry and moves outward with the surface as the ice accretes. Therefore, the control volume is always situated on either the clean or ice surface. Computationally, a control volume is placed over each segment defining the body geometry, as shown in Figure 4.8b. The equations resulting from the mass and energy balance can be expressed as follows:

Mass Balance:

$$\dot{m}_{r_{out}} = (1.0 - f)(\dot{m}_e + m_{r_{in}}) - \dot{m}_e \qquad (18)$$

Energy Balance:

$$\dot{m}_c \Big[c_{pw,s}(T_s - 273.15) + \frac{V_\infty^2}{2} \Big] +$$

$$\dot{m}_{r_{in}} \Big[c_{pw,sur(i-1)}(T_{sur(i+1)} - 273.15) \Big] + q_k \Delta s =$$

$$\dot{m}_e \Big[c_{pw,sur}[(T_{sur} - 273.15) + L_V \Big] +$$

$$\Big[(1 - f)(\dot{m}_c + \dot{m}_{r_{in}}) - \dot{m}_e \Big] c_{pw,sur}(T_{sur} - 273.15) +$$

$$f\dot{m}_c - \dot{m}_{r_{in}})\Big[c_{pi,sur}(T_{sur} - 273.15) - L_f \Big] +$$

$$h_c \Big[T_{sur} - T_L - \frac{r_c V_L^2}{2c_{pa}} \Big] \Delta s \qquad (19)$$

The complete derivation of Equations (18) and (19) is included in Appendix A.

4.3.1 Definitions

Before discussing the method used to solve Equations (18) and (19), it is necessary to discuss several of the terms that are important to the solution procedure.

As discussed in Section 3.1, the atmospheric and meterological parameters determine the type of ice that will form for a given icing condition. It has been found by various authors that the concept of a freezing fraction

can be used to determine the type of ice that will form. The freezing fraction, f, was defined by Messinger as the fraction of impinging liquid that freezes within the region of impingement. In this application, f is defined as the fraction of the total liquid entering the control volume that freezes within the control volume. It is given by the equation

$$f = \frac{\dot{m}_i}{\dot{m}_c + \dot{m}_{r_{in}}}$$ (20)

For colder icing conditions, the droplets tend to freeze immediately on impact, resulting in the formation of rime ice. Since all the water entering the control volume freezes within the control volume, the freezing fraction equals 1.0. Freezing fractions close to 0.0 characterize glaze or clear ice. Freezing fractions between approximately 0.3 and 1.0 will normally indicate that the ice has some combination of glaze and rime characteristics. As shown in Figure 3.1, ice accretions are often composed of glaze, rime, and intermediate regions. The local value of the freezing fraction therefore varies along the surface, and can be calculated using the mass and energy balances given by Equations (18) and (19).

4.3.2 Solution of the Energy Equation

The evaluation of Equation (19) is begun at the stagnation point because there will be no runback into the control volumes located on each side of the stagnation point, as shown in Figure 4.8b. Therefore,

$$\dot{m}_{r_{in}}|_{stag} = \dot{m}_{r_{in}}|_{stag-1} = 0.0$$ (21)

It is first assumed that the equilibrium surface temperature, T_{sur}, equals 273.15 K. The terms of Equation (19) are then evaluated at this temperature, and the resulting expression is solved to determine the freezing fraction, f. This calculation is performed in subroutine COMPF. The value of f will be either 1) less than 0.0, 2) between 0.0 and 1.0, inclusive, or 3) greater than 1.0.

For $0.0 < f < 1.0$, $T_{sur} = 273.15K$, and the initial assumption was correct. A value of $f < 0.0$ indicates that the surface temperature is greater than 273.15 K. Therefore, the solution is obtained by setting $f = 0.0$ and solving for T_{sur} in subroutine COMPT. Note that an iterative procedure

is required since many of the terms of Equation (19) are functions of T_{sur}. Similarly, $f > 1.0$ indicates that T_{sur} is less than 273.15K, and f should be set equal to 1.0. Again, an iterative procedure must be applied to determine T_{sur}.

When the thermodynamic characteristics of the control volume are known, the mass balance given by Equation (18) is used to determine the mass flow rate of runback water out of the control volume. Any water flow out of the control volume will be away from the stagnation point and into the next control volume.

The above procedure is then repeated for the adjacent downstream control volume and continued along the upper surface of the body. The entire procedure is then repeated again, starting at the stagnation point and proceding along the lower surface of the body.

4.4 Calculation of the Iced Geometry

When the freezing fraction has been determined for each segment (control volume) on the body, Equation (20) is used to calculate the local ice accumulation rate, rewritten below as

$$\dot{m}_i = f\left(\dot{m}_c + \dot{m}_{r_{in}}\right) \tag{22}$$

This ice growth rate must be interpreted as an ice thickness to form an ice accretion on the surface of the geometry. The thickness of the ice layer grown on a particular segment is given by the equation

$$d_i = \frac{\dot{m}_i \, \Delta t + \Delta s}{\rho_i} \tag{23}$$

where ρ_i is the density of the ice, Δs is the length of the segment, and Δt is a time increment specified by the user.

The density of the accreted ice is determined using the empirical expression developed by Macklin (Reference 18). This correlation was developed from predominantly rime ice accretions at low temperatures and velocities and is as follows:

25

$$\rho_i = 110 \left(\frac{-\bar{d}_m V_d}{2\,T_{sur}} \right)^{.76} \tag{24}$$

In this expression, $\bar{d}_m$ is the mass median droplet diameter in microns, V_d is the droplet impact velocity in m/sec, and T_{sur} is the surface temperature in °C. In the calculation, the freestream velocity V_∞ is used for V_d. The ice density has the units of kg/m^3. Equation (24) is used to determine the ice density when the atmospheric and meteorological parameters are such that

$$1 \frac{\mu m\ m}{sec\ °C} \le \frac{-\bar{d}_m V_d}{2\,T_{sur}} \le 17 \frac{\mu m\ m}{sec°C}$$

and $T_{sur} < -5°C$. When these conditions are not satified, it is assumed that the ice has a density of $917 kg/m^3$. In general, the inequality will be satisfied under conditions of small droplets, low velocities, and low surface temperatures. For example, with a droplet diameter of 12 microns and a velocity of 60 m/s, the surface temperature must be less than -20 °C, a rather extreme rime condition. The density of the ice accretion is evaluated for each surface segment to allow mixed ice accretions to form (mixed ice accretions contain both rime and glaze ice). The calculation of the ice density is performed in function RHOICE.

The new ice surface is formed by first adding the ice thickness, d_i, perpendicular to each segment, as shown in Figure 4.9. The adjacent endpoints of each of these new segments are then averaged to obtain the coordinates describing the new ice surface. The new ice surface is calculated in subroutine NWFOIL using this procedure.

When the new surface is formed, the length of a segment increases. The segments are allowed to grow but, at some point, must be split to maintain adequate definition of the surface. The segment length is allowed to increase until it is SEGTOL times the length of the original segment. The value of SEGTOL is input by the user. When a segment has grown to SEGTOL times the initial segment length, it is divided in half to form two new segments, and a new point is added to the set of coordinates. These two new segments will be allowed to grow to SEGTOL times their current length before being divided. Note that a value of SEGTOL < 2.0 will result in progressively shorter segments. Values greater than 2.0 will

result in progressively longer segments. The segment lengths are checked and, if necessary, divided in subroutine NWPTS.

As the ice accretion grows, it is also possible for two lobes of the accretion to grow together, causing some of the points to lie in the interior of the body, as shown in Figure 4.10. These points must be removed in order to continue the calculations.

The point removal procedure is begun by applying the same procedure used to determine if two segments intersect, as shown in Figure 4. In this case, each body segment is checked with every other segment, excluding the two adjacent segments. As shown in Figure 10, if an intersection is found, all segments between the two intersecting segments are removed, and the set of coordinates is revised to reflect these changes. This procedure is performed in subroutine SEGSEC.

4.5 General Computational Procedure

The previous sections discussed each of the individual phenomena of the ice accretion process that are evaluated in LEWICE. The purpose of this section is to describe how these individual calculations are implemented to form a complete ice accretion.

As discussed in the Introduction, LEWICE applies a time-stepping procedure to grow an ice accretion. The flow field and droplet impingement characteristics are initially determined for the clean geometry. The ice growth rate on each segment defining the surface is determined by applying the thermodynamic model. The new surface is then formed by specifying an icing time and applying the procedure described in the previous section to account for the accreted ice on the clean surface. After calculating this initial ice layer, two options are available.

The most desirable option is to repeat the entire procedure, beginning with the calculation of the flow field about the iced geometry, to obtain revised local collection efficiency and thermodynamic data. Unfortunately, since the majority of the computational time is spent calculating droplet trajectories, this option also increases the computational time required to accrete a layer of ice. Therefore, a second option was made available.

27

If the amount of ice accreted during the time step is small or no new protuberances, such as glaze horns, were formed, it is possible to accrete another layer of ice using the same local collection efficiency curve calculated from the previous time step. This option, of course, does not produce results that are as accurate as those in the first option, especially for glaze ice accretions. The advantage is that the computational time required is significantly reduced.

Each of these options will require that another time increment be specified. The above procedure is repeated by specifying discrete time increments until the desired icing time is reached. Guidelines for choosing an appropriate time increment are also given in Section 5.3.1.

Ice accretions can have many geometrical shapes ranging from the smooth, aerodynamically-shaped rime accretions to rough glaze accretions with deep center grooves. LEWICE is therefore required to calculate sufficiently accurate flow fields and particle trajectories about what can be very irregular geometries where viscous effects such as boundary layer separation and reattachment are important. This can, at times, exceed the capabilities of the potential flow code and produce non-physical results. Much work has been done to identify and correct inaccuracies in the flow field calculations. The techniques that have been implemented in the code to overcome these flow field inadequacies will be discussed in many of the following sections.
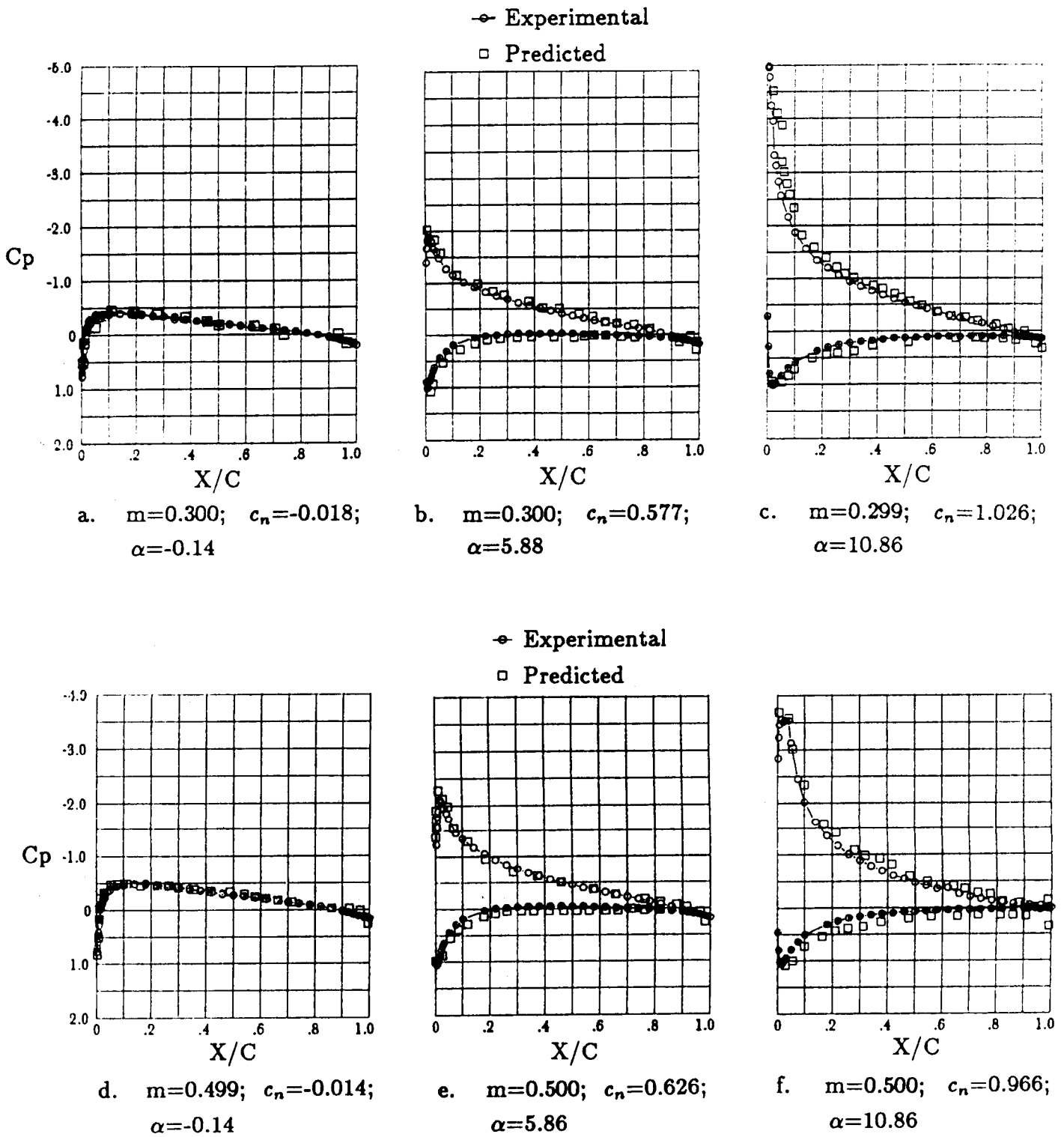
Figure 4.1 Comparison to experiment of pressure coefficient over a NACA
0012 airfoil calculated by the Douglas 2-dimensional flow code.

g. m=0.698; c_n=-0.018;
    α=-0.14

h. m=0.697; c_n=0.716;
    α=5.86
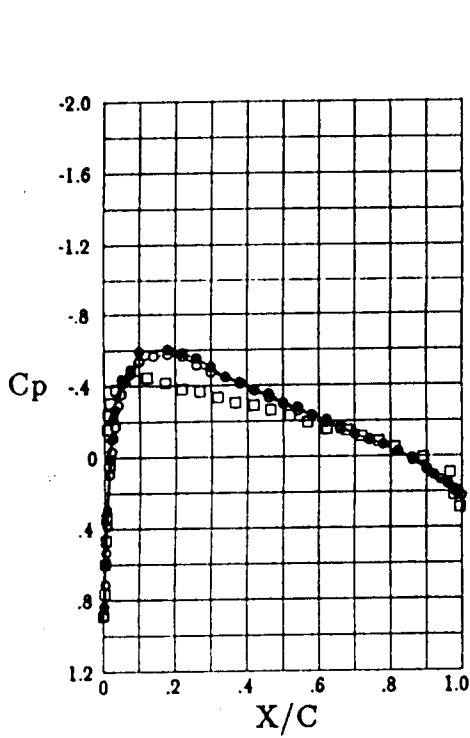
i. m=0.801; c_n=0.021;
    α=0.14

-● Experimental

□ Predicted
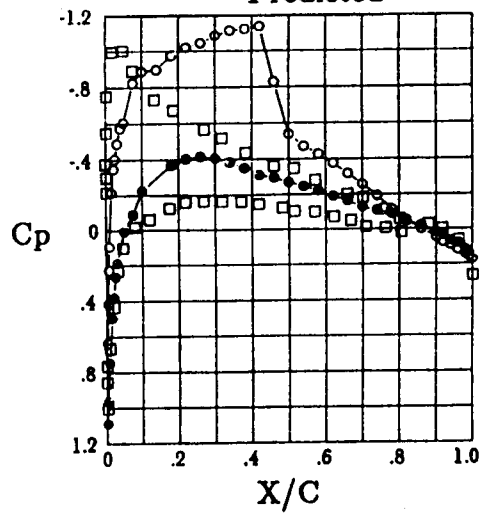
j. m=0.798; c_n=0.367;
    α=2.86

Figure 4.1: Continued.

30
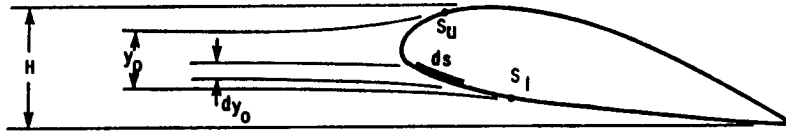
s_u = Upper − Surface Impingement Limit

s_l = Lower − Surface Impingement Limit

H = Forward Projection of the Airfoil Height

Total Collection Efficiency

$$E_m = \frac{y_o}{H}$$

$$E_m = \frac{1}{H} \int_{S_l}^{S_u} \beta \, ds$$

Local Collection Efficiency

$$\beta = \frac{dy_o}{ds}$$

Figure 4.2: Definition of total and local collection efficiency
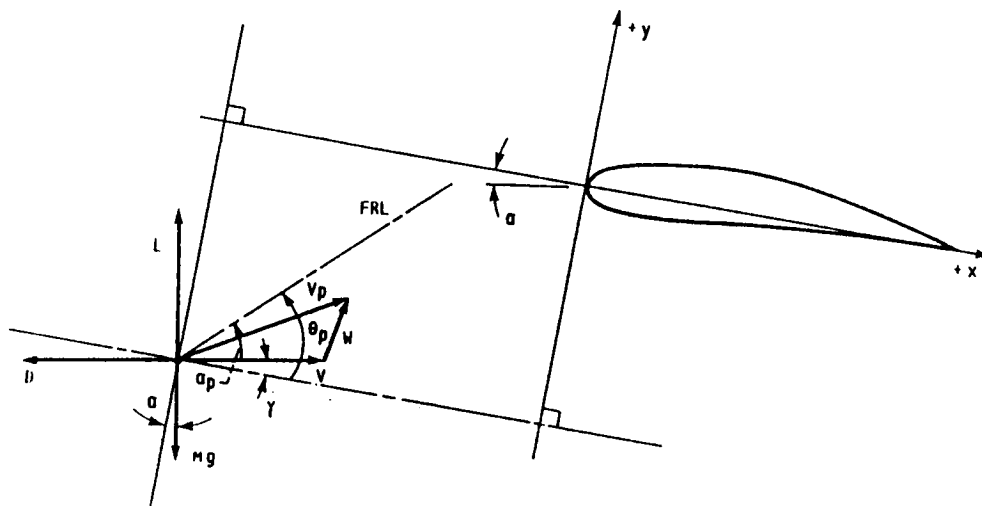
Figure 4.3: Forces acting on an arbitrarily-shaped particle
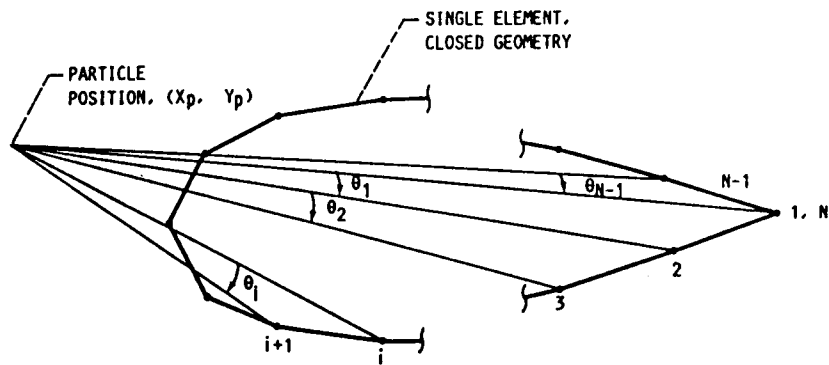
$$\theta_T = \sum_1^N \theta_i,$$

N = number of points describing the geometry (point 1 is the same as poing N).

If x_p, y_p lies outside the body, $\theta_T = 0$. If x_p, y_p lies on the body, $\theta_T = \pi$. If x_p, y_p lies inside the body, $\theta_T = 2\pi$

Figure 4.4: Illustration of the method to determine particle impact
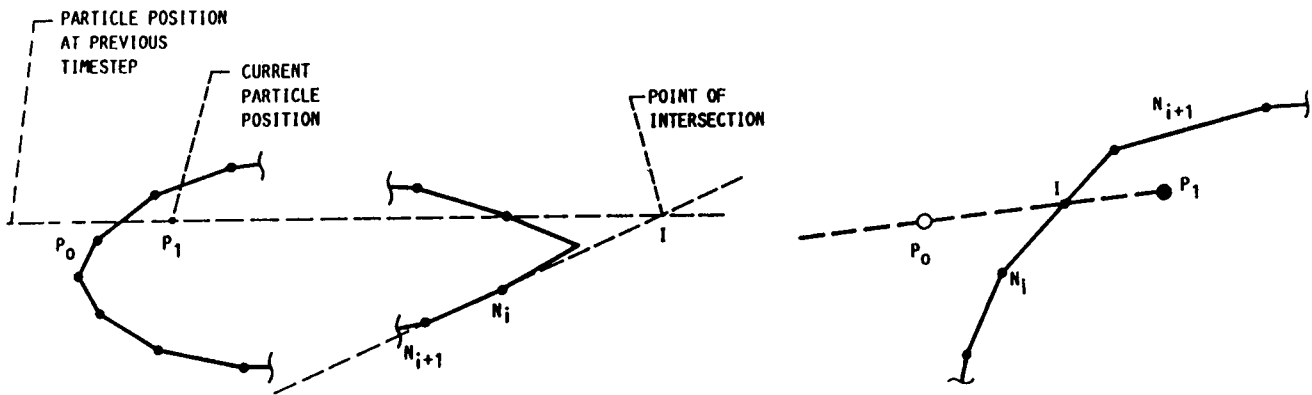
I. Particle does not pass through the segment being evaluated.

II. Particle passes through the segment being evaluated.

The particle passed through the segment being evaluated if all of the following criteria are satisfied:

$$\overline{IP_1} < \overline{P_0 P_1}$$

$$\overline{IN_{i+1}} < \overline{N_i N_{i+1}}$$

$$\overline{IP_0} < \overline{P_0 P_1}$$

$$\overline{IN_i} < \overline{N_i N_{i+1}}$$

Figure 4.5: Illustration of the method to determine the location of particle impingement
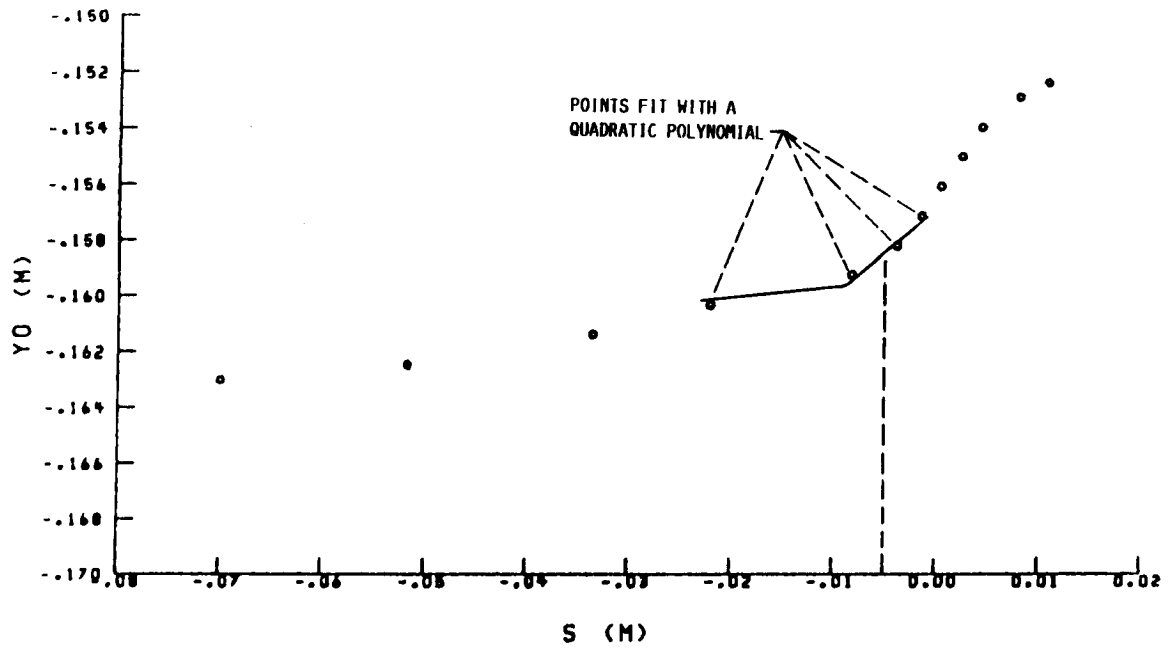
Figure 4.6: Particle release position, y_0, vs. surface impace distances, s, points used to determine the polynomial
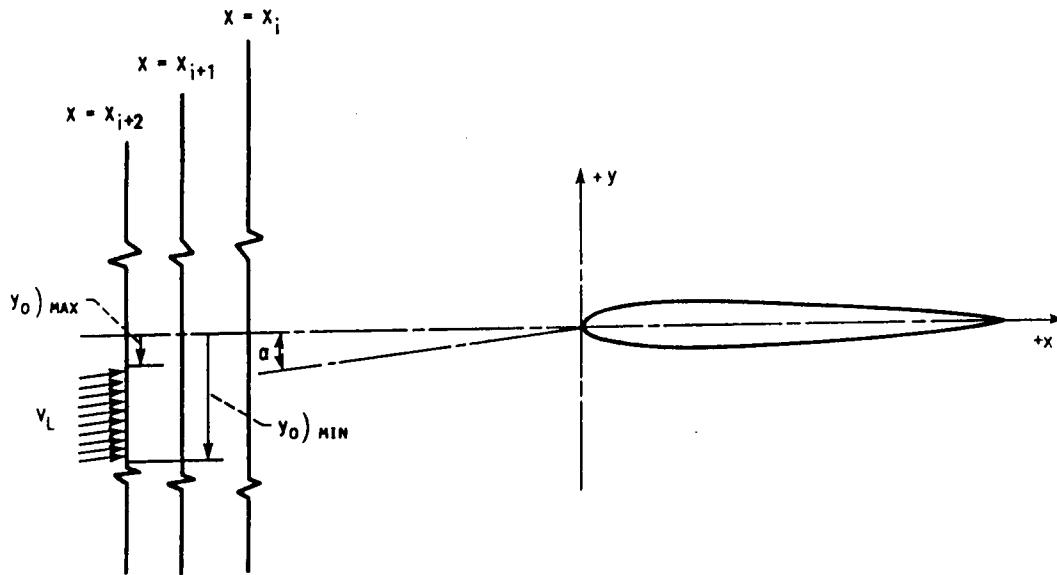
$$x = x_0 \quad if \ \left|1 - \frac{V_L}{V_\infty}\right|_{y_0|_{min}}^{y_0|_{max}} \leq \epsilon$$

a. Criteria to determine the particle release location.
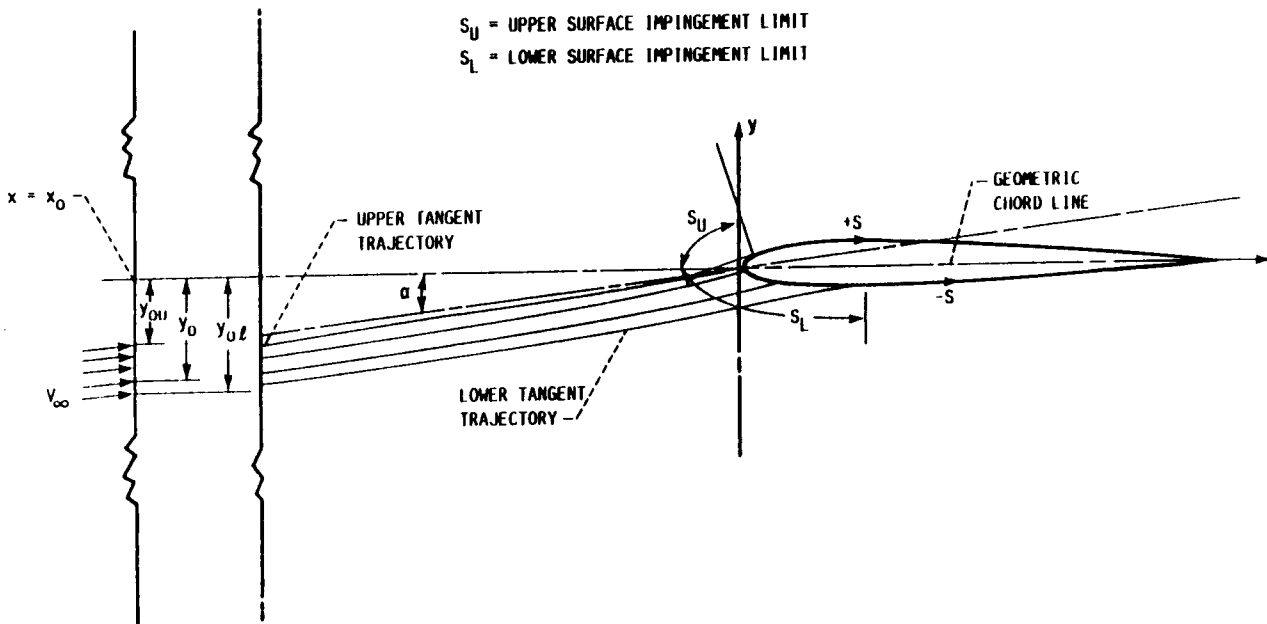
b. Particle release locations for the upper and lower surface tangent trajectories

Figure 4.7: Definition of terms used to determine the Local Collection Efficiency.

34
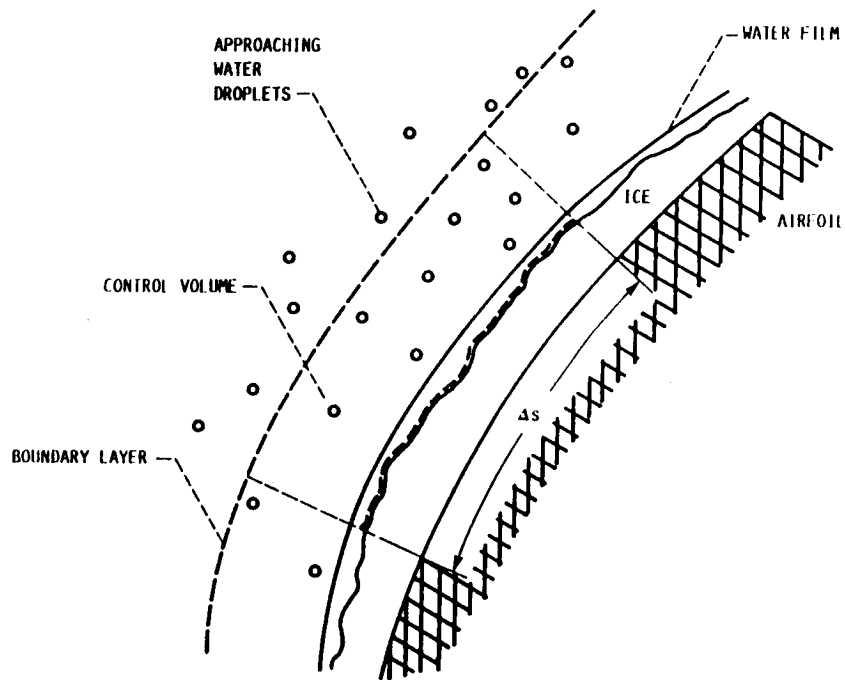
a. Single control volume on the icing surface.
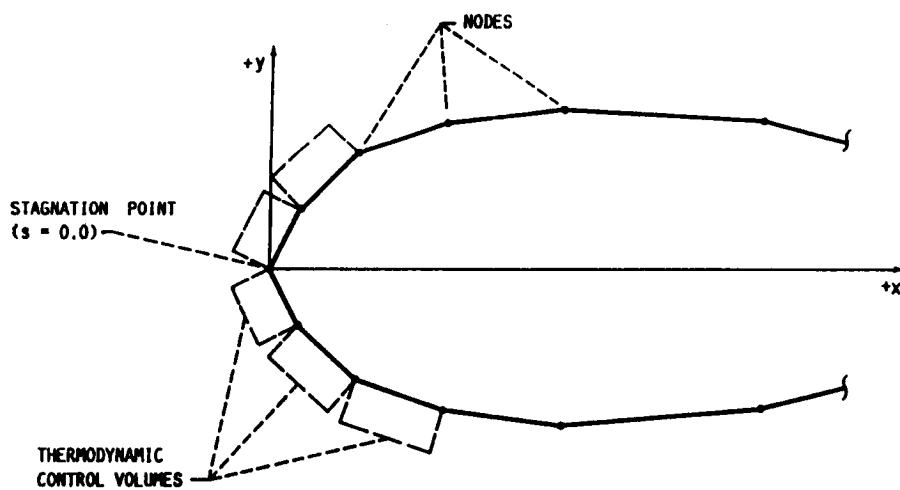
b. Thermodynamic control volumes over each segment defining the body geometry

Figure 4.8: Identification of the control volume used to formulate the thermodynamic equations
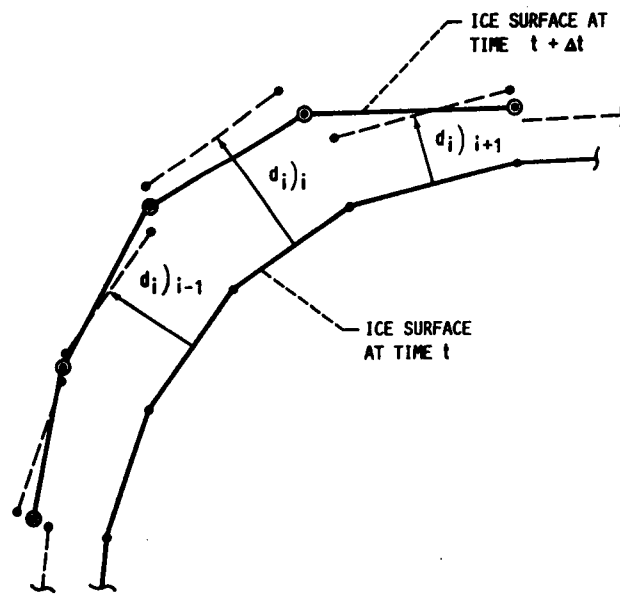
Figure 4.9: Illustration of the method to calculate the iced geometry
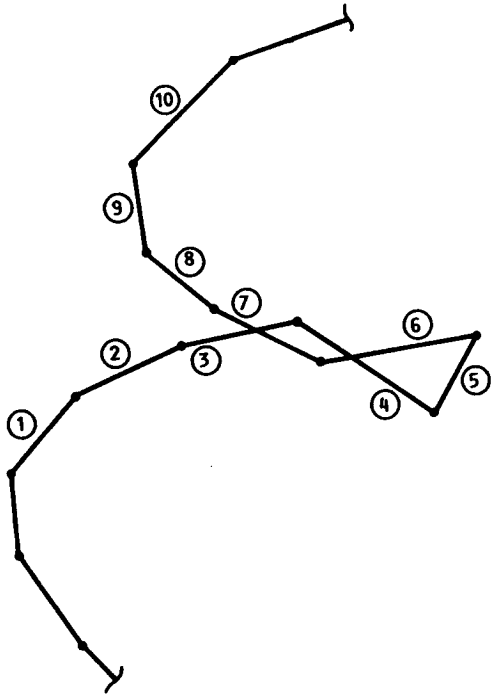
a. Geometry with intersecting segments ③ and ⑦
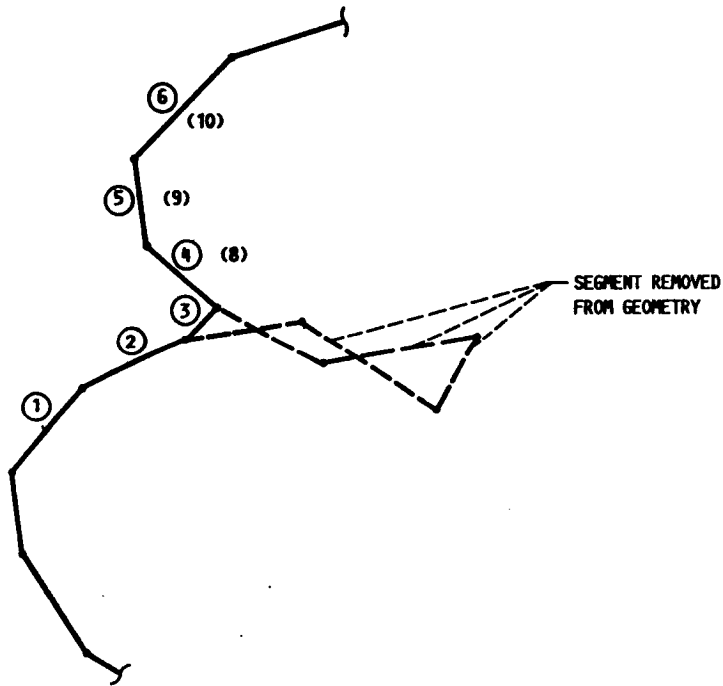
b. Revised geometry with the intersecting segments removed. (The original segment numbers from a. are in parenthesis)

Figure 4.10: Illustration of the method to remove points from the body geometry

Chapter 5

LEWICE INPUTS

This chapter presents the input format for a LEWICE input card deck. Section 5.1 contains the documentation that is needed to set up, execute, and make changes to the data deck. When more explanation is required, the user should consult Section 5.2 which includes additional information concerning input definitions and program options. Examples of the input files are shown in Section 7.0. The interactive input requested by the program is discussed in Section 5.3.

5.1 Input Format

The purpose of this section is to provide a quick reference to the input parameters used in LEWICE. Additional information can be found in Section 5.2 and in various sections throughout the text. Where applicable, the sections that contain additional information about the parameters are identified.

5.1.1 Potential Flow Input

CARD 01   Run Identification Card (8A4)
            IDR

CARD 02   Potential Flow Code Control Parameters (NAMELIST S24Y)

        Variable   Description

            ILIFT   Lift Control Flag
                          = 0 This is not a lifting body
                          = 1 This is a lifting body

IPARA	Element Geometry Flag
	= 0 Linear Elements
	= 1 Parabolic Elements
IFIRST	First-order Terms Flag
	= 0 No first-order terms
	= 1 First derivative term
	= 2 Curvature term
	= 3 Both first-order terms
ISECND	Second-order terms flag
	= 0 No second- order terms
	= 1 Second derivative term
	= 2 Curvature squared term
	= 3 Both second- order terms
IPVOR	Vorticity Distribution Flag
	= 0 Use constant vorticity between body elements
	= 1 Use variable vorticity distribution
INCLT	c_l, α Flag
	= 0 Angle of attack, α, is input
	= 1 Total lift coefficient, c_l, is input
CLT	Value of angle of attack (degrees) or lift coefficient depending on the value of INCLT
ICHORD	Reference Length Flag
	= 0 The reference length used in calculating c_l is to be set $= 1.0$
	= 1 The reference length used in calculating c_l will be input as CCL
CCL	The value for the reference length (chord) used in calculating c_l

IND	Individual Solution Flag
	S24Y is capable of calculating the potential flow about up to 6 bodies and then superimpose the results of each. The possible values of IND are as follows:
	= 0 Edge velocities are not calculated for each body
	= 1 Edge velocities are calculated for each body
	In LEWICE, only one body is input and the edge velocities are always required. Therefore, IND = 1
ISOL	Matrix Solution Method Control Flag
	= 0 Use routine SOLVIT for the matrix solution (used when a very large number of geometry points have been input)
	= 1 Use routine QUASI for the matrix solution
	= 2 Use routine MIS1 for the matrix solution. Maximum number of geometry points is 101. If the number of points is greater than 101, the program will automatically use SOLVIT.
IPRINT	Print/Punch Flag
	= 0 Normal output
	= 2 Print the individual matrices
	= 7 Punch the output on cards
	IPRINT should be set equal to 0 to reduce the amount of printed output
IFILL	Parabolic Integration Flag
	S24Y calculates the forces and moments acting on the body using both trapezoidal and parabolic integration of the calculated pressure coefficient. The results of the trapezoidal calculations are always output.

The value of IFILL determines whether the parabolic results are printed.

= 0 Results of the parabolic integration are not printed

= 1 Results of the parabolic integrations are printed

ICOMB   Combination Solution Flag

= 0 No combination solution calculated

= 1 Combination solution calculated

CARD 03   x-Coordinates (6F12.7,2X,I1,1X,I1,1X,I1)

Column	Variable	Description
01-12	X(1)	x-coordinate of the geometry. Up to
13-24	X(2)	six coordinates may be input on each
25-36	X(3)	card depending on how the INO flag is
37-48	X(4)	set.
49-60	X(5)	
61-72	X(6)	
75	INO	Number of data points per card. If there are 6 values per card, INO may be left blank.
77	ISTAT	Last Card Flag =0 This is not the last x-coordinate card. More cards will follow. =1 This is the last x-coordinate card.
79	ITYPE	x-Coordinate Flag = 3

CARD 04   y-Coordinates (6F12.7,2X,I1,1X,I1,1X,I1)

Column	Variable	Description
01-12	Y(1)	y-coordinate of the geometry. Up
13-24	Y(2)	to six points may be input on each
25-36	Y(3)	card depending upon how the INO flag
37-48	Y(4)	is set.
49-60	Y(5)	
61-72	Y(6)	
75	INO	Number of data points per card. If there are six values per card, INO may be left blank.
77	ISTAT	Last Card Flag = 0 This is not the last y-coordinate card. More cards will follow. = 1 This is the last y-coordinate card.
79	ITYPE	y-Coordinate Flag = 4

5.1.2   Trajectory Code Input

CARD 05   Tajectory Input I (NAMELIST TRAJ1)

Variable	Description
GEPS	Convergence criterion for the integration method of Gear
VEPS	Accuracy criterion for the case when LXOR = 1 (Section 4.2.6)

DSHIFT	x-distance to shift coordinates after the potential flow calculation to avoid discretization errors
LCMB	Combination Correction Flag = 0 Calculates the combination solution using the method of S24Y = 1 Calculates the combination solution using the method of COMBIN-2D
LCMP	Compressiblity Correction Flag = 0 No correction for compressibility = 1 Correct velocity values to account for compressibility
LEQM	Particle Initial Condition Flag = 0 The initial x- and y-components of the particle velocity will be input = 1 The initial particle velocity is equal to the flow at the initial particle location (in equilibrium with the flow)
LSYM	Symmetric Flow Field Flag = 0 Unsymmetric flow field (general case) = 1 Symmetric flow field (only half plane is computed)
LYOR	y-Coordinate Particle Release Flag = 0 Particle is released from the position specified by YORC = 1 Program determines the vertical particle release position using Y0MAX and Y0MIN as the initial guesses
LXOR	x-Coordinate Particle Release Flag = 0 Particle is released from the position specified by XORC = 1 Particle release position is determined using the criteria $\left\|1 - \frac{V_L}{V_\infty}\right\| < VEPS$

NEQ	Number of equations to be solved to determine the particle trajectories = 4 Spherical, non-lifting particle = 6 Lifting, rotating particle
NPL	Number of particle trajectories to be computed to define the y_0 vs. s curve. If NPL is set equal to 1, a single trajectory is to be calculated.
NSEAR	Maximum number of trajectories allowed to be calculated in the search for the upper and lower impingement limits
NSI	Number of droplet sizes used to characterize the cloud droplet distribution (maximum of 10)
TIMSTP	Initial value of the time step used in the integration of the particle trajectory equation (Gear's integration method)

CARD 06   Trajectory Input II (NAMELIST TRAJ2)

Variable	Description
CHORD	Airfoil chord (m)
G	Acceleration of gravity (m/s^2)
PIT	Initial angle of the particle flight reference line (Figure 4.3) (degrees)
PRATK	Initial value of the particle angle of attack (Figure 4.3) (degrees)
XORC	x-coordinate position of particle release (x_0/chord). XORC need not be input if LXOR = 1.
YORC	y-coordinate position of particle release (y_0/chord). YORC need not be input if LYOR = 1.

XSTOP	Maximum downstream distance, normalized by the chord of the airfoil, for which particle trajectories are calculated
Y0LIM	Accuracy criterion for computing the surface impingement limits (Section 4.2.6)
Y0MAX	Initial guess for the y-coordinate of the upper surface tangent trajectory release point (y_0/chord) (Section 4.2.6)
Y0MIN	Initial guess for the y-coordinate of the lower surface tangent trajectory release point (y_0/chord) (Section 4.2.6)
VXPIN, VYPIN	x- and y-components of the particle release velocity. They are input only when LEQM = 0.

CARD 07   Droplet Distribution Characterization Card (NAMELIST DIST)

Variable	Description
DPD	Droplet sizes in the distribution (maximum of 10) (microns)
FLWC	Fraction of LWC for each droplet size specified in the distribution
CFP	Cunningham correction factor (Section 4.2.2, Table 4.2)

5.1.3   Ice Accretion Input

CARD 08   Ice Accretion Data (NAMELIST ICE)

Variable	Description
VINF	Free-stream velocity (m/s)
TAMB	Static temperature (K)
PAMB	Static pressure (Pa)
LWC	Liquid water content (g/m^3)
DPMM	Mass median droplet diameter of the specified droplet distribution (microns)
RH	Percent relative humidity
XKINIT	Initial value of the equivalent sand-grain roughness of the icing surface (Chapter 4.3, Appendix F)
SEGTOL	Maximum amount any segment may grow before it is divided in two (Chapter 4.4)

5.2   User's Guide to Input Format

5.2.1   Potential Flow Input

As discussed in Section 4.1, the flow field used in LEWICE is calculated using the Douglas potential flow method (S24Y). This code was developed to calculate the flow field about a wide variety of geometries. Using this code in an ice accretion prediction method decreases the generality required by the potential flow code, and many of the input parameters and program options are not necessary for this application. The input to the potential flow code required by LEWICE users was simplified to include only the applicable parameters. However, the potential flow computer code was not modified and remains in its original form in LEWICE. Therefore, the original input format to the potential flow code is still used and all input parameters are required. The input parameters not found in NAMELIST S24Y are set to default values in subroutine SETUP. In this subroutine, the input file to the potential flow code is set up and written to unit 45. A description of the complete input to the potential flow code written to unit 45 is given in Appendix C. Further details concerning the input parameters can be found in Reference C-1 and C-2.

5.2.2 Trajectory Code Input

This section provides the user with additional information about many of the input parameters to the particle trajectory code. Suggested values of the parameters are also given.

5.2.2.1 Trajectory Input 1 (NAMELIST TRAJ1)

GEPS

This variable is the error test constant used in the integration method of Gear. Single step error estimates made in the integration algorithm must be less than GEPS in the Euclidean norm. The step size and/or order is adjusted so that this criteria is met. See References 16 and 17 for additional information on the parameter and the integration scheme in general.

Parametric studies were made to evaluate the effect of changing the value of GEPS from 0.001 to 0.00001. Increasing the value of GEPS was found to reduce the cpu time required to calculate each trajectory by allowing larger integration step sizes to be used. Figure 5.1 shows how increasing GEPS decreases the computational time per trajectory.

Unfortunately, larger values of GEPS also allow larger computational errors which are reflected in the calculated particle impingement locations. Computationally, GEPS should approach 0.0, but the required computational time would be excessive, as shown in Figure 5.1. A value of GEPS=0.00005 was therefore used for all calculations.

VEPS

This parameter is used when the program is to locate the proper x location at which to release the particles. The particles will be released from an x location where, between Y0MIN and Y0MAX,

$$\left| 1 - \frac{V_L}{V_\infty} \right| \leq VEPS$$

Increasing the value of VEPS will allow particles to be released closer to the body and thereby decrease the number of integration timesteps required for the particle to strike the body. The computational time will therefore be decreased.

No studies have been made to show the effect of releasing the particles closer to the body. The particles must be released in essentially free stream conditions for physically accurate trajectories to be calculated. For this reason, a VEPS value of 1.0×10^{-3} has been used for all calculations.

DSHIFT

The potential flow computer program has a relatively large discretization error very close to the body. Figure 5.2, taken from Reference 12, shows the longitudinal and vertical velocities around the leading edge of a Joukowski airfoil. The velocity is computed for different constant values of separation distance (DSHIFT) from the body, as illustrated in the insert. Note the large oscillations in the flow field velocity near the surface. These oscillations can cause erratic particle trajectories close to the body, especially for small particles that are effected by small flow field perturbations, and can cause fatal program errors to occur, thereby terminating the program.

To overcome the effect of the discretization error near the body, an artificial impingement surface is generated by the computer program. This surface is defined by displacing each point of the body by a small increment DSHIFT in the upstream x direction. This displacement essentially increases the size of the body to include the region where discretization errors are present. DSHIFT values of approximately .2 to .6 percent of the chord length are commonly used. If irregularties in the impingement curves or droplet trajectory calculations persist for a specific case, the DSHIFT value should be increased. Additional information concerning this flowfield correction can be found in Appendix C.

The artificial impingement surface is generated in the computer program after the potential flow calculation. Thus, the flow field is not influenced by the creation of the pseudo-surface. Also, this surface is discarded after the collection efficiency has been calculated, and is not used when a new ice surface is formed.

LEQM

This parameter is the flag to specify the initial velocity of the particle. In cases where an ice accretion is to be formed, the particles should be released in equilibrium with the flow, i.e., LEQM = 1. The option exists to specify the x- and y- components of the initial particle velocity when

LEQM = 0. This option could be used along with the options to specify the particle release position to simulate a droplet being ejected from a spray nozzle.

LSYM

If a body and flow field are symmetrical, the local collection efficiency distribution will also be symmetrical. Therefore, particle trajectory and impingement locations need to be calculated only for either the upper or lower surface. The local collection efficiency distribution is then assumed to be identical for the opposite surface. When LSYM = 1, the droplet impingement characteristics will be calculated only on the upper surface, and the local collection efficiency distribution is specified to be identical on the lower surface. When LSYM = 0, the droplet impingement characteristics are calculated for both the upper and lower surfaces.

While some clean geometries are exactly symmetrical, the ice shapes rarely have exactly symmetrical surface coordinates. Forcing symmetrical collection efficiency distributions onto these surfaces has caused inaccurate ice shapes to form. Therefore, it is suggested that, unless three or fewer time-steps are to be performed, LSYM be set equal to 0 even for symmetrical bodies at zero angle of attack. Of course, the computational time will be longer, but, in general, fewer problems will be encountered.

LYOR, LXOR

These are the x- and y-coordinate particle release flags used to indicate whether the particle release position will be specified by the user or determined in the computer program using the criteria discussed in Section 4.2.6. When using the code to predict ice accretions, it is better to let the code determine the particle release positions. The positions that might be specified by the user for the clean geometry may be unsatisfactory as an ice accretion grows. These options have been included so that the code can also be used to calculate individual trajectories of particles released from a specific person.

NPL

This parameter is used to specify the number of particle trajectories calculated in subroutine COLLEC to define the y_o vs. s curve. The curve will be better defined when more trajectories and impingement locations are calculated. This, of course, is done at the expense of computational time. While a maximum of 50 trajectories can be calculated, NPL = 15 is normally specified.

If NPL is set equal to 1, the impingement limits will not be calculated and the program will calculate the trajectory of only one particle. The particle will be released from a position specified by XORC, YORC.

NSEAR

The criteria to identify an impingement limit are specified by the parameter Y0LIM. If this specified parameter is specified too small, an excessive number of trajectories could be calculated. This parameter limits the number of trajectories that can be calculated while searching for the impingement limits; a value of NSEAR = 50 is normally input. Calculations of excessive numbers of trajectories can also be caused by erroneous input values and coordinates defining the body geometry.

TIMSTP

As mentioned in the description of the GEPS parameter, the integration step size is determined in the program so that the single step error estimate is less than GEPS. Since the program automatically determines the step size during the integration, the value of the initial step size is not critical. A value of TIMSTP = 0.0005 has been used consistently for all calculations. This value is then decreased or increased as required in the computer program.

NSI

This parameter specifies the number of droplet size increments used to characterize the cloud droplet size distribution. If a monodispersed cloud is to be input, NSI = 1. The effect of using a multidispersed droplet distribution as opposed to a monodispersed distribution to determine an ice accretion shape is discussed in Section 7.4.

5.2.2.2 Trajectory Input II (NAMELIST TRAJ2)

CHORD

The chord of the airfoil (or diameter for a cylindrical body) is used as the reference length for the coordinate release inputs discussed in this section. The chord is input in meters.

G

The acceleration of gravity is input in m/s^2. If it is input as zero, the effect of gravity on the particle trajectories is neglected. The effect of gravity on the trajectories of droplets less than 50.0 microns is usually negligible, and is therefore omitted in most icing studies[19]. The effect of gravity was omitted for all of the sample cases in this report except for the ones using a multidispersed droplet distribution containing droplets larger than 50.0 microns.

PIT, PRATK

PIT is the initial particle pitch angle, which is defined as the angle between the axis oriented parallel to the airfoil x- axis and the flight reference line (See Figure 4.3 and Section 4.2.2). For spherical, non-rotating particles (such as water droplets) PIT = 0.0. PRATK is the initial particle angle of attack and should also be set equal to 0.0 for spherical particles.

When LEWICE is used to calculate ice accretion shapes, PIT and PRATK should both equal 0.0. The option to calculate the trajectories for non-spherical, rotating particles has been included so that the particle trajectory calculation may be useful for alternate applications, however, appropriate equations for the lift, drag, and moment coefficients must be supplied by the user and placed in subroutine COEFF. The subroutine was developed so that the coefficients are functions of the Reynolds number and the particle angle of attack.

XORC, YORC

These parameters are used to specify the particle release location when LXOR = 0 and LYOR = 0. XORC and YORC should be input normalized with respect to the airfoil chord length.

XSTOP

51

This parameter is the maximum downstream value of x/chord for which particle trajectories are calculated. If a particle reaches a location where x > XSTOP, it is considered to have missed the body and moved out of range. This rear boundary of the computational box should extend at least past the location of maximum thickness, and often further, depending on the geometry and angle of attack. If the value of XSTOP is greater than the maximum x-coordinate defining the body (XREAR), XSTOP is set equal to XREAR.

YOMAX, YOMIN

These are the initial guesses for the y-coordinate of the upper and lower surface tangent trajectory release points, normalized with respect to the chord.

YOLIM

YOLIM is the accuracy criteria to be used in determining when an impingement limit has been reached. As discussed in Section 4.2.6, when the release points of two trajectories (one that hit the body and one that missed the body) are within YOLIM, the trajectory that hit the body is identified as either the upper or lower surface tangent trajectory. The smaller the value of YOLIM, the greater the number of trajectories that will have to be calculated to identify the tangent trajectory. A practical value for YOLIM is 0.0001; this value is used for all sample calculations.

VXPIN, VYPIN

These values are the x- and y-components of the initial particle velocity in m/s. These values need to be input only when LEQM = 0.

5.2.2.3 Droplet Distribution Input (NAMELIST DIST)

DPD

This array is used to specify the droplet sizes characterizing the distribution. The droplet sizes should be input in microns.

FLWC

FLWC is the fraction of the total liquid water content contained in each droplet size increment.

CFP

This parameter is the Cunningham correction factor (Reference 15). Small particles, i.e., those less than 10.0 microns, have a drag slightly less than that given by the equation for spheres in cross-flow. The Cunningham correction factor is used to correct the drag coefficient given by the equations in subroutine COEFF. The correction factors are found in Table 4.2.

5.2.3   Ice Accretion Input (NAMELIST ICE)

VINF, TAMB, PAMB, LWC, DPMM, RH

These variables are used to specify the icing condition. The pressure and temperature inputs are static conditions. The variable DPMM is the mass median droplet diameter of the specified droplet distribution in microns. If a monodispersed cloud is specified (NSI = 1), DPMM is equal to the droplet size specified as DPD. When a multidispersed cloud is specified (NSI = 1), DPMM should still be input because it is used as a label on the parameter plots.

XKINIT

This parameter is the initial value of the equivalent sand-grain roughness of the icing surface. The integral boundary layer method applied to calculate the convective heat transfer coefficient uses this variable to account for the effect of surface roughness. The value of XKINIT is input by the user and obtained using a relationship that expresses XKINIT as a function of static temperature, velocity, and LWC. The value of XKINIT is constant throughout the icing encounter. A discussion of the procedure used to determine this relationship is given in Appendix F.

SEGTOL

To maintain adequate definition of the body geometry, it is necessary to divide segments as they grow. This variable is the maximum fractional amount by which a segment may increase in length before being divided in

two. A value of SEGTOL < 2.0 will result in progressively shorter segments. Values greater than 2.0 will allow the segments to grow progressively longer. A value of SEGTOL = 1.5 has been found to work well in most icing predictions.

QCOND

This variable is used to input heat flow either to or from the body surface. The values of QCOND are input in W/m^2 as a function of surface distance. It can be used to simulate thermal anti-icing systems, but is not applicable to de-icing systems since the thermodynamics of the ice-to-liquid phase change at the surface of the body are not modeled. The results can only be assumed to be correct for the first timestep because, the effect of conduction through an ice layer formed during the first timestep is not modeled.

5.3   Interactive Input

The timestepping feature of LEWICE can, at times, cause conditions to exist that require the user's interaction. This section describes the primary interactive prompts and responses required in the computer code. Several interactive prompts are also made to indicate an unusual condition requiring analysis by the user. These will be discussed as they occur in the examples in Section 7.0.

After the primary input file (unit 35) has been read and the potential flow and particle trajectory files have been set up, the program will prompt the user to enter the desired icing time (in seconds). The icing time is considered to be the total length of time that the accretion is to be grown. The prompt will read as follows:

TIME = 0
ENTER DESIRED ICING TIME (SEC), (F10.0)

Upon entering the icing time, the program will then prompt the user to enter the desired time increment for the first timestep with the following statement:

ENTER DESIRED TIME INCREMENT (SEC), (F10.0)

A general guideline for selecting an icing time increment for a given icing condition is discussed in Section 5.3.1.

The user will then be asked to select the desired plot options. The prompt will be as follows:

                AVAILABLE PLOT OPTIONS
                    0 - NO PLOTS
                    1 - PARAMETER PLOTS ONLY
                    2 - TRAJECTORY PLOTS ONLY
                    3 - PARAMETER AND TRAJECTORY PLOTS
                ENTER PLOT OPTION ( )

If plot option 2 or 3 is chosen, the trajectories will be plotted immediately after each is calculated. The trajectory points are not saved and, therefore, are lost when subsequent trajectories are calculated. Plot options 1 and 3 will send the program into a plotting routine after the completion of the timestep so that the significant parameters can be plotted. The plotting routine uses a menu from which the following plots can be selected:

01 - Iced airfoil
02 - Particle release point (y_0) vs. Surface impact distance(s)
03 - Local collection efficieny (β) vs. Surface distance(s)
04 - Edge velocity (V_e) vs. Surface distance(s)
05 - Edge temperature (T_e) vs. Surface distance(s)
06 - Edge pressure (P_e) vs. Surface distance(s)
07 - Surface temperature (T_{sur}) vs. Surface distance(s)
08 - Convective heat transfer coefficient (h_c) vs. Surface distance(s)
09 - Equivalent sand-grain roughness height (k_s) vs. Surface distance(s)
10 - Ice density (ρ_i) vs. surface distance(s)
11 - Freezing fraction (f) vs. surface distance(s)

Examples of these plots are given in Section 6.0, LEWICE Output.

5.3.1 Selection of an Icing Time Increment

The timestepping procedure makes LEWICE unique among ice accretion prediction methods because it allows the physics of the ice accretion to

55

be more accurately modeled. Unfortunately, the procedure also adds complexity to the model because a proper time increment must be selected by the user. Also, the timestep will influence the ice accretion shape for a specific icing condition; the shape is not uniquely determined by the icing conditions. For example, Figure 5.3 shows three glaze ice accretion shapes calculated for the same icing condition, but with different timesteps. In Figure 5.3a, the accretion was formed in a single timestep. This shape has the basic shape of the experimental ice accretion but lacks much of the detail. Figures 5.3b and c show the same accretion formed at shorter timesteps. Note that, as the timestep is decreased, the predicted accretion takes on more of the characteristics of the experimental ice shape. Similar results for a rime ice accretion are shown in Figure 5.4. These results indicate that there is some maximum amount of ice that should be deposited during a single timestep. On the other hand, when a short timestep is selected, more steps are required to form the final ice shape, which increases the computational time required for each icing condition.

Many ice accretion shapes have been calculated during the development of LEWICE, and a criterion has been developed to help the user select an appropriate timestep. Various authors have developed a term known as the accumulation parameter, which is given by the following equation:

$$A_c = \frac{\beta|_{max} \, V_\infty \, LWC \, \Delta t}{c \, \rho_i} \tag{25}$$

where c is the chord length of the body geometry (Some authors omit the factor $\beta|_{max}$ in the definition of A_c[19].) The accumulation parameter is representative of the non-dimensional maximum thickness of the ice accreted during time Δt. Therefore, a limiting value of A_c could be used to determine the length of a timestep. However, it was found that when ice shapes were formed on an airfoil at an angle of attack, better results were obtained using timesteps shorter than those used when the airfoil was at 0.0 . Equation (25) was modified as follows:

$$\bar{A}_c = \frac{\beta|_{max} \, V_\infty \, (LWC) \, \Delta t \, (1 + \frac{\alpha}{20})}{c \, \rho_i} \tag{26}$$

where α is in degrees. When comparisons with experimental ice accretions, the modified accumulation parameter was generally less than .1. Therefore, the following equation can be used to calculate the time step:

$$\Delta t \leq \frac{(.1)\left(9.17 \times 10^5 \frac{g}{m^3}\right) c}{\beta|_{max} V_\infty LWC \left(1 + \frac{\alpha}{20}\right)} \tag{27}$$

Suppose that an ice accretion is to be formed on an airfoil with a chord of 0.3 m at the following icing condition:

Velocity	= 80.0 m/s
LWC	= 1.2 g/m^3
Angle of attack	= 4.0
Icing time	= 5.0 min

If the value of $\beta|_{max}$, the maximum value of the local collection efficiency, is known, it should be used to evaluate Equation (27). If not, a value of 0.80 is a reasonable upper limit and can be substituted into Equation (27). The equation is evaluated as follows:

$$\Delta t \leq \frac{(.1)\left(9.17 \times 10^5 g/m^3\right)(.3m)}{0.80\,(80m/s)\,(1.2g/m^3)\left(1 + \frac{4}{20}\right)}$$
$$\leq 29.85 seconds \sim 30.0 seconds$$

This indicates that the initial timesteps should be no greater than 30.0 seconds. Since Equation (27) was developed only to provide guidance in selecting a timestep, it is always appropriate to round the calculated time to a whole number.

Depending on the icing condition and size of the geometry, a time increment may be calculated that is greater than the total icing time. In this case, it is recommended that the total icing time be divided into at least two, and perhaps three, timesteps even though Equation (27) indicated the ice could be accreted in one step. If a single step were used, none of the time dependent features of the accretion would be calculated by LEWICE. It was found that more realistic ice accretions are predicted if at least two timesteps are used.

There is one additional note concerning the selection of a timestep. Depending on the icing condition, the predicted shape can become very convoluted and irregular after several timesteps and computational inaccuracies, such as multiple calculated stagnation points, may occur. If the

multiple effects of these approximations cause the abnormal termination of the code or the formation of a non-physical ice accretion, increase the timestep and re-run the condition. By doing so, the user can get an idea of the general size and shape of the accretion. By comparing this result to the accretion obtained using the shorter timesteps, the accuracy of the prediction can be evaluated.
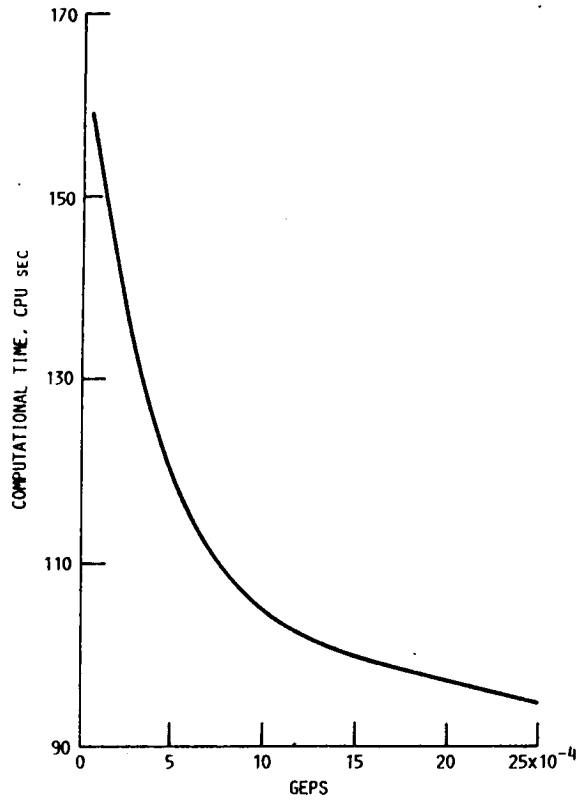
Figure 5.1: Computational time as a function of GEPS .
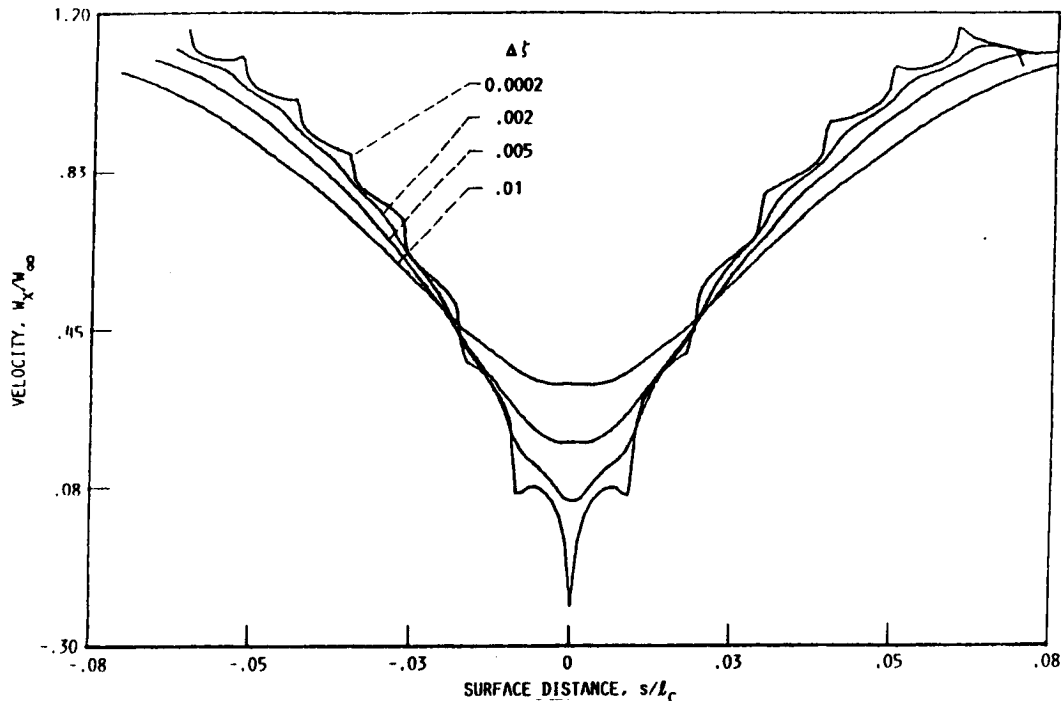
Figure 5.2: Discretization error in the flow field near the nose of a Joukowski airfoil.

59
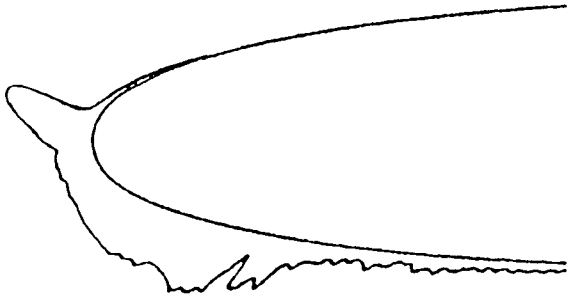
EXPERIMENTAL (REF. 20)
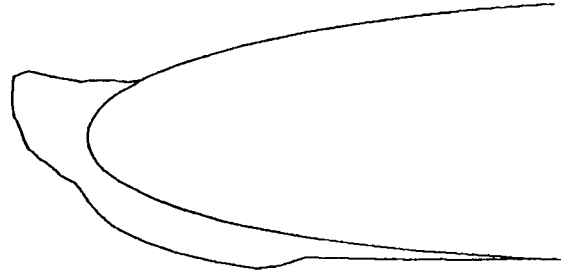
(a) Δt = 120.0 SEC.
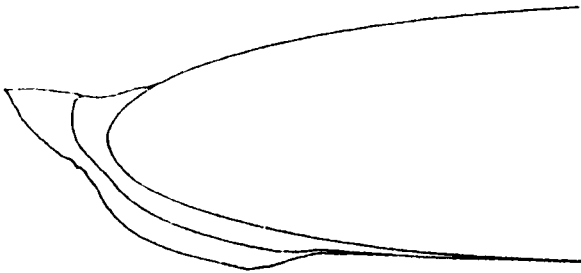
(b) Δt = 60.0 SEC.
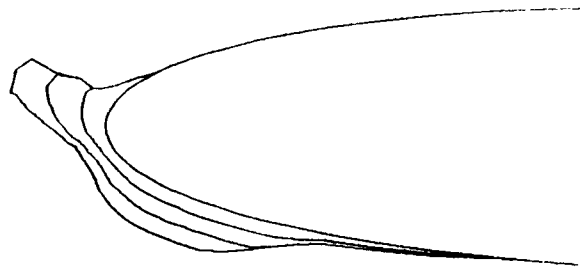
(c) Δt = 40.0 SEC.

VELOCITY (M/S)	129.00
TEMPERATURE (C)	-12.60
PRESSURE (KPA)	90.75
HUMIDITY (%)	100.00
LWC (G/M³)	1.00
DROP DIAM (MICRONS)	20.00
TIME (SEC)	120.00

Figure 5.3: Effect of icing time increment on a calcualted glaze ice accretion.

Δt = 120 SEC

Δt = 60 SEC

Δt = 40 SEC

TOTAL ICING TIME = 120 SEC
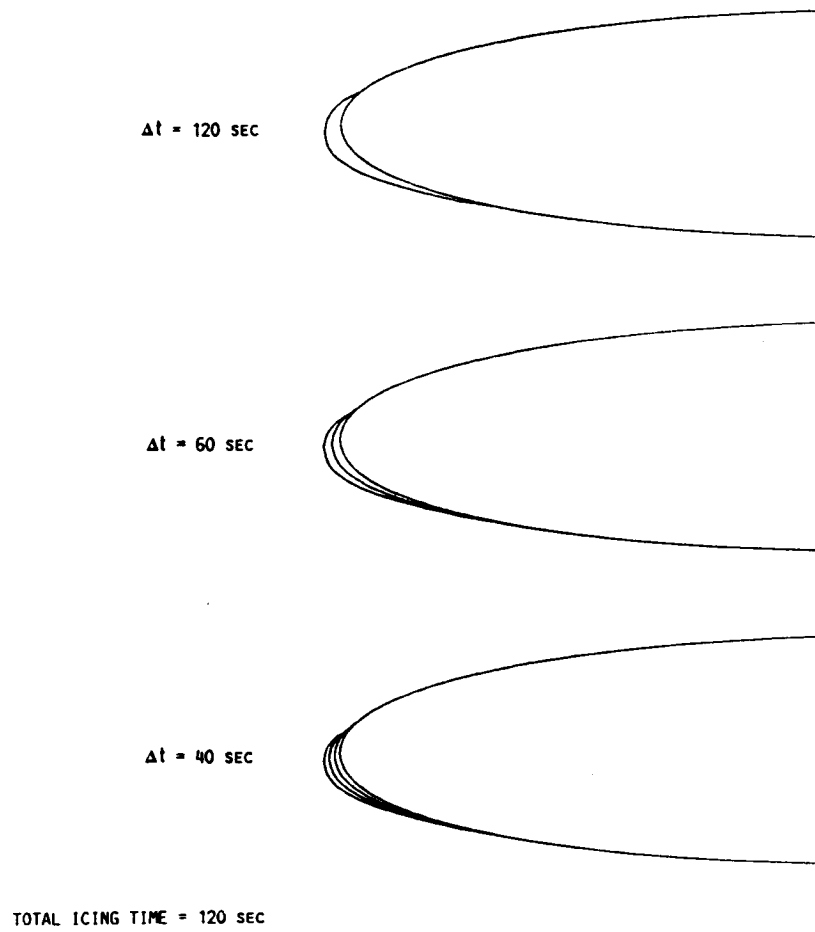
VELOCITY (M/S)	60.00
TEMPERATURE (C)	-26.15
PRESSURE (KPA)	98.80
HUMIDITY (%)	100.00
LWC (G/M**3)	1.00
DROP DIAM (MICRONS)	20.00
TIME (SEC)	120.00

Figure 5.4: Effect of icing time increment on a calculated rime ice accretion

Chapter 6

LEWICE Output

The standard output from LEWICE consists of both printed and plotted output. The printed output is made available primarily for diagnostic purposes and examination of the calculated values. Most comparisons of calculated variables and ice shapes are made with the graphics routines provided in the code. The output discussed in this section is the output for the sample case presented in Section 7.1.

6.1 Printed Output

Printed output is produced by the potential flow, particle trajectory, and ice accretion portions of the computer code. All output is printed on unit 56. The following sections describe the printed output from each of these portions.

6.1.1 Printed Output from the Potential Flow Code (S24Y)

All write statements contained in the original version of S24Y are included in LEWICE, however, many of these write statments have been commented out to reduce the amount of printed output.

The initial output from the potential flow code is a listing of the input geometry coordinates, as shown in Figure 6.1a. Following the coordinate listing are the calculated non-dimensional surface velocities and the body pressure coefficients, as shown in Figure 6.1b. A description of each of the parameters printed on this output page is as follows:

ALPHA	Angle of attack (degress) specified by the user
ALPHA O	Calculated angle of zero lift (degrees)
CL	Calculated lift coefficient. The reference length is that specified by CHORD
CHORD	Chord length (meters) specified by the user to use as the reference length in the calculation of CL
NO. OF ELEMENTS, TOTAL ELEMENTS	Number of segments specified to define the body geometry
I, J	Segment number
X, Y	x,y coordinates of the midpoint of each segment
S	Surface distance to the midpoint of each segment s = 0.0 corresponds to the trailing edge of the body (point number 1)
VT	Non-dimensional surface velocity given by the following equation:

$$VT = \frac{V_L}{V_\infty}$$

CP	Surface pressure coefficient, c_p calculated from VT using the following equation:

$$CP = 1.0 - VT^2$$

The force coefficients (lift, moment, normal, axial, and pressure drag) are calculated from the pressure coefficient data and printed after the data described above. These variables are calculated using two methods from the same set of pressure coefficient data. The first method integrates the pressure coefficient curve using the trapezoidal rule while the second uses Simpson's rule.

63

6.1.2 Printed Output from the Particle Trajectory Code

The first output from the particle trajectory code will be a statement identifying the x location from which the particles were released, X0. This output, shown in Figure 6.2, is a result of the calculations performed in subroutine RELEAS.

The next output consists of the identification of some of the geometry characteristics. All of the values are dimensional with standard units in the MKS system. Recall that the geometry coordinates have been adjusted to avoid the discretization errors in the flow field calculation (Appendix C). The values of the leading edge, trailing edge, and thickness are determined from these modified values and not from the original input coordinates. This computational correction is removed before the collection efficiency calculation and the calculation of the new ice surface.

The particle trajectory data begin after the geometry characteristics are printed. The first output is a statement identifying how the particles were released. If the particles are released in equilibrium with the air (LEQM = 1), the following message will be printed:

The particles are released in equilibrium with the air.

If LEQM = 0, no message is printed, and the particle release velocities are specified by the user. In this case, the initial particle velocities are printed in the line of data shown in Figure 6.2.

Note that when LEQM = 1, the initial particle velocities are shown to be 0.0 m/s. This indicates that the user did not specify the input velocity. The initial velocity of each particle is determined by the program and will depend on the particle release location.

The next statement will indicate the percent mass of each particle corresponding to the droplet diameter specified. Following this statement, the results of the integration of the particle trajectory equations are printed. This output indicates whether a particle released from a point X0, Y0 impinges on the body. The column headings used in this section of the output are defined as follows:

XO   = x-location of particle release

YO   = y-location of particle release

XP   = x-location where particle either impinged
        upon the body or moved out of range

YP   = y-location where the particle either impinged
        upon the body or moved out of range

S   = surface distance from the stagnation point
        to the particle impingement point (lower surface
        is negative)

DT   = size of the integration timestep when the particle
        either hit the body or moved out of range

NSTP = number of integration timesteps required for the
        particle to either impinge upon the body or move out
        of range

As discussed in Section 4.2.6, particle trajectories are first calculated to determine the impingement limits in subroutine IMPLIM. The release points for the upper and lower surface tangent trajectories are defined as the particle release positions. A particle released between these points will strike the body, and one released outside of these points will miss the body. When the impingement limits are found, they will be printed as shown in Figure 6.2. The remaining particle trajectory calculations, for particles released between the upper and lower surface tangent trajectory release points, are made in COLLEC. All of these particles should strike the body, and are used to determine the local collection efficiency. When a droplet distribution has been specified, the output shown in Figure 6.2 will be repeated for each droplet size before continuing with the collection efficiency calculation.

After completing the calculation of the impingement limits for each droplet size, the program enters subroutine EFFICY, where the local col-

lection efficiency is calculated. The output consists of the calculated y_o vs. s points that form the curve that is differentiated to determine the local collection efficiency, as shown in Figure 6.3a. This is followed by the surface distance and calculated local collection efficiency for each body segment. An example of this output is shown in Figure 6.4b. If a droplet distribution has been specified, the output shown in Figure 6.3a and b is printed for each droplet size.

When a droplet distribution has been specified, the local collection efficiencies for each droplet size in the distribution must be combined to form a cumulative local collection efficiency distribution. The local collection efficiency for each body segment corresponding to a specific droplet size is weighted using the fraction of the total mass specified on input. This weighting procedure is described in Section 4.2.5.1. These cumulative values are used in the thermodynamic and ice accretion portions of the code.

6.1.3   Printed Output from the Ice Accretion Code

The first page of output from the thermodynamic and ice accretion portions is shown in Figure 6.4a. This output contains the run identification specified by the user on input, and the current icing time in seconds. The free stream icing conditions are then printed, followed by general information concerning the thermodynamic and ice accretion calculations. This information contains the body segment numbers corresponding to the stagnation point, the upper and lower surface boundary layer transition points (transition from laminar to turbulent flow), and the upper and lower surface icing limits. The total number of points used in the calculation of this timestep is given, followed by the number of segments added to the geometry generated by the previous timestep.

Following this page are three pages containing the detailed output of the most significant aerodynamic, thermodynamic, and ice accretion parameters. All of these parameters are functions of the surface distance, s, and are shown in Figure 6.4b. The column headings in the computer output are defined as follows:

Page 1

I	- Body segment number
X	- x-coordinate of the iced surface corresponding

to segment I (m)

Y   - y-coordinate of the iced surface corresponding to segment I (m)

S   - Surface distance, s, to the midpoint of segment I (m)

VE   - Velocity at the outer edge of the boundary layer, V_e, (m/s)

TE   - Static temperature at the outer edge of the boundary layer, T_e, (K)

PE   - Static pressure at the outer edge of the boundary layer, P_e, (Pa)

RA   - Density of the air at the outer edge of the boundary layer, ρ_a, (kg/m^3)

SEGLENGTH   - Length of the body segment, s, (m)

Page 2

HTC   - Convective heat transfer coefficient, h_c, $(W/m^2/K)$

XK   - Equivalent sand-grain roughness height, k_s, (m)

BETA   - Local collection efficiency, β

FFRAC   - Freezing fraction, f

RI   - Density of the ice, ρ_i, (kg/m^3)

TSURF   - Equilibrium surface temperature, T_{sur}, (K)

DICE   - Thickness of the ice accreted in the current timestep, d_i, (m)

Page 3

QCOND   - Conductive heat flux from the body surface, q_c, (W/m^2)

MDOTC   - Mass flux of liquid impinging in segment I, $\dot{m}_c$ (kg/s)

MDOTRI   - Mass flux of liquid water running along the surface into the control volume, $\dot{m}_{rin}$, of segment I

MDOTE   - Mass flux of water vapor evaporating from

the control volume, $\dot{m}_e$, of segment I (kg/s)

MDOTTI — Total mass flux of water entering control volume, $\dot{m}_{T_{in}}$, of segment I (kg/s)

MDOTT — Total mass flux of water in to control volume $\dot{m}_T$, of segment I (kg/s)

This concludes the description of the printed output from LEWICE. All of the output described above is repeated for each time step.

6.2 Graphical Output

While the printed output is useful to verify whether the code is performing as expected, much of the output from LEWICE is displayed graphically to aid in the evaluation of the results.

The plotting commands used in LEWICE are unique to NASA Lewis Research Center and, therefore, are not likely to be directly applicable to another facility. GRAPH2D/GRAPH3D commands are used.

All plots discussed in this section have the same border, which contains title and icing condition information.

6.2.1 Droplet Trajectory Plots

As discussed in Section 5.3.1, when plot option 2 or 3 is selected, the particle trajectories will be plotted. An example of five such plots are shown in Figure 6.5. The axes limits (in meters) are determined by the program so that the entire body geometry is plotted. When a particle impinges upon the body, the y-coordinate of the release point, y_0, and the surface impingement distance, s, are displayed on the plot. If the particle misses the body, this information is omitted.

The plotting commands are located in subroutine PLTRAJ, which is called from subroutine INTIG after the calculation of the trajectory is completed. Each trajectory is plotted immediately after it is calculated and, once the calculation of a new trajectory is begun, the previous trajectory coordinates are erased.

6.2.2 Ice Accretion Data

Much of the ice accretion data (Section 6.1.3) can also be plotted to assist the user in interpreting the results. If plot option 1 or 2 has been selected, the program will enter the plotting routine (subroutine PLOTD) after completing the ice accretion calculations. The following plot menu will be displayed upon entering the plot routine:

```
        AVAILABLE PLOT OPTIONS
        0  -   NO PLOTS
        1  -   ICED GEOMETRY
        2  -   Z VS S
        3  -   BETA VS S
        4  -   VE VS S
        5  -   TE VS S
        6  -   PE VS S
        7  -   TSURF VS S
        8  -   HTC VS S
        9  -   XK VS S
        10 -   ICE DENSITY VS S
        11 -   FFRAC VS S
    ENTER OPTION NUMBER (I2)
```

The user then inputs the two-digit identifier for the desired plot.

When plot 01 is selected the iced geometry, with all preceding timesteps, will be plotted. Before plotting the geometry, the user will be asked to specify the percent of the geometry to be plotted with the following prompt:

ENTER PERCENT OF GEOMETRY TO BE PLOTTED (F10.0)

Since the size of the plot is fixed, the larger the portion of the airfoil to be plotted, the smaller the geometry will appear on the plot. For example, Figures 6.6a, b, and c show geometries plotted with the specified percent equal to 100., 50., and 25., respectively. After the geometry is plotted, the program will return to the plot menu.

Plots 02 to 11 are all parameters that are functions of the surface distance, s. The format for all of these plots is similar and is described below.

69

After selecting the desired plot, the minimum and maximum values on the ordinate and abcissa will be displayed. After each maximum and minimum is displayed, the user will be asked to specify the desired axis limit. After the desired limits are input, the program will ask if experimental data is to be plotted, i.e.,

ENTER 1 IF EXPERIMENTAL DATA IS TO BE PLOTTED IF NOT, ENTER O

If experimental data are to be plotted, the program will first ask for the number of data points, and then ask the user to manually input the data. After the last experimental data point is input, the plot will be displayed, and the experimental data will be represented as circles.

After viewing the plot, the user will be given the chance to change the axes limits with the following prompt:

IF YOU WOULD LIKE A DIFFERENT SCALE, ENTER 1. IF NOT, ENTER O.

If this is desired, the maximum and minimum ordinate and abcissa values will be displayed again, and the above procedure is repeated. If new axes limits are not desired, the plot menu will be returned to the screen.

As previously stated, plots 02 to 11 all use the operating format described above with the occasional exception of plot 02, y_o vs. s. When a droplet distribution is specified, the y_0 vs. s curve corresponding to each droplet size will be plotted. The correct droplet size for each plot will be printed in the parameter box in the upper left-hand corner of the plot. The user will be asked to input the maximum and minimum axes limits for the plot of each droplet size.

Examples of each of the parameter plots (02-11) are shown in Figures 6.7a-k.

UNTRANSFORMED COORDINATE DATA FOR BODY ID = 1,   NACA 0012 : EXAMPLE 1

I	X(I)	Y(I)	I	X(I)	Y(I)	I	X(I)	Y(I)
1	1.0000000	0.0000000	51	0.0150000	-0.0207970	101	0.1000000	0.0470040
2	0.9899999	-0.0018740	52	0.0100000	-0.0172480	102	0.1250000	0.0507320
3	0.9800000	-0.0036110	53	0.0075000	-0.0150780	103	0.1500000	0.0536360
4	0.9700000	-0.0052390	54	0.0050000	-0.0123860	104	0.1750000	0.0558790
5	0.9500000	-0.0082510	55	0.0037500	-0.0106990	105	0.2000000	0.0575700
6	0.9250000	-0.0117000	56	0.0025000	-0.0086200	106	0.2250000	0.0587940
7	0.9000000	-0.0149080	57	0.0022500	-0.0081360	107	0.2500000	0.0596120
8	0.8750000	-0.0179530	58	0.0020000	-0.0076230	108	0.2750000	0.0600760
9	0.8500000	-0.0208880	59	0.0017500	-0.0070750	109	0.3000000	0.0602260
10	0.8250000	-0.0237390	60	0.0015000	-0.0064850	110	0.3250000	0.0600940
11	0.8000000	-0.0265150	61	0.0012500	-0.0058470	111	0.3500000	0.0597070
12	0.7750000	-0.0292210	62	0.0010000	-0.0051460	112	0.3750000	0.0590900
13	0.7500000	-0.0318550	63	0.0008750	-0.0047660	113	0.4000000	0.0582620
14	0.7250000	-0.0344110	64	0.0007500	-0.0043630	114	0.4250000	0.0572430
15	0.7000000	-0.0368870	65	0.0006250	-0.0039310	115	0.4500000	0.0560510
16	0.6750000	-0.0392810	66	0.0005000	-0.0034620	116	0.4750000	0.0546980
17	0.6500000	-0.0415850	67	0.0003750	-0.0029450	117	0.5000000	0.0531980
18	0.6250000	-0.0437950	68	0.0002500	-0.0023560	118	0.5250000	0.0515600
19	0.6000000	-0.0459040	69	0.0001250	-0.0016320	119	0.5500000	0.0497930
20	0.5750000	-0.0479060	70	0.0000000	0.0000000	120	0.5750000	0.0479060
21	0.5500000	-0.0497930	71	0.0001250	0.0016320	121	0.6000000	0.0459040
22	0.5250000	-0.0515600	72	0.0002500	0.0023560	122	0.6250000	0.0437950
23	0.5000000	-0.0531980	73	0.0003750	0.0029450	123	0.6500000	0.0415850
24	0.4750000	-0.0546980	74	0.0005000	0.0034620	124	0.6750000	0.0392810
25	0.4500000	-0.0560510	75	0.0006250	0.0039310	125	0.7000000	0.0368870
26	0.4250000	-0.0572430	76	0.0007500	0.0043630	126	0.7250000	0.0344110
27	0.4000000	-0.0582620	77	0.0008750	0.0047660	127	0.7500000	0.0318550
28	0.3750000	-0.0590900	78	0.0010000	0.0051460	128	0.7750000	0.0292210
29	0.3500000	-0.0597070	79	0.0012500	0.0058470	129	0.8000000	0.0265150
30	0.3250000	-0.0600940	80	0.0015000	0.0064850	130	0.8250000	0.0237390
31	0.3000000	-0.0602260	81	0.0017500	0.0070750	131	0.8500000	0.0208880
32	0.2750000	-0.0600760	82	0.0020000	0.0076230	132	0.8750000	0.0179530
33	0.2500000	-0.0596120	83	0.0022500	0.0081360	133	0.9000000	0.0149080
34	0.2250000	-0.0587940	84	0.0025000	0.0086200	134	0.9250000	0.0117000
35	0.2000000	-0.0575700	85	0.0037500	0.0106990	135	0.9500000	0.0082510
36	0.1750000	-0.0558790	86	0.0050000	0.0123860	136	0.9700000	0.0052390
37	0.1500000	-0.0536360	87	0.0075000	0.0150780	137	0.9800000	0.0036110
38	0.1250000	-0.0507320	88	0.0100000	0.0172480	138	0.9899999	0.0018740
39	0.1000000	-0.0470040	89	0.0150000	0.0207970	139	1.0000000	0.0000000
40	0.0900000	-0.0452280	90	0.0200000	0.0237260			
41	0.0800000	-0.0432520	91	0.0250000	0.0262300			
42	0.0700000	-0.0410380	92	0.0300000	0.0284620			
43	0.0600000	-0.0385350	93	0.0350000	0.0304960			
44	0.0500000	-0.0356740	94	0.0400000	0.0323620			
45	0.0450000	-0.0340820	95	0.0450000	0.0340820			
46	0.0400000	-0.0323620	96	0.0500000	0.0356740			
47	0.0350000	-0.0304960	97	0.0600000	0.0385350			
48	0.0300000	-0.0284620	98	0.0700000	0.0410380			
49	0.0250000	-0.0262300	99	0.0800000	0.0432520			
50	0.0200000	-0.0237260	100	0.0900000	0.0452280			

a. Geomentry coordinates input.

DOUGLAS AIRCRAFT COMPANY TWO-DIMENSIONAL POTENTIAL FLOW PROGRAM

COMBINED FLOW   NACA 0012 : EXAMPLE 1

ALPHA =   0.000000   ALPHA O =   -0.000010   NO. OF BODIES   1

CL = -0.000001   CHORD = 1.000000   TOTAL ELEMENTS 138

BODY ID = 1   NACA 0012 : EXAMPLE 1   NO. OF ELEMENTS 138

I	X	Y	S	VT	CP	J	SIGMA	VN
1	0.9950030	-0.0009536	0.0024939	-0.8268576	0.3163066	1	-0.013142	0.000003
2	0.9850022	-0.0027573	0.0074755	-0.8886778	0.2102517	2	-0.013130	0.000004
3	0.9750018	-0.0044365	0.0124468	-0.9189486	0.1555335	3	-0.012671	0.000004
4	0.9600045	-0.0067780	0.0198878	-0.9451062	0.1067743	4	-0.012001	0.000004
5	0.9375044	-0.0100112	0.0310313	-0.9680851	0.0628113	5	-0.011208	0.000004
6	0.9125030	-0.0133284	0.0433954	-0.9839670	0.0318090	6	-0.010560	0.000003
7	0.8875018	-0.0164470	0.0557466	-0.9951780	0.0096207	7	-0.010141	0.000003
8	0.8625011	-0.0194323	0.0680897	-1.0043850	-0.0087891	8	-0.009908	0.000002
9	0.8375007	-0.0223233	0.0804271	-1.0128355	-0.0258350	9	-0.009761	0.000001
10	0.8125005	-0.0251359	0.0927601	-1.0208483	-0.0421305	10	-0.009632	0.000001
11	0.7875008	-0.0278768	0.1050892	-1.0285645	-0.0579443	11	-0.009518	0.000001
12	0.7625008	-0.0305473	0.1174146	-1.0361175	-0.0735426	12	-0.009385	0.000001
13	0.7375007	-0.0331427	0.1297361	-1.0434093	-0.0887022	13	-0.009215	0.000001
14	0.7125006	-0.0356590	0.1420537	-1.0504131	-0.1033669	14	-0.009038	0.000001
15	0.6875005	-0.0380946	0.1543674	-1.0573263	-0.1179380	15	-0.008855	0.000001
16	0.6625009	-0.0404444	0.1666770	-1.0641356	-0.1323843	16	-0.008629	0.000001
17	0.6375008	-0.0427021	0.1789825	-1.0707989	-0.1466093	17	-0.008389	0.000001
18	0.6125008	-0.0448624	0.1912838	-1.0773840	-0.1607561	18	-0.008116	0.000001
19	0.5875007	-0.0469188	0.2035809	-1.0838785	-0.1747923	19	-0.007818	0.000001
20	0.5625006	-0.0488641	0.2158735	-1.0902719	-0.1886921	20	-0.007483	0.000001
21	0.5375010	-0.0506920	0.2281619	-1.0966110	-0.2025557	21	-0.007134	0.000001
22	0.5125009	-0.0523956	0.2404459	-1.1029654	-0.2165318	22	-0.006745	0.000001
23	0.4875010	-0.0539657	0.2527257	-1.1092901	-0.2305241	23	-0.006321	0.000000
24	0.4625010	-0.0553936	0.2650014	-1.1156693	-0.2447176	24	-0.005863	0.000000
25	0.4375009	-0.0566678	0.2772729	-1.1220798	-0.2590628	25	-0.005340	0.000000
26	0.4125009	-0.0577752	0.2895406	-1.1285248	-0.2735682	26	-0.004772	0.000000
27	0.3875008	-0.0587010	0.3018047	-1.1350374	-0.2883091	27	-0.004120	0.000000
28	0.3625006	-0.0594260	0.3140656	-1.1414566	-0.3029222	28	-0.003377	0.000000

b. Surface flow characteristics

Figure 6.1: Printed output for the potential flow calculations in Example

I	X	Y	S	VT	CP	J	SIGMA	VN
29	0.3375004	-0.0599308	0.3263239	-1.1477957	-0.3174343	29	-0.002558	0.000000
30	0.3125001	-0.0601935	0.3385804	-1.1540527	-0.3318377	30	-0.001628	0.000000
31	0.2874997	-0.0601882	0.3508363	-1.1601448	-0.3459358	31	-0.000585	0.000000
32	0.2624992	-0.0598856	0.3630932	-1.1660824	-0.3597479	32	0.000589	0.000000
33	0.2374984	-0.0592503	0.3753533	-1.1718359	-0.3731985	33	0.001731	0.000000
34	0.2124973	-0.0582363	0.3876197	-1.1771927	-0.3857822	34	0.003497	0.000000
35	0.1874956	-0.0567876	0.3998969	-1.1819983	-0.3971195	35	0.005304	-0.000002
36	0.1624932	-0.0548323	0.4121914	-1.1859293	-0.4064274	36	0.007457	-0.000002
37	0.1374894	-0.0522749	0.4245132	-1.1885757	-0.4127121	37	0.010015	-0.000004
38	0.1124832	-0.0489800	0.4368784	-1.1891918	-0.4141769	38	0.013170	-0.000003
39	0.0949960	-0.0461379	0.4455638	-1.1883059	-0.4120703	39	0.015802	-0.000003
40	0.0849948	-0.0442662	0.4505519	-1.1872902	-0.4096575	40	0.017660	-0.000002
41	0.0749931	-0.0421762	0.4555610	-1.1851130	-0.4044924	41	0.019888	-0.000002
42	0.0649905	-0.0398243	0.4605983	-1.1808882	-0.3944960	42	0.022593	-0.000002
43	0.0549870	-0.0371499	0.4656748	-1.1729183	-0.3757372	43	0.025912	-0.000002
44	0.0474957	-0.0348913	0.4695106	-1.1636887	-0.3541708	44	0.028774	-0.000001
45	0.0424947	-0.0332373	0.4720928	-1.1553183	-0.3347597	45	0.030983	-0.000001
46	0.0374936	-0.0314462	0.4746970	-1.1443930	-0.3096352	46	0.033388	-0.000001
47	0.0324920	-0.0294985	0.4773243	-1.1306782	-0.2784328	47	0.035952	-0.000000
48	0.0274892	-0.0273701	0.4799935	-1.1155024	-0.2443447	48	0.038617	-0.000001
49	0.0224832	-0.0250116	0.4827065	-1.0984278	-0.2065430	49	0.042161	-0.000000
50	0.0174724	-0.0223086	0.4854543	-1.0677700	-0.1401320	50	0.047986	-0.000000
51	0.0124526	-0.0190892	0.4884222	-1.0151653	-0.0305605	51	0.055116	0.000000
52	0.0087273	-0.0161891	0.4907374	-0.9530601	0.0916765	52	0.062405	0.000001
53	0.0062075	-0.0137715	0.4924501	-0.8769044	0.2310386	53	0.070770	0.000001
54	0.0043571	-0.0115558	0.4938659	-0.7800953	0.3914513	54	0.079197	0.000001
55	0.0030979	-0.0096758	0.4949795	-0.6789735	0.5389950	55	0.086045	0.000002
56	0.0023736	-0.0083787	0.4957039	-0.6001744	0.6397908	56	0.090240	0.000002
57	0.0021234	-0.0078803	0.4959772	-0.5699795	0.6751234	57	0.091479	0.000002
58	0.0018732	-0.0073498	0.4962647	-0.5368442	0.7117984	58	0.092791	0.000002
59	0.0016230	-0.0067808	0.4965694	-0.4998890	0.7501110	59	0.094172	0.000002
60	0.0013727	-0.0061669	0.4968944	-0.4601299	0.7882805	60	0.095317	0.000002
61	0.0011222	-0.0054975	0.4972447	-0.4157784	0.8271284	61	0.096394	0.000002
62	0.0009367	-0.0049563	0.4975251	-0.3790950	0.8562871	62	0.097154	0.000002
63	0.0008116	-0.0045648	0.4977266	-0.3526587	0.8756319	63	0.097512	0.000002
64	0.0006864	-0.0041473	0.4979402	-0.3240126	0.8950159	64	0.097782	0.000002
65	0.0005612	-0.0036968	0.4981694	-0.2925072	0.9144396	65	0.098000	0.000002
66	0.0004359	-0.0032039	0.4984187	-0.2576460	0.9336185	66	0.098023	0.000003
67	0.0003101	-0.0026510	0.4986966	-0.2174368	0.9527213	67	0.097767	-0.000003
68	0.0001830	-0.0019948	0.4990243	-0.1691881	0.9713754	68	0.097009	-0.000009
69	0.0000337	-0.0008182	0.4996058	-0.0722346	0.9947822	69	0.096000	-0.000026
70	0.0000337	0.0008182	0.5004088	0.0722347	0.9947821	70	0.096000	-0.000027
71	0.0001830	0.0019948	0.5009904	0.1691873	0.9713757	71	0.097008	-0.000013
72	0.0003101	0.0026510	0.5013180	0.2174352	0.9527220	72	0.097767	-0.000003
73	0.0004359	0.0032039	0.5015960	0.2576444	0.9336194	73	0.098023	0.000001
74	0.0005612	0.0036968	0.5018453	0.2925053	0.9144407	74	0.098000	0.000002
75	0.0006864	0.0041473	0.5020745	0.3240107	0.8950171	75	0.097782	0.000002
76	0.0008116	0.0045648	0.5022881	0.3526556	0.8756340	76	0.097512	0.000001
77	0.0009367	0.0049563	0.5024896	0.3790935	0.8562882	77	0.097154	0.000001
78	0.0011222	0.0054975	0.5027700	0.4157771	0.8271290	78	0.096394	0.000002
79	0.0013727	0.0061669	0.5031203	0.4601290	0.7882814	79	0.095317	0.000001
80	0.0016230	0.0067808	0.5034453	0.4998873	0.7501127	80	0.094172	0.000001
81	0.0018732	0.0073498	0.5037500	0.5368432	0.7117994	81	0.092791	0.000002
82	0.0021234	0.0078803	0.5040374	0.5699789	0.6751241	82	0.091479	0.000001
83	0.0023736	0.0083787	0.5043108	0.6001900	0.6399925	83	0.090240	0.000001
84	0.0030979	0.0096758	0.5050392	0.6789733	0.5389953	84	0.086045	0.000002
85	0.0043571	0.0115558	0.5061488	0.7800953	0.3914514	85	0.079197	0.000001
86	0.0062075	0.0137715	0.5075645	0.8769052	0.2310373	86	0.070770	0.000000
87	0.0087273	0.0161891	0.5092772	0.9530600	0.0916766	87	0.062404	-0.000000
88	0.0124526	0.0190892	0.5115924	1.0151653	-0.0305605	88	0.055116	-0.000001
89	0.0174724	0.0223086	0.5145167	1.0677710	-0.1401348	89	0.047986	-0.000002
90	0.0224832	0.0250116	0.5173082	1.0984278	-0.2065430	90	0.042161	-0.000002
91	0.0274892	0.0273701	0.5200211	1.1155024	-0.2443447	91	0.038617	-0.000003
92	0.0324920	0.0294985	0.5226864	1.1306782	-0.2784328	92	0.035951	-0.000003
93	0.0374936	0.0314462	0.5253177	1.1443920	-0.3096323	93	0.033388	-0.000003
94	0.0424947	0.0332373	0.5279219	1.1553183	-0.3347597	94	0.030982	-0.000003
95	0.0474957	0.0348913	0.5305041	1.1636887	-0.3541708	95	0.028774	-0.000003
96	0.0549870	0.0371499	0.5343399	1.1729183	-0.3757372	96	0.025912	-0.000003
97	0.0649905	0.0398243	0.5394163	1.1808882	-0.3944960	97	0.022593	-0.000003
98	0.0749931	0.0421762	0.5444537	1.1851130	-0.4044924	98	0.019888	-0.000004
99	0.0849948	0.0442662	0.5494628	1.1872892	-0.4096556	99	0.017660	-0.000003
100	0.0949960	0.0461379	0.5544509	1.1883039	-0.4120655	100	0.015802	-0.000004
101	0.1124832	0.0489800	0.5631363	1.1891899	-0.4141722	101	0.013169	-0.000003
102	0.1374894	0.0522749	0.5755014	1.1885748	-0.4127092	102	0.010015	-0.000002
103	0.1624932	0.0548323	0.5878233	1.1859283	-0.4064255	103	0.007457	-0.000002
104	0.1874956	0.0567876	0.6001178	1.1819983	-0.3971195	104	0.005304	-0.000002
105	0.2124973	0.0582363	0.6123950	1.1771927	-0.3857822	105	0.003497	0.000000
106	0.2374984	0.0592503	0.6246614	1.1718359	-0.3731985	106	0.001931	0.000000
107	0.2624992	0.0598856	0.6369215	1.1660814	-0.3597450	107	0.000589	0.000000
108	0.2874997	0.0601882	0.6491783	1.1601439	-0.3459330	108	-0.000585	0.000000
109	0.3125001	0.0601935	0.6614342	1.1540527	-0.3318377	109	-0.001628	0.000000
110	0.3375004	0.0599308	0.6736907	1.1477957	-0.3174343	110	-0.002558	0.000000
111	0.3625006	0.0594260	0.6859490	1.1414566	-0.3029222	111	-0.003377	0.000000
112	0.3875008	0.0587010	0.6982099	1.1350374	-0.2883091	112	-0.004120	0.000000
113	0.4125009	0.0577752	0.7104740	1.1285248	-0.2735682	113	-0.004772	0.000000
114	0.4375009	0.0566678	0.7227417	1.1220808	-0.2590647	114	-0.005340	0.000000
115	0.4625010	0.0553936	0.7350133	1.1156693	-0.2447176	115	-0.005863	0.000000
116	0.4875010	0.0539657	0.7472889	1.1092901	-0.2305241	116	-0.006321	0.000000
117	0.5125009	0.0523956	0.7595688	1.1029654	-0.2165318	117	-0.006746	0.000001
118	0.5375010	0.0506920	0.7718528	1.0966110	-0.2025557	118	-0.007134	0.000001
119	0.5625006	0.0488641	0.7841411	1.0902719	-0.1886921	119	-0.007483	0.000001
120	0.5875007	0.0469188	0.7964338	1.0838785	-0.1747923	120	-0.007818	0.000001
121	0.6125008	0.0448624	0.8087308	1.0773830	-0.1607542	121	-0.008116	0.000001
122	0.6375008	0.0427021	0.8210322	1.0707949	-0.1466093	122	-0.008389	0.000001
123	0.6625009	0.0404444	0.8333377	1.0641356	-0.1323843	123	-0.008629	0.000001
124	0.6875005	0.0380946	0.8456473	1.0573254	-0.1179361	124	-0.008855	0.000001
125	0.7125006	0.0356590	0.8579609	1.0504131	-0.1033669	125	-0.009038	0.000001
126	0.7375007	0.0331427	0.8702785	1.0434093	-0.0887022	126	-0.009215	0.000001
127	0.7625008	0.0305473	0.8826001	1.0361190	-0.0735426	127	-0.009385	0.000001
128	0.7875008	0.0278768	0.8949254	1.0285645	-0.0579443	128	-0.009518	0.000001
129	0.8125005	0.0251359	0.9072545	1.0208483	-0.0421305	129	-0.009632	0.000001
130	0.8375007	0.0223233	0.9195876	1.0128345	-0.0258331	130	-0.009761	0.000001
131	0.8625011	0.0194323	0.9319250	1.0043850	-0.0087891	131	-0.009908	0.000001
132	0.8875018	0.0164470	0.9442680	0.9951776	0.0096216	132	-0.010141	0.000001
133	0.9125030	0.0133284	0.9566193	0.9839664	0.0318101	133	-0.010560	0.000001

Surface flow characteristics (continued)

Figure 6.1: continued

I	X	Y	S	VT	CP	J	SIGMA	VN
134	0.9375044	0.0100112	0.9689832	0.9680846	0.0628123	134	-0.011208	0.000004
135	0.9500045	0.0067780	0.9801267	0.9451060	0.1067747	135	-0.012001	0.000004
136	0.9750018	0.0044365	0.9875676	0.9189485	0.1555337	136	-0.012671	0.000004
137	0.9850022	0.0027573	0.9925388	0.8886768	0.2102537	137	-0.013130	0.000005
138	0.9950030	0.0009536	0.9975204	0.8268565	0.3163084	138	-0.013142	0.000004

INTEGRATED VALUES

CY = 0.00000   CX = 0.00010

CL = 0.00000   CD = 0.00010   CM = 0.00000

PARABOLIC INTEGRATION

INTEGRATED VALUES

CY = 0.00000   CX = 0.00014

CL = 0.00000   CD = 0.00014   CM = -0.00000

TOTAL CM = 0.00000

TOTAL CM = -0.00000   (PARABOLIC)

Surface flow characteristics (continued)

Figure 6.1: Concluded

THE PARTICLES ARE RELEASED FROM X = -1.26000E 00
WHICH IS OBTAINED AT THE   1 LOOP OF   50 LOOPS

GEOMETRY CHARACTERISTICS:

```
        LEADING EDGE (X,Y)      -2.0000E-03      0.0000
        TRAILING EDGE (X,Y)    j 3.0200E-01      0.0000
        THICKNESS               4.0136E-02
        CHORD                   3.0000E-01
        ANGLE OF ATTACK         0.0000

        UPPER BOUNDARY          2.2075E-02
        LOWER BOUNDARY         -2.2075E-02
```

PARTICLE TRAJECTORY DATA:

THE PARTICLES ARE RELEASED IN EQUILIBRIUM WITH THE AIR

PARTICLE DIAMETER (MICRONS)	INITIAL VX (M/S)	INITIAL VY (M/S)	PARTICLE AOA (DEGREES)	PITCH ANGLE (DEGREES)	PIT DOT (DEG/SEC)	GRAVT CONST (M/S**2)	ERROR CRITERIA
20.00	0.00	0.00	0.00	0.00	0.00	0.00	5.00E-05

THE PARTICLES OF SIZE 20.00CONTAIN 1.0000 OF THE TOTAL MASS

X0	Y0		XP	YP	S	DT	NSTP
-1.2599993	0.0150000	OUT OF RANGE	0.0471370	0.0224023		3.6440E-05	58
-1.2599993	-0.0150000	OUT OF RANGE	0.0473017	-0.0224352		3.5853E-05	67

YOMAX= 1.5000E-02   YOMIN= -1.5000E-02

X0	Y0		XP	YP	S	DT	NSTP
-1.2599993	0.0000000	HIT BODY AT	-0.0019999	0.0000010	0.0000011	5.9902E-06	46
-1.2599993	0.0075000	HIT BODY AT	0.0123249	0.0100423	0.0197897	1.1801E-05	67
-1.2599993	0.0112500	OUT OF RANGE	0.0732779	0.0228669		4.9098E-05	74
-1.2599993	0.0093750	OUT OF RANGE	0.0846801	0.0229987		6.0772E-05	83
-1.2599993	0.0084375	HIT BODY AT	0.0227204	0.0127862	0.0305664	1.7692E-05	65
-1.2599993	0.0089062	OUT OF RANGE	0.0793477	0.0221173		5.7872E-05	84
-1.2599993	0.0086719	OUT OF RANGE	0.0863379	0.0227919		5.5584E-05	83
-1.2599993	0.0085547	OUT OF RANGE	0.0862296	0.0227190		5.9460E-05	99
-1.2599993	0.0084961	HIT BODY AT	0.0258700	0.0134200	0.0337822	2.4208E-05	69
-1.2599993	-0.0032520	HIT BODY AT	0.0000620	-0.0037906	-0.0055256	5.8164E-06	59
-1.2599993	-0.0091260	OUT OF RANGE	0.0826181	-0.0226274		5.8351E-05	83
-1.2599993	-0.0061890	HIT BODY AT	0.0063645	-0.0077377	-0.0133298	9.1509E-06	61
-1.2599993	-0.0076575	HIT BODY AT	0.0133570	-0.0103734	-0.0208795	1.1755E-05	65
-1.2599993	-0.0083917	HIT BODY AT	0.0216431	-0.0125515	-0.0294638	1.9979E-05	69
-1.2599993	-0.0087588	OUT OF RANGE	0.0826917	-0.0224242		4.8719E-05	87
-1.2599993	-0.0085753	OUT OF RANGE	0.0873171	-0.0228487		7.0857E-05	86
-1.2599993	-0.0084835	HIT BODY AT	0.0237963	-0.0130158	-0.0316695	1.7371E-05	74

UPPER SURFACE LIMIT		LOWER SURFACE LIMIT	
YOU	SU	YOL	SL
0.8496E-02	0.3378E-01	-0.8483E-02	-0.3167E-01

-1.2599993	0.0076471	HIT BODY AT	0.0132636	0.0103448	0.0207819	1.1751E-05	69

Figure 6.2: Printed output for the individual particle trajectory calculations in Example 1.

X0	Y0		XP	YP	S	DT	NSTP
-1.2599993	0.0065556	HIT BODY AT	0.0077701	0.0083489	0.0148929	8.6830E-06	52
-1.2599993	0.0054640	HIT BODY AT	0.0042313	0.0066797	0.0109037	7.9091E-06	56
-1.2599993	0.0043725	HIT BODY AT	0.0018271	0.0052005	0.0080055	6.0560E-06	52
-1.2599993	0.0032809	HIT BODY AT	0.0000979	0.0038238	0.0055745	6.1364E-06	53
-1.2599993	0.0021894	HIT BODY AT	-0.0010394	0.0025188	0.0035691	5.9198E-06	50
-1.2599993	0.0010978	HIT BODY AT	-0.0017108	0.0012562	0.0017999	6.9843E-06	44
-1.2599993	0.0000063	HIT BODY AT	-0.0019994	0.0000057	0.0000057	5.9947E-06	46
-1.2599993	-0.0010852	HIT BODY AT	-0.0017167	-0.0012406	-0.0017832	7.1043E-06	47
-1.2599993	-0.0021768	HIT BODY AT	-0.0010524	-0.0025049	-0.0035500	6.1744E-06	43
-1.2599993	-0.0032683	HIT BODY AT	0.0000774	-0.0038049	-0.0055467	6.4569E-06	46
-1.2599993	-0.0043599	HIT BODY AT	0.0017959	-0.0051801	-0.0079682	7.3536E-06	49
-1.2599993	-0.0054514	HIT BODY AT	0.0041859	-0.0066553	-0.0108521	9.0981E-06	61
-1.2599993	-0.0065430	HIT BODY AT	0.0077176	-0.0083265	-0.0148358	8.6736E-06	52
-1.2599993	-0.0076345	HIT BODY AT	0.0132047	-0.0103267	-0.0207203	1.7346E-05	57

Figure 6.2: Concluded

YO VS S DATA FOR DROPLET DIAMETER= 20.00000 MICRONS
17 POINTS HAVE BEEN CALCULATED

I	S	YO
1	0.033782	0.008496
2	0.020782	0.007647
3	0.014893	0.006556
4	0.010904	0.005464
5	0.008005	0.004372
6	0.005575	0.003281
7	0.003569	0.002189
8	0.001800	0.001098
9	0.000006	0.000006
10	-0.001783	-0.001085
11	-0.003550	-0.002177
12	-0.005547	-0.003268
13	-0.007968	-0.004360
14	-0.010852	-0.005451
15	-0.014836	-0.006543
16	-0.020720	-0.007635
17	-0.031670	-0.008483

ORIGINAL PAGE IS OF POOR QUALITY

a. Calculate y_o vs s points

CALCULATED LOCAL COLLECTION EFFICIENCY FOR DROPLET DIAMETER= 20.00000 MICRONS

SEG	S	BETA	SEG	S	BETA	SEG	S	BETA
1	-0.309069	0.000000	26	-0.132014	0.000000	51	-0.009002	0.387632
2	-0.304890	0.000000	27	-0.124494	0.000000	52	-0.007390	0.440836
3	-0.301823	0.000000	28	-0.116974	0.000000	53	-0.006131	0.483091
4	-0.297245	0.000000	29	-0.109454	0.000000	54	-0.005052	0.522569
5	-0.290405	0.000000	30	-0.101933	0.000000	55	-0.004194	0.557831
6	-0.282821	0.000000	31	-0.094410	0.000000	56	-0.003623	0.581140
7	-0.275249	0.000000	32	-0.086884	0.000000	57	-0.003371	0.581300
8	-0.267686	0.000000	33	-0.079353	0.000000	58	-0.003144	0.585409
9	-0.260129	0.000000	34	-0.071814	0.000000	59	-0.002904	0.589759
10	-0.252576	0.000000	35	-0.064264	0.000000	60	-0.002649	0.594386
11	-0.245025	0.000000	36	-0.056696	0.000000	61	-0.002381	0.599225
12	-0.237477	0.000000	37	-0.049102	0.000000	62	-0.002162	0.603208
13	-0.229931	0.000000	38	-0.041482	0.000000	63	-0.001995	0.606220
14	-0.222386	0.000000	39	-0.036113	0.000000	64	-0.001826	0.609284
15	-0.214844	0.000000	40	-0.033010	0.000000	65	-0.001643	0.613915
16	-0.207304	0.000000	41	-0.029899	0.023592	66	-0.001442	0.613387
17	-0.199766	0.000000	42	-0.026761	0.067630	67	-0.001212	0.612782
18	-0.192231	0.000000	43	-0.023597	0.112024	68	-0.000895	0.611950
19	-0.184697	0.000000	44	-0.021192	0.145775	69	-0.000351	0.610521
20	-0.177165	0.000000	45	-0.019556	0.168733	70	0.000351	0.610452
21	-0.169635	0.000000	46	-0.017911	0.191828	71	0.000895	0.611482
22	-0.162108	0.000000	47	-0.016242	0.215251	72	0.001212	0.612082
23	-0.154582	0.000000	48	-0.014540	0.251020	73	0.001442	0.612518
24	-0.147058	0.000000	49	-0.012786	0.289074	74	0.001643	0.612899
25	-0.139536	0.000000	50	-0.010945	0.328992	75	0.001826	0.608128

b. Local collection efficiency for each body segment.

Figure 6.3: Summary of the particle trajectory and local collection efficiency calculations in Example 1.

74

SEG	S	BETA		SEG	S	BETA
76	0.001995	0.605038		108	0.094410	0.000000
77	0.002162	0.602000		109	0.101933	0.000000
78	0.002381	0.597982		110	0.109454	0.000000
79	0.002649	0.593102		111	0.116974	0.000000
80	0.002904	0.588435		112	0.124494	0.000000
81	0.003144	0.584047		113	0.132014	0.000000
82	0.003371	0.579904		114	0.139536	0.000000
83	0.003628	0.580444		115	0.147058	0.000000
84	0.004194	0.557125		116	0.154582	0.000000
85	0.005052	0.521846		117	0.162108	0.000000
86	0.006131	0.482057		118	0.169635	0.000000
87	0.007390	0.440096		119	0.177165	0.000000
88	0.009002	0.387285		120	0.184697	0.000000
89	0.010945	0.328975		121	0.192231	0.000000
90	0.012786	0.289406		122	0.199766	0.000000
91	0.014540	0.251683		123	0.207304	0.000000
92	0.016242	0.215806		124	0.214844	0.000000
93	0.017911	0.192810		125	0.222386	0.000000
94	0.019556	0.170136		126	0.229931	0.000000
95	0.021192	0.147597		127	0.237477	0.000000
96	0.023597	0.114461		128	0.245025	0.000000
97	0.026761	0.070877		129	0.252576	0.000000
98	0.029899	0.027642		130	0.260129	0.000000
99	0.033010	0.000000		131	0.267686	0.000000
100	0.036113	0.000000		132	0.275249	0.000000
101	0.041482	0.000000		133	0.282821	0.000000
102	0.049102	0.000000		134	0.290405	0.000000
103	0.056696	0.000000		135	0.297245	0.000000
104	0.064264	0.000000		136	0.301823	0.000000
105	0.071814	0.000000		137	0.304890	0.000000
106	0.079353	0.000000		138	0.309069	0.000000
107	0.086884	0.000000				

b. Local collection efficiency for each body segment (continued).

Figure 6.3: Concluded

SEG	S	QCOND	MDOTC	MDOTRI	MDOTE	MDOTTI	MDOTT
1	-0.30721E 00	0.00000	0.00000	0.00000	0.00000	0.00000	0.00000
2	-0.30416E 00	0.00000	0.00000	0.00000	0.00000	0.00000	0.00000
3	-0.30112E 00	0.00000	0.00000	0.00000	0.00000	0.00000	0.00000
4	-0.29656E 00	0.00000	0.00000	0.00000	0.00000	0.00000	0.00000
5	-0.28974E 00	0.00000	0.00000	0.00000	0.00000	0.00000	0.00000
6	-0.28218E 00	0.00000	0.00000	0.00000	0.00000	0.00000	0.00000
7	-0.27462E 00	0.00000	0.00000	0.00000	0.00000	0.00000	0.00000
8	-0.26707E 00	0.00000	0.00000	0.00000	0.00000	0.00000	0.00000
9	-0.25952E 00	0.00000	0.00000	0.00000	0.00000	0.00000	0.00000
10	-0.25197E 00	0.00000	0.00000	0.00000	0.00000	0.00000	0.00000
11	-0.24442E 00	0.00000	0.00000	0.00000	0.00000	0.00000	0.00000
12	-0.23688E 00	0.00000	0.00000	0.00000	0.00000	0.00000	0.00000
13	-0.22934E 00	0.00000	0.00000	0.00000	0.00000	0.00000	0.00000
14	-0.22180E 00	0.00000	0.00000	0.00000	0.00000	0.00000	0.00000
15	-0.21427E 00	0.00000	0.00000	0.00000	0.00000	0.00000	0.00000
16	-0.20673E 00	0.00000	0.00000	0.00000	0.00000	0.00000	0.00000
17	-0.19920E 00	0.00000	0.00000	0.00000	0.00000	0.00000	0.00000
18	-0.19168E 00	0.00000	0.00000	0.00000	0.00000	0.00000	0.00000
19	-0.18415E 00	0.00000	0.00000	0.00000	0.00000	0.00000	0.00000
20	-0.17663E 00	0.00000	0.00000	0.00000	0.00000	0.00000	0.00000
21	-0.16911E 00	0.00000	0.00000	0.00000	0.00000	0.00000	0.00000
22	-0.16159E 00	0.00000	0.00000	0.00000	0.00000	0.00000	0.00000
23	-0.15408E 00	0.00000	0.00000	0.00000	0.00000	0.00000	0.00000
24	-0.14656E 00	0.00000	0.00000	0.00000	0.00000	0.00000	0.00000
25	-0.13905E 00	0.00000	0.00000	0.00000	0.00000	0.00000	0.00000
26	-0.13155E 00	0.00000	0.00000	0.00000	0.00000	0.00000	0.00000
27	-0.12404E 00	0.00000	0.00000	0.00000	0.00000	0.00000	0.00000
28	-0.11654E 00	0.00000	0.00000	0.00000	0.00000	0.00000	0.00000
29	-0.10904E 00	0.00000	0.00000	0.00000	0.00000	0.00000	0.00000
30	-0.10154E 00	0.00000	0.00000	0.00000	0.00000	0.00000	0.00000
31	-0.94037E-01	0.00000	0.00000	0.00000	0.00000	0.00000	0.00000
32	-0.86537E-01	0.00000	0.00000	0.00000	0.00000	0.00000	0.00000
33	-0.79034E-01	0.00000	0.00000	0.00000	0.00000	0.00000	0.00000
34	-0.71528E-01	0.00000	0.00000	0.00000	0.00000	0.00000	0.00000
35	-0.64015E-01	0.00000	0.00000	0.00000	0.00000	0.00000	0.00000
36	-0.56491E-01	0.00000	0.00000	0.00000	0.00000	0.00000	0.00000
37	-0.48951E-01	0.00000	0.00000	0.00000	0.00000	0.00000	0.00000
38	-0.41384E-01	0.00000	0.00000	0.00000	0.00000	0.00000	0.00000
39	-0.36069E-01	0.00000	0.00000	0.00000	0.00000	0.00000	0.00000
40	-0.33017E-01	0.00000	0.00000	0.00000	0.00000	0.00000	0.00000
41	-0.29948E-01	0.00000	0.46756E-05	0.00000	0.93274E-05	0.46756E-05	0.00000
42	-0.26853E-01	0.00000	0.13490E-04	0.00000	0.30625E-05	0.13490E-04	0.10428E-04
43	-0.23729E-01	0.00000	0.22546E-04	0.00000	0.35536E-05	0.22546E-04	0.18993E-04
44	-0.21363E-01	0.00000	0.14801E-04	0.00000	0.19748E-05	0.14801E-04	0.12827E-04
45	-0.19763E-01	0.00000	0.17264E-04	0.00000	0.21182E-05	0.17264E-04	0.15146E-04

a. Icing condition and summary of ice accretion data

Figure 6.4: Printed output from the ice accretion calculations in Example 1.

75

SEG	S	QCOND	MDOTC	MDOTRI	MDOTE	MDOTTI	MDOTT
46	-0.18146E-01	0.00000	0.19810E-04	0.00000	0.22692E-05	0.19810E-04	0.17540E-04
47	-0.16506E-01	0.00000	0.22483E-04	0.00000	0.24326E-05	0.22483E-04	0.20050E-04
48	-0.14833E-01	0.00000	0.26596E-04	0.00000	0.26663E-05	0.26596E-04	0.23930E-04
49	-0.13110E-01	0.00000	0.31279E-04	0.00000	0.29390E-05	0.31279E-04	0.28340E-04
50	-0.11302E-01	0.00000	0.36889E-04	0.00000	0.32710E-05	0.36889E-04	0.33618E-04
51	-0.93693E-02	0.00000	0.45990E-04	0.00000	0.37734E-05	0.45990E-04	0.42217E-04
52	-0.77677E-02	0.00000	0.28238E-04	0.00000	0.21648E-05	0.28238E-04	0.26074E-04
53	-0.64879E-02	0.00000	0.34342E-04	0.00000	0.24859E-05	0.34342E-04	0.31856E-04
54	-0.53333E-02	0.00000	0.21231E-04	0.18432E-05	0.15491E-05	0.23074E-04	0.21525E-04
55	-0.43923E-02	0.00000	0.26185E-04	0.85131E-05	0.20664E-05	0.34698E-04	0.32631E-04
56	-0.37712E-02	0.00000	0.61258E-05	0.93358E-05	0.43172E-06	0.15462E-04	0.15030E-04
57	-0.34932E-02	0.00000	0.64190E-05	0.99246E-05	0.43325E-06	0.16344E-04	0.15910E-04
58	-0.32417E-02	0.00000	0.68230E-05	0.10286E-04	0.44195E-06	0.17109E-04	0.16667E-04
59	-0.29800E-02	0.00000	0.73125E-05	0.10377E-04	0.45292E-06	0.17690E-04	0.17237E-04
60	-0.27048E-02	0.00000	0.78811E-05	0.10151E-04	0.46528E-06	0.18032E-04	0.17567E-04
61	-0.24173E-02	0.00000	0.86295E-05	0.95637E-05	0.48563E-06	0.18193E-04	0.17708E-04
62	-0.21846E-02	0.00000	0.46692E-05	0.91048E-05	0.25283E-06	0.13774E-04	0.13521E-04
63	-0.29137E-02	0.00000	0.49495E-05	0.85090E-05	0.26031E-06	0.13459E-04	0.13198E-04
64	-0.18393E-02	0.00000	0.53020E-05	0.77708E-05	0.27181E-06	0.13073E-04	0.12801E-04
65	-0.16529E-02	0.00000	0.57658E-05	0.68596E-05	0.28796E-06	0.12625E-04	0.12337E-04
66	-0.14501E-02	0.00000	0.63131E-05	0.58027E-05	0.31115E-06	0.12116E-04	0.11805E-04
67	-0.12199E-02	0.00000	0.71395E-05	0.45832E-05	0.35022E-06	0.11723E-04	0.11372E-04
68	-0.91868E-03	0.00000	0.86999E-05	0.31432E-05	0.43012E-06	0.11843E-04	0.11413E-04
69	-0.37066E-03	0.00000	0.19336E-04	0.00000	0.95677E-06	0.19336E-04	0.18379E-04
70	0.37066E-03	0.00000	0.19334E-04	0.00000	0.95677E-06	0.19334E-04	0.18377E-04
71	0.91867E-03	0.00000	0.86932E-05	0.31413E-05	0.43012E-06	0.11835E-04	0.11404E-04
72	0.12199E-02	0.00000	0.71313E-05	0.45755E-05	0.35022E-06	0.11707E-04	0.11357E-04
73	0.14500E-02	0.00000	0.63042E-05	0.57880E-05	0.31115E-06	0.12092E-04	0.11781E-04
74	0.16528E-02	0.00000	0.57563E-05	0.68372E-05	0.28796E-06	0.12593E-04	0.12305E-04
75	0.18392E-02	0.00000	0.52920E-05	0.77401E-05	0.27181E-06	0.13032E-04	0.12760E-04
76	0.20136E-02	0.00000	0.49399E-05	0.84697E-05	0.26031E-06	0.13410E-04	0.13149E-04
77	0.21845E-02	0.00000	0.46598E-05	0.90572E-05	0.25283E-06	0.13717E-04	0.13464E-04
78	0.24171E-02	0.00000	0.86117E-05	0.95080E-05	0.48563E-06	0.18120E-04	0.17634E-04
79	0.27047E-02	0.00000	0.78641E-05	0.10080E-04	0.46528E-06	0.17944E-04	0.17479E-04
80	0.29798E-02	0.00000	0.72961E-05	0.10292E-04	0.45292E-06	0.17588E-04	0.17135E-04
81	0.32415E-02	0.00000	0.68071E-05	0.10186E-04	0.44191E-06	0.16993E-04	0.16551E-04
82	0.34930E-02	0.00000	0.64036E-05	0.98116E-05	0.43325E-06	0.16215E-04	0.15782E-04
83	0.37710E-02	0.00000	0.61185E-05	0.92095E-05	0.43172E-06	0.15328E-04	0.14896E-04
84	0.43922E-02	0.00000	0.26151E-04	0.83804E-05	0.20664E-05	0.34532E-04	0.32465E-04
85	0.53337E-02	0.00000	0.21202E-04	0.16818E-05	0.15393E-05	0.22883E-04	0.21344E-04
86	0.64871E-02	0.00000	0.34268E-04	0.00000	0.24826E-05	0.34268E-04	0.31786E-04
87	0.77652E-02	0.00000	0.28191E-04	0.00000	0.21627E-05	0.28191E-04	0.26028E-04
88	0.93664E-02	0.00000	0.45949E-04	0.00000	0.37718E-05	0.45949E-04	0.42177E-04
89	0.11299E-01	0.00000	0.36887E-04	0.00000	0.32709E-05	0.36887E-04	0.33616E-04
90	0.13107E-01	0.00000	0.31315E-04	0.00000	0.29405E-05	0.31315E-04	0.28374E-04
91	0.14830E-01	0.00000	0.26666E-04	0.00000	0.26693E-05	0.26666E-04	0.23997E-04
92	0.16503E-01	0.00000	0.22541E-04	0.00000	0.24350E-05	0.22541E-04	0.20106E-04
93	0.18143E-01	0.00000	0.19911E-04	0.00000	0.22734E-05	0.19911E-04	0.17638E-04
94	0.19759E-01	0.00000	0.17407E-04	0.00000	0.21242E-05	0.17407E-04	0.15283E-04
95	0.21360E-01	0.00000	0.14986E-04	0.00000	0.19825E-05	0.14986E-04	0.13004E-04
96	0.23726E-01	0.00000	0.23037E-04	0.00000	0.35737E-05	0.23037E-04	0.19463E-04
97	0.26851E-01	0.00000	0.14138E-04	0.00000	0.30885E-05	0.14138E-04	0.11049E-04
98	0.29946E-01	0.00000	0.54782E-05	0.00000	0.93274E-05	0.54782E-05	0.00000
99	0.33015E-01	0.00000	0.00000	0.00000	0.00000	0.00000	0.00000
100	0.36067E-01	0.00000	0.00000	0.00000	0.00000	0.00000	0.00000
101	0.41382E-01	0.00000	0.00000	0.00000	0.00000	0.00000	0.00000
102	0.48949E-01	0.00000	0.00000	0.00000	0.00000	0.00000	0.00000
103	0.56489E-01	0.00000	0.00000	0.00000	0.00000	0.00000	0.00000
104	0.64013E-01	0.00000	0.00000	0.00000	0.00000	0.00000	0.00000
105	0.71526E-01	0.00000	0.00000	0.00000	0.00000	0.00000	0.00000
106	0.79032E-01	0.00000	0.00000	0.00000	0.00000	0.00000	0.00000
107	0.86535E-01	0.00000	0.00000	0.00000	0.00000	0.00000	0.00000
108	0.94035E-01	0.00000	0.00000	0.00000	0.00000	0.00000	0.00000
109	0.10154E 00	0.00000	0.00000	0.00000	0.00000	0.00000	0.00000
110	0.10904E 00	0.00000	0.00000	0.00000	0.00000	0.00000	0.00000
111	0.11654E 00	0.00000	0.00000	0.00000	0.00000	0.00000	0.00000
112	0.12404E 00	0.00000	0.00000	0.00000	0.00000	0.00000	0.00000
113	0.13155E 00	0.00000	0.00000	0.00000	0.00000	0.00000	0.00000
114	0.13905E 00	0.00000	0.00000	0.00000	0.00000	0.00000	0.00000
115	0.14656E 00	0.00000	0.00000	0.00000	0.00000	0.00000	0.00000
116	0.15407E 00	0.00000	0.00000	0.00000	0.00000	0.00000	0.00000
117	0.16159E 00	0.00000	0.00000	0.00000	0.00000	0.00000	0.00000
118	0.16911E 00	0.00000	0.00000	0.00000	0.00000	0.00000	0.00000
119	0.17663E 00	0.00000	0.00000	0.00000	0.00000	0.00000	0.00000
120	0.18415E 00	0.00000	0.00000	0.00000	0.00000	0.00000	0.00000
121	0.19167E 00	0.00000	0.00000	0.00000	0.00000	0.00000	0.00000
122	0.19920E 00	0.00000	0.00000	0.00000	0.00000	0.00000	0.00000
123	0.20673E 00	0.00000	0.00000	0.00000	0.00000	0.00000	0.00000
124	0.21427E 00	0.00000	0.00000	0.00000	0.00000	0.00000	0.00000
125	0.22180E 00	0.00000	0.00000	0.00000	0.00000	0.00000	0.00000
126	0.22934E 00	0.00000	0.00000	0.00000	0.00000	0.00000	0.00000
127	0.23688E 00	0.00000	0.00000	0.00000	0.00000	0.00000	0.00000
128	0.24442E 00	0.00000	0.00000	0.00000	0.00000	0.00000	0.00000
129	0.25197E 00	0.00000	0.00000	0.00000	0.00000	0.00000	0.00000
130	0.25951E 00	0.00000	0.00000	0.00000	0.00000	0.00000	0.00000
131	0.26706E 00	0.00000	0.00000	0.00000	0.00000	0.00000	0.00000
132	0.27462E 00	0.00000	0.00000	0.00000	0.00000	0.00000	0.00000
133	0.28218E 00	0.00000	0.00000	0.00000	0.00000	0.00000	0.00000
134	0.28974E 00	0.00000	0.00000	0.00000	0.00000	0.00000	0.00000
135	0.29656E 00	0.00000	0.00000	0.00000	0.00000	0.00000	0.00000
136	0.30112E 00	0.00000	0.00000	0.00000	0.00000	0.00000	0.00000
137	0.30416E 00	0.00000	0.00000	0.00000	0.00000	0.00000	0.00000
138	0.30721E 00	0.00000	0.00000	0.00000	0.00000	0.00000	0.00000

b. Calculated surface characteristics (continued)

Figure 6.4: continued

NACA 0012 : EXAMPLE 1 : TIME= 60.000 SEC

ICING CONDITION:

STATIC TEMPERATURE (C)	260.55
STATIC PRESSURE (PA)	90748.00
VELOCITY (M/S)	129.00
LWC (G/M**3)	0.50
DROPLET DIAMETER (MICRONS)	20.00

ORIGINAL PAGE IS
OF POOR QUALITY

ICE ACCRETION DATA:

STAGNATION POINT	70	
TRANSITION POINTS (LOWER,UPPER)	68	71
ICING LIMITS (LOWER,UPPER)	42	97
NUMBER OF POINTS	139	
NUMBER OF SEGMENTS ADDED	0	

SEG	X	Y	S	VE	TE	PRESS	RA	SEGLENGTH
1	0.30000E 00	0.00000	-0.30721E 00	0.10282E 03	0.26357E 03	0.94482E 05	0.12469E 01	0.30523E-02
2	0.29700E 00	-0.56220E-03	-0.30416E 00	0.11347E 03	0.26242E 03	0.93052E 05	0.12334E 01	0.30449E-02
3	0.29400E 00	-0.10833E-02	-0.30112E 00	0.11731E 03	0.26198E 03	0.92506E 05	0.12282E 01	0.30395E-02
4	0.29100E 00	-0.15717E-02	-0.29656E 00	0.12094E 03	0.26155E 03	0.91976E 05	0.12231E 01	0.60676E-02
5	0.28500E 00	-0.24753E-02	-0.28974E 00	0.12423E 03	0.26115E 03	0.91482E 05	0.12185E 01	0.75710E-02
6	0.27750E 00	-0.35100E-02	-0.28218E 00	0.12655E 03	0.26086E 03	0.91129E 05	0.12151E 01	0.75615E-02
7	0.27000E 00	-0.44724E-02	-0.27462E 00	0.12819E 03	0.26065E 03	0.90874E 05	0.12127E 01	0.75554E-02
8	0.26250E 00	-0.53859E-02	-0.26707E 00	0.12954E 03	0.26048E 03	0.90664E 05	0.12107E 01	0.75515E-02
9	0.25500E 00	-0.62664E-02	-0.25952E 00	0.13075E 03	0.26032E 03	0.90473E 05	0.12088E 01	0.75486E-02
10	0.24750E 00	-0.71217E-02	-0.25197E 00	0.13189E 03	0.26017E 03	0.90292E 05	0.12071E 01	0.75461E-02
11	0.24000E 00	-0.79545E-02	-0.24442E 00	0.13298E 03	0.26003E 03	0.90117E 05	0.12054E 01	0.75438E-02
12	0.23250E 00	-0.87663E-02	-0.23688E 00	0.13404E 03	0.25989E 03	0.89946E 05	0.12038E 01	0.75414E-02
13	0.22500E 00	-0.95565E-02	-0.22934E 00	0.13507E 03	0.25975E 03	0.89779E 05	0.12022E 01	0.75391E-02
14	0.21750E 00	-0.10323E-01	-0.22180E 00	0.13607E 03	0.25962E 03	0.89617E 05	0.12007E 01	0.75367E-02
15	0.21000E 00	-0.11066E-01	-0.21427E 00	0.13704E 03	0.25949E 03	0.89457E 05	0.11991E 01	0.75343E-02
16	0.20250E 00	-0.11784E-01	-0.20673E 00	0.13801E 03	0.25935E 03	0.89298E 05	0.11976E 01	0.75318E-02
17	0.19500E 00	-0.12475E-01	-0.19920E 00	0.13895E 03	0.25922E 03	0.89141E 05	0.11961E 01	0.75292E-02
18	0.18750E 00	-0.13138E-01	-0.19168E 00	0.13989E 03	0.25909E 03	0.88985E 05	0.11946E 01	0.75266E-02
19	0.18000E 00	-0.13771E-01	-0.18415E 00	0.14081E 03	0.25896E 03	0.88831E 05	0.11931E 01	0.75240E-02
20	0.17250E 00	-0.14372E-01	-0.17663E 00	0.14171E 03	0.25884E 03	0.88677E 05	0.11917E 01	0.75214E-02
21	0.16500E 00	-0.14938E-01	-0.16911E 00	0.14262E 03	0.25871E 03	0.88524E 05	0.11902E 01	0.75187E-02
22	0.15750E 00	-0.15468E-01	-0.16159E 00	0.14352E 03	0.25858E 03	0.88371E 05	0.11887E 01	0.75160E-02
23	0.15000E 00	-0.15959E-01	-0.15408E 00	0.14442E 03	0.25845E 03	0.88216E 05	0.11872E 01	0.75135E-02
24	0.14250E 00	-0.16409E-01	-0.14656E 00	0.14533E 03	0.25832E 03	0.88061E 05	0.11857E 01	0.75110E-02
25	0.13500E 00	-0.16815E-01	-0.13905E 00	0.14624E 03	0.25819E 03	0.87903E 05	0.11842E 01	0.75085E-02
26	0.12750E 00	-0.17173E-01	-0.13155E 00	0.14715E 03	0.25806E 03	0.87745E 05	0.11827E 01	0.75062E-02
27	0.12000E 00	-0.17479E-01	-0.12404E 00	0.14806E 03	0.25792E 03	0.87585E 05	0.11811E 01	0.75041E-02
28	0.11250E 00	-0.17727E-01	-0.11654E 00	0.14896E 03	0.25779E 03	0.87426E 05	0.11796E 01	0.75023E-02
29	0.10500E 00	-0.17912E-01	-0.10904E 00	0.14985E 03	0.25766E 03	0.87270E 05	0.11781E 01	0.75009E-02
30	0.97500E-01	-0.18028E-01	-0.10154E 00	0.15072E 03	0.25753E 03	0.87115E 05	0.11766E 01	0.75002E-02
31	0.90000E-01	-0.18068E-01	-0.94037E-01	0.15157E 03	0.25740E 03	0.86966E 05	0.11752E 01	0.75001E-02
32	0.82500E-01	-0.18023E-01	-0.86537E-01	0.15237E 03	0.25728E 03	0.86821E 05	0.11738E 01	0.75012E-02
33	0.75000E-01	-0.17884E-01	-0.79034E-01	0.15314E 03	0.25716E 03	0.86684E 05	0.11725E 01	0.75041E-02
34	0.67500E-01	-0.17638E-01	-0.71528E-01	0.15383E 03	0.25706E 03	0.86559E 05	0.11713E 01	0.75089E-02
35	0.60000E-01	-0.17271E-01	-0.64015E-01	0.15441E 03	0.25697E 03	0.86454E 05	0.11702E 01	0.75171E-02
36	0.52500E-01	-0.16764E-01	-0.56491E-01	0.15483E 03	0.25690E 03	0.86379E 05	0.11695E 01	0.75301E-02
37	0.45000E-01	-0.16091E-01	-0.48957E-01	0.15500E 03	0.25688E 03	0.86348E 05	0.11692E 01	0.75504E-02
38	0.37500E-01	-0.15220E-01	-0.41384E-01	0.15478E 03	0.25691E 03	0.86388E 05	0.11696E 01	0.75829E-02
39	0.30000E-01	-0.14101E-01	-0.36069E-01	0.15426E 03	0.25699E 03	0.86482E 05	0.11705E 01	0.30469E-02
40	0.27000E-01	-0.13568E-01	-0.33017E-01	0.15380E 03	0.25706E 03	0.86565E 05	0.11713E 01	0.30580E-02
41	0.24000E-01	-0.12976E-01	-0.29948E-01	0.15308E 03	0.25717E 03	0.86694E 05	0.11726E 01	0.30799E-02
42	0.20965E-01	-0.12450E-01	-0.26853E-01	0.15196E 03	0.25734E 03	0.86895E 05	0.11745E 01	0.31094E-02
43	0.17900E-01	-0.11926E-01	-0.23729E-01	0.15022E 03	0.25760E 03	0.87205E 05	0.11775E 01	0.31386E-02
44	0.14842E-01	-0.11223E-01	-0.21363E-01	0.14830E 03	0.25789E 03	0.87543E 05	0.11807E 01	0.15939E-02
45	0.13291E-01	-0.10854E-01	-0.19763E-01	0.14664E 03	0.25813E 03	0.87833E 05	0.11835E 01	0.16068E-02
46	0.11743E-01	-0.10425E-01	-0.18146E-01	0.14460E 03	0.25843E 03	0.88186E 05	0.11869E 01	0.16265E-02
47	0.10187E-01	-0.99488E-02	-0.16506E-01	0.14207E 03	0.25879E 03	0.88618E 05	0.11911E 01	0.16536E-02
48	0.86129E-02	-0.94430E-02	-0.14833E-01	0.13891E 03	0.25923E 03	0.89148E 05	0.11962E 01	0.16921E-02
49	0.70109E-02	-0.88981E-02	-0.13110E-01	0.13473E 03	0.25980E 03	0.89835E 05	0.12027E 01	0.17543E-02
50	0.53760E-02	-0.82622E-02	-0.11302E-01	0.12866E 03	0.26059E 03	0.90801E 05	0.12120E 01	0.18612E-02
51	0.36757E-02	-0.75051E-02	-0.93693E-02	0.11954E 03	0.26172E 03	0.92182E 05	0.12251E 01	0.20044E-02
52	0.19168E-02	-0.65439E-02	-0.77677E-02	0.10892E 03	0.26293E 03	0.93678E 05	0.12393E 01	0.11989E-02
53	0.89327E-03	-0.59196E-02	-0.64879E-02	0.98295E 02	0.26402E 03	0.95052E 05	0.12522E 01	0.13607E-02
54	-0.20987E-03	-0.51230E-02	-0.53333E-02	0.87417E 02	0.26503E 03	0.96324E 05	0.12642E 01	0.94852E-03
55	-0.10241E-02	-0.46363E-02	-0.43923E-02	0.77850E 02	0.26581E 03	0.97328E 05	0.12736E 01	0.93358E-03
56	-0.15952E-02	-0.38979E-02	-0.37712E-02	0.71259E 02	0.26630E 03	0.97956E 05	0.12794E 01	0.30853E-03
57	-0.16134E-02	-0.35899E-02	-0.34932E-02	0.68248E 02	0.26651E 03	0.98226E 05	0.12820E 01	0.24737E-03
58	-0.16399E-02	-0.33439E-02	-0.32417E-02	0.65594E 02	0.26669E 03	0.98454E 05	0.12841E 01	0.25563E-03
59	-0.16748E-02	-0.30907E-02	-0.29800E-02	0.62800E 02	0.26687E 03	0.98685E 05	0.12862E 01	0.26787E-03
60	-0.17045E-02	-0.28245E-02	-0.27048E-02	0.59880E 02	0.26704E 03	0.98915E 05	0.12884E 01	0.28247E-03
61	-0.17332E-02	-0.25435E-02	-0.24173E-02	0.56913E 02	0.26722E 03	0.99139E 05	0.12905E 01	0.29266E-03
62	-0.17677E-02	-0.22528E-02	-0.21846E-02	0.54569E 02	0.26735E 03	0.99308E 05	0.12920E 01	0.17260E-03
63	-0.17728E-02	-0.20803E-02	-0.20137E-02	0.52861E 02	0.26744E 03	0.99427E 05	0.12931E 01	0.16919E-03
64	-0.17852E-02	-0.19116E-02	-0.18393E-02	0.51209E 02	0.26752E 03	0.99538E 05	0.12942E 01	0.17973E-03
65	-0.18036E-02	-0.17328E-02	-0.16529E-02	0.49522E 02	0.26761E 03	0.99648E 05	0.12952E 01	0.19311E-03

b. Calculated surface characteristics (continued)

Figure 6.4: continued

77

SEG	X	Y	S	VE	TE	PRESS	RA	SEGLENGTH
66	-0.18269E-02	-0.15411E-02	-0.14501E-02	0.47811E 02	0.26769E 03	0.99756E 05	0.12962E 01	0.21248E-03
67	-0.18597E-02	-0.13312E-02	-0.12199E-02	0.46063E 02	0.26777E 03	0.99863E 05	0.12972E 01	0.24780E-03
68	-0.19107E-02	-0.10887E-02	-0.91868E-03	0.44066E 02	0.26786E 03	0.99980E 05	0.12983E 01	0.35471E-03
69	-0.19736E-02	-0.73960E-03	-0.37066E-03	0.41887E 02	0.26796E 03	0.10010E 06	0.12994E 01	0.74133E-03
70	-0.20243E-02	-0.12515E-08	0.37066E-03	0.41887E 02	0.26796E 03	0.10010E 06	0.12994E 01	0.74132E-03
71	-0.19735E-02	0.73957E-03	0.91867E-03	0.44066E 02	0.26786E 03	0.99980E 05	0.12983E 01	0.35470E-03
72	-0.19104E-02	0.10886E-02	0.12199E-02	0.46063E 02	0.26777E 03	0.99863E 05	0.12972E 01	0.24778E-03
73	-0.18593E-02	0.13311E-02	0.14500E-02	0.47811E 02	0.26769E 03	0.99756E 05	0.12962E 01	0.21246E-03
74	-0.18263E-02	0.15410E-02	0.16528E-02	0.49522E 02	0.26761E 03	0.99648E 05	0.12952E 01	0.19309E-03
75	-0.18030E-02	0.17326E-02	0.18392E-02	0.51209E 02	0.26752E 03	0.99538E 05	0.12942E 01	0.17970E-03
76	-0.17845E-02	0.19114E-02	0.20136E-02	0.52861E 02	0.26744E 03	0.99427E 05	0.12931E 01	0.16918E-03
77	-0.17721E-02	0.20801E-02	0.21845E-02	0.54569E 02	0.26735E 03	0.99308E 05	0.12920E 01	0.17258E-03
78	-0.17671E-02	0.22526E-02	0.24171E-02	0.56913E 02	0.26722E 03	0.99139E 05	0.12905E 01	0.29264E-03
79	-0.17325E-02	0.25432E-02	0.27047E-02	0.59880E 02	0.26704E 03	0.98915E 05	0.12884E 01	0.28244E-03
80	-0.17038E-02	0.28242E-02	0.29798E-02	0.62800E 02	0.26687E 03	0.98685E 05	0.12862E 01	0.26781E-03
81	-0.16740E-02	0.30903E-02	0.32415E-02	0.65590E 02	0.26669E 03	0.98454E 05	0.12841E 01	0.25560E-03
82	-0.16391E-02	0.33435E-02	0.34930E-02	0.68248E 02	0.26651E 03	0.98226E 05	0.12820E 01	0.24746E-03
83	-0.16129E-02	0.35896E-02	0.37710E-02	0.71259E 02	0.26630E 03	0.97956E 05	0.12794E 01	0.30859E-03
84	-0.15949E-02	0.38977E-02	0.43922E-02	0.77850E 02	0.26581E 03	0.97328E 05	0.12736E 01	0.93380E-03
85	-0.10159E-02	0.46303E-02	0.53337E-02	0.87420E 02	0.26503E 03	0.96323E 05	0.12642E 01	0.94904E-03
86	-0.20030E-03	0.51156E-02	0.64871E-02	0.98295E 02	0.26402E 03	0.95052E 05	0.12522E 01	0.13579E-02
87	0.89589E-03	0.59169E-02	0.77652E-02	0.10892E 03	0.26293E 03	0.93678E 05	0.12393E 01	0.11984E-02
88	0.19182E-02	0.65421E-02	0.93664E-02	0.11954E 03	0.26172E 03	0.92182E 05	0.12251E 01	0.20040E-02
89	0.36761E-02	0.75045E-02	0.11299E-01	0.12866E 03	0.26059E 03	0.90801E 05	0.12120E 01	0.18611E-02
90	0.53757E-02	0.82628E-02	0.13107E-01	0.13473E 03	0.25980E 03	0.89835E 05	0.12027E 01	0.17542E-02
91	0.70101E-02	0.89000E-02	0.14830E-01	0.13891E 03	0.25923E 03	0.89148E 05	0.11962E 01	0.16922E-02
92	0.86119E-02	0.94454E-02	0.16503E-01	0.14206E 03	0.25879E 03	0.88618E 05	0.11911E 01	0.16537E-02
93	0.10186E-01	0.99518E-02	0.18143E-01	0.14459E 03	0.25843E 03	0.88186E 05	0.11869E 01	0.16265E-02
94	0.11741E-01	0.10429E-01	0.19759E-01	0.14664E 03	0.25813E 03	0.87833E 05	0.11835E 01	0.16068E-02
95	0.13287E-01	0.10861E-01	0.21360E-01	0.14830E 03	0.25789E 03	0.87543E 05	0.11807E 01	0.15940E-02
96	0.14839E-01	0.11231E-01	0.23726E-01	0.15022E 03	0.25760E 03	0.87205E 05	0.11775E 01	0.31387E-02
97	0.17897E-01	0.11938E-01	0.26851E-01	0.15196E 03	0.25734E 03	0.86895E 05	0.11745E 01	0.31100E-02
98	0.20964E-01	0.12456E-01	0.29946E-01	0.15308E 03	0.25717E 03	0.86694E 05	0.11726E 01	0.30804E-02
99	0.24000E-01	0.12976E-01	0.33015E-01	0.15380E 03	0.25706E 03	0.86566E 05	0.11713E 01	0.30580E-02
100	0.27000E-01	0.13568E-01	0.36067E-01	0.15426E 03	0.25699E 03	0.86482E 05	0.11705E 01	0.30469E-02
101	0.30000E-01	0.14101E-01	0.41382E-01	0.15478E 03	0.25691E 03	0.86388E 05	0.11696E 01	0.75829E-02
102	0.37500E-01	0.15220E-01	0.48949E-01	0.15500E 03	0.25688E 03	0.86348E 05	0.11692E 01	0.75504E-02
103	0.45000E-01	0.16091E-01	0.56489E-01	0.15483E 03	0.25690E 03	0.86379E 05	0.11695E 01	0.75301E-02
104	0.52500E-01	0.16764E-01	0.64013E-01	0.15441E 03	0.25697E 03	0.86454E 05	0.11702E 01	0.75171E-02
105	0.60000E-01	0.17271E-01	0.71526E-01	0.15383E 03	0.25706E 03	0.86559E 05	0.11713E 01	0.75089E-02
106	0.67500E-01	0.17638E-01	0.79032E-01	0.15314E 03	0.25716E 03	0.86684E 05	0.11725E 01	0.75041E-02
107	0.75000E-01	0.17884E-01	0.86535E-01	0.15237E 03	0.25728E 03	0.86821E 05	0.11738E 01	0.75012E-02
108	0.82500E-01	0.18023E-01	0.94035E-01	0.15157E 03	0.25740E 03	0.86966E 05	0.11752E 01	0.75001E-02
109	0.90000E-01	0.18068E-01	0.10154E 00	0.15072E 03	0.25753E 03	0.87115E 05	0.11766E 01	0.75002E-02
110	0.97500E-01	0.18028E-01	0.10904E 00	0.14985E 03	0.25766E 03	0.87270E 05	0.11781E 01	0.75009E-02
111	0.10500E 00	0.17912E-01	0.11654E 00	0.14896E 03	0.25779E 03	0.87426E 05	0.11796E 01	0.75023E-02
112	0.11250E 00	0.17727E-01	0.12404E 00	0.14806E 03	0.25792E 03	0.87585E 05	0.11811E 01	0.75041E-02
113	0.12000E 00	0.17479E-01	0.13155E 00	0.14715E 03	0.25806E 03	0.87745E 05	0.11827E 01	0.75062E-02
114	0.12750E 00	0.17173E-01	0.13905E 00	0.14624E 03	0.25819E 03	0.87903E 05	0.11842E 01	0.75085E-02
115	0.13500E 00	0.16815E-01	0.14656E 00	0.14533E 03	0.25832E 03	0.88061E 05	0.11857E 01	0.75110E-02
116	0.14250E 00	0.16409E-01	0.15407E 00	0.14442E 03	0.25845E 03	0.88216E 05	0.11872E 01	0.75135E-02
117	0.15000E 00	0.15959E-01	0.16159E 00	0.14352E 03	0.25858E 03	0.88371E 05	0.11887E 01	0.75160E-02
118	0.15750E 00	0.15468E-01	0.16911E 00	0.14262E 03	0.25871E 03	0.88524E 05	0.11902E 01	0.75187E-02
119	0.16500E 00	0.14938E-01	0.17663E 00	0.14171E 03	0.25884E 03	0.88677E 05	0.11917E 01	0.75214E-02
120	0.17250E 00	0.14372E-01	0.18415E 00	0.14081E 03	0.25896E 03	0.88831E 05	0.11931E 01	0.75240E-02
121	0.18000E 00	0.13771E-01	0.19167E 00	0.13989E 03	0.25909E 03	0.88985E 05	0.11946E 01	0.75266E-02
122	0.18750E 00	0.13138E-01	0.19920E 00	0.13895E 03	0.25922E 03	0.89141E 05	0.11961E 01	0.75292E-02
123	0.19500E 00	0.12475E-01	0.20673E 00	0.13801E 03	0.25935E 03	0.89298E 05	0.11976E 01	0.75318E-02
124	0.20250E 00	0.11784E-01	0.21427E 00	0.13704E 03	0.25949E 03	0.89457E 05	0.11991E 01	0.75343E-02
125	0.21000E 00	0.11066E-01	0.22180E 00	0.13607E 03	0.25962E 03	0.89617E 05	0.12007E 01	0.75367E-02
126	0.21750E 00	0.10323E-01	0.22934E 00	0.13507E 03	0.25975E 03	0.89779E 05	0.12022E 01	0.75391E-02
127	0.22500E 00	0.95565E-02	0.23688E 00	0.13404E 03	0.25989E 03	0.89946E 05	0.12038E 01	0.75414E-02
128	0.23250E 00	0.87663E-02	0.24442E 00	0.13298E 03	0.26003E 03	0.90118E 05	0.12054E 01	0.75438E-02
129	0.24000E 00	0.79545E-02	0.25197E 00	0.13188E 03	0.26018E 03	0.90292E 05	0.12071E 01	0.75461E-02
130	0.24750E 00	0.71217E-02	0.25951E 00	0.13075E 03	0.26032E 03	0.90473E 05	0.12088E 01	0.75486E-02
131	0.25500E 00	0.62664E-02	0.26706E 00	0.12953E 03	0.26048E 03	0.90664E 05	0.12107E 01	0.75515E-02
132	0.26250E 00	0.53859E-02	0.27462E 00	0.12819E 03	0.26065E 03	0.90874E 05	0.12127E 01	0.75554E-02
133	0.27000E 00	0.44724E-02	0.28218E 00	0.12654E 03	0.26086E 03	0.91129E 05	0.12151E 01	0.75615E-02
134	0.27750E 00	0.35100E-02	0.28974E 00	0.12423E 03	0.26115E 03	0.91482E 05	0.12185E 01	0.75710E-02
135	0.28500E 00	0.24753E-02	0.29656E 00	0.12094E 03	0.26155E 03	0.91976E 05	0.12231E 01	0.60676E-02
136	0.29100E 00	0.15717E-02	0.30112E 00	0.11731E 03	0.26198E 03	0.92506E 05	0.12282E 01	0.30395E-02
137	0.29400E 00	0.10833E-02	0.30416E 00	0.11347E 03	0.26242E 03	0.93052E 05	0.12334E 01	0.30449E-02
138	0.29700E 00	0.56220E-03	0.30721E 00	0.10282E 03	0.26357E 03	0.94482E 05	0.12469E 01	0.30523E-02
139	0.30000E 00	0.00000	0.00000	0.00000	0.00000	0.00000	0.00000	0.00000

SEG	S	HTC	XK	BETA	FFRAC	RI	TSURF	DICE
1	-0.30721E 00	0.00000	0.35000E-03	0.00000	0.10000E 01	0.35791E 03	0.00000	0.00000
2	-0.30416E 00	0.36935E 03	0.35000E-03	0.00000	0.10000E 01	0.35791E 03	0.00000	0.00000
3	-0.30112E 00	0.39015E 03	0.35000E-03	0.00000	0.10000E 01	0.35791E 03	0.00000	0.00000
4	-0.29656E 00	0.41048E 03	0.35000E-03	0.00000	0.10000E 01	0.35791E 03	0.00000	0.00000
5	-0.28974E 00	0.42982E 03	0.35000E-03	0.00000	0.10000E 01	0.35791E 03	0.00000	0.00000
6	-0.28218E 00	0.44425E 03	0.35000E-03	0.00000	0.10000E 01	0.35791E 03	0.00000	0.00000
7	-0.27462E 00	0.45520E 03	0.35000E-03	0.00000	0.10000E 01	0.35791E 03	0.00000	0.00000
8	-0.26707E 00	0.46462E 03	0.35000E-03	0.00000	0.10000E 01	0.35791E 03	0.00000	0.00000
9	-0.25952E 00	0.47350E 03	0.35000E-03	0.00000	0.10000E 01	0.35791E 03	0.00000	0.00000
10	-0.25197E 00	0.48217E 03	0.35000E-03	0.00000	0.10000E 01	0.35791E 03	0.00000	0.00000
11	-0.24442E 00	0.49078E 03	0.35000E-03	0.00000	0.10000E 01	0.35791E 03	0.00000	0.00000
12	-0.23688E 00	0.49946E 03	0.35000E-03	0.00000	0.10000E 01	0.35791E 03	0.00000	0.00000
13	-0.22934E 00	0.50816E 03	0.35000E-03	0.00000	0.10000E 01	0.35791E 03	0.00000	0.00000
14	-0.22180E 00	0.51689E 03	0.35000E-03	0.00000	0.10000E 01	0.35791E 03	0.00000	0.00000
15	-0.21427E 00	0.52580E 03	0.35000E-03	0.00000	0.10000E 01	0.35791E 03	0.00000	0.00000
16	-0.20673E 00	0.53492E 03	0.35000E-03	0.00000	0.10000E 01	0.35791E 03	0.00000	0.00000
17	-0.19920E 00	0.54424E 03	0.35000E-03	0.00000	0.10000E 01	0.35791E 03	0.00000	0.00000
18	-0.19168E 00	0.55382E 03	0.35000E-03	0.00000	0.10000E 01	0.35791E 03	0.00000	0.00000
19	-0.18415E 00	0.56370E 03	0.35000E-03	0.00000	0.10000E 01	0.35791E 03	0.00000	0.00000
20	-0.17663E 00	0.57390E 03	0.35000E-03	0.00000	0.10000E 01	0.35791E 03	0.00000	0.00000

b. Calculated surface characteristics (continued)

Figure 6.4: continued

SEG	S	HTC	XK	BETA	FFRAC	RI	TSURF	DICE
21	-0.16911E 00	0.58452E 03	0.35000E-03	0.00000	0.10000E 01	0.35791E 03	0.00000	0.00000
22	-0.16159E 00	0.59563E 03	0.35000E-03	0.00000	0.10000E 01	0.35791E 03	0.00000	0.00000
23	-0.15408E 00	0.60729E 03	0.35000E-03	0.00000	0.10000E 01	0.35791E 03	0.00000	0.00000
24	-0.14656E 00	0.61962E 03	0.35000E-03	0.00000	0.10000E 01	0.35791E 03	0.00000	0.00000
25	-0.13905E 00	0.63271E 03	0.35000E-03	0.00000	0.10000E 01	0.35791E 03	0.00000	0.00000
26	-0.13155E 00	0.64663E 03	0.35000E-03	0.00000	0.10000E 01	0.35791E 03	0.00000	0.00000
27	-0.12404E 00	0.66158E 03	0.35000E-03	0.00000	0.10000E 01	0.35791E 03	0.00000	0.00000
28	-0.11654E 00	0.67753E 03	0.35000E-03	0.00000	0.10000E 01	0.35791E 03	0.00000	0.00000
29	-0.10904E 00	0.69471E 03	0.35000E-03	0.00000	0.10000E 01	0.35791E 03	0.00000	0.00000
30	-0.10154E 00	0.71332E 03	0.35000E-03	0.00000	0.10000E 01	0.35791E 03	0.00000	0.00000
31	-0.94037E-01	0.73360E 03	0.35000E-03	0.00000	0.10000E 01	0.35791E 03	0.00000	0.00000
32	-0.86537E-01	0.75594E 03	0.35000E-03	0.00000	0.10000E 01	0.35791E 03	0.00000	0.00000
33	-0.79034E-01	0.78085E 03	0.35000E-03	0.00000	0.10000E 01	0.35791E 03	0.00000	0.00000
34	-0.71528E-01	0.80885E 03	0.35000E-03	0.00000	0.10000E 01	0.35791E 03	0.00000	0.00000
35	-0.64015E-01	0.84079E 03	0.35000E-03	0.00000	0.10000E 01	0.35791E 03	0.00000	0.00000
36	-0.56491E-01	0.87784E 03	0.35000E-03	0.00000	0.10000E 01	0.35791E 03	0.00000	0.00000
37	-0.48951E-01	0.92188E 03	0.35000E-03	0.00000	0.10000E 01	0.35791E 03	0.00000	0.00000
38	-0.41384E-01	0.97611E 03	0.35000E-03	0.00000	0.10000E 01	0.35791E 03	0.00000	0.00000
39	-0.36069E-01	0.10231E 04	0.35000E-03	0.00000	0.10000E 01	0.35791E 03	0.00000	0.00000
40	-0.33017E-01	0.10552E 04	0.35000E-03	0.00000	0.10000E 01	0.35791E 03	0.00000	0.00000
41	-0.29942E-01	0.10916E 04	0.35000E-03	0.23592E-01	0.10000E 01	0.35791E 03	0.00000	0.00000
42	-0.26853E-01	0.11327E 04	0.35000E-03	0.67630E-01	0.10000E 01	0.91700E 03	0.26639E 03	0.28542E-03
43	-0.23729E-01	0.11790E 04	0.35000E-03	0.11202E 00	0.10000E 01	0.91700E 03	0.26684E 03	0.47277E-03
44	-0.21363E-01	0.12172E 04	0.35000E-03	0.14578E 00	0.10000E 01	0.91700E 03	0.26716E 03	0.61521E-03
45	-0.19763E-01	0.12451E 04	0.35000E-03	0.16873E 00	0.10000E 01	0.91700E 03	0.26737E 03	0.71210E-03
46	-0.18146E-01	0.12752E 04	0.35000E-03	0.19183E 00	0.10000E 01	0.91700E 03	0.26757E 03	0.80957E-03
47	-0.16506E-01	0.13082E 04	0.35000E-03	0.21525E 00	0.10000E 01	0.91700E 03	0.26777E 03	0.90842E-03
48	-0.14833E-01	0.13452E 04	0.35000E-03	0.25102E 00	0.10000E 01	0.91700E 03	0.26807E 03	0.10594E-02
49	-0.13110E-01	0.13848E 04	0.35000E-03	0.28907E 00	0.10000E 01	0.91700E 03	0.26838E 03	0.12200E-02
50	-0.11302E-01	0.14194E 04	0.35000E-03	0.32899E 00	0.10000E 01	0.91700E 03	0.26872E 03	0.13884E-02
51	-0.93693E-02	0.14388E 04	0.35000E-03	0.38763E 00	0.10000E 01	0.91700E 03	0.26924E 03	0.16359E-02
52	-0.77677E-02	0.14174E 04	0.35000E-03	0.44084E 00	0.10000E 01	0.91700E 03	0.26982E 03	0.18605E-02
53	-0.64879E-02	0.13593E 04	0.35000E-03	0.48309E 00	0.10000E 01	0.91700E 03	0.27040E 03	0.20388E-02
54	-0.53333E-02	0.12691E 04	0.35000E-03	0.52257E 00	0.10000E 01	0.91700E 03	0.27150E 03	0.23969E-02
55	-0.43923E-02	0.11726E 04	0.35000E-03	0.55783E 00	0.88732E 00	0.91700E 03	0.27315E 03	0.27681E-02
56	-0.37712E-02	0.10996E 04	0.35000E-03	0.58114E 00	0.42148E 00	0.91700E 03	0.27315E 03	0.26091E-02
57	-0.34932E-02	0.10570E 04	0.35000E-03	0.58130E 00	0.40227E 00	0.91700E 03	0.27315E 03	0.25127E-02
58	-0.32417E-02	0.10245E 04	0.35000E-03	0.58541E 00	0.39408E 00	0.91700E 03	0.27315E 03	0.24413E-02
59	-0.29800E-02	0.98977E 03	0.35000E-03	0.58976E 00	0.39295E 00	0.91700E 03	0.27315E 03	0.23660E-02
60	-0.27048E-02	0.95358E 03	0.35000E-03	0.59439E 00	0.39869E 00	0.91700E 03	0.27315E 03	0.22883E-02
61	-0.24173E-02	0.91894E 03	0.35000E-03	0.59922E 00	0.41536E 00	0.91700E 03	0.27315E 03	0.22145E-02
62	-0.21846E-02	0.89199E 03	0.35000E-03	0.60321E 00	0.28732E 00	0.91700E 03	0.27315E 03	0.21577E-02
63	-0.20137E-02	0.87198E 03	0.35000E-03	0.60622E 00	0.30415E 00	0.91700E 03	0.27315E 03	0.21159E-02
64	-0.18393E-02	0.85545E 03	0.35000E-03	0.60928E 00	0.32831E 00	0.91700E 03	0.27315E 03	0.20815E-02
65	-0.16529E-02	0.84088E 03	0.35000E-03	0.61391E 00	0.36170E 00	0.91700E 03	0.27315E 03	0.20520E-02
66	-0.14501E-02	0.83024E 03	0/35000E-03	0.61339E 00	0.40815E 00	0.91700E 03	0.27315E 03	0.20277E-02
67	-0.12199E-02	0.82660E 03	0.35000E-03	0.61278E 00	0.47513E 00	0.91700E 03	0.27315E 03	0.20175E-02
68	-0.91868E-03	0.83319E 03	0.35000E-03	0.61195E 00	0.57669E 00	0.91700E 03	0.27315E 03	0.20275E-02
69	-0.37066E-03	0.83319E 03	0.35000E-03	0.61052E 00	0.78796E 00	0.91700E 03	0.27315E 03	0.20302E-02
70	0.37066E-03	0.83319E 03	0.35000E-03	0.61045E 00	0.78804E 00	0.91700E 03	0.27315E 03	0.20302E-02
71	0.91867E-03	0.83319E 03	0.35000E-03	0.61148E 00	0.57703E 00	0.91700E 03	0.27315E 03	0.20272E-02
72	0.12199E-02	0.82660E 03	0.35000E-03	0.61208E 00	0.47567E 00	0.91700E 03	0.27315E 03	0.20171E-02
73	0.14500E-02	0.83024E 03	0.35000E-03	0.61252E 00	0.40885E 00	0.91700E 03	0.27315E 03	0.20272E-02
74	0.16528E-02	0.84088E 03	0.35000E-03	0.61290E 00	0.36252E 00	0.91700E 03	0.27315E 03	0.20515E-02
75	0.18392E-02	0.85545E 03	0.35000E-03	0.60813E 00	0.32923E 00	0.91700E 03	0.27315E 03	0.20808E-02
76	0.20136E-02	0.87198E 03	0.35000E-03	0.60504E 00	0.30516E 00	0.91700E 03	0.27315E 03	0.21152E-02
77	0.21845E-02	0.89199E 03	0.35000E-03	0.60200E 00	0.28841E 00	0.91700E 03	0.27315E 03	0.21570E-02
78	0.24171E-02	0.91894E 03	0.35000E-03	0.59798E 00	0.41691E 00	0.91700E 03	0.27315E 03	0.22138E-02
79	0.27047E-02	0.95358E 03	0.35000E-03	0.59310E 00	0.40052E 00	0.91700E 03	0.27315E 03	0.22875E-02
80	0.29798E-02	0.98977E 03	0.35000E-03	0.58843E 00	0.39510E 00	0.91700E 03	0.27315E 03	0.23652E-02
81	0.32415E-02	0.10245E 04	0.35000E-03	0.58405E 00	0.39660E 00	0.91700E 03	0.27315E 03	0.24403E-02
82	0.34930E-02	0.10570E 04	0.35000E-03	0.57990E 00	0.40533E 00	0.91700E 03	0.27315E 03	0.25119E-02
83	0.37710E-02	0.10996E 04	0.35000E-03	0.58044E 00	0.42509E 00	0.91700E 03	0.27315E 03	0.26087E-02
84	0.43922E-02	0.11726E 04	0.35000E-03	0.55712E 00	0.89146E 00	0.91700E 03	0.27315E 03	0.27677E-02
85	0.53337E-02	0.12691E 04	0.35000E-03	0.52185E 00	0.10000E 01	0.91700E 03	0.27146E 03	0.23770E-02
86	0.64871E-02	0.13592E 04	0.35000E-03	0.48206E 00	0.10000E 01	0.91700E 03	0.27039E 03	0.20344E-02
87	0.77652E-02	0.14174E 04	0.35000E-03	0.44010E 00	0.10000E 01	0.91700E 03	0.26981E 03	0.18573E-02
88	0.93664E-02	0.14388E 04	0.35000E-03	0.38728E 00	0.10000E 01	0.91700E 03	0.26924E 03	0.16344E-02
89	0.11299E-01	0.14193E 04	0.35000E-03	0.32898E 00	0.10000E 01	0.91700E 03	0.26872E 03	0.13884E-02
90	0.13107E-01	0.13848E 04	0.35000E-03	0.28941E 00	0.10000E 01	0.91700E 03	0.26838E 03	0.12214E-02
91	0.14830E-01	0.13452E 04	0.35000E-03	0.25168E 00	0.10000E 01	0.91700E 03	0.26807E 03	0.10622E-02
92	0.16503E-01	0.13082E 04	0.35000E-03	0.21581E 00	0.10000E 01	0.91700E 03	0.26778E 03	0.91076E-03
93	0.18143E-01	0.12752E 04	0.35000E-03	0.19281E 00	0.10000E 01	0.91700E 03	0.26758E 03	0.81371E-03
94	0.19759E-01	0.12451E 04	0.35000E-03	0.17014E 00	0.10000E 01	0.91700E 03	0.26738E 03	0.71802E-03
95	0.21360E-01	0.12173E 04	0.35000E-03	0.14760E 00	0.10000E 01	0.91700E 03	0.26718E 03	0.62290E-03
96	0.23726E-01	0.11790E 04	0.35000E-03	0.11446E 00	0.10000E 01	0.91700E 03	0.26687E 03	0.48306E-03
97	0.26851E-01	0.11327E 04	0.35000E-03	0.70877E-01	0.10000E 01	0.91700E 03	0.26643E 03	0.29912E-03
98	0.29946E-01	0.10916E 04	0.35000E-03	0.27642E-01	0.10000E 01	0.35791E 03	0.00000	0.00000
99	0.33015E-01	0.10552E 04	0.35000E-03	0.00000	0.10000E 01	0.35791E 03	0.00000	0.00000
100	0.36067E-01	0.10231E 04	0.35000E-03	0.00000	0.10000E 01	0.35791E 03	0.00000	0.00000
101	0.41382E-01	0.97609E 03	0.35000E-03	0.00000	0.10000E 01	0.35791E 03	0.00000	0.00000
102	0.48949E-01	0.92187E 03	0.35000E-03	0.00000	0.10000E 01	0.35791E 03	0.00000	0.00000
103	0.56489E-01	0.87784E 03	0.35000E-03	0.00000	0.10000E 01	0.35791E 03	0.00000	0.00000
104	0.64013E-01	0.84079E 03	0.35000E-03	0.00000	0.10000E 01	0.35791E 03	0.00000	0.00000
105	0.71526E-01	0.80885E 03	0.35000E-03	0.00000	0.10000E 01	0.35791E 03	0.00000	0.00000
106	0.79032E-01	0.78086E 03	0.35000E-03	0.00000	0.10000E 01	0.35791E 03	0.00000	0.00000
107	0.86535E-01	0.75594E 03	0.35000E-03	0.00000	0.10000E 01	0.35791E 03	0.00000	0.00000
108	0.94035E-01	0.73360E 03	0.35000E-03	0.00000	0.10000E 01	0.35791E 03	0.00000	0.00000
109	0.10154E 00	0.71332E 03	0.35000E-03	0.00000	0.10000E 01	0.35791E 03	0.00000	0.00000
110	0.10904E 00	0.69471E 03	0.35000E-03	0.00000	0.10000E 01	0.35791E 03	0.00000	0.00000
111	0.11654E 00	0.67753E 03	0.35000E-03	0.00000	0.10000E 01	0.35791E 03	0.00000	0.00000
112	0.12404E 00	0.66158E 03	0.35000E-03	0.00000	0.10000E 01	0.35791E 03	0.00000	0.00000
113	0.13155E 00	0.64663E 03	0.35000E-03	0.00000	0.10000E 01	0.35791E 03	0.00000	0.00000
114	0.13905E 00	0.63271E 03	0.35000E-03	0.00000	0.10000E 01	0.35791E 03	0.00000	0.00000
115	0.14656E 00	0.61962E 03	0.35000E-03	0.00000	0.10000E 01	0.35791E 03	0.00000	0.00000
116	0.15407E 00	0.60729E 03	0.35000E-03	0.00000	0.10000E 01	0.35791E 03	0.00000	0.00000
117	0.16159E 00	0.59563E 03	0.35000E-03	0.00000	0.10000E 01	0.35791E 03	0.00000	0.00000
118	0.16911E 00	0.58452E 03	0.35000E-03	0.00000	0.10000E 01	0.35791E 03	0.00000	0.00000
119	0.17663E 00	0.57390E 03	0.35000E-03	0.00000	0.10000E 01	0.35791E 03	0.00000	0.00000

b. Calculated surface characteristics (continued)

Figure 6.4: continued

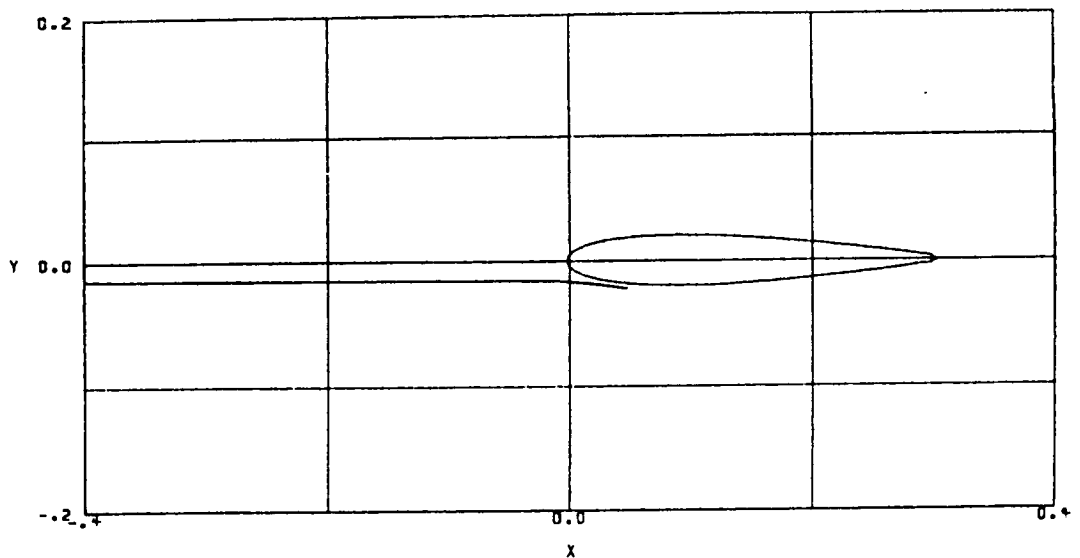| SEG	S	HTC	XK	BETA	FFRAC	RI	TSURF	DICE
120	0.18415E 00	0.56370E 03	0.35000E-03	0.00000	0.10000E 01	0.35791E 03	0.00000	0.00000
121	0.19167E 00	0.55383E 03	0.35000E-03	0.00000	0.10000E 01	0.35791E 03	0.00000	0.00000
122	0.19920E 00	0.54424E 03	0.35000E-03	0.00000	0.10000E 01	0.35791E 03	0.00000	0.00000
123	0.20673E 00	0.53492E 03	0.35000E-03	0.00000	0.10000E 01	0.35791E 03	0.00000	0.00000
124	0.21427E 00	0.52580E 03	0.35000E-03	0.00000	0.10000E 01	0.35791E 03	0.00000	0.00000
125	0.22180E 00	0.51689E 03	0.35000E-03	0.00000	0.10000E 01	0.35791E 03	0.00000	0.00000
126	0.22934E 00	0.50814E 03	0.35000E-03	0.00000	0.10000E 01	0.35791E 03	0.00000	0.00000
127	0.23688E 00	0.49944E 03	0.35000E-03	0.00000	0.10000E 01	0.35791E 03	0.00000	0.00000
128	0.24442E 00	0.49077E 03	0.35000E-03	0.00000	0.10000E 01	0.35791E 03	0.00000	0.00000
129	0.25197E 00	0.48216E 03	0.35000E-03	0.00000	0.10000E 01	0.35791E 03	0.00000	0.00000
130	0.25951E 00	0.47349E 03	0.35000E-03	0.00000	0.10000E 01	0.35791E 03	0.00000	0.00000
131	0.26706E 00	0.46460E 03	0.35000E-03	0.00000	0.10000E 01	0.35791E 03	0.00000	0.00000
132	0.27462E 00	0.45518E 03	0.35000E-03	0.00000	0.10000E 01	0.35791E 03	0.00000	0.00000
133	0.28218E 00	0.44424E 03	0.35000E-03	0.00000	0.10000E 01	0.35791E 03	0.00000	0.00000
134	0.28974E 00	0.42981E 03	0.35000E-03	0.00000	0.10000E 01	0.35791E 03	0.00000	0.00000
135	0.29656E 00	0.41048E 03	0.35000E-03	0.00000	0.10000E 01	0.35791E 03	0.00000	0.00000
136	0.30112E 00	0.39015E 03	0.35000E-03	0.00000	0.10000E 01	0.35791E 03	0.00000	0.00000
137	0.30416E 00	0.36936E 03	0.35000E-03	0.00000	0.10000E 01	0.35791E 03	0.00000	0.00000
138	0.30721E 00	0.31466E 03	0.35000E-03	0.00000	0.10000E 01	0.35791E 03	0.00000	0.00000

b. Calculated surface characteristics (continued)

Figure 6.4: Concluded

VELOCITY (M/S)   129.00
TEMPERATURE (C)   -12.60
PRESSURE (KPA)   90.75
HUMIDITY (%)   100.00
LWC (G/M**3)   0.50
DROP DIAM (MICRONS)   20.00
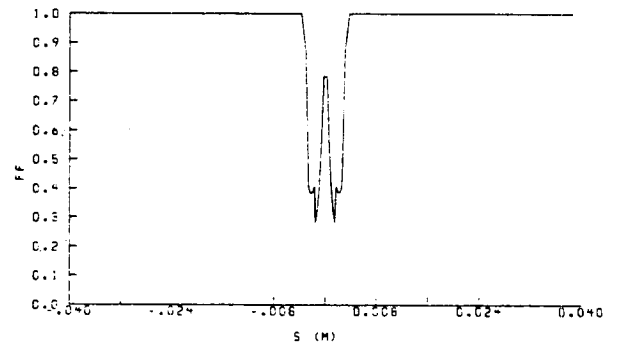TIME (SEC)   0.00

0.2

Y 0.0

-.2
       -.4   0.0   0.4
                              X
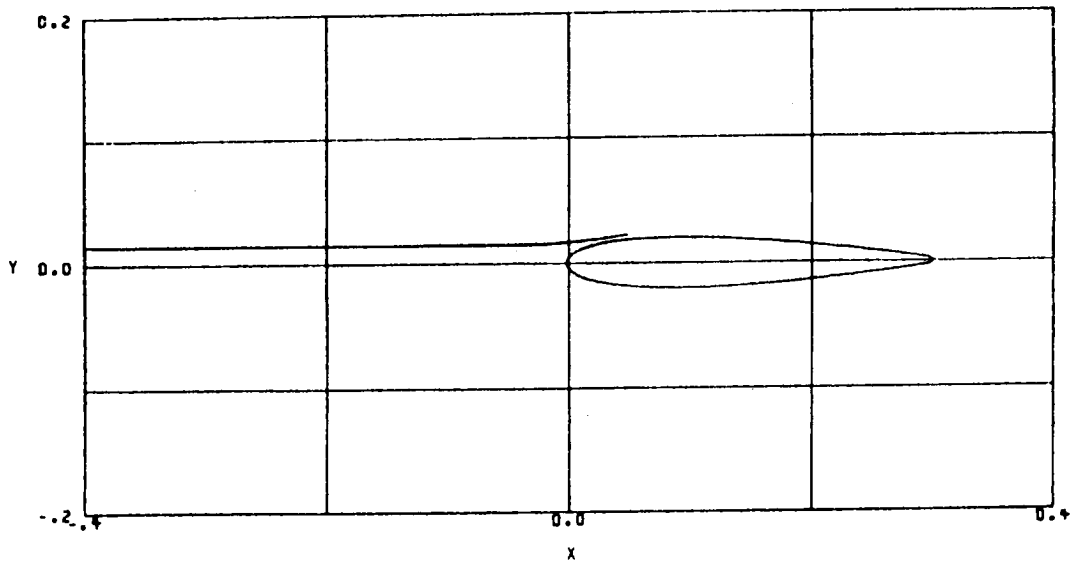
a. Trajectory of particle released from Y0MAX

VELOCITY (M/S)   129.00
TEMPERATURE (C)   -12.60
PRESSURE (KPA)   90.75
HUMIDITY (%)   100.00
LWC (G/M**3)   0.50
DROP DIAM (MICRONS)   20.00
TIME (SEC)   0.00

0.2

Y 0.0

-.2
       -.4   0.0   0.4
                              X

b. Trajectory of particle released from Y0MIN

Figure 6.5: Examples of droplet trajectory plots from Example 1.

81

```
VELOCITY (M/S)          129.00
TEMPERATURE (C)         -12.60
PRESSURE (KPA)           90.75
HUMIDITY (%)            100.00
LWC (G/M**3)              0.50
DROP DIAM (MICRONS)      20.00
TIME (SEC)               0.00
```

```
IW=     1
YO=  0.00000
S =  0.00000
```
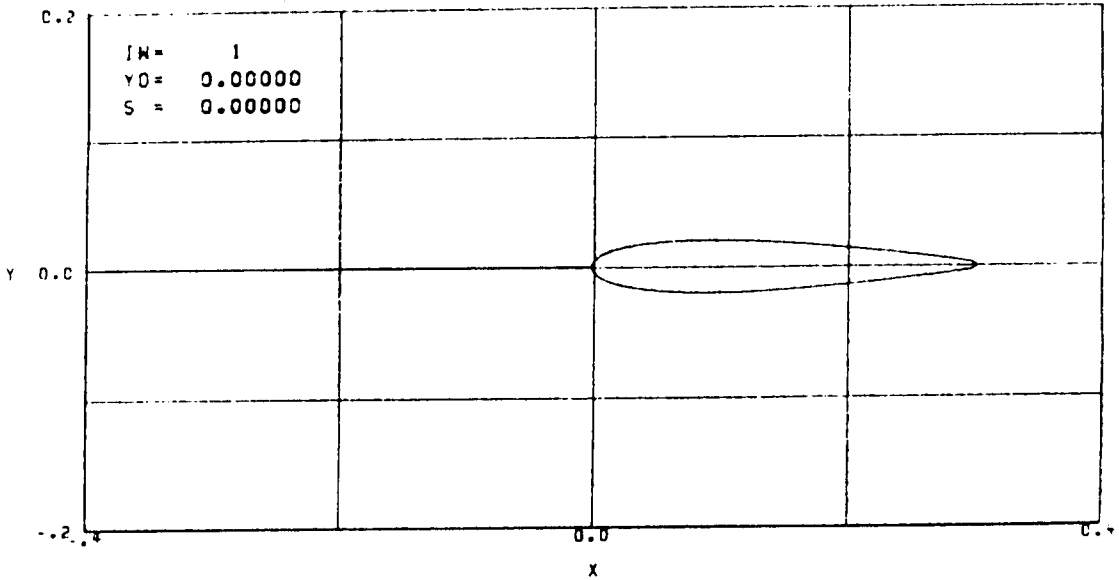
c. Trajectory released from $\frac{YOMAX+YOMIN}{2}$

```
VELOCITY (M/S)          129.00
TEMPERATURE (C)         -12.60
PRESSURE (KPA)           90.75
HUMIDITY (%)            100.00
LWC (G/M**3)              0.50
DROP DIAM (MICRONS)      20.00
TIME (SEC)               0.00
```
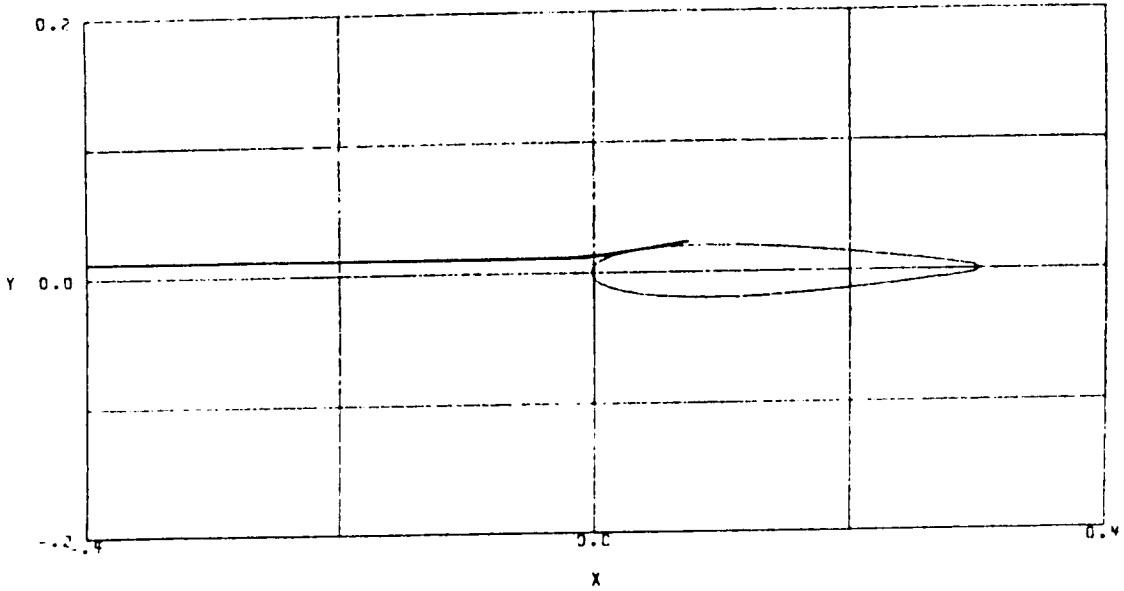
d. Trajectory calculated while searching for the upper impingement limit.

Figure 6.5: continued

82

```
VELOCITY (M/S)          129.00
TEMPERATURE (C)         -12.60
PRESSURE (KPA)           90.75
HUMIDITY (%)            100.00
LWC (G/M**3)              0.50
DROP DIAM (MICRONS)      20.00
TIME (SEC)               0.00
```
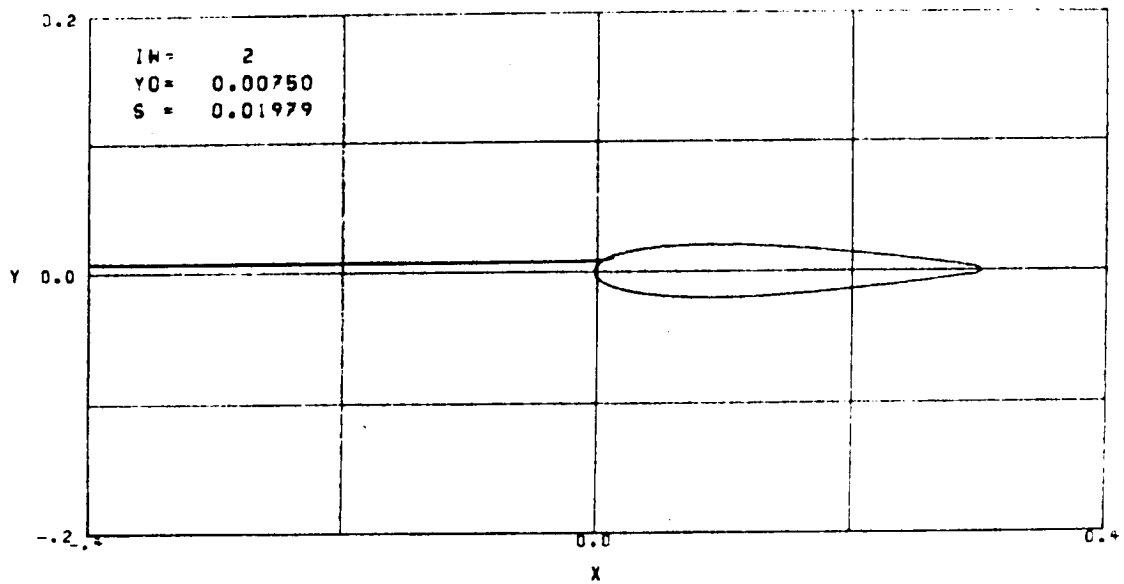

e. Trajectory calculated while searching for the upper impingement limit.

Figure 6.5: Concluded
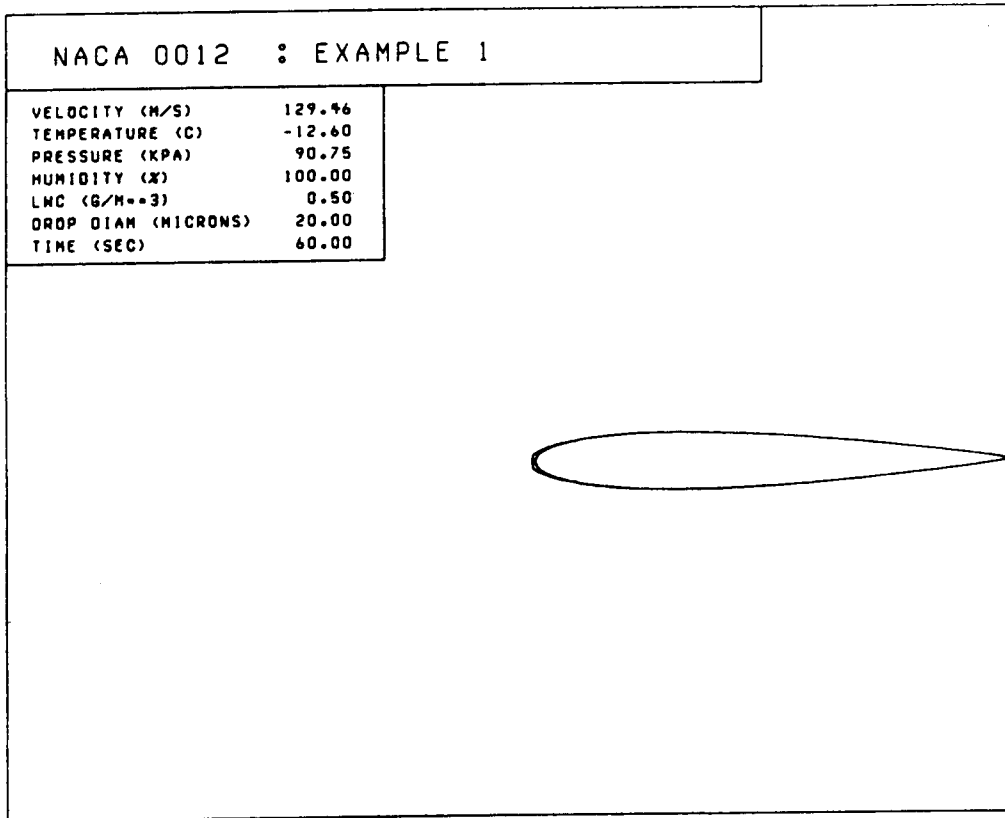
a. Percent plotted = 100%
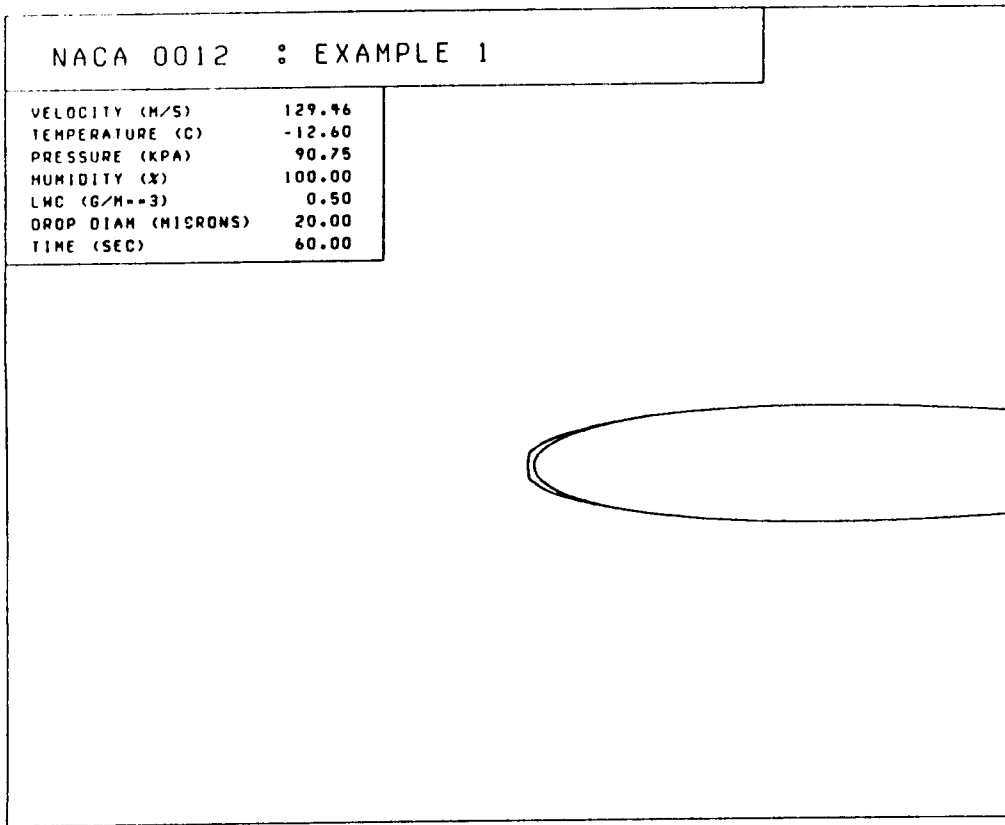
b. Percent plotted = 50%

Figure 6.6: Size of the plotted geometry as a function of the percent plotted.
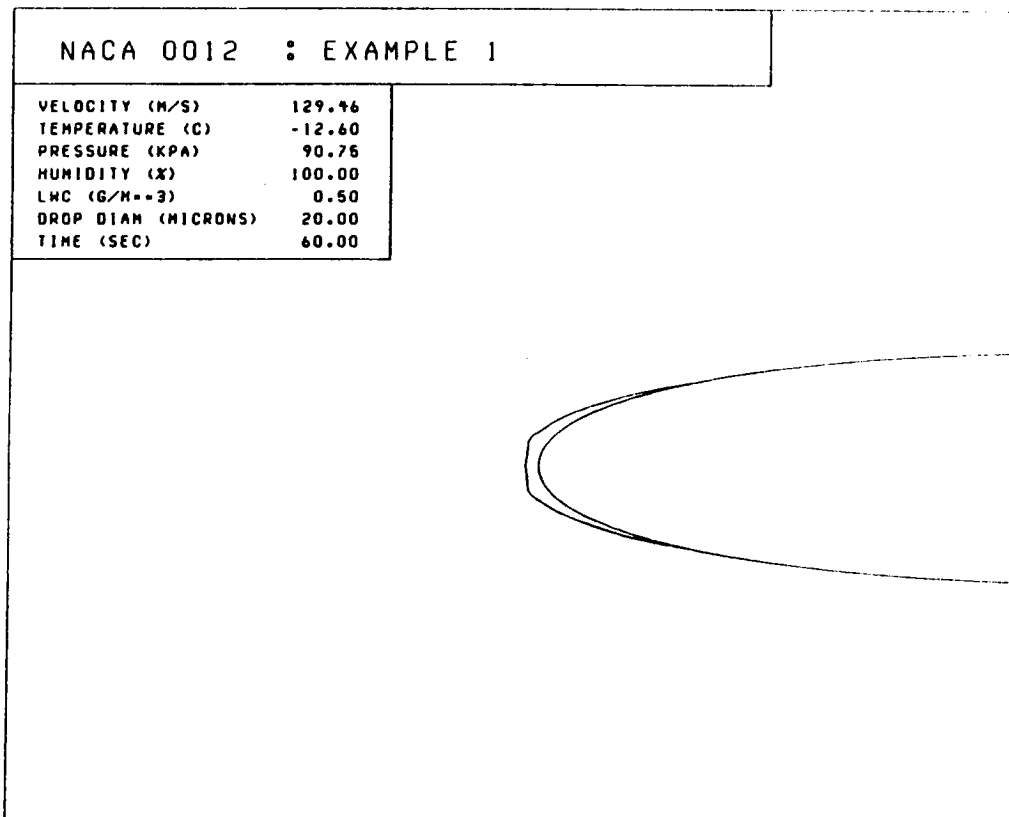
c. Percent plotted = 25%

Figure 6.6: Concluded

VELOCITY (M/S)	129.46
TEMPERATURE (C)	-12.60
PRESSURE (KPA)	90.75
HUMIDITY (%)	100.00
LHC (G/M**3)	0.50
DROP DIAM (MICRON)	20.00
TIME (SEC)	60.00
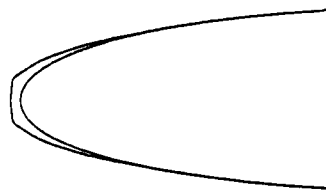
a. Iced airfoil geometry
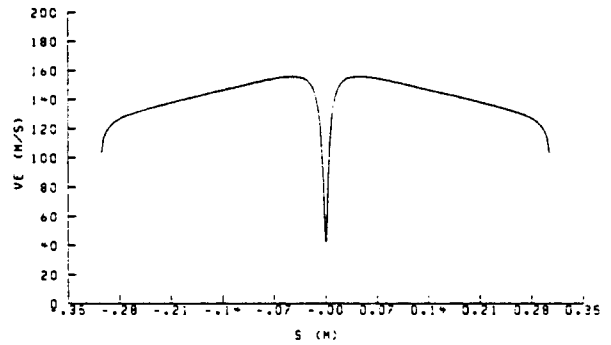
d. Edge velocity vs. surface location
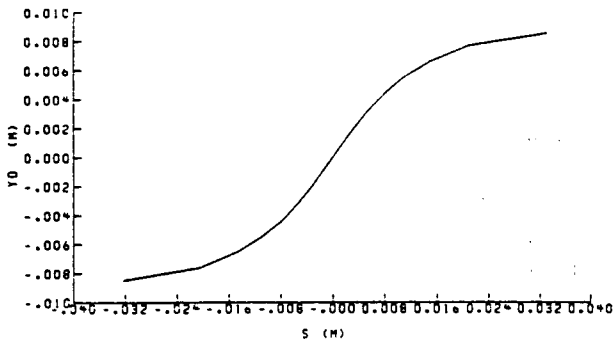
b. Particle release position vs. surface
    impact distance
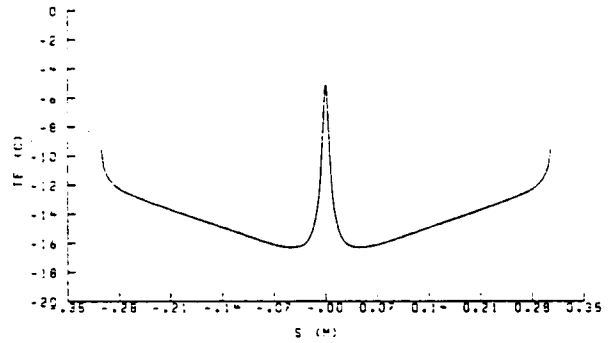
e. Edge temperature vs. surface location
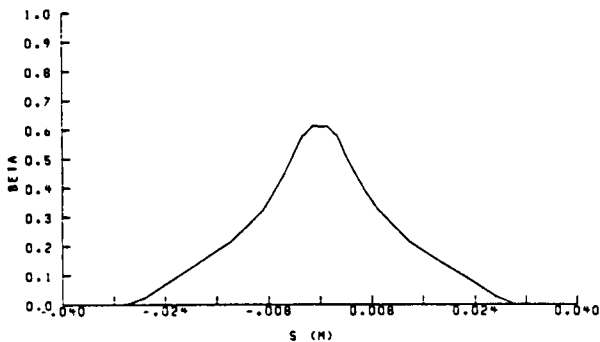
c. Local collection efficiency vs. surface
    location
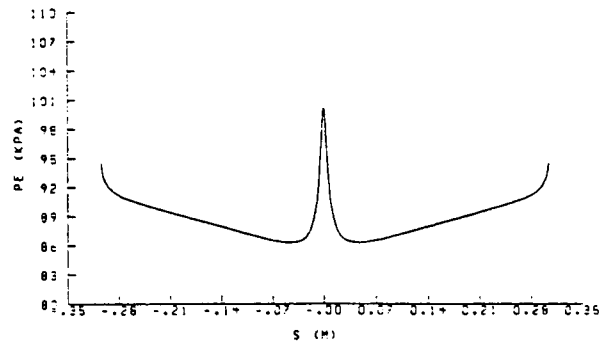
f. Edge pressure vs. surface location

Figure 6.7 Icing parameter plots for the first timestep of Example 1.

VELOCITY (M/S)	129.46
TEMPERATURE (C)	-12.60
PRESSURE (KPA)	90.75
HUMIDITY (%)	100.00
LWC (G/M**3)	0.50
DROP DIAM (MICRON)	20.00
TIME (SEC)	60.00
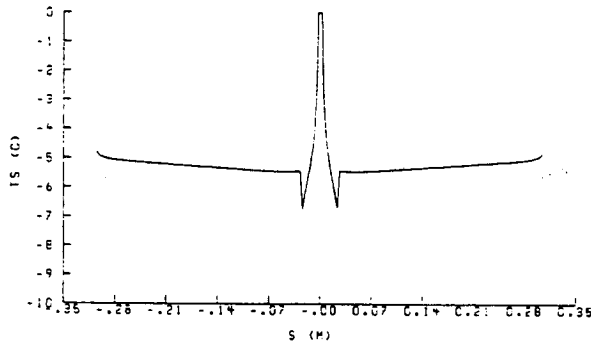
g. **Equilibrium surface temperature vs. surface location**
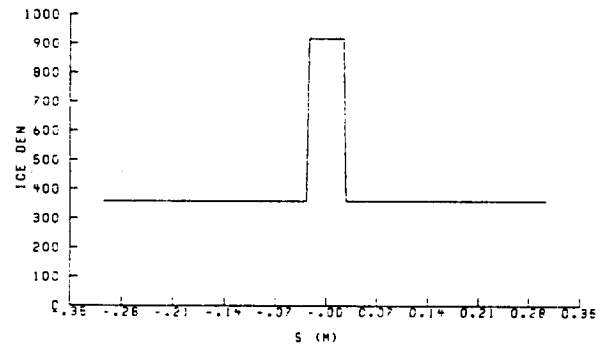
j. **Ice density vs. surface location**
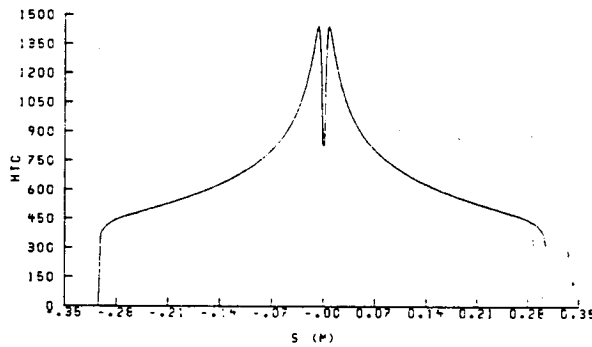
h. **Convective heat transfer coefficient vs. surface location**

k. **Freezing fraction vs. surface location**
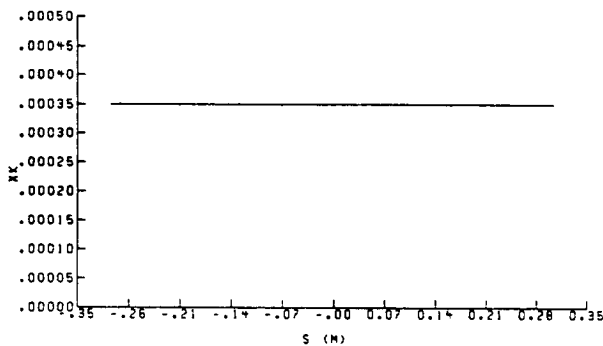
i. **Equivalent sand-grain roughness height vs. surface location**

Figure 6.7: Concluded.

87

Chapter 7

EXAMPLE CASES

In this section, the capabilities of LEWICE are illustrated through the presentation of five example cases. These examples include the input data sets and the printed and plotted output data; however, printed output is included for example 1 only.

7.1 Example 1: Glaze Icing on a NACA 0012 Airfoil, $\alpha = 0.0^o$

In this example, a 2-minute glaze ice accretion will be formed on a NACA 0012 airfoil at an angle of attack of 0.0 degree. The accretion will be formed in two 1-min timesteps. The icing conditions are shown below:

Velocity	= 129.46 m/s
Static Temperature	= 260.55 K
Static Pressure	= 90748.0 Pa
LWC	= 0.50 g/m^3
Droplet Diameter	= 20.0 microns (monodispersed cloud)
Roughness Height	= 0.00035 m

The input file and the interactive input for the first timestep in Example 1 are shown in Figures 7.1a and b, respectively. Plot option 3 was selected in the interactive input, therefore, the particle trajectories and icing parameters were plotted. Figures 6.5a-e show the first five particle trajectory plots from this example case. Figures 6.5a and b show the trajectories of particles released from Y0MAX and Y0MIN. As discussed in Chapter 5, these trajectories are calculated to identify the release point of a particle that passes above the body and one that passes below the body. These calculations are performed in subroutine RANGE.

After locating an upper and lower boundary trajectory, the search for the upper and lower impingement limit is begun by releasing a particle from a position halfway between the release points of the two trajectories identified in Figures 6.5a and b. When a particle impinges on the body,

the particle number (IW), particle release ordinate (Y0), and the surface impact distance (S) are displayed, as shown in Figure 6.5c. Using the Newton iteration scheme described in Chapter 4.2.6, the search for the upper impingement limit is continued, as shown in Figures 6.5d and e. These calculations are performed in subroutine IMPLIM. When plot option 3 is selected, all of the trajectories will be plotted. Only the first five have been shown in this example.

After calculating the particle trajectories, the program will prompt the user to preview the y_0 vs. s data or to continue with the collection efficiency calculation with the following statement.

ENTER 1 TO PREVIEW Y0 VS S DATA
ENTER 0 TO CONTINUE WITH THE COLLECTION EFFICIENCY CALCULATION (I1)

If option 1 is selected and the axes limits are specified as follows:

smin	= -0.04	smax	= 0.04
$y_0$min	= -0.01	$y_0$max	= 0.01

the y_0 vs. s points calculated in subroutine COLLEC will be plotted as shown in Figure 7.2. Upon producing the plot, the following statement will be printed on the screen:

THE CALCULATED SURFACE IMPACT DISTANCES (S) AND RELEASE POINTS (Y0) ARE AS FOLLOWS

I	Y0	S	I	Y0	S
1	0.00850	0.03378	10	-0.00109	-0.00178
2	0.00765	0.02078	11	-0.00218	-0.00355
3	0.00656	0.01489	12	-0.00327	-0.00555
4	0.00546	0.01090	13	-0.00436	-0.00797
5	0.00437	0.00801	14	-0.00545	-0.01085
6	0.00328	0.00557	15	-0.00654	-0.01484
7	0.00219	0.00357	16	-0.00763	-0.02072
8	0.00110	0.00180	17	-0.00848	-0.03167
9	0.00001	0.00001	18	0.00000	0.00000

HOW MANY TRAJECTORIES ARE TO BE DELETED BEFORE THE COLLECTION EFFICIENCY CALCULATION? (I2)

At this time, y_0 vs. s points can be removed, if necessary. Non-physical impact locations can occur when inaccurate flow fields are calculated around the horns of glaze ice accretions. In this example, it is not necessary to remove any points, so option 0 was selected.

The title of the run, icing condition parameters, ice accretion data, and parameter plot menu are then printed on the screen as follows:

NACA 0012 : EXAMPLE 1   : TIME = 60.000 SEC
ICING CONDITION:

STATIC TEMPERATURE (C)	260.55
STATIC PRESSURE (PA)	90748.00
VELOCITY (M/S)	129.00
LWC (G/M^3)	0.50
DROPLET DIAMETER (MICRONS)	20.00

ICE ACCRETION DATA

STAGNATION POINT	70
TRANSITION POINTS (LOWER,UPPER)	68 71
ICING LIMITS (LOWER,UPPER)	42 97
NUMBER OF POINTS	139
NUMBER OF SEGMENTS ADDED	0

AVAILABLE PLOT OPTIONS

```
     0  -  NO PLOTS
     1  -  ICED GEOMETRY
     2  -  Z VS S
     3  -  BETA VS S
     4  -  VE VS S
     5  -  TE VS S
     6  -  PE VS S
     7  -  TSURF VS S
     8  -  HTC VS S
     9  -  XK VS S
    10  -  ICE DENSITY VS S
    11  -  FFRAC VS S
```
ENTER OPTIONS NUMBER (12)

C-2

All of the parameter plots for the first time-step are shown in Figures 6.7a-k. When the option for no plots is selected, the computer will respond with the following message:

TIME STEP COMPLETE: TIME = 60.0

ICING TIME INPUT HAS BEEN REACHED

PROGRAMS OPTIONS
      1 - CONTINUE ICING, USE PREVIOUS FLOW FIELD
      2 - CONTINUE ICING, CALCULATE NEW FLOW FIELD
      3 - TERMINATE PROGRAM

Since a second 1-min timestep with a new flow field calculation is desired, option 2 is selected.

The second timestep proceeds in a manner similar to the first. The plots, computer prompts, and responses are shown in the order of their occurrence in Figure 7.3. The printed output from the first timestep in this example is shown in Figures 6.1-6.4. The icing parameter plots for the second timestep are shown in Figure 7.4a-k. The printed output for the second timestep is shown in Figure 7.5.

The overall accuracy of LEWICE is checked by comparing calculated and experimental ice accretion shapes. The experimental ice accretion for the condition was obtained by Gent (Reference 20), and is compared to the calculated shape in Figure 7.6.

7.2   Example 2: Glaze Icing on a NACA 0012 Airfoil, $\alpha = 4.0^o$

This example is identical to Example 1 except that the airfoil is now at a 4.0 angle of attack. The icing time for this condition is also 2-minute and the accretion is formed in two 1-minute timesteps. The input file is shown in Figure 7.7. Note that the value of CLT in namelist S24Y is now equal to 4.0.

Figures 7.8 show the particle trajectories calculated in subroutine RANGE, where the program searches for a trajectory that passes above

and below the body. More accurate selections of YOMIN and YOMAX would have resulted in fewer trajectories being calculated while the code searches for the two boundary trajectories. The first three trajectories calculated in subroutine IMPLIM are shown in Figures 7.9. These trajectories are calculated while the program was searching for the upper surface impingement limit. No additional trajectories will be shown for this example, but all trajectories will be plotted when plot option 3 is selected. The y_0 vs. s points calculated in subroutine COLLEC are shown in Figure 7.10. After the plot is completed, the following prompts are printed to the screen to allow the user to remove any incorrect points:

THE CALCULATED SURFACE IMPACT DISTANCES (S) AND
RELEASE POINTS (YO) ARE AS FOLLOWS

I	YO	S	I	YO	S
1	-0.11162	0.01610	10	-0.12296	-0.00836
2	-0.11263	0.01042	11	-0.12425	-0.01156
3	-0.11392	0.00727	12	-0.12554	-0.01528
4	-0.11521	0.00473	13	-0.12683	-0.01979
5	-0.11650	0.00276	14	-0.12812	-0.02534
6	-0.11779	0.00081	15	-0.12942	-0.03270
7	-0.11908	-0.00103	16	-0.13071	-0.04386
8	-0.12037	-0.00315	17	-0.13171	-0.06252
9	-0.12167	-0.00561	18	0.00000	0.00000

HOW MANY TRAJECTORIES ARE TO BE DELETED BEFORE
THE COLLECTION EFFICIENCY CALCULATION? (12)

As in Example 1, option 0 was selected because it was not necessary to remove any points. The program then entered displays the plot menu to the screen, and the plots shown in Figures 7.11a-i were obtained. The results of the first timestep are similar to those obtained in Example 1.

After plot option 0 was selected, the prompts for the program option were printed, and, as in Example 1, option 2 was selected. The plot option was not changed from the first timestep and the calculation of the potential flow field was begun. When the program entered subroutine STAG, it was found that two "stagnation points" had been calculated. This is indicated by the following message and prompt:

2 STAGNATION POINTS HAVE BEEN CALCULATED. ENTER 1 TO SHOW THE LOCATIONS OF THE CALCULATED STAGNATION POINTS. ENTER 0 TO DISPLAY OPTIONS.

When this situation occurs, it may be necessary to form a pseudo-surface over the region where the multiple stagnation points exist. The procedure to form the pseudo-surface is described in the following section. Appendix C discusses additional causes for the calculation of multiple stagnation points.

7.2.1 Application of the Pseudo-Surface

In normal operation, select option 1 to display the locations of the stagnation points. The locations of the stagnation points are indicated by X's, as shown in Figure 7.12. After displaying the plot, the x, y, and s locations of the stagnation points will be displayed, and the user will be asked either to select one of the points for use as the stagnation point in the remaining calculations, or to form the pseudo-surface.

THE FOLLOWING MULTIPLE STAGNATION POINTS HAVE BEEN CALCULATED

I	X	Y	S
57	-0.00089	-0.00336	0.00123
59	-0.00111	-0.00309	0.00172

AVAILABLE OPTIONS

0 - CONTINUE CALCULATIONS WITH MANUALLY-SELECTED STAGNATION POINT

1 - RECOMPUTE FLOW FIELD USING A PSEUDO-SURFACE

In this example, option 1 was selected.

In Figure 7.12, the axes scales were such that it was difficult to identify the locations of the stagnation points. Therefore, the user will be asked if the plotting scales should be changed to enlarge the region of interest. In this example, the axes limits were changed as shown below:

$$x_{max} = y_{max} = 0.02$$

$$x_{min} = y_{min} = -0.02$$

The locations of the stagnation points will then be re-plotted using the new axes limits, as shown in Figure 7.13.

The circular arc that will be placed over the multiple stagnation points is defined by specifying two points on the arc and the radius. The two points on the arc are the locations where the pseudo-surface intersects the actual ice surface. The best results are obtained when the ends of the pseudo-surface arc intersect on a tangent to the ice surface. Figure 7.13 shows that this may be possible near y values near -0.006 and -0.001. These values are input by the user as shown below:

ENTER THE Y COORDINATE OF THE DESIRED LOWER
LIMIT OF THE PSEUDO-SURFACE (F10.0)
-.006
ENTER THE Y COORDINATE OF THE DESIRED UPPER
LIMIT OF THE PSEUDO-SURFACE (F10.0)
-.001

The computer will respond with the two body coordinates closest to the desired upper and lower limits as shown below:

THE POINTS CLOSEST TO THE LOWER LIMIT ARE
   X=   0.0019641   Y= -0.0065025   I= 52
   X=   0.0012161   Y= -0.0055978   I= 53
THE POINTS CLOSEST TO THE UPPER LIMIT ARE
   X= -0.0028274   Y= -0.0010464   I= 74
   X= -0.0029714   Y= -0.0008570   I= 75

The user is then prompted to enter the segment number of the desired upper and lower limits. In this example, segments 52 and 75 were selected as the lower and upper limits of the pseudo-surface, respectively. The program will then request that a radius be input. In this example the radius is 0.03. The input of these values is shown below.

ENTER THE I VALUE OF THE DESIRED LOWER AND UPPER
LIMITS (2I3) 52 75
ENTER THE DESIRED RADIUS (F10.0) .03

Because the selection of an appropriate radius is a manual iteration, there are no general criteria for selecting a radius. If an arc with the desired

radius cannot be formed between the two points specified, the program will respond by asking for another radius. The iced airfoil with the pseudo-surface will then be plotted, as shown in Figure 7.14. After the plot is completed, the following menu is displayed:

THE FOLLOWING OPTIONS ARE NOW AVAILABLE (11)
- 0 - SPECIFY NEW UPPER AND LOWER LIMITS
- 1 - SPECIFY A NEW RADIUS
- 2 - PSEUDO-SURFACE SATISFACTORY, CONTINUE CALCULATIONS
- 3 - PSEUDO-SURFACE UNSATISFACTORY, CONTINUE CALCULATIONS WITH THE ACTUAL ICE SURFACE

At this time, new upper and lower limits or a new radius can be selected, and the above procedure will be repeated. Option 2 will cause the program to re-calculate the flow field using the pseudo-surface. Option 3 is selected when a satifactory pseudo-surface cannot be formed and any errors in the flow field must be accepted. In this example, the pseudo-surface was satisfactory, therefore, option 2 was selected.

While it did not occur in this example, multiple stagnation points may still be calculated after the pseudo-surface has been formed. Unless a smoother pseudo-surface can be formed, it is usually best to select one of the points and continue with the calculations. Select the point that is closest to the stagnation point calculated in the previous timestep. This point can be identified by the value of surface distance, s. (Recall that s = 0.0 denotes the stagnation point.)

In this example, a single stagnation point was calculated when the pseudo-surface was placed on the iced surface, and the second timestep proceeded in a manner similar to the first. It was not necessary to remove any y_0 vs. s points from the plot shown in Figure 7.15 when the following prompt was displayed:

HOW MANY TRAJECTORIES ARE TO BE DELETED BEFORE THE COLLECTION EFFICIENCY CALCULATION? (12)

The plots obtained from the plot menu for the second timestep are shown in Figures 7.16a-i. The calculated airfoil shape is compared to the

experimental ice accretion shape, obtained from Reference 20, in Figure 7.17.

7.3 Example 3: Rime Icing on an NACA 0012 Airfoil, $\alpha = 0.0^o$

In this example, ice will be accreted on an NACA 0012 airfoil at an angle of attack of 0.0 for 2 min. As in Examples 1 and 2, the accretion will be formed in two 1-min time steps. The icing conditions, which should produce a rime ice accretion, are as follows:

Velocity	= 64.73 m/s
Static Temperature	= 260.55 K
Static Pressure	= 90748.0 Pa
LWC	= 0.50 g/m^3
Droplet Diameter	= 20.0 microns (monodispersed cloud)
Roughness Height	= 0.00025 m

The input file for this example is shown in Figure 7.18.

The program executes in a manner similar to Example 1. The parameter plots for the first and second timesteps are shown in Figures 7.19a-i and 7.20a-i, respectively. The predicted ice accretion shape is compared to the experimental shape (Reference 20) in Figure 7.21.

As discussed in Section 4.3.1, the difference between rime and glaze ice is determined by the calculated value of the freezing fraction, f (FFRAC in LEWICE). Figure 7.19k shows that the freezing fraction was equal to 1.0 over the entire surface for the first timestep. This would be indicative of a solid rime ice accretion. On the second timestep, the freezing fraction was slightly less than 1.0 near the stagnation point, as shown in Figure 7.20k. This indicates that the accretion is starting to take on some glaze ice accretion characteristics in that region, and would therefore constitute a mixed ice accretion. Glaze characteristics become more evident as the freezing fraction approaches 0.0. Experimentally, these initial glaze characteristics would probably not be observed until the ice accretion grew larger and the size of the glaze portion increased.

7.4 Example 4: Specification of a Droplet Size Distribution

The atmospheric conditions in this example are identical to those in Example 1. However, in this example, a droplet size distribution was used to characterize the icing cloud instead of a single droplet size. The icing time for this case is 60.0 sec, and the ice will be accreted in a single timestep.

The droplet size distribution was specified to have a normal volume (mass) distribution with a mean of 20 microns and $\sigma = 5$, as shown in Figure 7.22. As discussed in Section 4.2.5.1, the droplet size distribution is input into the code by specifying the mass fraction corresponding to a discrete droplet diameter. The procedure for quantifying a known distribution for input into LEWICE is discussed below.

The volume fraction (fraction LWC) corresponding to each droplet size used to produce Figure 7.22 is shown in Table 7.1. The cumulative volume fraction (CVF) is calculated for each droplet size, d_i, using the equation

$$CVF_i = CVF_{(i-1)} + \frac{V_{f_i}}{\Sigma V_{f_i}} \qquad (29)$$

The resulting plot of CVF vs. d is shown in Figure 7.23. For input into LEWICE, the droplet size range must be divided into a number of discrete droplet size bins of a constant width. The size of the bin width is arbitrary, but no more than 10 bins can be input to the code. Using more bins will increase the accuracy of the calculations but will also increase computational time. Five bins with a width of 8.0 microns were used in this example. The droplet diameter corresponding to the middle and the right-hand side of each bin is shown in Table 7.2.

97

Table 7.1 Volume Fraction for a Normal Mass Distribution of Droplet Size with a Mean of 20mm and $\sigma = 5$

d (microns)	Volume Fraction
0	0.0000
2	0.0002
4	0.0010
6	0.0032
8	0.0090
10	0.0216
12	0.0444
14	0.0776
16	0.1158
18	0.1474
20	0.1596
22	0.1474
24	0.1158
26	0.0776
28	0.0444
30	0.0216
32	0.0090
34	0.0032
36	0.0010
38	0.0002
40	0.0000

The cumulative volume fraction at the right-hand side of each bin must be determined using the data in Table 7.1 and Figure 7.23 using the following equation:

$$V_{f_i} = CVF_i - CVF_{i-1} \tag{30}$$

This volume fraction is assigned to the droplet size at the middle of the bin and assumes a uniform distribution of droplets inside the bin. The values of V_{f_i} for each droplet size bin are shown in Table 7.2. This data is input into LEWICE using namelist DIST, as shown in Figure 7.24.

Table 7.2 Volume Fraction for Each Droplet Size Bin Specified in Example 4

Bin	Droplet Diameter Middle	Droplet Diameter Right-Hand Endpoint	Cumulative Volume Fraction	Volume Fraction
1	4	8	0.0082	0.0082
2	12	16	0.2119	0.2037
3	20	24	0.7881	0.5762
4	28	32	0.9918	0.2037
5	36	40	1.0000	0.0082

When a droplet size distribution is input, the execution of the program is similar to when a single droplet size is specified. The difference is that the particle trajectory calculations must be performed for each droplet size specified. Since five discrete droplet sizes were specified in this example, the impingement limits and y_0 vs. s data were calculated for each of the droplet sizes. This will require significantly more computational time.

This example will require user interaction when asked to preview the y_0 vs. s data. This question will be asked for each droplet diameter, and the user will have the opportunity to remove points from each set of y_0 vs. s data. The procedure for removing the points was discussed in Example 1.

Figures 7.25a-o show the plotted output created from the plot menu. Note that Figures 7.25b-f show the y_0 vs. s curves for each of the droplet diameters specified. These plots are made from a single selection of plot option 2. The user will be requested to input the axes limit for each set of y_0 vs. s data. The total local collection efficiency curve (Figure 7.25g) is calculated by summing the contributions from each of the droplet diameters, as described in Section 4.2.5.1. The local collection efficiency for each droplet size is not stored by the program.

Recall that in Example 1, an ice accretion was formed for this same icing condition except that a single droplet diameter of 20 microns was specified. A comparison of the local collection efficiency from the first timestep of

99

Examples 1 and 4 is shown in Figure 7.26. The local collection efficiency curves are similar near the stagnation point (s = 0.0). However, the region over which droplets impinge is much greater when a droplet distribution is specified because of the presence of the larger droplets. This result is similar to that concluded by previous investigators (Chang, Reference 13).

The increased region of droplet impingement is also noticeable in comparisons among the predicted ice accretion shapes. However, because of the small amount of mass present at the impingement limits, the effect on the total ice accretion shape is small. These results are not sufficient for determining the total effect of using a multidispersed droplet size distribution to characterize an icing cloud as opposed to a monodispersed distribution. The effect of wider distributions with similar mass median droplet diameters must be evaluated. The effects must also be determined for various types of icing conditions and ice accretions.

7.5   Example 5: Thermal Anti-icing

The formulation of the thermodynamic equations in LEWICE allows the surface of the body to be a heat source or sink. However, since conduction through an existing ice layer is not modeled, the equations are valid only on the first timestep when ice is accreted on the clean airfoil. Also, since the melting of previously deposited ice from the surface of the body is not modeled, the equations are not applicable to a de-icing system. They are applicable, however, to the evaluation of a thermal anti-icing system. This example demonstrates the capability of LEWICE to determine the minimum thermal anti-icing heating requirements for maintaining an ice-free surface for a specified set of icing conditions. A discussion of the applicability of the thermodynamic model is presented in Appendix A.

The NACA 0012 airfoil evaluated in this example has an electro-thermal anti-icing heater covering the first 20 percent of the airfoil, as shown in Figure 7.27. A uniform heat flux of 6000.0 W/m² was specified over the entire surface. Lewice is to be applied to determine whether this heat flux is sufficient to maintain an ice-free surface at the following icing condition:

Angle of attack   = 6.0
Velocity   = 128.41 m/sec

100

Static Temperature	= 265.0 K
Static Pressure	= 90748.0 Pa
LWC	= 0.50 g/m^3
Droplet Diameter	= 20.0 microns
Roughness Height	= 0.0002 m

The input file is shown in **Figure 7.28**. The heat flux from the surface (into the thermodynamic control volume) is input in namelist ICE through the variable QCOND.

The icing time for this case was arbitrarily specified to be 120.0 sec so that any ice that did form would be easily visible on the plots. No user interaction, except the standard responses discussed in Examples 1 and 3, was required. As shown in **Figure 7.29a**, the heat input was not sufficient to maintain an ice-free surface. The ice accretion on the lower surface was formed as liquid water flowed off the heater and onto the colder airfoil surface. This result indicates that it is possible for ice to form aft of the heater but, since the shedding of water droplets from the surface are not modeled, the amount of ice may be over-predicted. The ice accretion on the upper surface was formed on the heater itself because the increased velocity (**Figure 7.29d**) over the upper surface caused a large decrease in the local static temperature (**Figure 7.29e**). It is also interesting to note the calculated surface temperature and convective heat transfer coefficient profiles over the surface (**Figures 7.29g** and **h**, respectively). The convective heat transfer was at a maximum on the upper surface which, when combined with the decreased local static temperature, contributed to the ice growth. The surface temperature profile shows that the temperature was greater than 0.0° C over a large portion of the heater, but was less than 0.0 over a small portion of the upper surface.

These results indicate that the heat flux should be increased in this region to maintain an ice-free surface. The actual minimum icing requirement could be determined by incrementally increasing the heat input and re-calculating the ice accretion shape. Unfortunately, there was no experimental data to verify these calculations. This example was presented to demonstrate the capability of the thermal model. It is expected that this capability be further exercised to evaluate its accuracy.

```
NACA 0012  : EXAMPLE 1
&S24Y
ILIFT= 1
IPARA= 1
IFIRST= 3
ISECND= 3
IPVOR= 1
INCLT= 0
CLT= 0.0
ICHORD= 0
CCL= 0.0
IND= 1
ISOL= 0
IPRINT= 0
IFLLL= 1
&END
```

```
   1.0000300    0.9899999    0.9800000    0.9700000    0.9500000    0.9250000   6 0 3
   0.9000000    0.8750000    0.8500000    0.8250000    0.8000000    0.7750000   6 0 3
   0.7500000    0.7250000    0.7000000    0.6750000    0.6500000    0.6250000   6 0 3
   0.6000000    0.5750000    0.5500000    0.5250000    0.5000000    0.4750000   6 0 3
   0.4500000    0.4250000    0.4000000    0.3750000    0.3500000    0.3250000   6 0 3
   0.3000000    0.2750000    0.2500000    0.2250000    0.2000000    0.1750000   6 0 3
   0.1500000    0.1250000    0.1000000    0.0900000    0.0800000    0.0700000   6 0 3
   0.0600000    0.0500000    0.0450000    0.0400000    0.0350000    0.0300000   6 0 3
   0.0250000    0.0200000    0.0150000    0.0100000    0.0075000    0.0050000   6 0 3
   0.0037500    0.0025000    0.0022500    0.0020000    0.0017500    0.0015000   6 0 3
   0.0012500    0.0010000    0.0008750    0.0007500    0.0006250    0.0005000   6 0 3
   0.0003750    0.0002500    0.0001250    0.0000000    0.0001250    0.0002500   6 0 3
   0.0003750    0.0005000    0.0006250    0.0007500    0.0008750    0.0010000   6 0 3
   0.0012500    0.0015000    0.0017500    0.0020000    0.0022500    0.0025000   6 0 3
   0.0037500    0.0050000    0.0075000    0.0100000    0.0150000    0.0200000   6 0 3
   0.0250000    0.0300000    0.0350000    0.0400000    0.0450000    0.0500000   6 0 3
   0.0600000    0.0700000    0.0800000    0.0900000    0.1000000    0.1250000   6 0 3
   0.1500000    0.1750000    0.2000000    0.2250000    0.2500000    0.2750000   6 0 3
   0.3000000    0.3250000    0.3500000    0.3750000    0.4000000    0.4250000   6 0 3
   0.4500000    0.4750000    0.5000000    0.5250000    0.5500000    0.5750000   6 0 3
   0.6000000.   0.6250000    0.6500000    0.6750000    0.7000000    0.7250000   6 0 3
   0.7500000    0.7750000    0.8000000    0.8250000    0.8500000    0.8750000   6 0 3
   0.9000000    0.9250000    0.9500000    0.9700000    0.9800000    0.9899999   6 0 3
   1.0000000    0.0000000    0.0000000    0.0000000    0.0000000    0.0000000   1 1 3
   0.0000000   -0.0018740   -0.0036110   -0.0052390   -0.0082510   -0.0117000   6 0 4
  -0.0149080   -0.0179530   -0.0208880   -0.0237390   -0.0265150   -0.0292210   6 0 4
  -0.0318550   -0.0344110   -0.0368870   -0.0392810   -0.0415850   -0.0437950   6 0 4
  -0.0459040   -0.0479060   -0.0497930   -0.0515600   -0.0531980   -0.0546980   6 0 4
  -0.0560510   -0.0572430   -0.0582620   -0.0590900   -0.0597070   -0.0600940   6 0 4
  -0.0602260   -0.0600760   -0.0596120   -0.0587940   -0.0575700   -0.0558790   6 0 4
  -0.0536360   -0.0507320   -0.0470040   -0.0452280   -0.0432520   -0.0410330   6 0 4
  -0.0385350   -0.0356740   -0.0340820   -0.0323620   -0.0304960   -0.0284623   6 0 4
  -0.0262300   -0.0237260   -0.0207970   -0.0172480   -0.0150780   -0.0123860   6 0 4
  -0.0106990   -0.0086200   -0.0081360   -0.0076230   -0.0070750   -0.0064850   6 0 4
  -0.0058470   -0.0051460   -0.0047660   -0.0043630   -0.0039310   -0.0034620   6 0 4
  -0.0029450   -0.0023560   -0.0016320    0.0000000    0.0016320    0.0023560   6 0 4
   0.0029450    0.0034620    0.0039310    0.0043630    0.0047660    0.0051460   6 0 4
   0.0058470    0.0064850    0.0070750    0.0076230    0.0081360    0.0086200   6 0 4
   0.0106990    0.0123860    0.0150780    0.0172480    0.0207970    0.0237260   6 0 4
   0.0262300    0.0284620    0.0304960    0.0323620    0.0340820    0.0356740   6 0 4
   0.0385350    0.0410380    0.0432520    0.0452280    0.0470040    0.0507320   6 0 4
   0.0536360    0.0558790    0.0575700    0.0587940    0.0596120    0.0600760   6 0 4
   0.0602260    0.0600940    0.0597070    0.0590900    0.0582620    0.0572430   6 0 4
   0.0560510    0.0546980    0.0531980    0.0515600    0.0497930    0.0479060   6 0 4
   0.0459040    0.0437950    0.0415850    0.0392810    0.0368870    0.0344110   6 0 4
   0.0318550    0.0292210    0.0265150    0.0237390    0.0208880    0.0179530   6 0 4
   0.0149080    0.0117000    0.0082510    0.0052390    0.0036110    0.0018740   6 0 4
   0.0000000    0.0000000    0.0000000    0.0000000    0.0000000    0.0000000   1 1 4
```

```
&TRAJ1
GEPS= 0.4999999E-04
DSHIFT= 0.20E-02
VEPS= 0.9999999E-03
LCMB= 0
LCMP= 0
LEQM= 1
LSTM= 0
LYOR= 1
LXOR= 1
NBDY= 1
NEQ= 4
NPL= 15
NSEAR= 50
NSI= 1
TIMSTP= 0.9999999E-03
&END
&TRAJ2
CHORD= 0.30
G= 0.0
PIT= 0.0
PITDOT= 0.0
PRATK= 0.0
XORC= -4.0
XSTOP= 0.50
YOLIM= 0.9999999E-04
YOMAX= 0.50E-01
YOMIN= -0.50E-01
YORC= 0.9999996E-01
&END
&DIST
FLWC= 1.0, 9*0.0
DPD= 20.0, 9*0.0
CFP= 1.0, 9*0.0
&END
&ICE
VINF= 129.460
LWC= 0.50
TAMB= 260.5498
PAMB= 90748.0
RH= 100.0
DPMM= 20.0
XKINIT= 0.00035
SEGTOL= 1.50
```

a. Input data file

Figure 7.1: Input data for Example 1

102

```
TIME =  0.

ENTER DESIRED ICING TIME (SEC), (F10.0)
120.
ENTER DESIRED TIME INCREMENT (SEC), (F10.0)
60.

ARE NEW PLOT OPTIONS DESIRED? (Y/N)
Y

AVAILABLE PLOT OPTIONS
  0 - NO PLOTS
  1 - PARAMETER PLOTS ONLY
  2 - TRAJECTORY PLOTS ONLY
  3 - PARAMETER AND TRAJECTORY PLOTS
ENTER PLOT OPTION (I1)
3

THE POTENTIAL FLOW FIELD IS NOW BEING CALCULATED
```

b. Interactive input

Figure 7.1: Concluded

```
VELOCITY (M/S)        129.00
TEMPERATURE (C)       -12.60
PRESSURE (KPA)         90.75
HUMIDITY (%)          100.00
LWC (G/M**3)            0.50
DROP DIAM (MICRONS)    20.00
TIME (SEC)              0.00
```
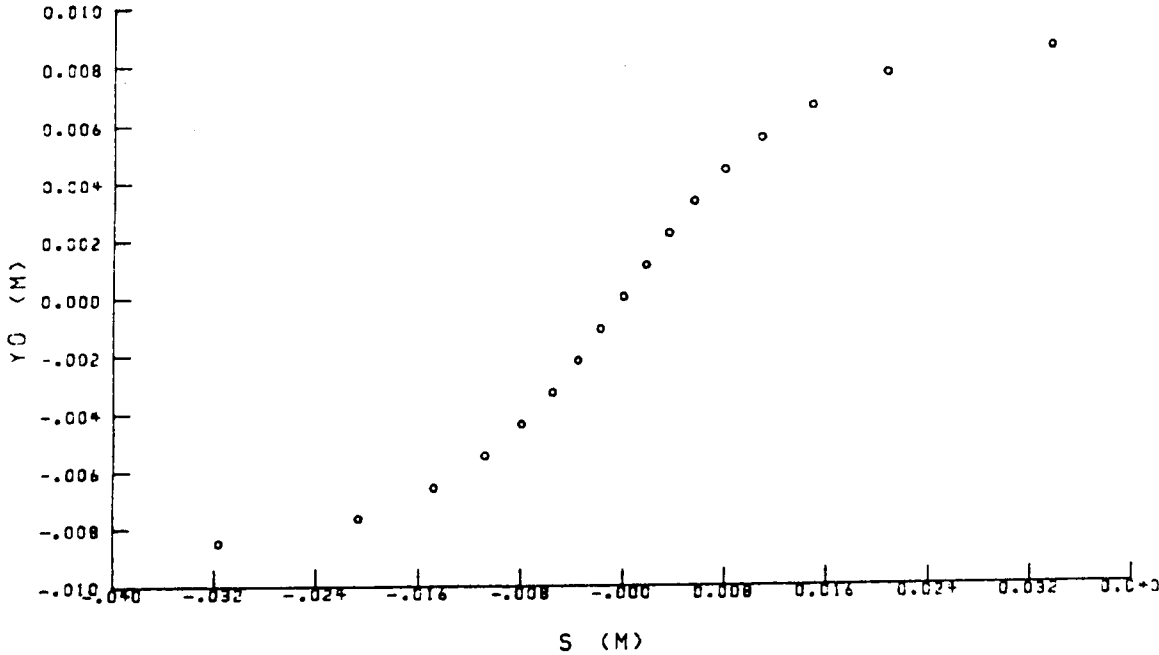
Figure 7.2: y_0 vs s points calculated in subroutine COLLEC for Example 1

```
THE CALCULATED SURFACE IMPACT DISTANCES (S) AND  RELEASE POINTS (Y0)
ARE AS FOLLOWS
:        Y0              S              I          Y0              S

1       0.00796        0.02715        10      -0.00106        -0.00160
2       0.00716        0.01944        11      -0.00208        -0.00256
3       0.00613        0.01302        12      -0.00311        -0.00385
4       0.00511        0.00964        13      -0.00414        -0.00734
5       0.02408        0.00694        14      -0.00517        -0.00983
6       0.00305        0.00378        15      -0.00619        -0.01326
7       0.00203        0.00249        16      -0.00722        -0.01886
8       0.00100        0.00154        17      -0.00802        -0.03702
9      -0.00003       -0.00003        18       0.00000         0.00000


HOW MANY TRAJECTORIES ARE TO BE DELETED BEFORE
THE COLLECTION EFFICIENCY CALCULATION? (I2)


NACA 0012  : EXAMPLE 1        : TIME= 120.000 SEC

ICING CONDITION
        STATIC TEMPERATURE (C)           260.55
        STATIC PRESSURE (PA)           90748.00
        VELOCITY (M/S)                   129.00
        LWC (G/M**3)                       0.50
        DROPLET DIAMETER (MICRONS)        20.00


ICE ACCRETION DATA
        STAGNATION POINT                  74
        TRANSITION POINTS (LOWER,UPPER)   72        75
        ICING LIMITS (LOWER,UPPER)        43       103
        NUMBER OF POINTS                 147
        NUMBER OF SEGMENTS ADDED           8

            AVAILABLE PLOT OPTIONS
            0  -  NO PLOTS
            1  -  ICED GEOMETRY
            2  -  Z VS S
            3  -  BETA VS S
            4  -  VE VS S
            5  -  TE VS S
            6  -  PE VS S
            7  -  TSURF VS S
            8  -  HTC VS S
            9  -  XK VS S
           10  -  ICE DENSITY VS S
           11  -  FFRAC VS S
        ENTER OPTION NUMBER (I2)
```
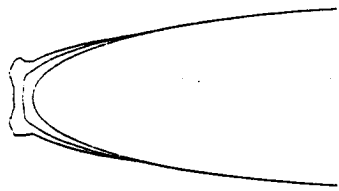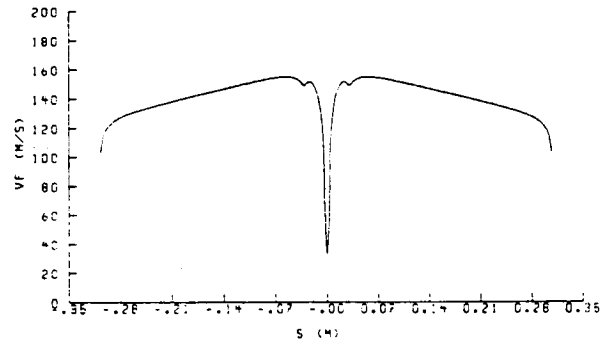
Figure 7.3: Interactive input and output for the second time step of Example 1.

104

```
VELOCITY (M/S)       129.46
TEMPERATURE (C)      -12.60
PRESSURE (KPA)        90.75
HUMIDITY (%)         100.00
LWC (G/M**3)           0.50
DROP DIAM (MICRON)    20.00
TIME (SEC)           120.00
```
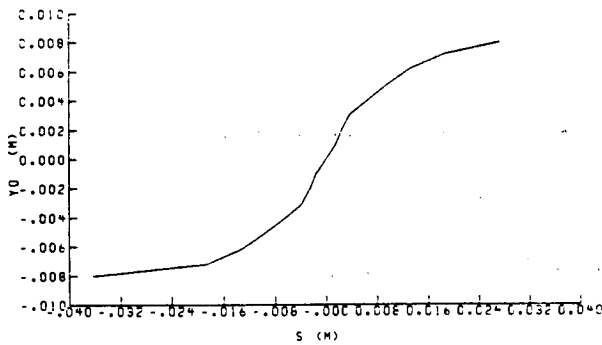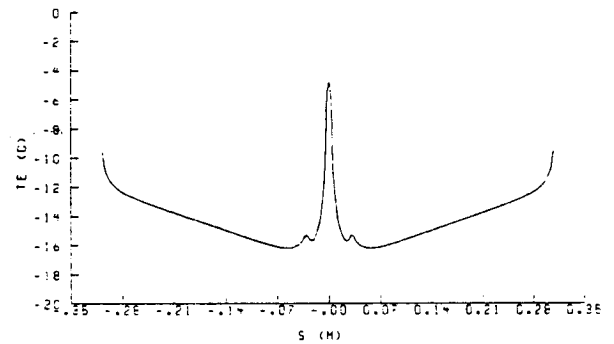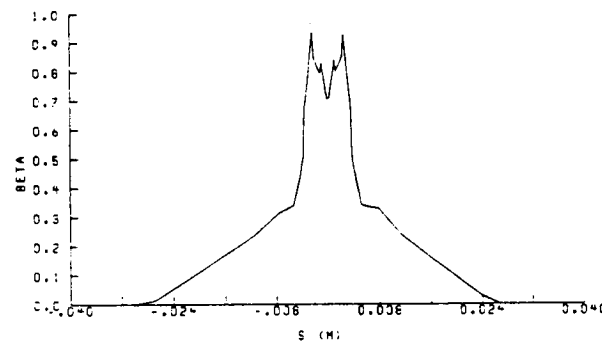
a. Iced airfoil geometry

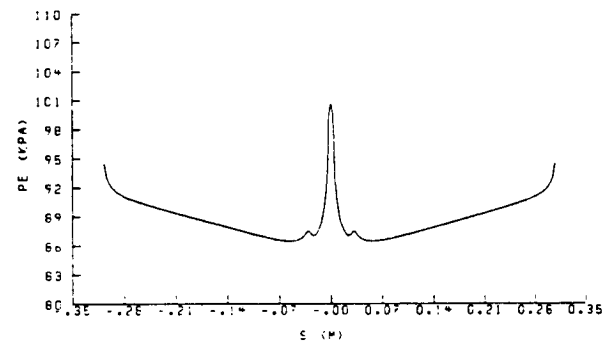d. Edge velocity vs. surface location

b. Particle release position vs. surface
    impact distance

e. Edge temperature vs. surface location

c. Local collection efficiency vs. surface
    location

f. Edge pressure vs. surface location

Figure 7.4: Icing parameter plots for the second timestep of Example 1.

105

VELOCITY (M/S)	129.46
TEMPERATURE (C)	-12.60
PRESSURE (KPA)	90.75
HUMIDITY (%)	100.00
LWC (G/M**3)	0.50
DROP DIAM (MICRON)	20.00
TIME (SEC)	120.00
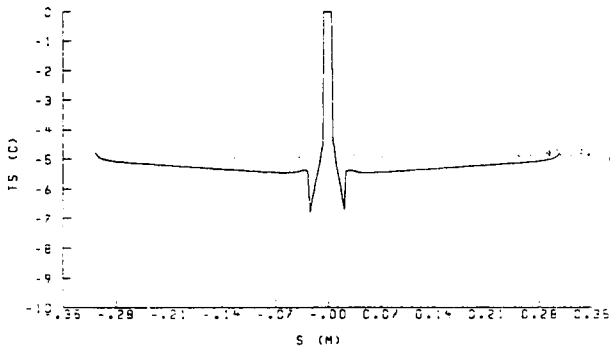
g. Equilibrium surface temperature vs. surface location
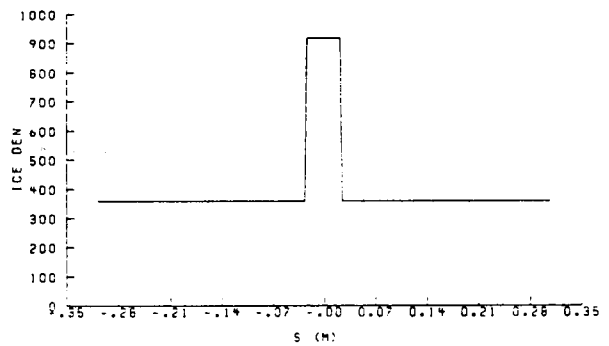
j. Ice density vs. surface location
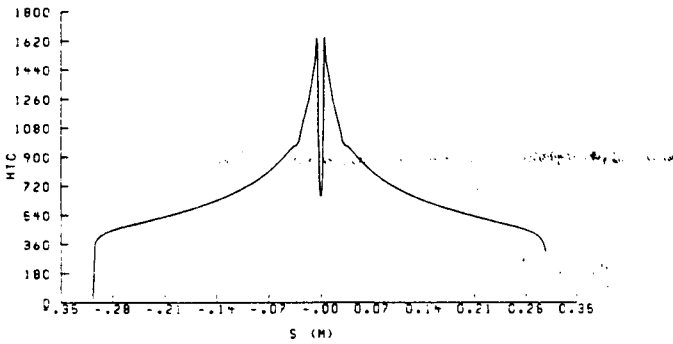
h. Convective heat transfer coefficient vs. surface location

k. Freezing fraction vs. surface location

i. Equivalent sand-grain roughness height vs. surface location

Figure 7.4: Concluded

106

UNTRANSFORMED COORDINATE DATA FOR BODY ID = 1,   NACA 0012 : EXAMPLE 1

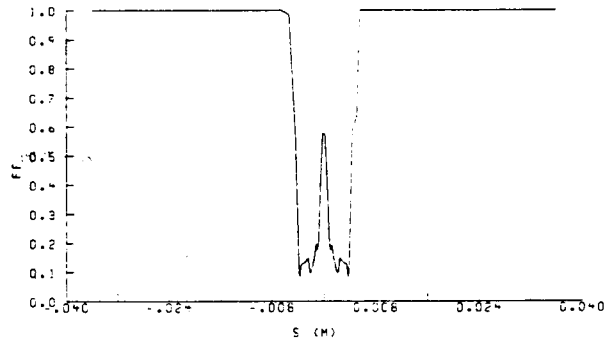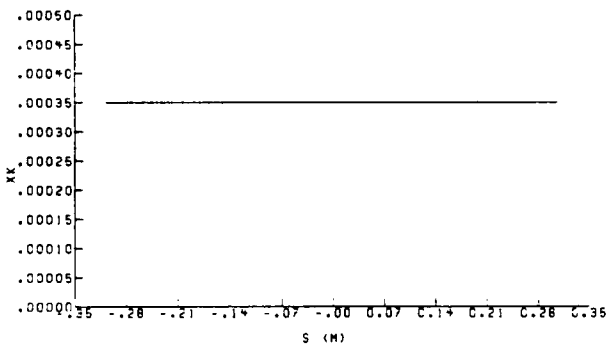| I	X(I)	Y(I)	I	X(I)	Y(I)	I	X(I)	Y(I)
1	1.0000000	0.0000000	51	0.0122522	-0.0250171	101	0.0339538	0.0331726
2	0.9899997	-0.0018740	52	0.0063893	-0.0218130	102	0.0391365	0.0347642
3	0.9799998	-0.0036110	53	0.0029776	-0.0197319	103	0.0442957	0.0362028
4	0.9699997	-0.0052390	54	-0.0006996	-0.0170765	104	0.0494636	0.0374372
5	0.9499997	-0.0082510	55	-0.0020565	-0.0162655	105	0.0596575	0.0397926
6	0.9249998	-0.0117000	56	-0.0034135	-0.0154545	106	0.0698789	0.0415216
7	0.8999999	-0.0149080	57	-0.0053174	-0.0129929	107	0.0799799	0.0432520
8	0.8749999	-0.0179530	58	-0.0053478	-0.0124796	108	0.0899999	0.0452280
9	0.8499998	-0.0208880	59	-0.0053782	-0.0119662	109	0.0993998	0.0470040
10	0.8249999	-0.0237390	60	-0.0054665	-0.0111464	110	0.1250000	0.0507320
11	0.7999997	-0.0265150	61	-0.0055827	-0.0103023	111	0.1499999	0.0536360
12	0.7749997	-0.0292210	62	-0.0056817	-0.0094149	112	0.1749999	0.0558790
13	0.7500000	-0.0318550	63	-0.0057773	-0.0084782	113	0.1999999	0.0575700
14	0.7249998	-0.0344110	64	-0.0058924	-0.0075095	114	0.2249998	0.0587940
15	0.6999997	-0.0368870	65	-0.0059092	-0.0069344	115	0.2500000	0.0596120
16	0.6749998	-0.0392810	66	-0.0059506	-0.0063720	116	0.2749997	0.0600760
17	0.6499997	-0.0415850	67	-0.0060122	-0.0057760	117	0.2999997	0.0602260
18	0.6249999	-0.0437950	68	-0.0060896	-0.0051370	118	0.3249999	0.0600940
19	0.5999998	-0.0459040	69	-0.0061991	-0.0044373	119	0.3499998	0.0597070
20	0.5749999	-0.0479060	70	-0.0063691	-0.0036290	120	0.3749999	0.0590900
21	0.5499997	-0.0497930	71	-0.0064739	-0.0030471	121	0.3999999	0.0582620
22	0.5249997	-0.0515600	72	-0.0065787	-0.0024653	122	0.4249998	0.0572430
23	0.5000000	-0.0531980	73	-0.0066632	-0.0012327	123	0.4499997	0.0560510
24	0.4749998	-0.0546980	74	-0.0067476	0.0000000	124	0.4749998	0.0546980
25	0.4499997	-0.0560510	75	-0.0066629	0.0012326	125	0.5000000	0.0531980
26	0.4249998	-0.0572430	76	-0.0065782	0.0024652	126	0.5249997	0.0515600
27	0.3999999	-0.0582620	77	-0.0064731	0.0030470	127	0.5499997	0.0497930
28	0.3749999	-0.0590900	78	-0.0063680	0.0036287	128	0.5749999	0.0479060
29	0.3499998	-0.0597070	79	-0.0061976	0.0044369	129	0.5999998	0.0459040
30	0.3249999	-0.0600940	80	-0.0060878	0.0051366	130	0.6249999	0.0437950
31	0.2999997	-0.0602260	81	-0.0060101	0.0057755	131	0.6499999	0.0415850
32	0.2749997	-0.0600760	82	-0.0059485	0.0063713	132	0.6749998	0.0392810
33	0.2500000	-0.0596120	83	-0.0059070	0.0069337	133	0.6999997	0.0368870
34	0.2249998	-0.0587940	84	-0.0058902	0.0075087	134	0.7249998	0.0344110
35	0.1999999	-0.0575700	85	-0.0057750	0.0084774	135	0.7500000	0.0318550
36	0.1749999	-0.0558790	86	-0.0056794	0.0094139	136	0.7749997	0.0292210
37	0.1499999	-0.0536360	87	-0.0055800	0.0103011	137	0.7999997	0.0265150
38	0.1250000	-0.0507320	88	-0.0054638	0.0111451	138	0.8249999	0.0237390
39	0.0999998	-0.0470040	89	-0.0053764	0.0119654	139	0.8499998	0.0208880
40	0.0899997	-0.0452280	90	-0.0053463	0.0124788	140	0.8749999	0.0179530
41	0.0799999	-0.0432520	91	-0.0053162	0.0129922	141	0.8999999	0.0149080
42	0.0698845	-0.0414994	92	-0.0033864	0.0154345	142	0.9249998	0.0117000
43	0.0596677	-0.0397540	93	-0.0020270	0.0162432	143	0.9499997	0.0082510
44	0.0494722	-0.0374086	94	-0.0006677	0.0170519	144	0.9699997	0.0052390
45	0.0443028	-0.0361813	95	0.0029863	0.0197231	145	0.9799998	0.0036110
46	0.0391421	-0.0347484	96	0.0063941	0.0218071	146	0.9899997	0.0018740
47	0.0339577	-0.0331625	97	0.0122537	0.0250150	147	1.0000000	0.0000000
48	0.0287098	-0.0314767	98	0.0179189	0.0275427.			
49	0.0233698	-0.0296603	99	0.0233668	0.0296667			
50	0.0179198	-0.0275407	100	0.0287064	0.0314846			

DOUGLAS AIRCRAFT COMPANY TWO-DIMENSIONAL POTENTIAL FLOW PROGRAM

COMBINED FLOW   NACA 0012 : EXAMPLE 1

ALPHA =   0.000000   ALPHA O =   0.000013   NO. OF BODIES   1

CL =   0.000002   CHORD =   1.000000   TOTAL ELEMENTS   146

BODY ID = 1   NACA 0012 : EXAMPLE 1   NO. OF ELEMENTS   146

I	X	Y	S	VT	CP	J	SIGMA	VN
1	0.9950025	-0.0009536	0.0024715	-0.8268182	0.3163716	1	-0.013141	0.000004
2	0.9850022	-0.0027573	0.0074045	-0.8886436	0.2103125	2	-0.013129	0.000004
3	0.9750013	-0.0044365	0.0123352	-0.9189040	0.1556154	3	-0.012670	0.000004
4	0.9600045	-0.0067780	0.0197094	-0.9450629	0.1068562	4	-0.012000	0.000004
5	0.9375044	-0.0100112	0.0307528	-0.9680377	0.0629031	5	-0.011207	0.000004
6	0.9125025	-0.0133284	0.0430058	-0.9839131	0.0319150	6	-0.010559	0.000004
7	0.8875018	-0.0164470	0.0552462	-0.9951214	0.0170703	7	-0.010140	0.000003
8	0.8625011	-0.0194323	0.0674784	-1.0043230	-0.0086641	8	-0.009907	0.000002
9	0.8375007	-0.0223233	0.0797051	-1.0127668	-0.0256953	9	-0.009760	0.000001
10	0.8125005	-0.0251359	0.0919275	-1.0207739	-0.0419788	10	-0.009630	0.000001
11	0.7875003	-0.0278768	0.1041459	-1.0284805	-0.0577717	11	-0.009516	0.000001
12	0.7625008	-0.0305473	0.1163605	-1.0360298	-0.0733576	12	-0.009384	0.000001
13	0.7375007	-0.0331427	0.1285714	-1.0433102	-0.0884953	13	-0.009213	0.000001
14	0.7125006	-0.0356590	0.1407784	-1.0503035	-0.1031370	14	-0.009036	0.000001
15	0.6875005	-0.0380946	0.1529815	-1.0572052	-0.1176825	15	-0.008853	0.000001
16	0.6625004	-0.0404444	0.1651806	-1.0640011	-0.1320982	16	-0.008626	0.000001
17	0.6375008	-0.0427021	0.1773756	-1.0706520	-0.1462955	17	-0.008386	0.000001
18	0.6125008	-0.0448624	0.1895665	-1.0772190	-0.1604004	18	-0.008112	0.000001
19	0.5875007	-0.0469188	0.2017531	-1.0836945	-0.1743937	19	-0.007813	0.000001
20	0.5625006	-0.0488641	0.2139356	-1.0900660	-0.1882429	20	-0.007477	0.000001
21	0.5375005	-0.0506920	0.2261137	-1.0963774	-0.2020426	21	-0.007127	0.000001
22	0.5125009	-0.0523956	0.2382874	-1.1027031	-0.2159538	22	-0.006738	0.000001
23	0.4875009	-0.0539657	0.2504569	-1.1089926	-0.2298641	23	-0.006311	0.000000
24	0.4625008	-0.0553936	0.2626224	-1.1153297	-0.2439604	24	-0.005851	0.000000
25	0.4375007	-0.0566678	0.2747838	-1.1216908	-0.2581892	25	-0.005326	0.000000
26	0.4125007	-0.0577752	0.2869414	-1.1280737	-0.2725496	26	-0.004755	0.000000
27	0.3875006	-0.0587010	0.2990954	-1.1345110	-0.2871151	27	-0.004099	0.000000
28	0.3625005	-0.0594260	0.3112462	-1.1408377	-0.3015099	28	-0.003351	0.000000
29	0.3375003	-0.0599308	0.3233944	-1.1470585	-0.3157425	29	-0.002524	0.000000
30	0.3124999	-0.0601935	0.3355410	-1.1531639	-0.3297263	30	-0.001583	0.000000
31	0.2874994	-0.0601882	0.3476869	-1.1590567	-0.3434114	31	-0.000526	0.000000
32	0.2624970	-0.0598856	0.3598337	-1.1647253	-0.3565845	32	0.000671	-0.000000
33	0.2374983	-0.0592503	0.3719836	-1.1701040	-0.3691425	33	0.002047	-0.000000
34	0.2124971	-0.0582363	0.3841400	-1.1749191	-0.3804340	34	0.003666	0.000000
35	0.1874956	-0.0567876	0.3963069	-1.1788921	-0.3897858	35	0.005558	-0.000000
36	0.1624931	-0.0548323	0.4084910	-1.1814556	-0.3958368	36	0.007853	-0.000002
37	0.1374893	-0.0522749	0.4207022	-1.1815958	-0.3961678	37	0.010653	-0.000004
38	0.1124831	-0.0489800	0.4329554	-1.1766272	-0.3844509	38	0.014243	-0.000004
39	0.0949959	-0.0461379	0.4415639	-1.1659498	-0.3594389	39	0.017408	-0.000004
40	0.0849999	-0.0442400	0.4465072	-1.1386347	-0.2964888	40	0.019940	-0.000003
41	0.0749438	-0.0423663	0.4514770	-1.1286554	-0.2738628	41	0.014238	-0.000003

Figure 7.5: Printed output for the second time step of Example 1

DOUGLAS AIRCRAFT COMPANY TWO-DIMENSIONAL POTENTIAL FLOW PROGRAM

COMBINED FLOW   NACA 0012 : EXAMPLE 1

ALPHA = 0.000000   ALPHA O = 0.000013   NO. OF BODIES   1

CL = 0.000002   CHORD = 1.000000   TOTAL ELEMENTS 146

BODY ID = 1   NACA 0012 : EXAMPLE 1   NO. OF ELEMENTS 146

I	X	Y	S	VT	CP	J	SIGMA	VN
42	0.0647761	-0.0406267	0.4564884	-1.1665764	-0.3608999	42	0.011522	-0.000002
43	0.0545632	-0.0386106	0.4615475	-1.1738958	-0.3780308	43	0.019424	-0.000002
44	0.0468854	-0.0368035	0.4653795	-1.1783762	-0.3885698	44	0.018503	-0.000002
45	0.0417168	-0.0354850	0.4679711	-1.1814480	-0.3958187	45	0.023559	-0.000001
46	0.0365461	-0.0339678	0.4705892	-1.1633625	-0.3534117	46	0.026692	-0.000002
47	0.0313305	-0.0323297	0.4732450	-1.1495943	-0.3215666	47	0.027136	-0.000001
48	0.0260337	-0.0305865	0.4759541	-1.1521044	-0.3273439	48	0.027243	-0.000001
49	0.0206328	-0.0286313	0.4787447	-1.1499968	-0.3224916	49	0.031244	-0.000001
50	0.0150664	-0.0263229	0.4816726	-1.1401501	-0.2999420	50	0.034985	-0.000001
51	0.0092924	-0.0234670	0.4848031	-1.0972996	-0.2040663	51	0.042964	-0.000000
52	0.0046702	-0.0207942	0.4873973	-1.0642109	-0.1325445	52	0.049018	0.000000
53	0.0011390	-0.0184042	0.4894699	-0.9627361	0.0731393	53	0.023584	0.000002
54	-0.0013779	-0.0166708	0.4909557	-0.9737462	0.0518184	54	0.009558	0.000003
55	-0.0027350	-0.0158600	0.4917236	-1.1018343	-0.2140379	55	0.043306	0.000004
56	-0.0045892	-0.0143968	0.4928801	-1.2881260	-0.6592684	56	0.126043	-0.000032
57	-0.0053327	-0.0127363	0.4937775	-0.8853139	0.2162194	57	0.128969	-0.000030
58	-0.0053630	-0.0122229	0.4940273	-0.7104751	0.4952251	58	0.128295	-0.000026
59	-0.0054181	-0.0115558	0.4943524	-0.6279104	0.6057286	59	0.123520	-0.000018
60	-0.0055246	-0.0107243	0.4947596	-0.5720486	0.6727604	60	0.124837	-0.000024
61	-0.0056339	-0.0098588	0.4951834	-0.5080939	0.7418406	61	0.124833	-0.000025
62	-0.0057295	-0.0089465	0.4956290	-0.4414389	0.8051318	62	0.127661	-0.000024
63	-0.0058348	-0.0079938	0.4960946	-0.4165254	0.8265067	63	0.125630	-0.000032
64	-0.0059008	-0.0072219	0.4964712	-0.3197475	0.8977616	64	0.131645	-0.000023
65	-0.0059274	-0.0066530	0.4967479	-0.3052155	0.9068435	65	0.136477	-0.000023
66	-0.0059797	-0.0060738	0.4970304	-0.2758528	0.9239053	66	0.135210	-0.000022
67	-0.0060489	-0.0054563	0.4973322	-0.2470832	0.9389499	67	0.134670	-0.000015
68	-0.0061407	-0.0047866	0.4976606	-0.2164860	0.9531339	68	0.133490	-0.000002
69	-0.0062841	-0.0040331	0.4980332	-0.2118799	0.9551069	69	0.124528	-0.000002
70	-0.0064215	-0.0033380	0.4983774	-0.1746964	0.9694812	70	0.119806	-0.000010
71	-0.0065263	-0.0027562	0.4986646	-0.1783613	0.9681873	71	0.114872	-0.000008
72	-0.0066215	-0.0018490	0.4991083	-0.0935943	0.9912401	72	0.118039	-0.000025
73	-0.0067059	-0.0006164	0.4997085	-0.0607150	0.9963138	73	0.116084	-0.000027
74	-0.0067052	0.0006163	0.5003088	0.0602920	0.9963649	74	0.116209	-0.000026
75	-0.0066205	0.0018489	0.5009090	0.0944792	0.9910737	75	0.118143	-0.000027
76	-0.0065258	0.0027561	0.5013527	0.1792508	0.9678692	76	0.114737	-0.000007
77	-0.0064206	0.0033372	0.5016398	0.1750311	0.9693642	77	0.119728	-0.000008
78	-0.0062828	0.0040328	0.5019841	0.2121464	0.9549940	78	0.124492	-0.000003
79	-0.0061390	0.0047862	0.5023567	0.2167311	0.9530277	79	0.133458	-0.000015
80	-0.0060470	0.0054558	0.5026851	0.2474253	0.9387807	80	0.134660	-0.000021
81	-0.0059776	0.0060732	0.5029869	0.2760307	0.9238071	81	0.135213	-0.000023
82	-0.0059253	0.0066523	0.5032694	0.3056121	0.9066013	82	0.136443	-0.000026
83	-0.0058986	0.0072212	0.5035461	0.3200547	0.8975651	83	0.131615	-0.000026
84	-0.0058326	0.0079930	0.5039227	0.4169908	0.8261187	84	0.125575	-0.000019
85	-0.0057272	0.0089456	0.5043883	0.4419479	0.8046821	85	0.127589	-0.000023
86	-0.0056314	0.0098577	0.5048338	0.5088874	0.7410337	86	0.124722	-0.000021
87	-0.0055219	0.0107231	0.5052575	0.5725745	0.6721895	87	0.123468	-0.000018
88	-0.0054158	0.0115548	0.5056649	0.6287807	0.6046349	88	0.128303	-0.000026
89	-0.0053313	0.0122221	0.5059901	0.7130577	0.4915488	89	0.128798	-0.000025
90	-0.0053312	0.0127355	0.5062309	0.8891031	0.2094958	90	0.125787	-0.000024
91	-0.0045729	0.0143884	0.5071375	1.2907629	-0.6660681	91	0.041929	0.000004
92	-0.0027067	0.0158388	0.5082944	1.0958996	-0.2009954	92	0.009722	0.000001
93	-0.0013472	0.0166473	0.5090628	0.9688777	0.0612761	93	0.023746	-0.000001
94	0.0011593	0.0183875	0.5105464	0.9584563	0.0813615	94	0.050142	-0.000001
95	0.0046765	0.0207875	0.5126163	1.0659027	-0.1361485	95	0.043791	-0.000002
96	0.0092954	0.0234631	0.5152097	1.0972567	-0.2039719	96	0.043104	-0.000002
97	0.0150667	0.0263228	0.5183359	1.1400375	-0.2996855	97	0.035132	-0.000002
98	0.0206308	0.0286356	0.5212675	1.1501760	-0.3229046	98	0.031395	-0.000003
99	0.0260304	0.0305937	0.5240582	1.1523075	-0.3278122	99	0.027300	-0.000003
100	0.0313269	0.0323384	0.5267673	1.1492682	-0.3208170	100	0.027225	-0.000003
101	0.0365414	0.0339804	0.5294232	1.1631508	-0.3529196	101	0.026901	-0.000003
102	0.0417105	0.0355036	0.5320413	1.1817484	-0.3965292	102	0.023755	-0.000003
103	0.0468775	0.0368288	0.5346623	1.1791773	-0.3904591	103	0.018736	-0.000004
104	0.0545534	0.0386457	0.5384650	1.1760740	-0.3831501	104	0.019568	-0.000004
105	0.0647681	0.0406571	0.5435247	1.1687498	-0.3659754	105	0.011189	-0.000003
106	0.0749408	0.0423782	0.5485370	1.1282282	-0.2728987	106	0.013823	-0.000004
107	0.0849999	0.0442400	0.5535073	1.1373749	-0.2936211	107	0.019942	-0.000003
108	0.0949959	0.0461379	0.5584505	1.1656160	-0.3586607	108	0.017405	-0.000003
109	0.1124831	0.0489800	0.5670580	1.1764851	-0.3841162	109	0.014238	-0.000003
110	0.1374893	0.0522749	0.5793122	1.1815319	-0.3960171	110	0.010649	-0.000002
111	0.1624931	0.0548323	0.5915234	1.1814203	-0.3957539	111	0.007848	-0.000002
112	0.1874956	0.0567876	0.6037076	1.1788692	-0.3897324	112	0.005554	-0.000002
113	0.2124971	0.0582363	0.6158745	1.1749039	-0.3803988	113	0.003662	0.000000
114	0.2374983	0.0592503	0.6280308	1.1700935	-0.3691187	114	0.002044	0.000000
115	0.2624990	0.0598856	0.6401808	1.1647167	-0.3565645	115	0.000669	0.000000
116	0.2874994	0.0601882	0.6523275	1.1590490	-0.3433943	116	-0.000528	0.000000
117	0.3124999	0.0601935	0.6644735	1.1531582	-0.3297729	117	-0.001585	0.000000
118	0.3375003	0.0599308	0.6766200	1.1470537	-0.3157320	118	-0.002526	0.000000
119	0.3625005	0.0594260	0.6887682	1.1408339	-0.3015013	119	-0.003353	0.000000
120	0.3875006	0.0587010	0.7009190	1.1345081	-0.2871084	120	-0.004101	0.000000
121	0.4125007	0.0577752	0.7130730	1.1280708	-0.2725430	121	-0.004757	0.000000
122	0.4375007	0.0566678	0.7252306	1.1216888	-0.2581854	122	-0.005328	0.000000
123	0.4625008	0.0553936	0.7373920	1.1153278	-0.2439556	123	-0.005852	0.000000

Figure 7.5: continued

DOUGLAS AIRCRAFT COMPANY TWO-DIMENSIONAL POTENTIAL FLOW PROGRAM

COMBINED FLOW   NACA 0012 : EXAMPLE 1

ALPHA = 0.000000   ALPHA O = 0.000013   NO. OF BODIES   1

CL = 0.000002   CHORD = 1.000000   TOTAL ELEMENTS 146

BODY ID = 1   NACA 0012 : EXAMPLE 1   NO. OF ELEMENTS 146

I	X	Y	S	VT	CP	J	SIGMA	VN
124	0.4875009	0.0539657	0.7495575	1.1089916	-0.2298622	124	-0.006312	0.000000
125	0.5125009	0.0523956	0.7617270	1.1027021	-0.2159519	125	-0.006739	0.000001
126	0.5375005	0.0506920	0.7739007	1.0963764	-0.2020407	126	-0.007128	0.000001
127	0.5625006	0.0488641	0.7860789	1.0900640	-0.1882391	127	-0.007478	0.000001
128	0.5875007	0.0469188	0.7982613	1.0836935	-0.1743908	128	-0.007814	0.000001
129	0.6125008	0.0448624	0.8104479	1.0772171	-0.1603966	129	-0.008112	0.000001
130	0.6375008	0.0427021	0.8226388	1.0706501	-0.1462908	130	-0.008386	0.000001
131	0.6625004	0.0404444	0.8348338	1.0640001	-0.1320953	131	-0.008627	0.000001
132	0.6875005	0.0380946	0.8470329	1.0572042	-0.1176805	132	-0.008853	0.000001
133	0.7125006	0.0356590	0.8592360	1.0503025	-0.1031351	133	-0.009036	0.000001
134	0.7375007	0.0331427	0.8714430	1.0433102	-0.0884953	134	-0.009214	0.000001
135	0.7625008	0.0305473	0.8836539	1.0360289	-0.0733557	135	-0.009384	0.000001
136	0.7875003	0.0278768	0.8958685	1.0284805	-0.0577717	136	-0.009517	0.000001
137	0.8125005	0.0251359	0.9080870	1.0207729	-0.0419769	137	-0.009631	0.000001
138	0.8375007	0.0223233	0.9203093	1.0127659	-0.0256939	138	-0.009760	0.000001
139	0.8625011	0.0194323	0.9325360	1.0043221	-0.0086622	139	-0.009907	0.000001
140	0.8875018	0.0164470	0.9447682	0.9951208	0.0097346	140	-0.010141	0.000001
141	0.9125025	0.0133284	0.9570085	0.9839124	0.0319164	141	-0.010560	0.000001
142	0.9375044	0.0100112	0.9692615	0.9680369	0.0629046	142	-0.011207	0.000005
143	0.9600045	0.0067780	0.9803048	0.9450626	0.1068568	143	-0.012000	0.000005
144	0.9750013	0.0044365	0.9876790	0.9189037	0.1556160	144	-0.012670	0.000004
145	0.9850022	0.0027573	0.9926056	0.8886423	0.2103150	145	-0.013129	0.000005
146	0.9950025	0.0009536	0.9975426	0.8268158	0.3163756	146	-0.013141	0.000004

INTEGRATED VALUES

CY =   0.00003   CX = -0.00106

CL =   0.00003   CD = -0.00106   CM =   0.00000

PARABOLIC INTEGRATION

INTEGRATED VALUES

CY =   0.00002   CX = -0.00030

CL =   0.00002   CD = -0.00030   CM =   0.00000

TOTAL CM =   0.00000

TOTAL CM =   0.00000   (PARABOLIC)

THE PARTICLES ARE RELEASED FROM X = -1.26000E 00
WHICH IS OBTAINED AT THE   1 LOOP OF   50 LOOPS

GEOMETRY CHARACTERISTICS:

LEADING EDGE (X,Y)	-4.0243E-03	2.0715E-07
TRAILING EDGE (X,Y)	3.0200E-01	0.0000
THICKNESS	4.0136E-02	
CHORD	3.0000E-01	
ANGLE OF ATTACK	0.0000	
UPPER BOUNDARY	2.2075E-02	
LOWER BOUNDARY	-2.2075E-02	

PARTICLE TRAJECTORY DATA:

THE PARTICLES ARE RELEASED IN EQUILIBRIUM WITH THE AIR

PARTICLE DIAMETER (MICRONS)	INITIAL VX (M/S)	INITIAL VY (M/S)	PARTICLE AOA (DEGREES)	PITCH ANGLE (DEGREES)	PIT DOT (DEG/SEC)	GRAVT CONST (M/S**2)	ERROR CRITERIA
20.00	0.00	0.00	0.00	0.00	0.00	0.00	5.00E-05

THE PARTICLES OF SIZE 20.00 CONTAIN 1.0000 OF THE TOTAL MASS

X0	Y0		XP	YP	S	DT	NSTP
-1.2599993	0.0090961	OUT OF RANGE	0.0831582	0.0226937		4.6785E-05	101
-1.2599993	-0.0090835	OUT OF RANGE	0.0828083	-0.0226548		5.2456E-05	97

YOMAX= 9.0961E-03   YOMIN= -9.0835E-03

-1.2599993	0.0000063	HIT BODY AT	-0.0040239	0.0000050	0.0000050	8.1206E-06	41
-1.2599993	0.0045512	HIT BODY AT	-0.0009029	0.0054289	0.0082756	2.8464E-06	68
-1.2599993	0.0068123	HIT BODY AT	0.0061579	0.0088386	0.0162043	9.2295E-06	65
-1.2599993	0.0079599	HIT BODY AT	0.0166598	0.0117465	0.0271505	6.7323E-06	80
-1.2599993	0.0085280	OUT OF RANGE	0.0813009	0.0221908		4.7782E-05	95
-1.2599993	0.0082439	OUT OF RANGE	0.0829488	0.0222186		4.7512E-05	111
-1.2599993	0.0081019	OUT OF RANGE	0.0871353	0.0226163		6.1404E-05	116
-1.2599993	0.0080309	OUT OF RANGE	0.0864309	0.0225082		4.4515E-05	119
-1.2599993	-0.0005618	HIT BODY AT	-0.0039709	-0.0006448	-0.0007154	6.9591E-06	45
-1.2599993	-0.0048227	HIT BODY AT	-0.0003887	-0.0057987	-0.0089134	3.1107E-06	56
-1.2599993	-0.0069531	HIT BODY AT	0.0069689	-0.0091094	-0.0170804	1.1028E-05	58
-1.2599993	-0.0080183	HIT BODY AT	0.0263552	-0.0135138	-0.0370157	9.9582E-06	91
-1.2599993	-0.0085509	OUT OF RANGE	0.0868925	-0.0228065		4.9236E-05	87
-1.2599993	-0.0082846	OUT OF RANGE	0.0823606	-0.0221761		4.0522E-05	108
-1.2599993	-0.0081514	OUT OF RANGE	0.0851743	-0.0224173		5.1358E-05	111
-1.2599993	-0.0080849	OUT OF RANGE	0.0836582	-0.0222142		4.8017E-05	92

UPPER SURFACE LIMIT		LOWER SURFACE LIMIT	
YOU	SU	YOL	SL
0.7960E-02	0.2715E-01	-0.8018E-02	-0.3702E-01

| -1.2599993 | 0.0071610 | HIT BODY AT | 0.0082593 | 0.0095326 | 0.0184434 | 9.5929E-06 | 71 |
| -1.2599993 | 0.0061338 | HIT BODY AT | 0.0032192 | 0.0076855 | 0.0130234 | 7.8691E-06 | 68 |

Figure 7.5: continued

```
-1.2599993    0.0051066   HIT BODY AT     0.0002541    0.0061759    0.0096382   4.0084E-06     54
-1.2599993    0.0040795   HIT BODY AT    -0.0018151    0.0048164    0.0069433   2.4937E-06     52
-1.2599993    0.0030523   HIT BODY AT    -0.0036111    0.0035133    0.0037847   6.9544E-06     52
-1.2599993    0.0020251   HIT BODY AT    -0.0037484    0.0023366    0.0024918   1.0324E-05     56
-1.2599993    0.0009980   HIT BODY AT    -0.0038598    0.0011532    0.0015363   5.0499E-06     50
-1.2599993   -0.0000292   HIT BODY AT    -0.0040216   -0.0000330   -0.0000332   8.1260E-06     39
-1.2599993   -0.0010564   HIT BODY AT    -0.0038480   -0.0012178   -0.0016015   8.0285E-06     46
-1.2599993   -0.0020835   HIT BODY AT    -0.0037397   -0.0024063   -0.0025623   6.3720E-06     56
-1.2599993   -0.0031107   HIT BODY AT    -0.0036065   -0.0035786   -0.0038509   4.9189E-06     61
-1.2599993   -0.0041379   HIT BODY AT    -0.0016187   -0.0048994   -0.0073419   2.7035E-06     59
-1.2599993   -0.0051650   HIT BODY AT     0.0004149   -0.0062647   -0.0098281   4.3314E-06     60
-1.2599993   -0.0061922   HIT BODY AT     0.0034358   -0.0077756   -0.0132626   9.5905E-06     63
-1.2599993   -0.0072194   HIT BODY AT     0.0086581   -0.0096553   -0.0188647   7.5941E-06     55
```

Y0 VS S DATA FOR DROPLET DIAMETER=   20.00000 MICRONS
17 POINTS HAVE BEEN CALCULATED

I	S	Y0
1	0.027150	0.007960
2	0.018443	0.007161
3	0.013023	0.006134
4	0.009638	0.005107
5	0.006943	0.004079
6	0.003785	0.003052
7	0.002492	0.002025
8	0.001536	0.000998
9	-0.000033	-0.000029
10	-0.001602	-0.001056
11	-0.002562	-0.002084
12	-0.003851	-0.003111
13	-0.007342	-0.004138
14	-0.009828	-0.005165
15	-0.013263	-0.006192
16	-0.018865	-0.007219
17	-0.037016	-0.008018

CALCULATED LOCAL COLLECTION EFFICIENCY FOR DROPLET DIAMETER=   20.00000 MICRONS

SEG	S	BETA	SEG	S	BETA	SEG	S	BETA
1	-0.311805	0.000000	51	-0.011512	0.312600	101	0.020674	0.122772
2	-0.307626	0.000000	52	-0.009782	0.334206	102	0.022342	0.094780
3	-0.304559	0.000000	53	-0.008418	0.332866	103	0.023998	0.066991
4	-0.299981	0.000000	54	-0.007550	0.332015	104	0.026420	0.026342
5	-0.293141	0.000000	55	-0.006894	0.373618	105	0.029605	0.000000
6	-0.285557	0.000000	56	-0.005736	0.408603	106	0.032716	0.000000
7	-0.277985	0.000000	57	-0.004476	0.446685	107	0.035768	0.000000
8	-0.270422	0.000000	58	-0.003842	0.672177	108	0.038847	0.000000
9	-0.262865	0.000000	59	-0.003704	0.702001	109	0.044215	0.000000
10	-0.255312	0.000000	60	-0.003438	0.748906	110	0.051835	0.000000
11	-0.247761	0.000000	61	-0.003210	0.809049	111	0.059429	0.000000
12	-0.240213	0.000000	62	-0.002921	0.871553	112	0.066997	0.000000
13	-0.232667	0.000000	63	-0.002613	0.938362	113	0.074547	0.000000
14	-0.225122	0.000000	64	-0.002321	0.850024	114	0.082086	0.000000
15	-0.217580	0.000000	65	-0.002153	0.837777	115	0.089618	0.000000
16	-0.210040	0.000000	66	-0.002040	0.829479	116	0.097143	0.000000
17	-0.202502	0.000000	67	-0.001904	0.819519	117	0.104666	0.000000
18	-0.194966	0.000000	68	-0.001772	0.809902	118	0.112187	0.000000
19	-0.187433	0.000000	69	-0.001598	0.857995	119	0.119707	0.000000
20	-0.179901	0.000000	70	-0.001381	0.833184	120	0.127227	0.000000
21	-0.172371	0.000000	71	-0.001112	0.802574	121	0.134748	0.000000
22	-0.164844	0.000000	72	-0.000728	0.758828	122	0.142269	0.000000
23	-0.157318	0.000000	73	-0.000254	0.704716	123	0.149791	0.000000
24	-0.149794	0.000000	74	0.000254	0.712874	124	0.157315	0.000000
25	-0.142272	0.000000	75	0.000729	0.767481	125	0.164841	0.000000
26	-0.134750	0.000000	76	0.001113	0.811653	126	0.172369	0.000000
27	-0.127230	0.000000	77	0.001381	0.842557	127	0.179898	0.000000
28	-0.119710	0.000000	78	0.001599	0.802467	128	0.187430	0.000000
29	-0.112190	0.000000	79	0.001773	0.815026	129	0.194964	0.000000
30	-0.104669	0.000000	80	0.001904	0.824530	130	0.202500	0.000000
31	-0.097146	0.000000	81	0.002040	0.834363	131	0.210038	0.000000
32	-0.089620	0.000000	82	0.002153	0.842550	132	0.217578	0.000000
33	-0.082089	0.000000	83	0.002321	0.854658	133	0.225120	0.000000
34	-0.074550	0.000000	84	0.002612	0.924965	134	0.232664	0.000000
35	-0.067000	0.000000	85	0.002921	0.857384	135	0.240210	0.000000
36	-0.059432	0.000000	86	0.003210	0.794160	136	0.247759	0.000000
37	-0.051838	0.000000	87	0.003487	0.733540	137	0.255309	0.000000
38	-0.044218	0.000000	88	0.003702	0.686370	138	0.262863	0.000000
39	-0.038849	0.000000	89	0.003840	0.500825	139	0.270419	0.000000
40	-0.035770	0.000000	90	0.004483	0.473752	140	0.277982	0.000000
41	-0.032716	0.000000	91	0.005751	0.420415	141	0.285554	0.000000
42	-0.029607	0.019078	92	0.006902	0.372005	142	0.293138	0.000000
43	-0.026425	0.062426	93	0.007548	0.340757	143	0.299979	0.000000
44	-0.024004	0.095400	94	0.008408	0.337226	144	0.304556	0.000000
45	-0.022348	0.117956	95	0.009775	0.343233	145	0.307624	0.000000
46	-0.020680	0.140685	96	0.011507	0.298582	146	0.311802	0.000000
47	-0.019004	0.163511	97	0.013561	0.242132			
48	-0.017286	0.186925	98	0.015481	0.209926			
49	-0.015486	0.211437	99	0.017280	0.179721			
50	-0.013567	0.237579	100	0.018999	0.150880			

NACA 0012 : EXAMPLE 1   : TIME= 120.000 SEC

ICING CONDITION:

```
        STATIC TEMPERATURE (C)         260.55
        STATIC PRESSURE (PA)         90748.00
        VELOCITY (M/S)                 129.00
        LWC (G/M**3)                     0.50
        DROPLET DIAMETER (MICRONS)      20.00
```

ICE ACCRETION DATA:

```
        STAGNATION POINT                74
        TRANSITION POINTS (LOWER,UPPER)  72      75
        ICING LIMITS (LOWER,UPPER)       43     103
        NUMBER OF POINTS               147
        NUMBER OF SEGMENTS ADDED         8
```

Figure 7.5: continued

110

SEG	X	Y	S	VE	TE	PRESS	RA	SEGLENGTH
1	0.30000E 00	0.00000	-0.31233E 00	0.10281E 03	0.26357E 03	0.94483E 05	0.12469E 01	0.30523E-02
2	0.29700E 00	-0.56220E-03	-0.30929E 00	0.11347E 03	0.26242E 03	0.93053E 05	0.12334E 01	0.30449E-02
3	0.29400E 00	-0.10833E-02	-0.30624E 00	0.11730E 03	0.26198E 03	0.92507E 05	0.12282E 01	0.30395E-02
4	0.29100E 00	-0.15717E-02	-0.30169E 00	0.12093E 03	0.26155E 03	0.91977E 05	0.12232E 01	0.60676E-02
5	0.28500E 00	-0.24753E-02	-0.29487E 00	0.12422E 03	0.26115E 03	0.91483E 05	0.12185E 01	0.75710E-02
6	0.27750E 00	-0.35100E-02	-0.28730E 00	0.12654E 03	0.26086E 03	0.91130E 05	0.12151E 01	0.75615E-02
7	0.27000E 00	-0.44724E-02	-0.27975E 00	0.12819E 03	0.26065E 03	0.90875E 05	0.12127E 01	0.75554E-02
8	0.26250E 00	-0.53859E-02	-0.27219E 00	0.12953E 03	0.26048E 03	0.90665E 05	0.12107E 01	0.75515E-02
9	0.25500E 00	-0.62664E-02	-0.26464E 90	0.13074E 03	0.26032E 03	0.90474E 05	0.12088E 01	0.75488E-02
10	0.24750E 00	-0.71217E-02	-0.25710E 00	0.13188E 03	0.26018E 03	0.90294E 05	0.12071E 01	0.75461E-02
11	0.24000E 00	-0.79545E-02	-0.24955E 00	0.13297E 03	0.26003E 03	0.90119E 05	0.12055E 01	0.75438E-02
12	0.23250E 00	-0.87663E-02	-0.24201E 00	0.13403E 03	0.25989E 03	0.89948E 05	0.12038E 01	0.75414E-02
13	0.22500E 00	-0.95565E-02	-0.23447E 00	0.13506E 03	0.25975E 03	0.89781E 05	0.12022E 01	0.75391E-02
14	0.21750E 00	-0.10323E-01	-0.22693E 00	0.13605E 03	0.25962E 03	0.89620E 05	0.12007E 01	0.75367E-02
15	0.21000E 00	-0.11066E-01	-0.21939E 00	0.13703E 03	0.25949E 03	0.89460E 05	0.11991E 01	0.75343E-02
16	0.20250E 00	-0.11784E-01	-0.21186E 00	0.13799E 03	0.25936E 03	0.89301E 05	0.11976E 01	0.75318E-02
17	0.19500E 00	-0.12475E-01	-0.20433E 00	0.13893E 03	0.25923E 03	0.89144E 05	0.11961E 01	0.75292E-02
18	0.18750E 00	-0.13138E-01	-0.19680E 00	0.13986E 03	0.25910E 03	0.88989E 05	0.11946E 01	0.75266E-02
19	0.18000E 00	-0.13771E-01	-0.18928E 00	0.14078E 03	0.25897E 03	0.88835E 05	0.11932E 01	0.75240E-02
20	0.17250E 00	-0.14373E-01	-0.18176E 00	0.14169E 03	0.25884E 03	0.88682E 05	0.11917E 01	0.75214E-02
21	0.16500E 00	-0.14938E-01	-0.17424E 00	0.14258E 03	0.25871E 03	0.88530E 05	0.11902E 01	0.75187E-02
22	0.15750E 00	-0.15463E-01	-0.16672E 00	0.14348E 03	0.25859E 03	0.88377E 05	0.11888E 01	0.75160E-02
23	0.15000E 00	-0.15959E-01	-0.15920E 00	0.14438E 03	0.25846E 03	0.88224E 05	0.11873E 01	0.75135E-02
24	0.14250E 00	-0.16409E-01	-0.15169E 00	0.14528E 03	0.25833E 03	0.88069E 05	0.11858E 01	0.75110E-02
25	0.13500E 00	-0.16815E-01	-0.14418E 00	0.14618E 03	0.25820E 03	0.87913E 05	0.11843E 01	0.75085E-02
26	0.12750E 00	-0.17173E-01	-0.13667E 00	0.14708E 03	0.25807E 03	0.87756E 05	0.11828E 01	0.75062E-02
27	0.12000E 00	-0.17477E-01	-0.12917E 00	0.14798E 03	0.25793E 03	0.87598E 05	0.11813E 01	0.75041E-02
28	0.11250E 00	-0.17727E-01	-0.12167E 00	0.14887E 03	0.25780E 03	0.87442E 05	0.11798E 01	0.75023E-02
29	0.10500E 00	-0.17912E-01	-0.11416E 00	0.14974E 03	0.25767E 03	0.87289E 05	0.11783E 01	0.75009E-02
30	0.97500E-01	-0.18028E-01	-0.10666E 00	0.15059E 03	0.25755E 03	0.87138E 05	0.11768E 01	0.75002E-02
31	0.90000E-01	-0.18068E-01	-0.99164E-01	0.15141E 03	0.25742E 03	0.86994E 05	0.11754E 01	0.75001E-02
32	0.82500E-01	-0.18023E-01	-0.91662E-01	0.15218E 03	0.25731E 03	0.86857E 05	0.11741E 01	0.75012E-02
33	0.75000E-01	-0.17884E-01	-0.84160E-01	0.15289E 03	0.25720E 03	0.86730E 05	0.11729E 01	0.75041E-02
34	0.67500E-01	-0.17638E-01	-0.76654E-01	0.15350E 03	0.25711E 03	0.86619E 05	0.11718E 01	0.75089E-02
35	0.60000E-01	-0.17271E-01	-0.69141E-01	0.15396E 03	0.25704E 03	0.86536E 05	0.11710E 01	0.75171E-02
36	0.52500E-01	-0.16764E-01	-0.61617E-01	0.15418E 03	0.25700E 03	0.86497E 05	0.11706E 01	0.75301E-02
37	0.45000E-01	-0.16091E-01	-0.54077E-01	0.15398E 03	0.25703E 03	0.86713E 05	0.11727E 01	0.75504E-02
38	0.37500E-01	-0.15220E-01	-0.46510E-01	0.15298E 03	0.25719E 03	0.86713E 05	0.11727E 01	0.75829E-02
39	0.30000E-01	-0.14101E-01	-0.41196E-01	0.15113E 03	0.25747E 03	0.87043E 05	0.11759E 01	0.30469E-02
40	0.27000E-01	-0.13568E-01	-0.38143E-01	0.14899E 03	0.25778E 03	0.87422E 05	0.11796E 01	0.30580E-02
41	0.24000E-01	-0.12976E-01	-0.35074E-01	0.14822E 03	0.25790E 03	0.87558E 05	0.11809E 01	0.30799E-02
42	0.20965E-01	-0.12450E-01	-0.31974E-01	0.15026E 03	0.25760E 03	0.87198E 05	0.11774E 01	0.31197E-02
43	0.17871E-01	-0.12055E-01	-0.28841E-01	0.15094E 03	0.25749E 03	0.87077E 05	0.11762E 01	0.31464E-02
44	0.14766E-01	-0.11547E-01	-0.26464E-01	0.15047E 03	0.25756E 03	0.87161E 05	0.11771E 01	0.16085E-02
45	0.13178E-01	-0.11290E-01	-0.24847E-01	0.14985E 03	0.25766E 03	0.87271E 05	0.11781E 01	0.16249E-02
46	0.11589E-01	-0.10948E-01	-0.23214E-01	0.14848E 03	0.25786E 03	0.87512E 05	0.11804E 01	0.16406E-02
47	0.99949E-02	-0.10561E-01	-0.21560E-01	0.14692E 03	0.25809E 03	0.87784E 05	0.11831E 01	0.16673E-02
48	0.83404E-02	-0.10145E-01	-0.19867E-01	0.14544E 03	0.25830E 03	0.88040E 05	0.11855E 01	0.17202E-02
49	0.67222E-02	-0.96873E-02	-0.18107E-01	0.14339E 03	0.25860E 03	0.88392E 05	0.11889E 01	0.17985E-02
50	0.50103E-02	-0.91360E-02	-0.16234E-01	0.13991E 03	0.25909E 03	0.88980E 05	0.11946E 01	0.19477E-02
51	0.31554E-02	-0.85419E-02	-0.14216E-01	0.13396E 03	0.25990E 03	0.89960E 05	0.12039E 01	0.20887E-02
52	0.12332E-02	-0.77248E-02	-0.12529E-01	0.12711E 03	0.26079E 03	0.91042E 05	0.12143E 01	0.12855E-02
53	0.11461E-03	-0.70911E-02	-0.11088E-01	0.12068E 03	0.26158E 03	0.92014E 05	0.12235E 01	0.15971E-02
54	-0.14317E-02	-0.71324E-02	-0.96494E-02	0.11609E 03	0.26212E 03	0.92682E 05	0.12298E 01	0.12797E-02
55	-0.24579E-02	-0.79599E-02	-0.84380E-02	0.11149E 03	0.26264E 03	0.93328E 05	0.12360E 01	0.11431E-02
56	-0.34527E-02	-0.73968E-02	-0.65963E-02	0.10001E 03	0.26385E 03	0.94838E 05	0.12502E 01	0.25404E-02
57	-0.45539E-02	-0.51074E-02	-0.47253E-02	0.82295E 02	0.26546E 03	0.96875E 05	0.12693E 01	0.12016E-02
58	-0.44715E-02	-0.39115E-02	-0.40146E-02	0.72197E 02	0.26624E 03	0.97870E 05	0.12786E 01	0.21980E-03
59	-0.42430E-02	-0.38089E-02	-0.38291E-02	0.70010E 02	0.26639E 03	0.98069E 05	0.12805E 01	0.15117E-03
60	-0.42185E-02	-0.36598E-02	-0.36224E-02	0.66542E 02	0.26663E 03	0.98373E 05	0.12833E 01	0.26195E-03
61	-0.41702E-02	-0.34023E-02	-0.33270E-02	0.62158E 02	0.26691E 03	0.98736E 05	0.12867E 01	0.32922E-03
62	-0.41002E-02	-0.30806E-02	-0.30143E-02	0.57735E 02	0.26717E 03	0.99078E 05	0.12899E 01	0.29607E-03
63	-0.40200E-02	-0.27956E-02	-0.26673E-02	0.53236E 02	0.26742E 03	0.99401E 05	0.12929E 01	0.39804E-03
64	-0.39027E-02	-0.24152E-02	-0.23342E-02	0.49196E 02	0.26762E 03	0.99669E 05	0.12954E 01	0.26804E-03
65	-0.37705E-02	-0.21821E-02	-0.21448E-02	0.46975E 02	0.26773E 03	0.99803E 05	0.12967E 01	0.11081E-03
66	-0.37218E-02	-0.20285E-02	-0.20200E-02	0.45561E 02	0.26780E 03	0.99893E 05	0.12975E 01	0.13877E-03
67	-0.37003E-02	-0.19454E-02	-0.18772E-02	0.43950E 02	0.26787E 03	0.99986E 05	0.12983E 01	0.14695E-03
68	-0.36868E-02	-0.17991E-02	-0.17382E-02	0.42505E 02	0.26793E 03	0.10007E 06	0.12991E 01	0.13095E-03
69	-0.37021E-02	-0.16690E-02	-0.15595E-02	0.40822E 02	0.26800E 03	0.10016E 06	0.12999E 01	0.22637E-03
70	-0.37369E-02	-0.14454E-02	-0.13413E-02	0.38966E 02	0.26807E 03	0.10026E 06	0.13008E 01	0.21016E-03
71	-0.37261E-02	-0.12355E-02	-0.10974E-02	0.37010E 02	0.26815E 03	0.10035E 06	0.13017E 01	0.27754E-03
72	-0.37307E-02	-0.95797E-03	-0.72425E-03	0.34789E 02	0.26823E 03	0.10046E 06	0.13027E 01	0.46881E-03
73	-0.37427E-02	-0.48931E-03	-0.24492E-03	0.33281E 02	0.26828E 03	0.10052E 06	0.13033E 01	0.48984E-03
74	-0.37559E-02	0.35418E-06	0.24487E-03	0.33289E 02	0.26828E 03	0.10052E 06	0.13033E 01	0.48974E-03
75	-0.37478E-02	0.49002E-03	0.72446E-03	0.34796E 02	0.26823E 03	0.10046E 06	0.13027E 01	0.46945E-03
76	-0.37362E-02	0.95933E-03	0.10983E-02	0.37031E 02	0.26815E 03	0.10035E 06	0.13017E 01	0.27820E-03
77	-0.37321E-02	0.12375E-02	0.13405E-02	0.38993E 02	0.26807E 03	0.10025E 06	0.13008E 01	0.20621E-03
78	-0.37244E-02	0.14436E-02	0.15567E-02	0.40847E 02	0.26800E 03	0.10016E 06	0.12999E 01	0.22620E-03
79	-0.36882E-02	0.16669E-02	0.17365E-02	0.42529E 02	0.26793E 03	0.10007E 06	0.12991E 01	0.13346E-03
80	-0.36902E-02	0.18003E-02	0.18766E-02	0.43979E 02	0.26787E 03	0.99985E 05	0.12983E 01	0.14666E-03
81	-0.37036E-02	0.19463E-02	0.20190E-02	0.45589E 02	0.26779E 03	0.99891E 05	0.12974E 01	0.13826E-03
82	-0.37247E-02	0.20830E-02	0.21434E-02	0.46997E 02	0.26773E 03	0.99806E 05	0.12967E 01	0.11045E-03
83	-0.37733E-02	0.21822E-02	0.23311E-02	0.49222E 02	0.26762E 03	0.99668E 05	0.12954E 01	0.26500E-03
84	-0.39003E-02	0.24148E-02	0.26616E-02	0.53260E 02	0.26742E 03	0.99399E 05	0.12929E 01	0.39604E-03
85	-0.40121E-02	0.27947E-02	0.30079E-02	0.57761E 02	0.26717E 03	0.99076E 05	0.12899E 01	0.29641E-03
86	-0.40921E-02	0.30801E-02	0.33204E-02	0.62191E 02	0.26690E 03	0.98734E 05	0.12867E 01	0.32873E-03
87	-0.41613E-02	0.34015E-02	0.36146E-02	0.66557E 02	0.26662E 03	0.98372E 05	0.12833E 01	0.25957E-03
88	-0.42085E-02	0.36567E-02	0.38182E-02	0.70002E 02	0.26639E 03	0.98070E 05	0.12805E 01	0.14760E-03
89	-0.41875E-02	0.38028E-02	0.40096E-02	0.72190E 02	0.26624E 03	0.97871E 05	0.12786E 01	0.23530E-03
90	-0.43983E-02	0.39073E-02	0.47420E-02	0.82429E 02	0.26545E 03	0.96861E 05	0.12692E 01	0.12295E-02
91	-0.45587E-02	0.51263E-02	0.66297E-02	0.10016E 03	0.26384E 03	0.94810E 05	0.12500E 01	0.25459E-02
92	-0.34338E-02	0.74102E-02	0.84734E-02	0.11147E 03	0.26265E 03	0.93330E 05	0.12360E 01	0.11414E-02
93	-0.23837E-02	0.78575E-02	0.96778E-02	0.11596E 03	0.26214E 03	0.92699E 05	0.12300E 01	0.12675E-02
94	-0.14199E-02	0.70342E-02	0.11052E-01	0.12052E 03	0.26160E 03	0.92038E 05	0.12237E 01	0.15199E-02
95	-0.98083E-04	0.71093E-02	0.12476E-01	0.12702E 03	0.26080E 03	0.91056E 05	0.12144E 01	0.12896E-02
96	0.12378E-02	0.77127E-02	0.14167E-01	0.13392E 03	0.25991E 03	0.89966E 05	0.12040E 01	0.20912E-02
97	0.31654E-02	0.85237E-02	0.16183E-01	0.13989E 03	0.25909E 03	0.88984E 05	0.11946E 01	0.19423E-02
98	0.50066E-02	0.91421E-02	0.18055E-01	0.14339E 03	0.25860E 03	0.88393E 05	0.11889E 01	0.18000E-02
99	0.67269E-02	0.96717E-02	0.19815E-01	0.14545E 03	0.25830E 03	0.88039E 05	0.11855E 01	0.17213E-02
100	0.83922E-02	0.10107E-01	0.21510E-01	0.14693E 03	0.25809E 03	0.87783E 05	0.11831E 01	0.16679E-02
101	0.10013E-01	0.10503E-01	0.23164E-01	0.14850E 03	0.25786E 03	0.87509E 05	0.11804E 01	0.16402E-02
102	0.11611E-01	0.10870E-01	0.24796E-01	0.14990E 03	0.25765E 03	0.87261E 05	0.11780E 01	0.16231E-02
103	0.13202E-01	0.11191E-01	0.26414E-01	0.15057E 03	0.25755E 03	0.87142E 05	0.11769E 01	0.16139E-02
104	0.14806E-01	0.11369E-01	0.28792E-01	0.15113E 03	0.25746E 03	0.87043E 05	0.11759E 01	0.31430E-02
105	0.17897E-01	0.11938E-01	0.31919E-01	0.15043E 03	0.25757E 03	0.87167E 05	0.11771E 01	0.31100E-02
106	0.20964E-01	0.12456E-01	0.35014E-01	0.14822E 03	0.25790E 03	0.87558E 05	0.11809E 01	0.30804E-02
107	0.24000E-01	0.12976E-01	0.38083E-01	0.14891E 03	0.25780E 03	0.87437E 05	0.11797E 01	0.30580E-02
108	0.27000E-01	0.13568E-01	0.41136E-01	0.15108E 03	0.25747E 03	0.87051E 05	0.11760E 01	0.30469E-02
109	0.30000E-01	0.14101E-01	0.46451E-01	0.15296E 03	0.25719E 03	0.86716E 05	0.11728E 01	0.75829E-02
110	0.37500E-01	0.15220E-01	0.54017E-01	0.15397E 03	0.25703E 03	0.86534E 05	0.11710E 01	0.75504E-02

Figure 7.5: continued

SEG	X	Y	S	VE	TE	PRESS	RR	SEGLENGTH
111	0.45000E-01	0.16091E-01	0.61558E-01	0.15417E 03	0.25700E 03	0.86498E 05	0.11707E 01	0.75301E-02
112	0.52500E-01	0.16764E-01	0.69081E-01	0.15396E 03	0.25704E 03	0.86537E 05	0.11710E 01	0.75171E-02
113	0.60000E-01	0.17271E-01	0.76599E-01	0.15349E 03	0.25711E 03	0.86620E 05	0.11718E 01	0.75089E-02
114	0.67500E-01	0.17638E-01	0.84101E-01	0.15289E 03	0.25720E 03	0.86730E 05	0.11729E 01	0.75041E-02
115	0.75000E-01	0.17884E-01	0.91603E-01	0.15217E 03	0.25731E 03	0.86857E 05	0.11741E 01	0.75012E-02
116	0.82500E-01	0.18023E-01	0.99104E-01	0.15140E 03	0.25742E 03	0.86994E 05	0.11755E 01	0.75001E-02
117	0.90000E-01	0.18068E-01	0.10660E 00	0.15059E 03	0.25755E 03	0.87139E 05	0.11768E 01	0.75002E-02
118	0.97500E-01	0.18028E-01	0.11410E 00	0.14974E 03	0.25767E 03	0.87289E 05	0.11783E 01	0.75009E-02
119	0.10500E 00	0.17912E-01	0.12161E 00	0.14887E 03	0.25780E 03	0.87442E 05	0.11798E 01	0.75023E-02
120	0.11250E 00	0.17727E-01	0.12911E 00	0.14798E 03	0.25793E 03	0.87599E 05	0.11813E 01	0.75041E-02
121	0.12000E 00	0.17479E-01	0.13661E 00	0.14708E 03	0.25807E 03	0.87757E 05	0.11828E 01	0.75062E-02
122	0.12750E 00	0.17173E-01	0.14412E 00	0.14618E 03	0.25820E 03	0.87913E 05	0.11843E 01	0.75085E-02
123	0.13500E 00	0.16815E-01	0.15163E 00	0.14527E 03	0.25833E 03	0.88069E 05	0.11858E 01	0.75110E-02
124	0.14250E 00	0.16409E-01	0.15914E 00	0.14438E 03	0.25846E 03	0.88224E 05	0.11873E 01	0.75135E-02
125	0.15000E 00	0.15959E-01	0.16666E 00	0.14348E 03	0.25859E 03	0.88377E 05	0.11888E 01	0.75162E-02
126	0.15750E 00	0.15468E-01	0.17418E 00	0.14258E 03	0.25871E 03	0.88530E 05	0.11902E 01	0.75187E-02
127	0.16500E 00	0.14938E-01	0.18170E 00	0.14169E 03	0.25884E 03	0.88682E 05	0.11917E 01	0.75214E-02
128	0.17250E 00	0.14372E-01	0.18922E 00	0.14078E 03	0.25897E 03	0.88835E 05	0.11932E 01	0.75240E-02
129	0.18000E 00	0.13771E-01	0.19674E 00	0.13986E 03	0.25910E 03	0.88989E 05	0.11946E 01	0.75266E-02
130	0.18750E 00	0.13138E-01	0.20427E 00	0.13893E 03	0.25923E 03	0.89145E 05	0.11961E 01	0.75292E-02
131	0.19500E 00	0.12475E-01	0.21180E 00	0.13799E 03	0.25936E 03	0.89301E 05	0.11976E 01	0.75318E-02
132	0.20250E 00	0.11784E-01	0.21933E 00	0.13703E 03	0.25949E 03	0.89460E 05	0.11991E 01	0.75343E-02
133	0.21000E 00	0.11066E-01	0.22687E 00	0.13605E 03	0.25962E 03	0.89620E 05	0.12007E 01	0.75367E-02
134	0.21750E 00	0.10323E-01	0.23441E 00	0.13506E 03	0.25975E 03	0.89782E 05	0.12022E 01	0.75391E-02
135	0.22500E 00	0.95565E-02	0.24195E 00	0.13403E 03	0.25989E 03	0.89948E 05	0.12038E 01	0.75414E-02
136	0.23250E 00	0.87663E-02	0.24949E 00	0.13296E 03	0.26003E 03	0.90120E 05	0.12055E 01	0.75438E-02
137	0.24000E 00	0.79545E-02	0.25704E 00	0.13187E 03	0.26018E 03	0.90294E 05	0.12071E 01	0.75461E-02
138	0.24750E 00	0.71217E-02	0.26458E 00	0.13074E 03	0.26033E 03	0.90475E 05	0.12089E 01	0.75486E-02
139	0.25500E 00	0.62664E-02	0.27213E 00	0.12952E 03	0.26048E 03	0.90666E 05	0.12107E 01	0.75515E-02
140	0.26250E 00	0.53859E-02	0.27969E 00	0.12818E 03	0.26065E 03	0.90875E 05	0.12127E 01	0.75554E-02
141	0.27000E 00	0.44724E-02	0.28724E 00	0.12654E 03	0.26086E 03	0.91130E 05	0.12151E 01	0.75615E-02
142	0.27750E 00	0.35100E-02	0.29481E 00	0.12422E 03	0.26115E 03	0.91483E 05	0.12185E 01	0.75710E-02
143	0.28500E 00	0.24753E-02	0.30163E 00	0.12093E 03	0.26155E 03	0.91977E 05	0.12232E 01	0.60676E-02
144	0.29100E 00	0.15717E-02	0.30618E 00	0.11730E 03	0.26198E 03	0.92507E 05	0.12282E 01	0.30395E-02
145	0.29400E 00	0.10833E-02	0.30923E 00	0.11347E 03	0.26242E 03	0.93053E 05	0.12334E 01	0.30449E-02
146	0.29700E 00	0.56220E-03	0.31227E 00	0.10281E 03	0.26357E 03	0.94483E 05	0.12469E 01	0.30523E-02
147	0.30000E 00	0.00000	0.00000	0.00000	0.00000	0.00000	0.00000	0.00000

SEG	S	HTC	XK	BETA	FFRAC	RI	TSURF	DICE
1	-0.31233E 00	0.00000	0.35000E-03	0.00000	0.10000E 01	0.35791E 03	0.00000	0.00000
2	-0.30929E 00	0.36903E 03	0.35000E-03	0.00000	0.10000E 01	0.35791E 03	0.00000	0.00000
3	-0.30624E 00	0.38979E 03	0.35000E-03	0.00000	0.10000E 01	0.35791E 03	0.00000	0.00000
4	-0.30169E 00	0.41010E 03	0.35000E-03	0.00000	0.10000E 01	0.35791E 03	0.00000	0.00000
5	-0.29487E 00	0.42941E 03	0.35000E-03	0.00000	0.10000E 01	0.35791E 03	0.00000	0.00000
6	-0.28730E 00	0.44331E 03	0.35000E-03	0.00000	0.10000E 01	0.35791E 03	0.00000	0.00000
7	-0.27975E 00	0.45474E 03	0.35000E-03	0.00000	0.10000E 01	0.35791E 03	0.00000	0.00000
8	-0.27219E 00	0.46414E 03	0.35000E-03	0.00000	0.10000E 01	0.35791E 03	0.00000	0.00000
9	-0.26464E 00	0.47300E 03	0.35000E-03	0.00000	0.10000E 01	0.35791E 03	0.00000	0.00000
10	-0.25710E 00	0.48163E 03	0.35000E-03	0.00000	0.10000E 01	0.35791E 03	0.00000	0.00000
11	-0.24955E 00	0.49021E 03	0.35000E-03	0.00000	0.10000E 01	0.35791E 03	0.00000	0.00000
12	-0.24201E 00	0.49886E 03	0.35000E-03	0.00000	0.10000E 01	0.35791E 03	0.00000	0.00000
13	-0.23447E 00	0.50753E 03	0.35000E-03	0.00000	0.10000E 01	0.35791E 03	0.00000	0.00000
14	-0.22693E 00	0.51622E 03	0.35000E-03	0.00000	0.10000E 01	0.35791E 03	0.00000	0.00000
15	-0.21939E 00	0.52511E 03	0.35000E-03	0.00000	0.10000E 01	0.35791E 03	0.00000	0.00000
16	-0.21186E 00	0.53418E 03	0.35000E-03	0.00000	0.10000E 01	0.35791E 03	0.00000	0.00000
17	-0.20433E 00	0.54345E 03	0.35000E-03	0.00000	0.10000E 01	0.35791E 03	0.00000	0.00000
18	-0.19680E 00	0.55298E 03	0.35000E-03	0.00000	0.10000E 01	0.35791E 03	0.00000	0.00000
19	-0.18928E 00	0.56278E 03	0.35000E-03	0.00000	0.10000E 01	0.35791E 03	0.00000	0.00000
20	-0.18176E 00	0.57292E 03	0.35000E-03	0.00000	0.10000E 01	0.35791E 03	0.00000	0.00000
21	-0.17424E 00	0.58344E 03	0.35000E-03	0.00000	0.10000E 01	0.35791E 03	0.00000	0.00000
22	-0.16672E 00	0.59448E 03	0.35000E-03	0.00000	0.10000E 01	0.35791E 03	0.00000	0.00000
23	-0.15920E 00	0.60602E 03	0.35000E-03	0.00000	0.10000E 01	0.35791E 03	0.00000	0.00000
24	-0.15169E 00	0.61823E 03	0.35000E-03	0.00000	0.10000E 01	0.35791E 03	0.00000	0.00000
25	-0.14418E 00	0.63115E 03	0.35000E-03	0.00000	0.10000E 01	0.35791E 03	0.00000	0.00000
26	-0.13667E 00	0.64492E 03	0.35000E-03	0.00000	0.10000E 01	0.35791E 03	0.00000	0.00000
27	-0.12917E 00	0.65962E 03	0.35000E-03	0.00000	0.10000E 01	0.35791E 03	0.00000	0.00000
28	-0.12167E 00	0.67531E 03	0.35000E-03	0.00000	0.10000E 01	0.35791E 03	0.00000	0.00000
29	-0.11416E 00	0.69214E 03	0.35000E-03	0.00000	0.10000E 01	0.35791E 03	0.00000	0.00000
30	-0.10666E 00	0.71033E 03	0.35000E-03	0.00000	0.10000E 01	0.35791E 03	0.00000	0.00000
31	-0.99164E-01	0.73005E 03	0.35000E-03	0.00000	0.10000E 01	0.35791E 03	0.00000	0.00000
32	-0.91663E-01	0.75164E 03	0.35000E-03	0.00000	0.10000E 01	0.35791E 03	0.00000	0.00000
33	-0.84160E-01	0.77549E 03	0.35000E-03	0.00000	0.10000E 01	0.35791E 03	0.00000	0.00000
34	-0.76654E-01	0.80198E 03	0.35000E-03	0.00000	0.10000E 01	0.35791E 03	0.00000	0.00000
35	-0.69141E-01	0.83159E 03	0.35000E-03	0.00000	0.10000E 01	0.35791E 03	0.00000	0.00000
36	-0.61617E-01	0.86483E 03	0.35000E-03	0.00000	0.10000E 01	0.35791E 03	0.00000	0.00000
37	-0.54077E-01	0.90196E 03	0.35000E-03	0.00000	0.10000E 01	0.35791E 03	0.00000	0.00000
38	-0.46510E-01	0.94150E 03	0.35000E-03	0.00000	0.10000E 01	0.35791E 03	0.00000	0.00000
39	-0.41196E-01	0.96466E 03	0.35000E-03	0.00000	0.10000E 01	0.35791E 03	0.00000	0.00000
40	-0.38143E-01	0.96850E 03	0.35000E-03	0.00000	0.10000E 01	0.35791E 03	0.00000	0.00000
41	-0.35074E-01	0.99093E 03	0.35000E-03	0.00000	0.10000E 01	0.35791E 03	0.00000	0.00000
42	-0.31974E-01	0.10548E 04	0.35000E-03	0.19078E-01	0.10000E 01	0.91700E 03	0.26637E 03	0.26346E-03
43	-0.28841E-01	0.11152E 04	0.35000E-03	0.62426E-01	0.10000E 01	0.91700E 03	0.26669E 03	0.40261E-03
44	-0.26464E-01	0.11584E 04	0.35000E-03	0.95400E-01	0.10000E 01	0.91700E 03	0.26690E 03	0.49781E-03
45	-0.24847E-01	0.11895E 04	0.35000E-03	0.11796E 00	0.10000E 01	0.91700E 03	0.26711E 03	0.59373E-03
46	-0.23214E-01	0.12161E 04	0.35000E-03	0.14069E 00	0.10000E 01	0.91700E 03	0.26732E 03	0.69006E-03
47	-0.21560E-01	0.12472E 04	0.35000E-03	0.16351E 00	0.10000E 01	0.91700E 03	0.26750E 03	0.78887E-03
48	-0.19867E-01	0.12904E 04	0.35000E-03	0.18692E 00	0.10000E 01	0.91700E 03	0.26767E 03	0.89232E-03
49	-0.18107E-01	0.13411E 04	0.35000E-03	0.21144E 00	0.10000E 01	0.91700E 03	0.26787E 03	0.10027E-02
50	-0.16234E-01	0.13935E 04	0.35000E-03	0.23758E 00	0.10000E 01	0.91700E 03	0.26848E 03	0.11193E-02
51	-0.14216E-01	0.14409E 04	0.35000E-03	0.31260E 00	0.10000E 01	0.91700E 03	0.26867E 03	0.14104E-02
52	-0.12529E-01	0.14783E 04	0.35000E-03	0.33421E 00	0.10000E 01	0.91700E 03	0.26866E 03	0.14048E-02
53	-0.11088E-01	0.15282E 04	0.35000E-03	0.33287E 00	0.10000E 01	0.91700E 03	0.27203E 03	0.33552E-02
54	-0.96494E-02	0.16128E 04	0.35000E-03	0.33201E 00	0.10000E 01	0.91700E 03	0.27315E 03	0.38217E-02
55	-0.84380E-02	0.16337E 04	0.35000E-03	0.37362E 00	0.63189E 00	0.91700E 03	0.27315E 03	0.36620E-02
56	-0.65963E-02	0.15858E 04	0.35000E-03	0.40860E 00	0.59133E 00	0.91700E 03	0.27315E 03	0.30259E-02
57	-0.47253E-02	0.13187E 04	0.35000E-03	0.44668E 00	0.99940E-01	0.91700E 03	0.27315E 03	0.26501E-02
58	-0.40146E-02	0.10925E 04	0.35000E-03	0.67200E 00	0.84900E-01	0.91700E 03	0.27315E 03	0.26501E-02
59	-0.38291E-02	0.10769E 04	0.35000E-03	0.70200E 00	0.12827E 00	0.91700E 03	0.27315E 03	0.26288E-02

Figure 7.5: continued

SEG	S	HTC	XK	BETA	FFRAC	RI	TSURF	DICE
60	-0.36226E-02	0.10384E 04	0.35000E-03	0.74891E 00	0.13035E 00	0.91700E 03	0.27315E 03	0.25674E-02
61	-0.33270E-02	0.77539E 03	0.35000E-03	0.80905E 00	0.13388E 00	0.91700E 03	0.27315E 03	0.24625E-02
62	-0.30143E-02	0.91001E 03	0.35000E-03	0.87155E 00	0.14107E 00	0.91700E 03	0.27315E 03	0.23562E-02
63	-0.26673E-02	0.84022E 03	0.35000E-03	0.93836E 00	0.15023E 00	0.91700E 03	0.27315E 03	0.22453E-02
64	-0.23342E-02	0.76773E 03	0.35000E-03	0.85002E 00	0.98205E-01	0.91700E 03	0.27315E 03	0.20413E-02
65	-0.21448E-02	0.73253E 03	0.35000E-03	0.83778E 00	0.99926E-01	0.91700E 03	0.27315E 03	0.19603E-02
66	-0.20200E-02	0.71991E 03	0.35000E-03	0.82948E 00	0.11225E 00	0.91700E 03	0.27315E 03	0.19284E-02
67	-0.18772E-02	0.70410E 03	0.35000E-03	0.81952E 00	0.12827E 00	0.91700E 03	0.27315E 03	0.18889E-02
68	-0.17382E-02	0.69690E 03	0.35000E-03	0.80990E 00	0.15287E 00	0.91700E 03	0.27315E 03	0.18672E-02
69	-0.15595E-02	0.69038E 03	0.35000E-03	0.85799E 00	0.19733E 00	0.91700E 03	0.27315E 03	0.18803E-02
70	-0.13413E-02	0.67910E 03	0.35000E-03	0.83318E 00	0.18054E 00	0.91700E 03	0.27315E 03	0.18414E-02
71	-0.10974E-02	0.66015E 03	0.35000E-03	0.80257E 00	0.20821E 00	0.91700E 03	0.27315E 03	0.17839E-02
72	-0.72425E-03	0.66318E 03	0.35000E-03	0.75883E 00	0.40589E 00	0.91700E 03	0.27315E 03	0.17626E-02
73	-0.24492E-03	0.66318E 03	0.35000E-03	0.70472E 00	0.58275E 00	0.91700E 03	0.27315E 03	0.17332E-02
74	0.24487E-03	0.66334E 03	0.35000E-03	0.71287E 00	0.57777E 00	0.91700E 03	0.27315E 03	0.17382E-02
75	0.72446E-03	0.66334E 03	0.35000E-03	0.76748E 00	0.40104E 00	0.91700E 03	0.27315E 03	0.17679E-02
76	0.10983E-02	0.66065E 03	0.35000E-03	0.81165E 00	0.20501E 00	0.91700E 03	0.27315E 03	0.17902E-02
77	0.13405E-02	0.67970E 03	0.35000E-03	0.84256E 00	0.17775E 00	0.91700E 03	0.27315E 03	0.18431E-02
78	0.15567E-02	0.69090E 03	0.35000E-03	0.80247E 00	0.19606E 00	0.91700E 03	0.27315E 03	0.18491E-02
79	0.17365E-02	0.69735E 03	0.35000E-03	0.81503E 00	0.15388E 00	0.91700E 03	0.27315E 03	0.18711E-02
80	0.18766E-02	0.70467E 03	0.35000E-03	0.82453E 00	0.12892E 00	0.91700E 03	0.27315E 03	0.18930E-02
81	0.20190E-02	0.72042E 03	0.35000E-03	0.83436E 00	0.11268E 00	0.91700E 03	0.27315E 03	0.19322E-02
82	0.21434E-02	0.73285E 03	0.35000E-03	0.84255E 00	0.10019E 00	0.91700E 03	0.27315E 03	0.19638E-02
83	0.23311E-02	0.76815E 03	0.35000E-03	0.85466E 00	0.98379E-01	0.91700E 03	0.27315E 03	0.20449E-02
84	0.26616E-02	0.84057E 03	0.35000E-03	0.92496E 00	0.15036E 00	0.91700E 03	0.27315E 03	0.22382E-02
85	0.30079E-02	0.91042E 03	0.35000E-03	0.85738E 00	0.14160E 00	0.91700E 03	0.27315E 03	0.23489E-02
86	0.33204E-02	0.97594E 03	0.35000E-03	0.79416E 00	0.13474E 00	0.91700E 03	0.27315E 03	0.24550E-02
87	0.36146E-02	0.10385E 04	0.35000E-03	0.73354E 00	0.13152E 00	0.91700E 03	0.27315E 03	0.25587E-02
88	0.38182E-02	0.10764E 04	0.35000E-03	0.68637E 00	0.12976E 00	0.91700E 03	0.27315E 03	0.26187E-02
89	0.40096E-02	0.10921E 04	0.35000E-03	0.50082E 00	0.84962E-01	0.91700E 03	0.27315E 03	0.25496E-02
90	0.47420E-02	0.13219E 04	0.35000E-03	0.47375E 00	0.10410E 00	0.91700E 03	0.27315E 03	0.30489E-02
91	0.66297E-02	0.15886E 04	0.35000E-03	0.42042E 00	0.60508E 00	0.91700E 03	0.27315E 03	0.36758E-02
92	0.84734E-02	0.16323E 04	0.35000E-03	0.37200E 00	0.66049E 00	0.91700E 03	0.27315E 03	0.38174E-02
93	0.96778E-02	0.16094E 04	0.35000E-03	0.34076E 00	0.10000E 01	0.91700E 03	0.27166E 03	0.31282E-02
94	0.11072E-01	0.15252E 04	0.35000E-03	0.33723E 00	0.10000E 01	0.91700E 03	0.26870E 03	0.14232E-02
95	0.12476E-01	0.14776E 04	0.35000E-03	0.34323E 00	0.10000E 01	0.91700E 03	0.26874E 03	0.14485E-02
96	0.14167E-01	0.14411E 04	0.35000E-03	0.29858E 00	0.10000E 01	0.91700E 03	0.26837E 03	0.12601E-02
97	0.16183E-01	0.13939E 04	0.35000E-03	0.24213E 00	0.10000E 01	0.91700E 03	0.26791E 03	0.10219E-02
98	0.18055E-01	0.13416E 04	0.35000E-03	0.20993E 00	0.10000E 01	0.91700E 03	0.26766E 03	0.88595E-03
99	0.19815E-01	0.12909E 04	0.35000E-03	0.17972E 00	0.10000E 01	0.91700E 03	0.26743E 03	0.75847E-03
100	0.21510E-01	0.12476E 04	0.35000E-03	0.15088E 00	0.10000E 01	0.91700E 03	0.26720E 03	0.63675E-03
101	0.23164E-01	0.12166E 04	0.35000E-03	0.12277E 00	0.10000E 01	0.91700E 03	0.26694E 03	0.51813E-03
102	0.24796E-01	0.11905E 04	0.35000E-03	0.94780E-01	0.10000E 01	0.91700E 03	0.26667E 03	0.40000E-03
103	0.26414E-01	0.11599E 04	0.35000E-03	0.66991E-01	0.10000E 01	0.91700E 03	0.26639E 03	0.28272E-03
104	0.28792E-01	0.11177E 04	0.35000E-03	0.26342E-01	0.10000E 01	0.35791E 03	0.00000	0.00000
105	0.31919E-01	0.10566E 04	0.35000E-03	0.00000	0.10000E 01	0.35791E 03	0.00000	0.00000
106	0.35014E-01	0.99059E 03	0.35000E-03	0.00000	0.10000E 01	0.35791E 03	0.00000	0.00000
107	0.38083E-01	0.96731E 03	0.35000E-03	0.00000	0.10000E 01	0.35791E 03	0.00000	0.00000
108	0.41136E-01	0.96396E 03	0.35000E-03	0.00000	0.10000E 01	0.35791E 03	0.00000	0.00000
109	0.46451E-01	0.94117E 03	0.35000E-03	0.00000	0.10000E 01	0.35791E 03	0.00000	0.00000
110	0.54017E-01	0.90179E 03	0.35000E-03	0.00000	0.10000E 01	0.35791E 03	0.00000	0.00000
111	0.61558E-01	0.86473E 03	0.35000E-03	0.00000	0.10000E 01	0.35791E 03	0.00000	0.00000
112	0.69081E-01	0.83153E 03	0.35000E-03	0.00000	0.10000E 01	0.35791E 03	0.00000	0.00000
113	0.76594E-01	0.80192E 03	0.35000E-03	0.00000	0.10000E 01	0.35791E 03	0.00000	0.00000
114	0.84101E-01	0.77547E 03	0.35000E-03	0.00000	0.10000E 01	0.35791E 03	0.00000	0.00000
115	0.91603E-01	0.75161E 03	0.35000E-03	0.00000	0.10000E 01	0.35791E 03	0.00000	0.00000
116	0.99104E-01	0.73002E 03	0.35000E-03	0.00000	0.10000E 01	0.35791E 03	0.00000	0.00000
117	0.10660E 00	0.71029E 03	0.35000E-03	0.00000	0.10000E 01	0.35791E 03	0.00000	0.00000
118	0.11410E 00	0.69212E 03	0.35000E-03	0.00000	0.10000E 01	0.35791E 03	0.00000	0.00000
119	0.12161E 00	0.67530E 03	0.35000E-03	0.00000	0.10000E 01	0.35791E 03	0.00000	0.00000
120	0.12911E 00	0.65960E 03	0.35000E-03	0.00000	0.10000E 01	0.35791E 03	0.00000	0.00000
121	0.13561E 00	0.64490E 03	0.35000E-03	0.00000	0.10000E 01	0.35791E 03	0.00000	0.00000
122	0.14412E 00	0.63115E 03	0.35000E-03	0.00000	0.10000E 01	0.35791E 03	0.00000	0.00000
123	0.15163E 00	0.61821E 03	0.35000E-03	0.00000	0.10000E 01	0.35791E 03	0.00000	0.00000
124	0.15914E 00	0.60602E 03	0.35000E-03	0.00000	0.10000E 01	0.35791E 03	0.00000	0.00000
125	0.16666E 00	0.59466E 03	0.35000E-03	0.00000	0.10000E 01	0.35791E 03	0.00000	0.00000
126	0.17418E 00	0.58344E 03	0.35000E-03	0.00000	0.10000E 01	0.35791E 03	0.00000	0.00000
127	0.18170E 00	0.57292E 03	0.35000E-03	0.00000	0.10000E 01	0.35791E 03	0.00000	0.00000
128	0.18922E 00	0.56278E 03	0.35000E-03	0.00000	0.10000E 01	0.35791E 03	0.00000	0.00000
129	0.19674E 00	0.55296E 03	0.35000E-03	0.00000	0.10000E 01	0.35791E 03	0.00000	0.00000
130	0.20427E 00	0.54343E 03	0.35000E-03	0.00000	0.10000E 01	0.35791E 03	0.00000	0.00000
131	0.21180E 00	0.53416E 03	0.35000E-03	0.00000	0.10000E 01	0.35791E 03	0.00000	0.00000
132	0.21933E 00	0.52510E 03	0.35000E-03	0.00000	0.10000E 01	0.35791E 03	0.00000	0.00000
133	0.22687E 00	0.51622E 03	0.35000E-03	0.00000	0.10000E 01	0.35791E 03	0.00000	0.00000
134	0.23441E 00	0.50752E 03	0.35000E-03	0.00000	0.10000E 01	0.35791E 03	0.00000	0.00000
135	0.24195E 00	0.49885E 03	0.35000E-03	0.00000	0.10000E 01	0.35791E 03	0.00000	0.00000
136	0.24949E 00	0.49020E 03	0.35000E-03	0.00000	0.10000E 01	0.35791E 03	0.00000	0.00000
137	0.25704E 00	0.48162E 03	0.35000E-03	0.00000	0.10000E 01	0.35791E 03	0.00000	0.00000
138	0.26458E 00	0.47298E 03	0.35000E-03	0.00000	0.10000E 01	0.35791E 03	0.00000	0.00000
139	0.27213E 00	0.46412E 03	0.35000E-03	0.00000	0.10000E 01	0.35791E 03	0.00000	0.00000
140	0.27969E 00	0.45472E 03	0.35000E-03	0.00000	0.10000E 01	0.35791E 03	0.00000	0.00000
141	0.28724E 00	0.44380E 03	0.35000E-03	0.00000	0.10000E 01	0.35791E 03	0.00000	0.00000
142	0.29481E 00	0.42941E 03	0.35000E-03	0.00000	0.10000E 01	0.35791E 03	0.00000	0.00000
143	0.30163E 00	0.41009E 03	0.35000E-03	0.00000	0.10000E 01	0.35791E 03	0.00000	0.00000
144	0.30618E 00	0.38979E 03	0.35000E-03	0.00000	0.10000E 01	0.35791E 03	0.00000	0.00000
145	0.30923E 00	0.36903E 03	0.35000E-03	0.00000	0.10000E 01	0.35791E 03	0.00000	0.00000
146	0.31227E 00	0.31438E 03	0.35000E-03	0.00000	0.10000E 01	0.35791E 03	0.00000	0.00000

SEG	S	GCOND	MDOTC	MDOTRI	MDOTE	MDOTTI	MDOTT
1	-0.31233E 00	0.00000	0.00000	0.00000	0.00000	0.00000	0.00000
2	-0.30929E 00	0.00000	0.00000	0.00000	0.00000	0.00000	0.00000
3	-0.30624E 00	0.00000	0.00000	0.00000	0.00000	0.00000	0.00000
4	-0.30169E 00	0.00000	0.00000	0.00000	0.00000	0.00000	0.00000
5	-0.29487E 00	0.00000	0.00000	0.00000	0.00000	0.00000	0.00000
6	-0.28730E 00	0.00000	0.00000	0.00000	0.00000	0.00000	0.00000
7	-0.27975E 00	0.00000	0.00000	0.00000	0.00000	0.00000	0.00000
8	-0.27219E 00	0.00000	0.00000	0.00000	0.00000	0.00000	0.00000
9	-0.26464E 00	0.00000	0.00000	0.00000	0.00000	0.00000	0.00000
10	-0.25710E 00	0.00000	0.00000	0.00000	0.00000	0.00000	0.00000

Figure 7.5: continued

113

SEG	S	QCOND	MDOTC	MDOTRI	MDOTE	MDOTTI	MDOTT
11	-0.24955E 00	0.00000	0.00000	0.00000	0.00000	0.00000	0.00000
12	-0.24201E 00	0.00000	0.00000	0.00000	0.00000	0.00000	0.00000
13	-0.23447E 00	0.00000	0.00000	0.00000	0.00000	0.00000	0.00000
14	-0.22693E 00	0.00000	0.00000	0.00000	0.00000	0.00000	0.00000
15	-0.21939E 00	0.00000	0.00000	0.00000	0.00000	0.00000	0.00000
16	-0.21186E 00	0.00000	0.00000	0.00000	0.00000	0.00000	0.00000
17	-0.20433E 00	0.00000	0.00000	0.00000	0.00000	0.00000	0.00000
18	-0.19680E 00	0.00000	0.00000	0.00000	0.00000	0.00000	0.00000
19	-0.18928E 00	0.00000	0.00000	0.00000	0.00000	0.00000	0.00000
20	-0.18176E 00	0.00000	0.00000	0.00000	0.00000	0.00000	0.00000
21	-0.17424E 00	0.00000	0.00000	0.00000	0.00000	0.00000	0.00000
22	-0.16672E 00	0.00000	0.00000	0.00000	0.00000	0.00000	0.00000
23	-0.15920E 00	0.00000	0.00000	0.00000	0.00000	0.00000	0.00000
24	-0.15169E 00	0.00000	0.00000	0.00000	0.00000	0.00000	0.00000
25	-0.14418E 00	0.00000	0.00000	0.00000	0.00000	0.00000	0.00000
26	-0.13667E 00	0.00000	0.00000	0.00000	0.00000	0.00000	0.00000
27	-0.12917E 00	0.00000	0.00000	0.00000	0.00000	0.00000	0.00000
28	-0.12167E 00	0.00000	0.00000	0.00000	0.00000	0.00000	0.00000
29	-0.11416E 00	0.00000	0.00000	0.00000	0.00000	0.00000	0.00000
30	-0.10666E 00	0.00000	0.00000	0.00000	0.00000	0.00000	0.00000
31	-0.99164E-01	0.00000	0.00000	0.00000	0.00000	0.00000	0.00000
32	-0.91663E-01	0.00000	0.00000	0.00000	0.00000	0.00000	0.00000
33	-0.84160E-01	0.00000	0.00000	0.00000	0.00000	0.00000	0.00000
34	-0.76654E-01	0.00000	0.00000	0.00000	0.00000	0.00000	0.00000
35	-0.69141E-01	0.00000	0.00000	0.00000	0.00000	0.00000	0.00000
36	-0.61617E-01	0.00000	0.00000	0.00000	0.00000	0.00000	0.00000
37	-0.54077E-01	0.00000	0.00000	0.00000	0.00000	0.00000	0.00000
38	-0.46510E-01	0.00000	0.00000	0.00000	0.00000	0.00000	0.00000
39	-0.41196E-01	0.00000	0.00000	0.00000	0.00000	0.00000	0.00000
40	-0.38143E-01	0.00000	0.00000	0.00000	0.00000	0.00000	0.00000
41	-0.35074E-01	0.00000	0.00000	0.00000	0.00000	0.00000	0.00000
42	-0.31974E-01	0.00000	0.38262E-05	0.00000	0.90590E-05	0.38262E-05	0.00000
43	-0.28841E-01	0.00000	0.12637E-04	0.00000	0.30246E-05	0.12637E-04	0.96128E-05
44	-0.26464E-01	0.00000	0.98077E-05	0.00000	0.17221E-05	0.98077E-05	0.80856E-05
45	-0.24847E-01	0.00000	0.12225E-04	0.00000	0.18667E-05	0.12225E-04	0.10358E-04
46	-0.23214E-01	0.00000	0.14759E-04	0.00000	0.20171E-05	0.14759E-04	0.12742E-04
47	-0.21560E-01	0.00000	0.17440E-04	0.00000	0.21866E-05	0.17440E-04	0.15253E-04
48	-0.19867E-01	0.00000	0.20401E-04	0.00000	0.23951E-05	0.20401E-04	0.18006E-04
49	-0.18107E-01	0.00000	0.23924E-04	0.00000	0.26594E-05	0.23924E-04	0.21265E-04
50	-0.16234E-01	0.00000	0.28521E-04	0.00000	0.30173E-05	0.28521E-04	0.25504E-04
51	-0.14216E-01	0.00000	0.40414E-04	0.00000	0.37175E-05	0.40414E-04	0.36696E-04
52	-0.12529E-01	0.00000	0.25844E-04	0.00000	0.23204E-05	0.25844E-04	0.23523E-04
53	-0.11088E-01	0.00000	0.29214E-04	0.00000	0.26696E-05	0.29214E-04	0.26545E-04
54	-0.96499E-02	0.00000	0.10156E-04	0.14163E-04	0.16858E-05	0.24319E-04	0.22633E-04
55	-0.84380E-02	0.00000	0.11429E-04	0.32409E-04	0.19745E-05	0.43838E-04	0.41864E-04
56	-0.65963E-02	0.00000	0.24604E-04	0.63755E-04	0.37003E-05	0.88360E-04	0.84659E-04
57	-0.47253E-02	0.00000	0.44446E-05	0.66940E-04	0.49544E-06	0.71385E-04	0.70889E-04
58	-0.40146E-02	0.00000	0.66885E-05	0.66905E-04	0.40532E-06	0.73594E-04	0.73188E-04
59	-0.38291E-02	0.00000	0.11201E-04	0.66282E-04	0.63905E-06	0.77483E-04	0.76844E-04
60	-0.36226E-02	0.00000	0.12348E-04	0.64599E-04	0.63436E-06	0.76947E-04	0.76312E-04
61	-0.33270E-02	0.00000	0.13978E-04	0.61323E-04	0.62154E-06	0.75302E-04	0.74680E-04
62	-0.30143E-02	0.00000	0.15879E-04	0.56225E-04	0.60886E-06	0.72104E-04	0.71495E-04
63	-0.26673E-02	0.00000	0.17713E-04	0.49135E-04	0.58010E-06	0.66848E-04	0.66268E-04
64	-0.23342E-02	0.00000	0.94628E-05	0.45368E-04	0.31155E-06	0.54831E-04	0.54519E-04
65	-0.21448E-02	0.00000	0.91427E-05	0.41585E-04	0.29091E-06	0.50728E-04	0.50437E-04
66	-0.20200E-02	0.00000	0.96156E-05	0.37570E-04	0.30337E-06	0.47186E-04	0.46882E-04
67	-0.18772E-02	0.00000	0.10208E-04	0.33256E-04	0.31844E-06	0.43463E-04	0.43145E-04
68	-0.17382E-02	0.00000	0.11100E-04	0.28566E-04	0.34643E-06	0.39666E-04	0.39319E-04
69	-0.15595E-02	0.00000	0.13713E-04	0.22374E-04	0.39979E-06	0.36087E-04	0.35687E-04
70	-0.13413E-02	0.00000	0.95311E-05	0.18115E-04	0.28112E-06	0.27646E-04	0.27365E-04
71	-0.10974E-02	0.00000	0.91810E-05	0.14043E-04	0.27295E-06	0.23224E-04	0.22951E-04
72	-0.72425E-03	0.00000	0.18142E-04	0.64580E-05	0.57233E-06	0.24600E-04	0.24028E-04
73	-0.24492E-03	0.00000	0.16848E-04	0.00000	0.57185E-06	0.16848E-04	0.16276E-04
74	0.24487E-03	0.00000	0.17043E-04	0.00000	0.57198E-06	0.17043E-04	0.16471E-04
75	0.72446E-03	0.00000	0.18349E-04	0.66241E-05	0.57246E-06	0.24973E-04	0.24400E-04
76	0.10983E-02	0.00000	0.92846E-05	0.14385E-04	0.27315E-06	0.23670E-04	0.23397E-04
77	0.13405E-02	0.00000	0.96381E-05	0.18544E-04	0.28137E-06	0.28182E-04	0.27901E-04
78	0.15567E-02	0.00000	0.12825E-04	0.22892E-04	0.40007E-06	0.35717E-04	0.35317E-04
79	0.17365E-02	0.00000	0.11169E-04	0.28314E-04	0.34663E-06	0.39483E-04	0.39136E-04
80	0.18766E-02	0.00000	0.10269E-04	0.33060E-04	0.31866E-06	0.43329E-04	0.43011E-04
81	0.20190E-02	0.00000	0.96711E-05	0.37424E-04	0.30355E-06	0.47095E-04	0.46792E-04
82	0.21434E-02	0.00000	0.91940E-05	0.41485E-04	0.29101E-06	0.50679E-04	0.50388E-04
83	0.23311E-02	0.00000	0.95134E-05	0.45310E-04	0.31170E-06	0.54824E-04	0.54512E-04
84	0.26616E-02	0.00000	0.17459E-04	0.49118E-04	0.58031E-06	0.66577E-04	0.65997E-04
85	0.30079E-02	0.00000	0.15619E-04	0.55986E-04	0.60909E-06	0.71606E-04	0.70997E-04
86	0.33204E-02	0.00000	0.13718E-04	0.60857E-04	0.62177E-06	0.74575E-04	0.73954E-04
87	0.36146E-02	0.00000	0.12093E-04	0.63905E-04	0.63436E-06	0.75999E-04	0.75364E-04
88	0.38182E-02	0.00000	0.10955E-04	0.65369E-04	0.63899E-06	0.76324E-04	0.75685E-04
89	0.40096E-02	0.00000	0.49842E-05	0.65781E-04	0.40524E-06	0.70765E-04	0.70360E-04
90	0.47420E-02	0.00000	0.47148E-05	0.64348E-04	0.49682E-06	0.69063E-04	0.68566E-04
91	0.66297E-02	0.00000	0.25322E-04	0.61376E-04	0.37085E-05	0.86698E-04	0.82989E-04
92	0.84734E-02	0.00000	0.11386E-04	0.30530E-04	0.19738E-05	0.41916E-04	0.39942E-04
93	0.96778E-02	0.00000	0.10429E-04	0.12257E-04	0.15952E-05	0.22686E-04	0.21091E-04
94	0.11072E-01	0.00000	0.29535E-04	0.00000	0.26774E-05	0.29535E-04	0.26858E-04
95	0.12476E-01	0.00000	0.26530E-04	0.00000	0.23484E-05	0.26530E-04	0.24181E-04
96	0.14167E-01	0.00000	0.38595E-04	0.00000	0.36402E-05	0.38595E-04	0.34955E-04
97	0.16183E-01	0.00000	0.29065E-04	0.00000	0.30405E-05	0.29065E-04	0.26025E-04
98	0.18055E-01	0.00000	0.23752E-04	0.00000	0.26527E-05	0.23752E-04	0.21100E-04
99	0.19815E-01	0.00000	0.19615E-04	0.00000	0.23631E-05	0.19615E-04	0.17252E-04
100	0.21510E-01	0.00000	0.16093E-04	0.00000	0.21315E-05	0.16093E-04	0.13962E-04
101	0.23164E-01	0.00000	0.12880E-04	0.00000	0.19406E-05	0.12880E-04	0.10939E-04
102	0.24796E-01	0.00000	0.98229E-05	0.00000	0.17700E-05	0.98229E-05	0.80530E-05
103	0.26414E-01	0.00000	0.68874E-05	0.00000	0.16059E-05	0.68874E-05	0.52815E-05
104	0.28792E-01	0.00000	0.53329E-05	0.00000	0.97099E-05	0.53329E-05	0.00000
105	0.31919E-01	0.00000	0.00000	0.00000	0.00000	0.00000	0.00000
106	0.35014E-01	0.00000	0.00000	0.00000	0.00000	0.00000	0.00000
107	0.38083E-01	0.00000	0.00000	0.00000	0.00000	0.00000	0.00000
108	0.41136E-01	0.00000	0.00000	0.00000	0.00000	0.00000	0.00000
109	0.46451E-01	0.00000	0.00000	0.00000	0.00000	0.00000	0.00000
110	0.54017E-01	0.00000	0.00000	0.00000	0.00000	0.00000	0.00000
111	0.61558E-01	0.00000	0.00000	0.00000	0.00000	0.00000	0.00000
112	0.69081E-01	0.00000	0.00000	0.00000	0.00000	0.00000	0.00000
113	0.76594E-01	0.00000	0.00000	0.00000	0.00000	0.00000	0.00000
114	0.84101E-01	0.00000	0.00000	0.00000	0.00000	0.00000	0.00000
115	0.91603E-01	0.00000	0.00000	0.00000	0.00000	0.00000	0.00000
116	0.99104E-01	0.00000	0.00000	0.00000	0.00000	0.00000	0.00000
117	0.10660E 00	0.00000	0.00000	0.00000	0.00000	0.00000	0.00000
118	0.11410E 00	0.00000	0.00000	0.00000	0.00000	0.00000	0.00000
119	0.12161E 00	0.00000	0.00000	0.00000	0.00000	0.00000	0.00000

Figure 7.5: continued

114

SEG	S	QCOND	MDOTC	MDOTRI	MDOTE	MDOTTI	MDOTT
120	0.12911E 00	0.00000	0.00000	0.00000	0.00000	0.00000	0.00000
121	0.13661E 00	0.00000	0.00000	0.00000	0.00000	0.00000	0.00000
122	0.14412E 00	0.00000	0.00000	0.00000	0.00000	0.00000	0.00000
123	0.15163E 00	0.00000	0.00000	0.00000	0.00000	0.00000	0.00000
124	0.15914E 00	0.00000	0.00000	0.00000	0.00000	0.00000	0.00000
125	0.16666E 00	0.00000	0.00000	0.00000	0.00000	0.00000	0.00000
126	0.17418E 00	0.00000	0.00000	0.00000	0.00000	0.00000	0.00000
127	0.18170E 00	0.00000	0.00000	0.00000	0.00000	0.00000	0.00000
128	0.18922E 00	0.00000	0.00000	0.00000	0.00000	0.00000	0.00000
129	0.19674E 00	0.00000	0.00000	0.00000	0.00000	0.00000	0.00000
130	0.20427E 00	0.00000	0.00000	0.00000	0.00000	0.00000	0.00000
131	0.21180E 00	0.00000	0.00000	0.00000	0.00000	0.00000	0.00000
132	0.21933E 00	0.00000	0.00000	0.00000	0.00000	0.00000	0.00000
133	0.22687E 00	0.00000	0.00000	0.00000	0.00000	0.00000	0.00000
134	0.23441E 00	0.00000	0.00000	0.00000	0.00000	0.00000	0.00000
135	0.24195E 00	0.00000	0.00000	0.00000	0.00000	0.00000	0.00000
136	0.24949E 00	0.00000	0.00000	0.00000	0.00000	0.00000	0.00000
137	0.25704E 00	0.00000	0.00000	0.00000	0.00000	0.00000	0.00000
138	0.26458E 00	0.00000	0.00000	0.00000	0.00000	0.00000	0.00000
139	0.27213E 00	0.00000	0.00000	0.00000	0.00000	0.00000	0.00000
140	0.27969E 00	0.00000	0.00000	0.00000	0.00000	0.00000	0.00000
141	0.28724E 00	0.00000	0.00000	0.00000	0.00000	0.00000	0.00000
142	0.29481E 00	0.00000	0.00000	0.00000	0.00000	0.00000	0.00000
143	0.30163E 00	0.00000	0.00000	0.00000	0.00000	0.00000	0.00000
144	0.30618E 00	0.00000	0.00000	0.00000	0.00000	0.00000	0.00000
145	0.30923E 00	0.00000	0.00000	0.00000	0.00000	0.00000	0.00000
146	0.31227E 00	0.00000	0.00000	0.00000	0.00000	0.00000	0.00000

Figure 7.5: Concluded
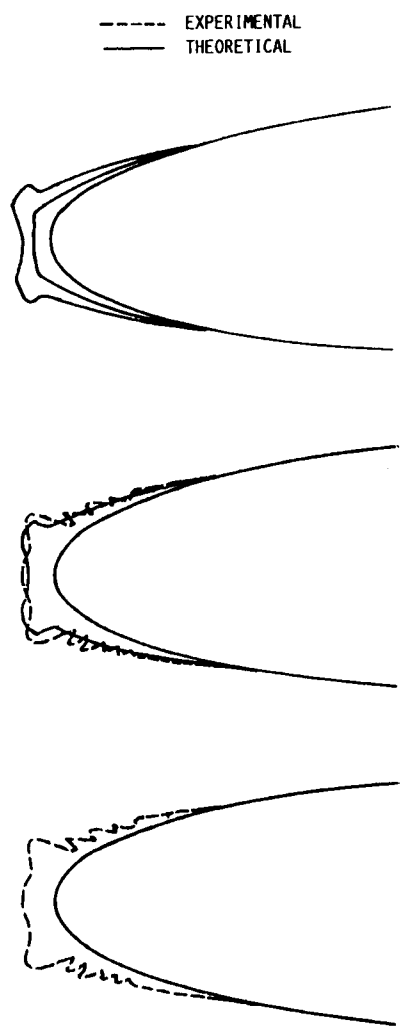
VELOCITY (M/S)	129.00
TEMPERATURE (C)	-12.60
PRESSURE (KPA)	90.75
HUMIDITY (%)	100.00
LWC (G/M³)	1.00
DROP DIAM (MICRONS)	20.00
TIME (SEC)	120.00

Figure 7.6: Comparison of the experimental and calculated ice shapes for Example 1.

```
NACA 0012  : EXAMPLE 2
&S24Y
ILIFT= 1
IPARA= 1
IFIRST= 3
ISECND= 3
IPVOR= 1
INCLT= 0
CLT= 4.0
ICHORD= 0
CCL= 0.0
IND= 1
ISOL= 0
IPRINT= 0
IFLLL= 1
&END
    1.0000000    0.9899999    0.9800000    0.9700000    0.9500000    0.9250000   6  0  3
    0.9000000    0.8750000    0.8500000    0.8250000    0.8000000    0.7750000   6  0  3
    0.7500000    0.7250000    0.7000000    0.6750000    0.6500000    0.6250000   6  0  3
    0.6000000    0.5750000    0.5500000    0.5250000    0.5000000    0.4750000   6  0  3
    0.4500000    0.4250000    0.4000000    0.3750000    0.3500000    0.3250000   6  0  3
    0.3000000    0.2750000    0.2500000    0.2250000    0.2000000    0.1750000   6  0  3
    0.1500000    0.1250000    0.1100000    0.0900000    0.0800000    0.0700000   6  0  3
    0.0600000    0.0500000    0.0450000    0.0400000    0.0350000    0.0300000   6  0  3
    0.0250000    0.0200000    0.0150000    0.0100000    0.0075000    0.0050000   6  0  3
    0.0037500    0.0025000    0.0022500    0.0020000    0.0017500    0.0015000   6  0  3
    0.0012500    0.0010000    0.0008750    0.0007500    0.0006250    0.0005000   6  0  3
    0.0003750    0.0002500    0.0001250    0.0000000    0.0001250    0.0002500   6  0  3
    0.0003750    0.0005000    0.0006250    0.0007500    0.0008750    0.0010000   6  0  3
    0.0012500    0.0015000    0.0017500    0.0020000    0.0022500    0.0025000   6  0  3
    0.0037500    0.0050000    0.0075000    0.0100000    0.0150000    0.0200000   6  0  3
    0.0250000    0.0300000    0.0350000    0.0400000    0.0450000    0.0500000   6  0  3
    0.0600000    0.0700000    0.0800000    0.0900000    0.1000000    0.1250000   6  0  3
    0.1500000    0.1750000    0.2000000    0.2250000    0.2500000    0.2750000   6  0  3
    0.3000000    0.3250000    0.3500000    0.3750000    0.4000000    0.4250000   6  0  3
    0.4500000    0.4750000    0.5000000    0.5250000    0.5500000    0.5750000   6  0  3
    0.6000000    0.6250000    0.6500000    0.6750000    0.7000000    0.7250000   6  0  3
    0.7500000    0.7750000    0.8000000    0.8250000    0.8500000    0.8750000   6  0  3
    0.9000000    0.9250000    0.9500000    0.9700000    0.9800000    0.9899999   6  0  3
    1.0000000    0.0000000    0.0000000    0.0000000    0.0000000    0.0000000   1  1  3
    0.0000000   -0.0018740   -0.0036110   -0.0052390   -0.0082510   -0.0117000   6  0  4
   -0.0149080   -0.0179530   -0.0208880   -0.0237390   -0.0265150   -0.0292210   6  0  4
   -0.0318550   -0.0344110   -0.0368870   -0.0392810   -0.0415850   -0.0437950   6  0  4
   -0.0459040   -0.0479060   -0.0497930   -0.0515600   -0.0531980   -0.0546980   6  0  4
   -0.0560510   -0.0572430   -0.0582620   -0.0590900   -0.0597070   -0.0600940   6  0  4
   -0.0602260   -0.0600760   -0.0596120   -0.0587940   -0.0575700   -0.0558790   6  0  4
   -0.0536360   -0.0507320   -0.0470040   -0.0452280   -0.0432520   -0.0410380   6  0  4
   -0.0385350   -0.0356740   -0.0340820   -0.0323620   -0.0304960   -0.0284620   6  0  4
   -0.0262300   -0.0237260   -0.0207970   -0.0172480   -0.0150780   -0.0123860   6  0  4
   -0.0106990   -0.0086200   -0.0081360   -0.0076230   -0.0070750   -0.0064850   6  0  4
   -0.0058470   -0.0051460   -0.0047660   -0.0043630   -0.0039310   -0.0034620   6  0  4
   -0.0029450   -0.0023560   -0.0016320    0.0000000    0.0016320    0.0023560   6  0  4
    0.0029450    0.0034620    0.0039310    0.0043630    0.0047660    0.0051460   6  0  4
    0.0058470    0.0064850    0.0070750    0.0076230    0.0081360    0.0086200   6  0  4

    0.0106990    0.0123860    0.0150780    0.0172480    0.0207970    0.0237260   6  0  4
    0.0262300    0.0284620    0.0304960    0.0323620    0.0340820    0.0356740   6  0  4
    0.0385350    0.0410380    0.0432520    0.0452280    0.0470040    0.0507320   6  0  4
    0.0536360    0.0558790    0.0575700    0.0587940    0.0596120    0.0600760   6  0  4
    0.0602260    0.0600940    0.0597070    0.0590900    0.0582620    0.0572430   6  0  4
    0.0560510    0.0546980    0.0531980    0.0515600    0.0497930    0.0479060   6  0  4
    0.0459040    0.0437950    0.0415850    0.0392810    0.0368870    0.0344110   6  0  4
    0.0318550    0.0292210    0.0265150    0.0237390    0.0208880    0.0179530   6  0  4
    0.0149080    0.0117000    0.0082510    0.0052390    0.0036110    0.0018740   6  0  4
    0.0000000    0.0000000    0.0000000    0.0000000    0.0000000    0.0000000   1  1  4
&TRAJ1
GEPS= 0.4999999E-04
DSHIFT= 0.20E-02
VEPS= 0.9999999E-03
LCMB= 0
LCMP= 0
LEQM= 1
LSYM= 0
LVOR= 1
LXOR= 1
NBDY= 1
NEQ= 4
NPL= 15
NSEAR= 50
NSI= 1
TIMSTP= 0.9999999E-03
&END
&TRAJ2
CHORD= 0.30
G= 0.0
PIT= 0.0
PITDOT= 0.0
PRATK= 0.0
XORC= -4.0
XSTOP= 0.50
YOLIM= 0.9999999E-04
YOMAX= 0.50E-01
YOMIN= -0.50E-01
YORC= 0.9999996E-01
&END
&DIST
FLWC= 1.0, 9*0.0
DPD= 20.0, 9*0.0
CFP= 1.0, 9*0.0
&END
&ICE
VINF= 129.460
LWC= 0.50
TAMB= 260.5498
PAMB= 90748.0
RH= 100.0
DPMM= 20.0
XKINIT= 0.00035
SEGTOL= 1.50
&END
```

Figure 7.7: Input data file for Example 2

VELOCITY (M/S)   129.00
TEMPERATURE (C)   -12.60
PRESSURE (KPA)   90.75
HUMIDITY (%)   100.00
LWC (G/M**3)   0.50
DROP DIAM (MICRONS)   20.00
TIME (SEC)   0.00
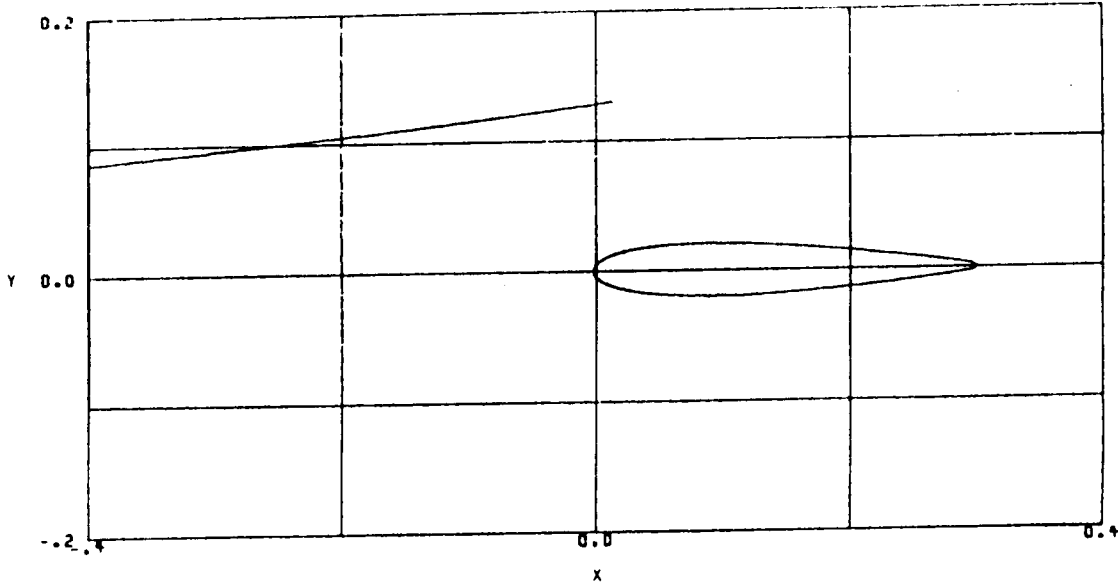
VELOCITY (M/S)   129.00
TEMPERATURE (C)   -12.60
PRESSURE (KPA)   90.75
HUMIDITY (%)   100.00
LWC (G/M**3)   0.50
DROP DIAM (MICRONS)   20.00
TIME (SEC)   0.00
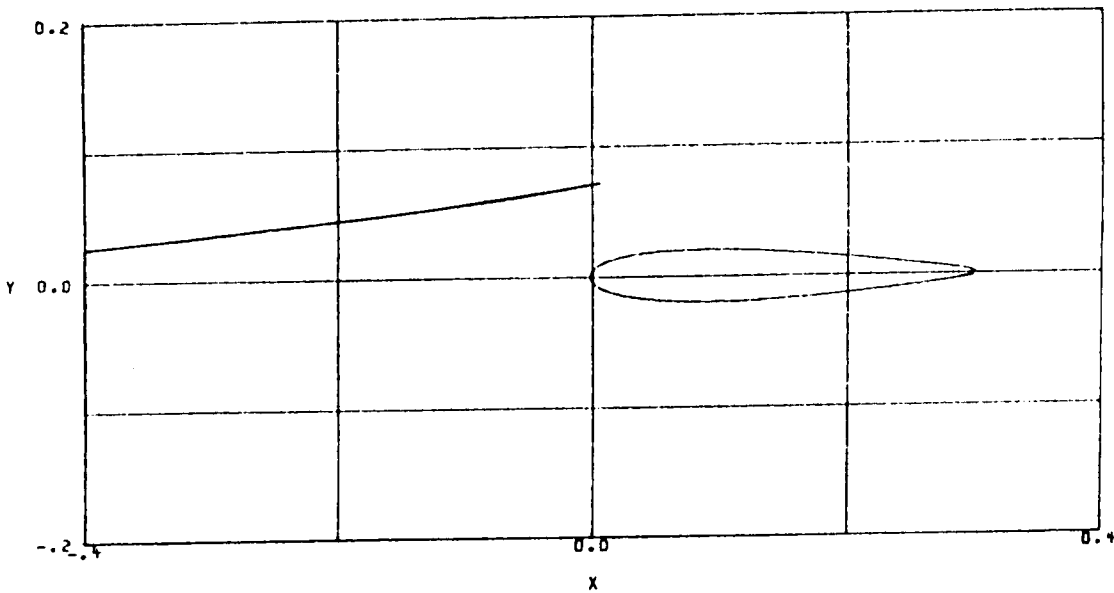
Figure 7.8: Plots of the particle trajectories calculated in subroutine RANGE.

118

VELOCITY (M/S)	129.00
TEMPERATURE (C)	-12.60
PRESSURE (KPA)	90.75
HUMIDITY (%)	100.00
LWC (G/M**3)	0.50
DROP DIAM (MICRONS)	20.00
TIME (SEC)	0.00

VELOCITY (M/S)	129.00
TEMPERATURE (C)	-12.60
PRESSURE (KPA)	90.75
HUMIDITY (%)	100.00
LWC (G/M**3)	0.50
DROP DIAM (MICRONS)	20.00
TIME (SEC)	0.00

Figure 7.8: Concluded

119

```
VELOCITY (M/S)          129.00
TEMPERATURE (C)         -12.60
PRESSURE (KPA)           90.75
HUMIDITY (%)            100.00
LWC (G/M**3)              0.50
DROP DIAM (MICRONS)      20.00
TIME (SEC)                0.00
```

IW=   1
YO= -0.12000
S = -0.00253

X

```
VELOCITY (M/S)          129.00
TEMPERATURE (C)         -12.60
PRESSURE (KPA)           90.75
HUMIDITY (%)            100.00
LWC (G/M**3)              0.50
DROP DIAM (MICRONS)      20.00
TIME (SEC)                0.00
```

IW=   2
YO= -0.11250
S =   0.01078

X

Figure 7.9: Sample of the plots of the particle trajectories calculated in subroutine IMPLIM.

VELOCITY (M/S)	129.00
TEMPERATURE (C)	-12.60
PRESSURE (KPA)	90.75
HUMIDITY (%)	100.00
LWC (G/M**3)	0.50
DROP DIAM (MICRONS)	20.00
TIME (SEC)	0.00
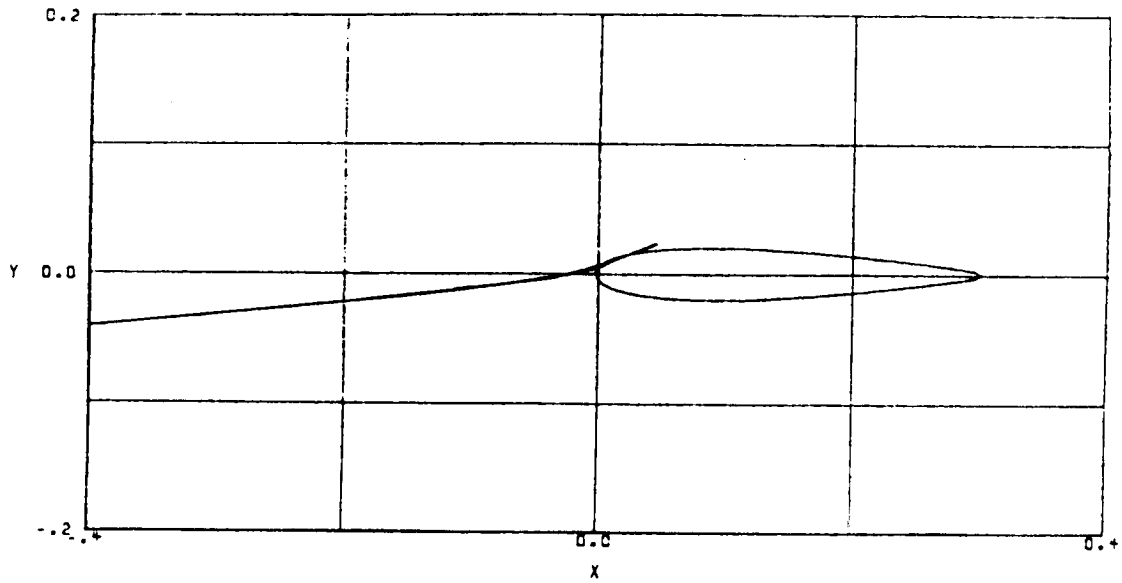
Figure 7.9: Concluded
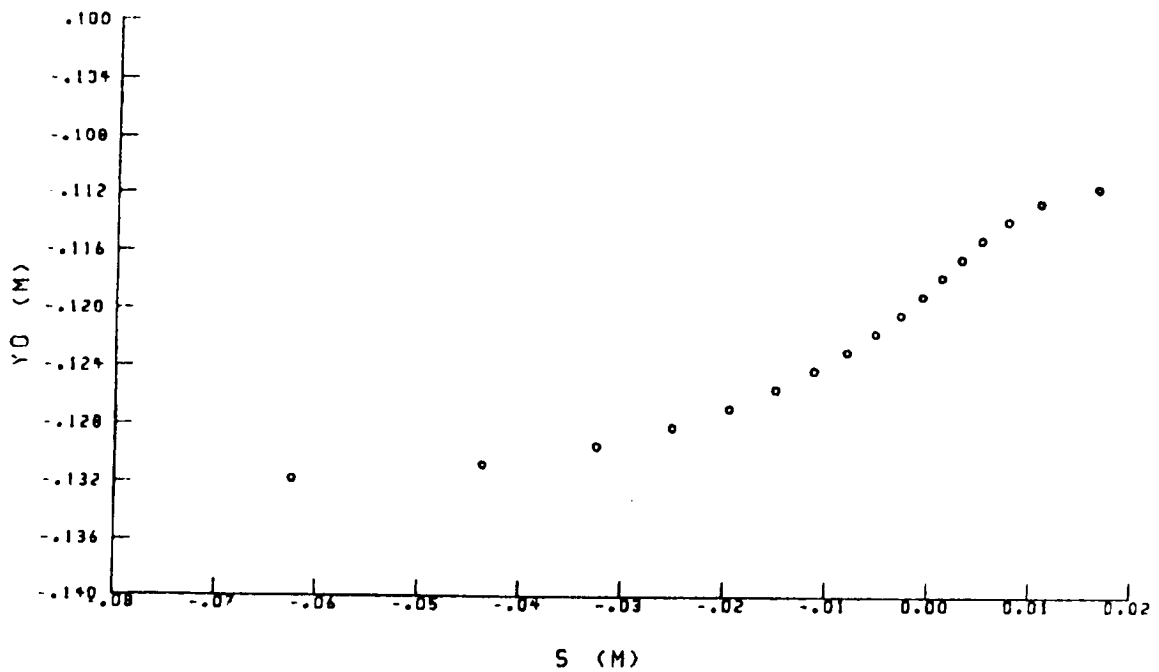
Figure 7.10: y_0 vs. s data calculated in subroutine COLLEC for Example 2

121

VELOCITY (M/S)	129.46
TEMPERATURE (C)	-12.60
PRESSURE (KPA)	90.75
HUMIDITY (%)	100.00
LWC (G/M**3)	0.50
DROP DIAM (MICRON)	20.00
TIME (SEC)	60.00
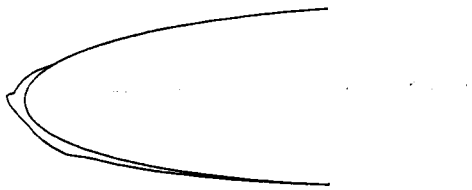
a. Iced airfoil geometry
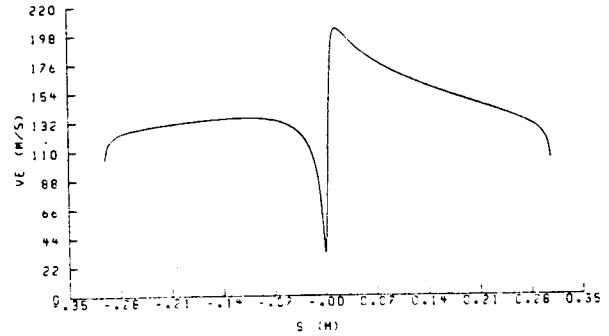
d. Edge velocity vs. surface location
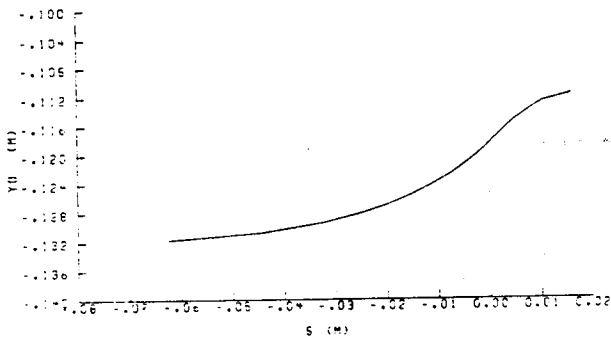
b. Particle release position vs. surface impact distance
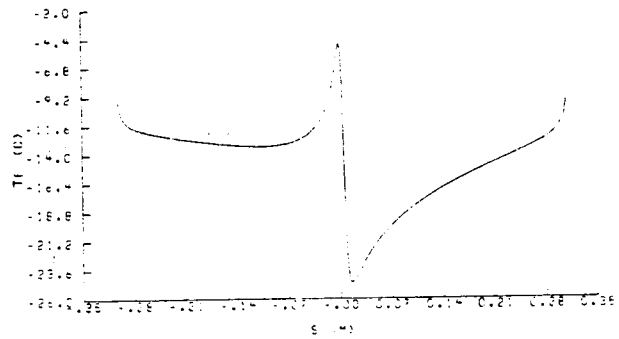
e. Edge temperature vs. surface location
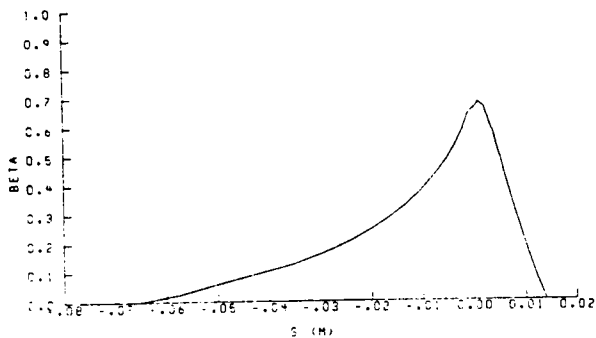
c. Local collection efficiency vs. surface location
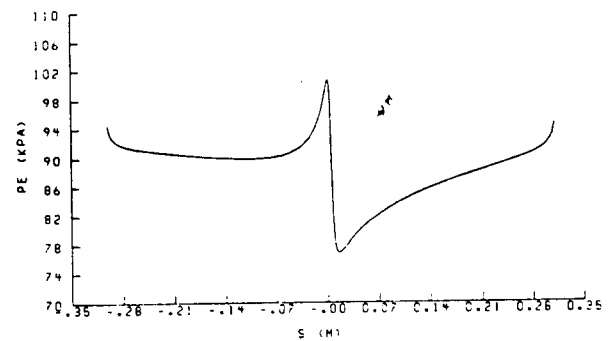
f. Edge pressure vs. surface location

Figure 7.11: Icing parameter plots for the first timestep of Example 2.

VELOCITY (M/S)	129.46
TEMPERATURE (C)	-12.60
PRESSURE (KPA)	90.75
HUMIDITY (%)	100.00
LWC (G/M**3)	0.50
DROP DIAM (MICRON)	20.00
TIME (SEC)	60.00
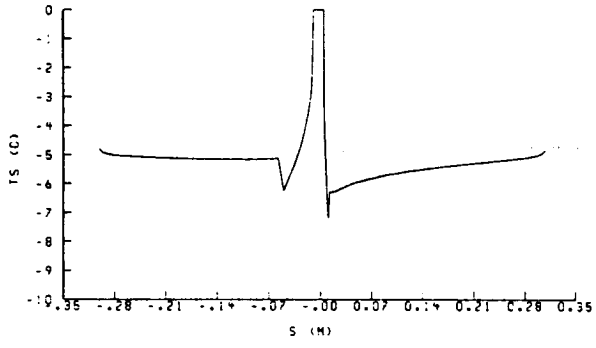
g. Equilibrium surface temperature vs. surface location

j. Ice density vs. surface location
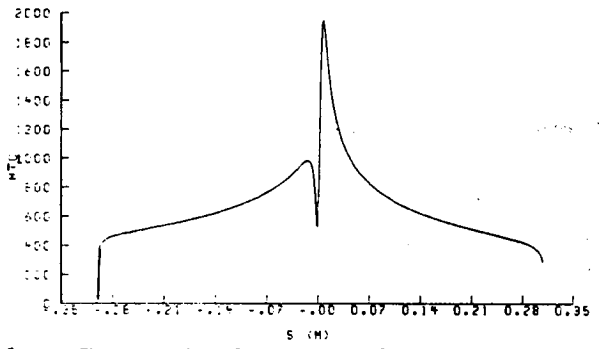
h. Convective heat transfer coefficient vs. surface location
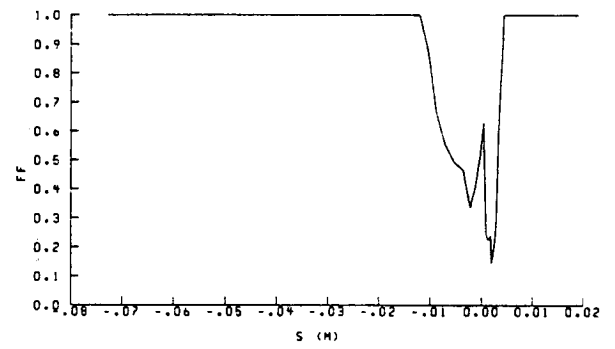
k. Freezing fraction vs. surface location
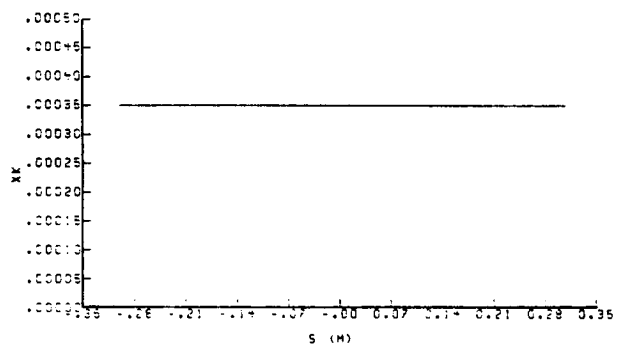
i. Equivalent sand-grain roughness height vs. surface location

Figure 7.11: Concluded

123
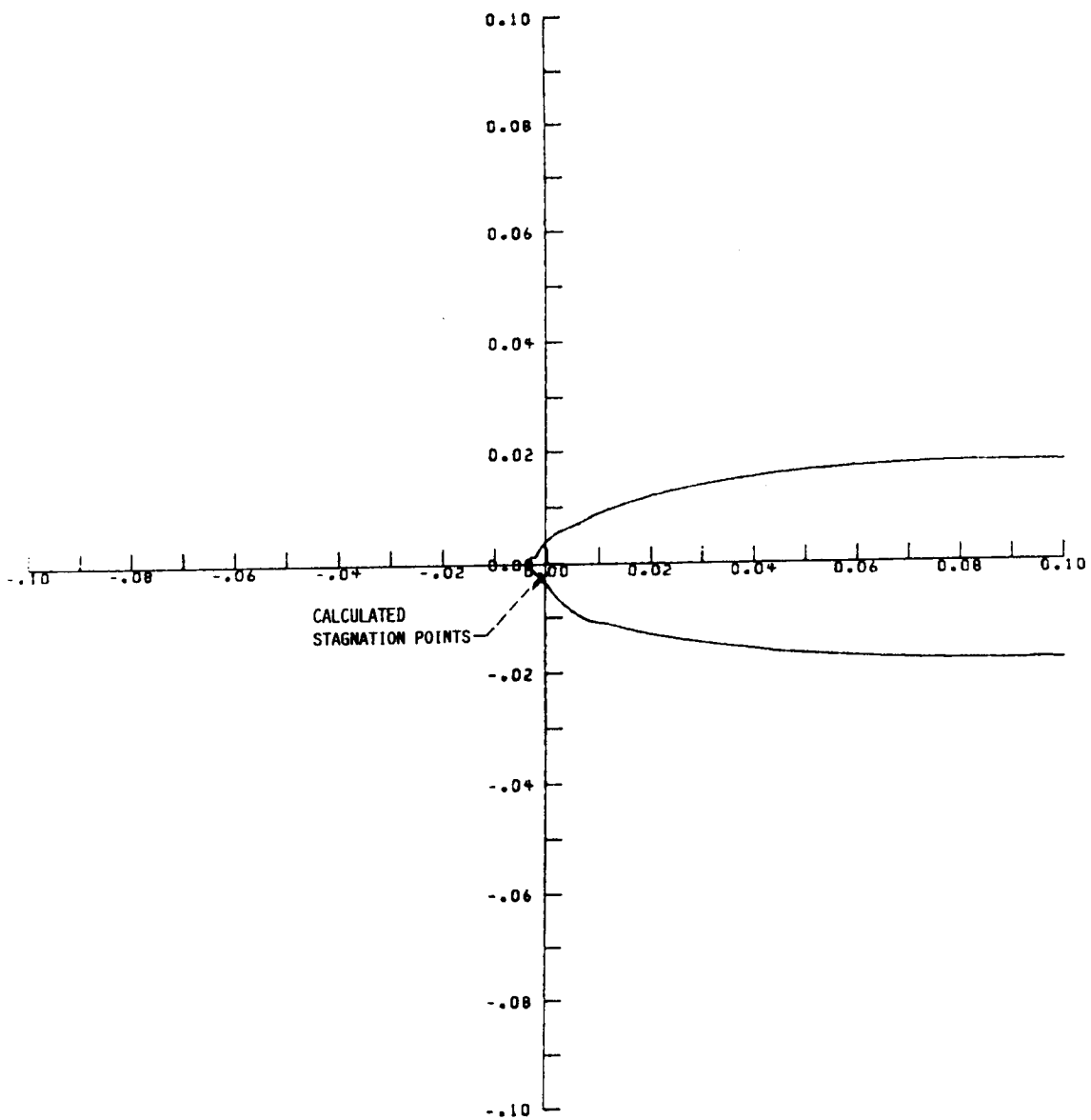
Figure 7.12: Locations of the multiple stagnation points in the second time step of Example 2
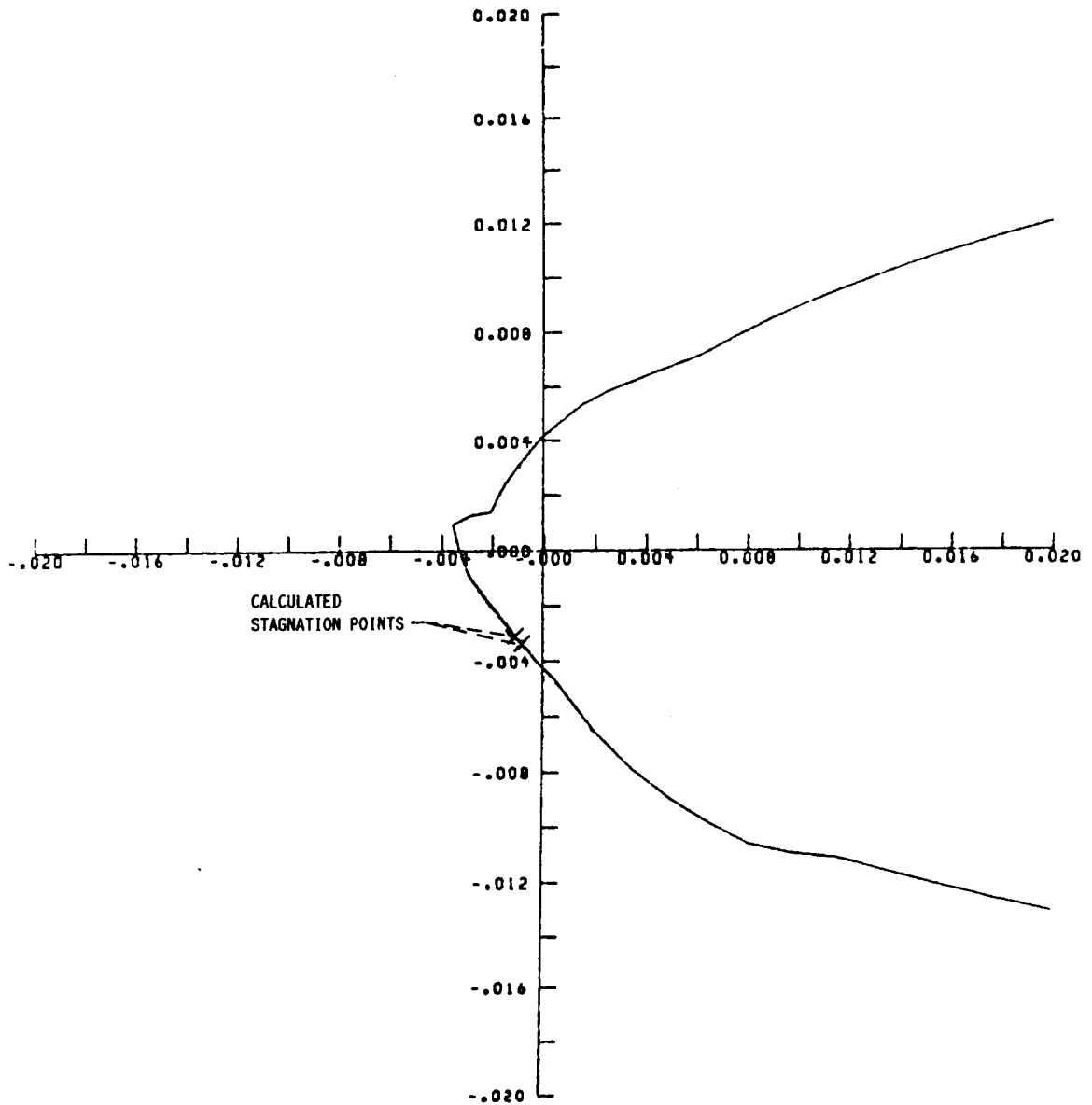
Figure 7.13: Locations of the multiple stagnation points in Example 2 after specifying new axes limits
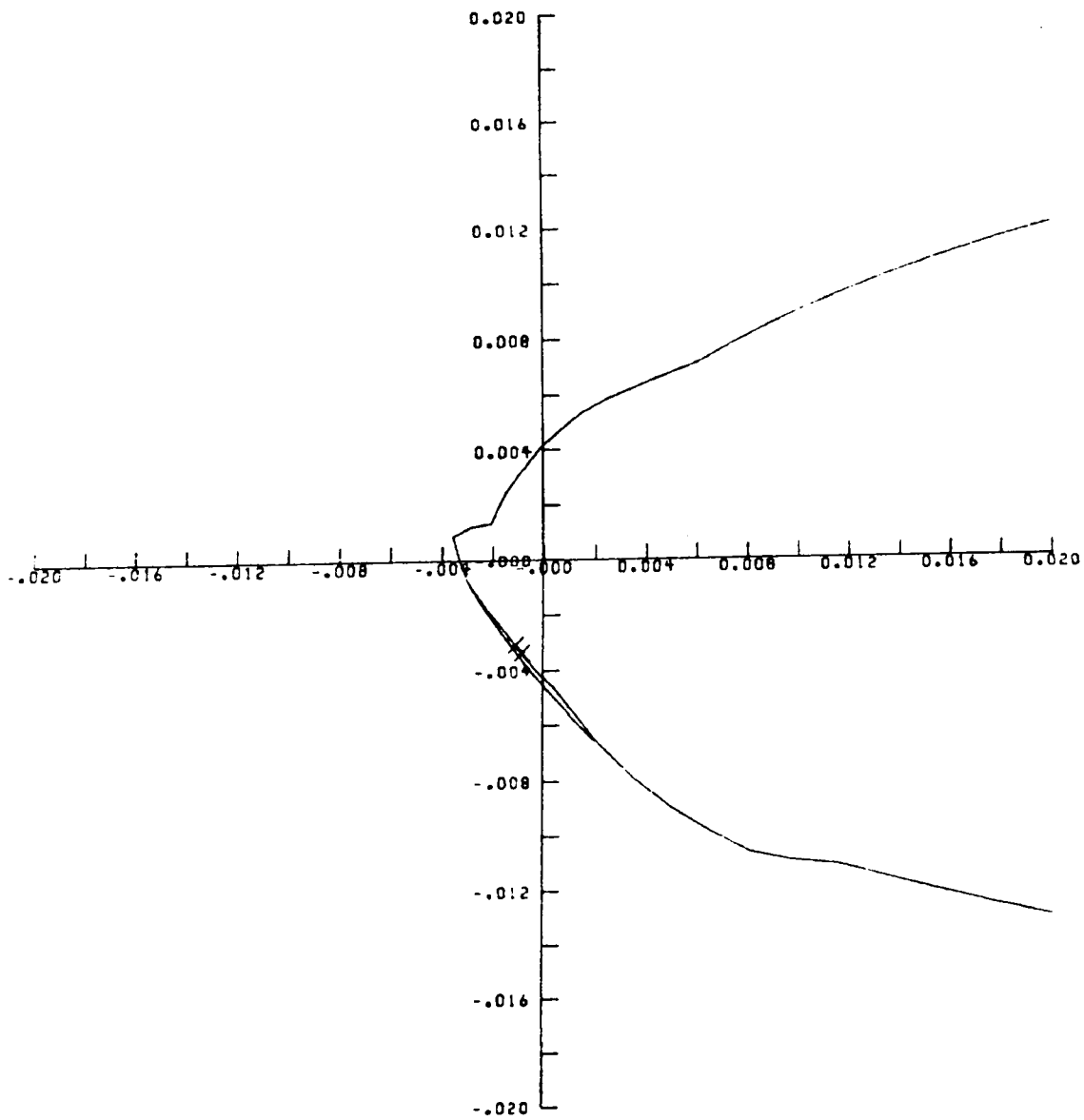
Figure 7.14: Iced airfoil with the pseudo-surface

126

VELOCITY (M/S)	129.00
TEMPERATURE (C)	-12.60
PRESSURE (KPA)	90.75
HUMIDITY (%)	100.00
LWC (G/M**3)	0.50
DROP DIAM (MICRONS)	20.00
TIME (SEC)	0.00
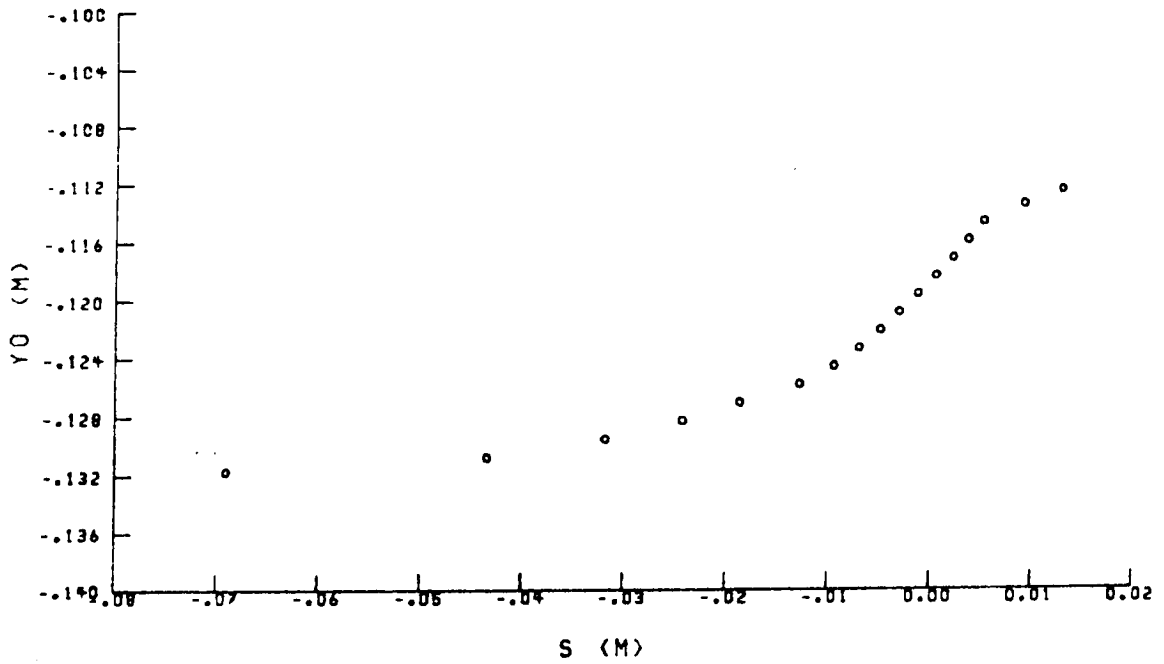
Figure 7.15: y_0 vs. s data calculated in subrouting COLLEC for the second time step of Example 2

VELOCITY (M/S)	129.46
TEMPERATURE (C)	-12.60
PRESSURE (KPA)	90.75
HUMIDITY (%)	100.00
LWC (G/M**3)	0.50
DROP DIAM (MICRON)	20.00
TIME (SEC)	120.00
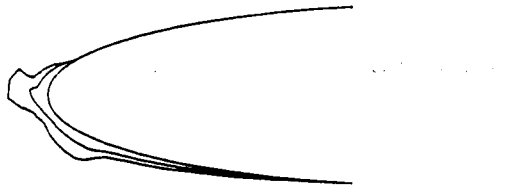
a. Iced airfoil geometry
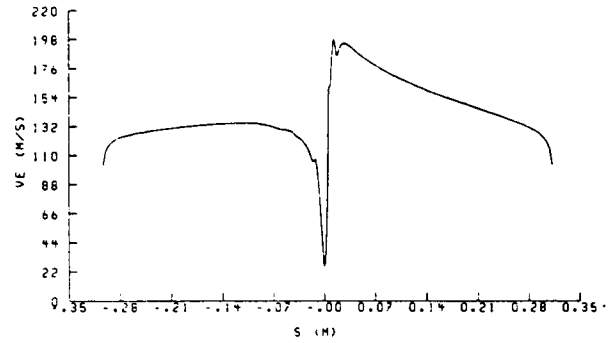
d. Edge velocity vs. surface location
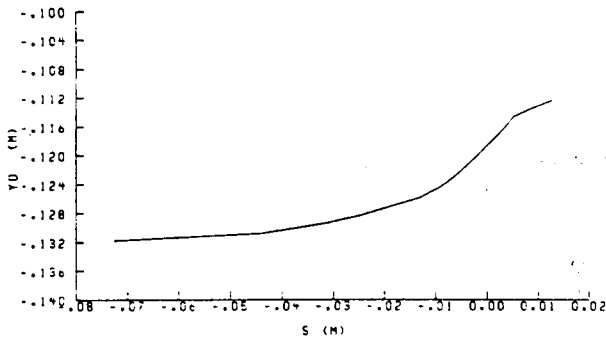
b. Particle release position vs. surface impact distance
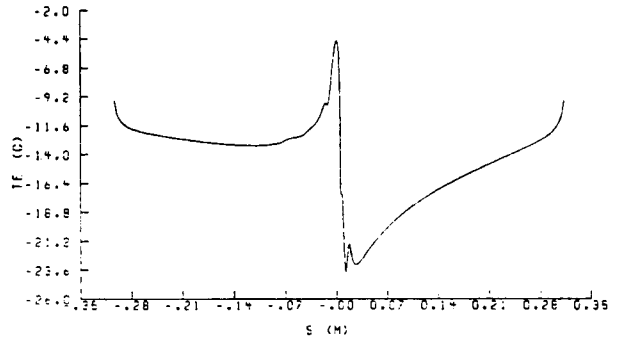
e. Edge temperature vs. surface location
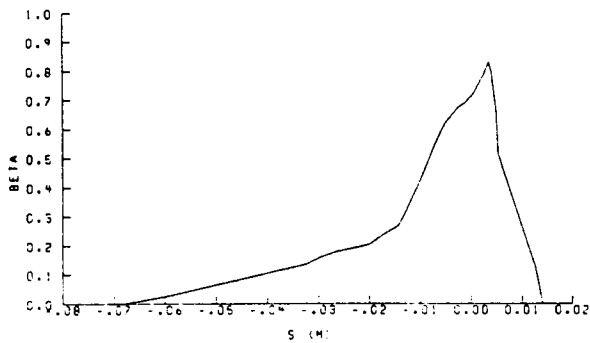
c. Local collection efficiency vs. surface location
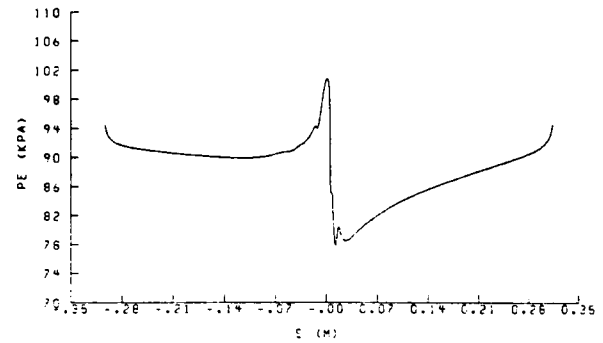
f. Edge pressure vs. surface location

Figure 7.16: Icing parameter plots for the second timestep of Example 2.

128

VELOCITY (M/S)	129.46
TEMPERATURE (C)	-12.60
PRESSURE (KPA)	90.75
HUMIDITY (%)	100.00
LWC (G/M**3)	0.50
DROP DIAM (MICRON)	20.00
TIME (SEC)	120.00
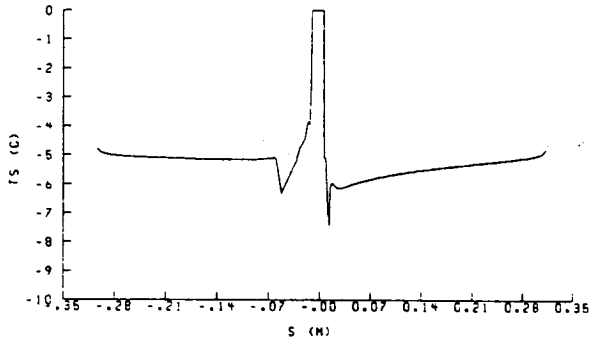
g. **Equilibrium surface temperature vs. surface location**
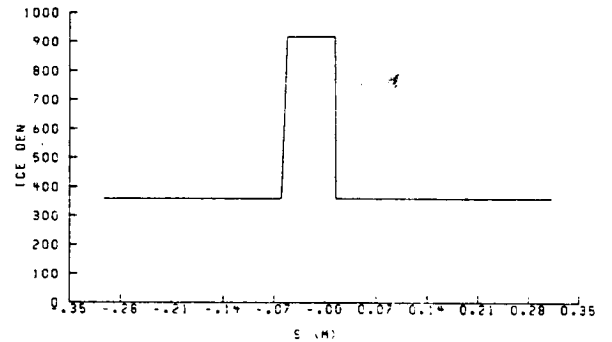
j. **Ice density vs. surface location**
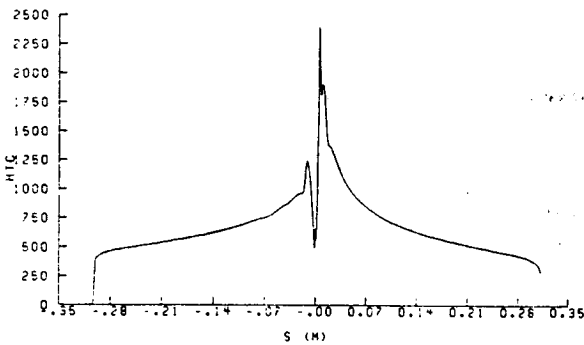
h. **Convective heat transfer coefficient vs. surface location**
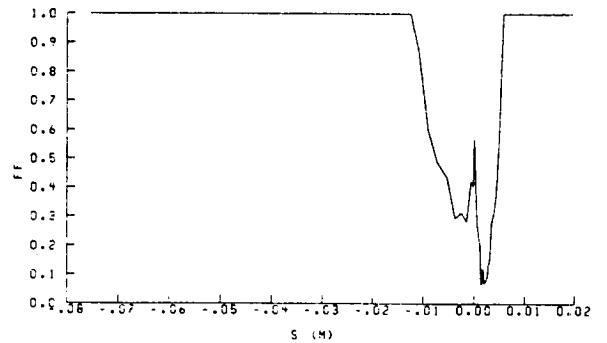
k. **Freezing fraction vs. surface location**
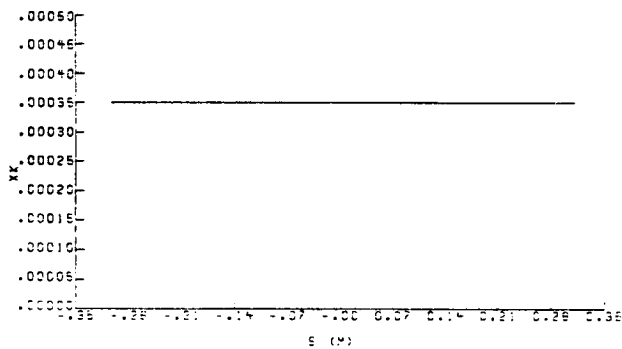
i. **Equivalent sand-grain roughness height vs. surface location**

Figure 7.16: Concluded
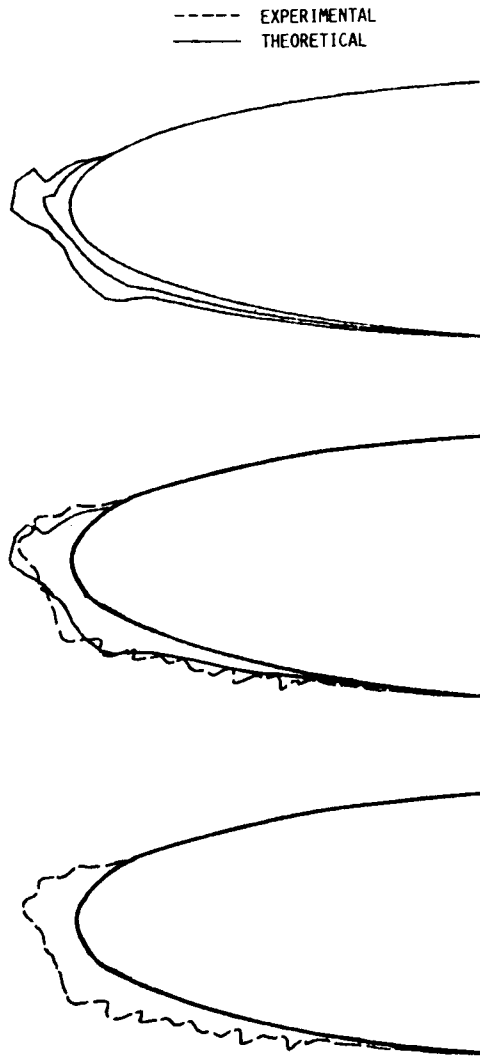
129

Figure 7.17: Comparison of experimental and calculated ice accretion shapes for Example 2.

```
NACA 0012 : EXAMPLE 3
&S24Y
ILIFT= 1
IPARA= 1
IFIRST= 3
ISECND= 3
IPVOR= 1
INCLT= 0
CLT= 0.0
ICHORD= 0
CCL= 0.0
IND= 1
ISOL= 0
IPRINT= 0
JFLLL= 1
&END
   1.0000000    0.9899999    0.9800000    0.9700000    0.9500000    0.9250000   6 0 3
   0.9000000    0.8750000    0.8500000    0.8250000    0.8000000    0.7750000   6 0 3
   0.7500000    0.7250000    0.7000000    0.6750000    0.6500000    0.6250000   6 0 3
  .0.6000000    0.5750000    0.5500000    0.5250000    0.5000000    0.4750000   6 0 3
   0.4500000    0.4250000    0.4000000    0.3750000    0.3500000    0.3250000   6 0 3
   0.3000000    0.2750000    0.2500000    0.2250000    0.2000000    0.1750000   6 0 3
   0.1500000    0.1250000    0.1000000    0.0900000    0.0800000    0.0700000   6 0 3
   0.0600000    0.0500000    0.0450000    0.0400000    0.0350000    0.0300000   6 0 3
   0.0250000    0.0200000    0.0150000    0.0100000    0.0075000    0.0050000   6 0 3
   0.0037500    0.0025000    0.0022500    0.0020000    0.0017500    0.0015000   6 0 3
   0.0012500    0.0010000    0.0008750    0.0007500    0.0006250    0.0005000   6 0 3
   0.0003750    0.0002500    0.0001250    0.0000000    0.0001250    0.0002500   6 0 3
   0.0003750    0.0005000    0.0006250    0.0007500    0.0008750    0.0010000   6 0 3
   0.0012500    0.0015000    0.0017500    0.0020000    0.0022500    0.0025000   6 0 3
   0.0037500    0.0050000    0.0075000    0.0100000    0.0150000    0.0200000   6 0 3
   0.0250000    0.0300000    0.0350000    0.0400000    0.0450000    0.0500000   6 0 3
   0.0600000    0.0700000    0.0800000    0.0900000    0.1000000    0.1250000   6 0 3
   0.1500000    0.1750000    0.2000000    0.2250000    0.2500000    0.2750000   6 0 3
   0.3000000    0.3250000    0.3500000    0.3750000    0.4000000    0.4250000   6 0 3
   0.4500000    0.4750000    0.5000000    0.5250000    0.5500000    0.5750000   6 0 3
   0.6000000    0.6250000    0.6500000    0.6750000    0.7000000    0.7250000   6 0 3
   0.7500000    0.7750000    0.8000000    0.8250000    0.8500000    0.8750000   6 0 3
   0.9000000    0.9250000    0.9500000    0.9700000    0.9800000    0.9899999   6 0 3
   1.0000000    0.0000000    0.0000000    0.0000000    0.0000000    0.0000000   1 1 3
   0.0000000   -0.0018740   -0.0036110   -0.0052390   -0.0082510   -0.0117000   6 0 4
  -0.0149080   -0.0179530   -0.0208880   -0.0237390   -0.0265150   -0.0292210   6 0 4
  -0.0318550   -0.0344110   -0.0368870   -0.0392810   -0.0415850   -0.0437950   6 0 4
  -0.0459040   -0.0479060   -0.0497930   -0.0515600   -0.0531980   -0.0546980   6 0 4
  -0.0560510   -0.0572430   -0.0582620   -0.0590900   -0.0597070   -0.0600940   6 0 4
  -0.0602260   -0.0600760   -0.0596120   -0.0587940   -0.0575700   -0.0558790   6 0 4
  -0.0536360   -0.0507320   -0.0470040   -0.0452280   -0.0432520   -0.0410380   6 0 4
  -0.0385350   -0.0356740   -0.0340820   -0.0323620   -0.0304960   -0.0284620   6 0 4
  -0.0262300   -0.0237260   -0.0207970   -0.0172480   -0.0150780   -0.0123860   6 0 4
  -0.0106990   -0.0086200   -0.0081360   -0.0076230   -0.0070750   -0.0064850   6 0 4
  -0.0058470   -0.0051460   -0.0047660   -0.0043630   -0.0039310   -0.0034620   6 0 4
  -0.0029450   -0.0023560   -0.0016320    0.0000000    0.0016320    0.0023560   6 0 4
   0.0029450    0.0034620    0.0039310    0.0043630    0.0047660    0.0051460   6 0 4
   0.0058470    0.0064850    0.0070750    0.0076230    0.0081360    0.0086200   6 0 4
   0.0106990    0.0123860    0.0150780    0.0172480    0.0207970    0.0237260   6 0 4
   0.0262300    0.0284620    0.0304960    0.0323620    0.0340820    0.0356740   6 0 4
   0.0385350    0.0410380    0.0432520    0.0452280    0.0470040    0.0507320   6 0 4
   0.0536360    0.0558790    0.0575700    0.0587940    0.0596120    0.0600760   6 0 4
   0.0602260    0.0600940    0.0597070    0.0590900    0.0582620    0.0572430   6 0 4
   0.0560510    0.0546980    0.0531980    0.0515600    0.0497930    0.0479060   6 0 4
   0.0459040    0.0437950    0.0415850    0.0392810    0.0368870    0.0344110   6 0 4
   0.0318550    0.0292210    0.0265150    0.0237390    0.0208880    0.0179530   6 0 4
   0.0149080    0.0117000    0.0082510    0.0052390    0.0036110    0.0018740   6 0 4
   0.0000000    0.0000000    0.0000000    0.0000000    0.0000000    0.0000000   1 1 4
&TRAJ1
GEPS= 0.4999999E-04
DSHIFT= 0.20E-02
VEPS= 0.9999999E-03
LCMB= 0
LCMP= 0
LEQM= 1
LSYM= 0
LYOR= 1
LXOR= 1
NBDY= 1
NEQ= 4
NPL= 15
NSEAR= 50
NSI= 1
TIMSTP= 0.9999999E-03
&END
&TRAJ2
CHORD= 0.30
G= 0.0
PIT= 0.0
PITDOT= 0.0
PRATK= 0.0
XORC= -4.0
XSTCP= 0.53
YOLIM= 0.9999999E-04
YOMAX= 9.50E-01
YOMIN= -0.50E-01
YORC= 0.9999996E-01
&END
&DIST
FLWC= 1.0, 9*0.0
DPD= 20.0, 9*0.0
CFP= 1.0, 9*0.0
&END
&ICE
VINF= 64.728
LWC= 0.500
TAMB= 260.55
PAMB= 90748.0
RH= 100.0
DPMM= 20.0
XKINIT= 0.25E-03
SEGTOL= 1.50
&END
```

Figure 7.18: Input data file for Example 3.

131

VELOCITY (M/S)	64.73
TEMPERATURE (C)	-12.60
PRESSURE (KPA)	90.75
HUMIDITY (%)	100.00
LWC (G/M**3)	0.50
DROP DIAM (MICRON)	20.00
TIME (SEC)	60.00
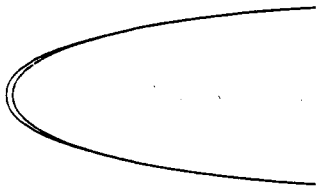
a. Iced airfoil geometry
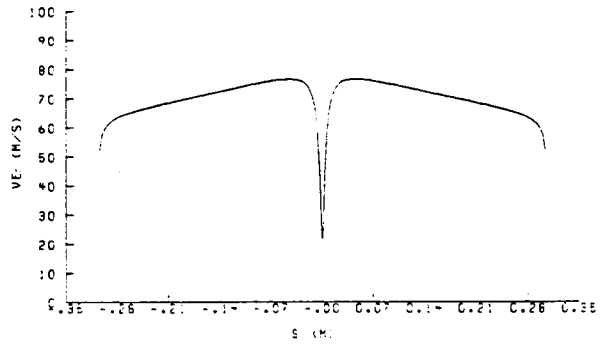
d. Edge velocity vs. surface location
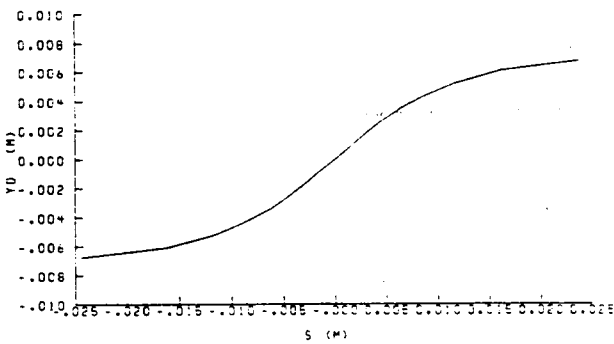
b. Particle release position vs. surface
    impact distance
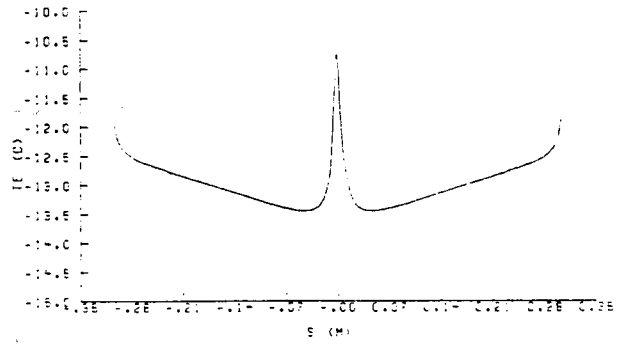
e. Edge temperature vs. surface location
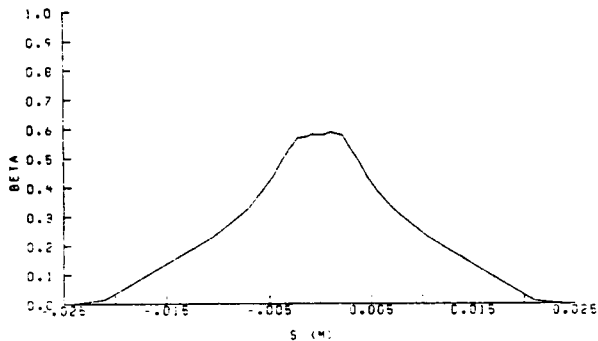
c. Local collection efficiency vs. surface
    location
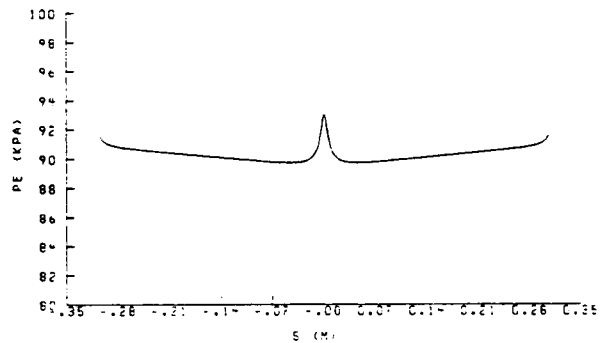
f. Edge pressure vs. surface location

Figure 7.19: Icing parameter plots for the first timestep of Example 3.

132

VELOCITY (M/S)	64.73
TEMPERATURE (C)	-12.60
PRESSURE (KPA)	90.75
HUMIDITY (%)	100.00
LWC (G/M**3)	0.50
DROP DIAM (MICRON)	20.00
TIME (SEC)	60.00
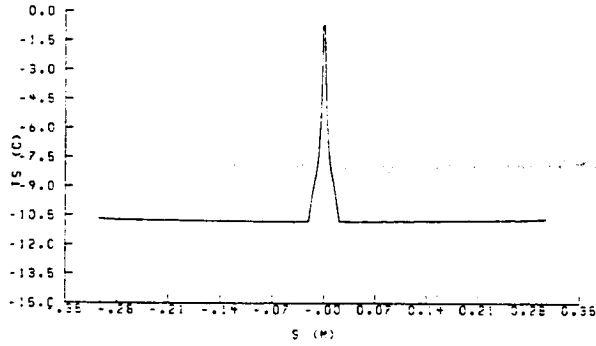
g. Equilibrium surface temperature vs. surface location
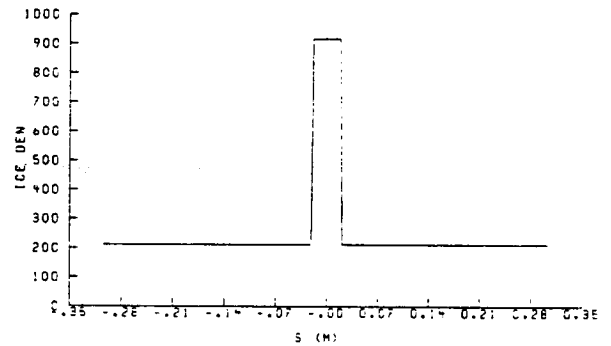
j. Ice density vs. surface location
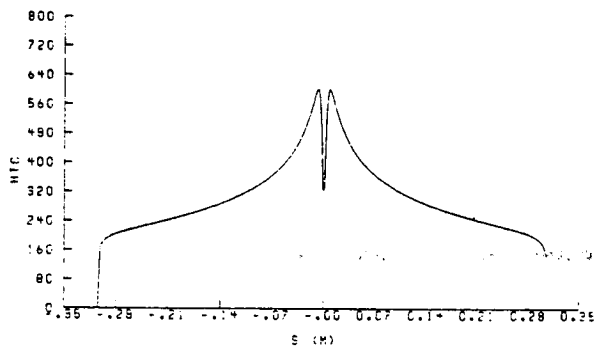
h. Convective heat transfer coefficient vs. surface location
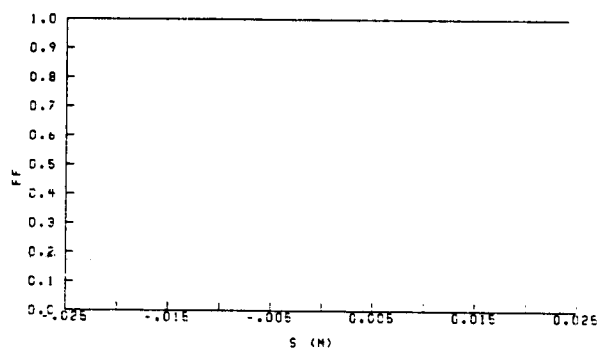
k. Freezing fraction vs. surface location
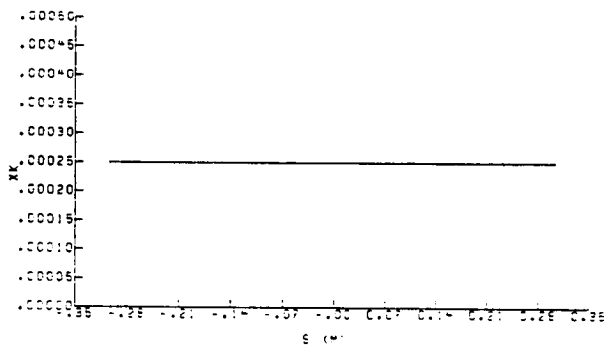
i. Equivalent sand-grain roughness height vs. surface location

Figure 7.19: Concluded.

133

```
VELOCITY (M/S)        64.73
TEMPERATURE (C)      -12.60
PRESSURE (KPA)        90.75
HUMIDITY (%)         100.00
LWC (G/M**3)           0.50
DROP DIAM (MICRON)    20.00
TIME (SEC)           120.00
```
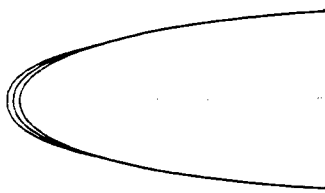
a. Iced airfoil geometry
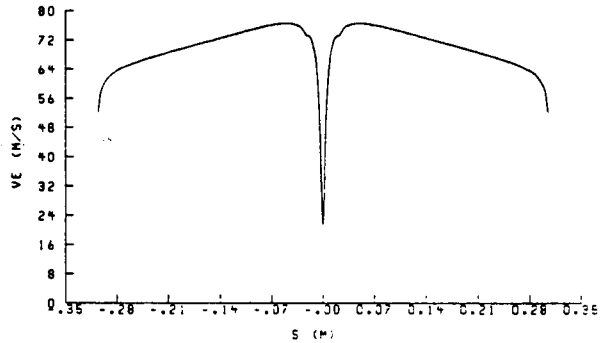
d. Edge velocity vs. surface location
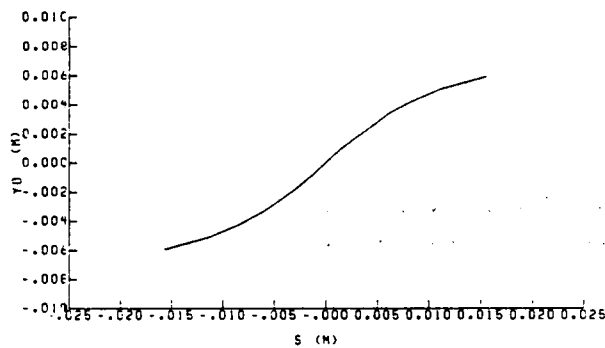
b. Particle release position vs. surface
    impact distance
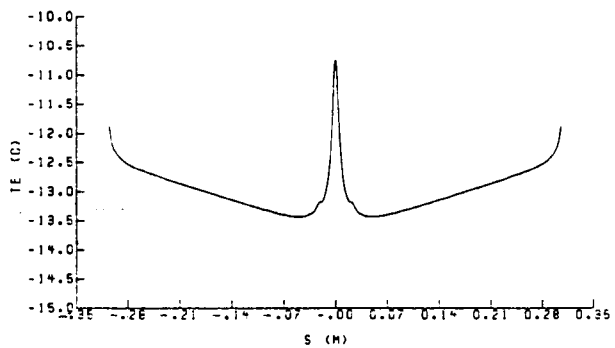
e. Edge temperature vs. surface location
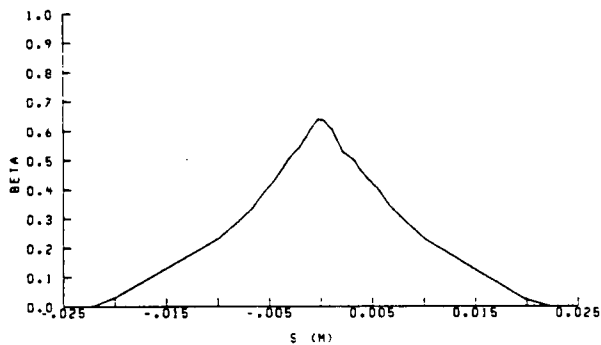
c. Local collection efficiency vs. surface
    location
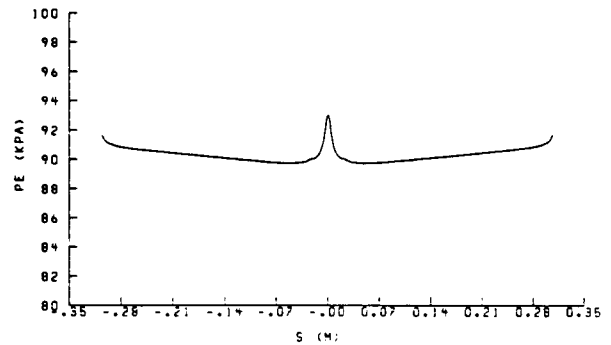
f. Edge pressure vs. surface location

Figure 7.20: Icing parameter plots for the second timestep of Example 3.

134

```
VELOCITY (M/S)        64.73
TEMPERATURE (C)      -12.60
PRESSURE (KPA)        90.75
HUMIDITY (%)         100.00
LHC (G/M**3)           0.50
DROP DIAM (MICRON)    20.00
TIME (SEC)           120.00
```
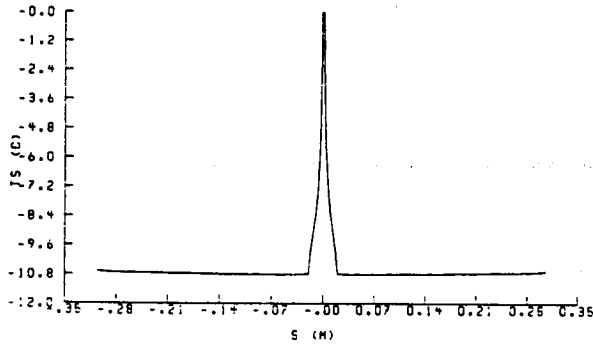
g. Equilibrium surface temperature vs.
    surface location
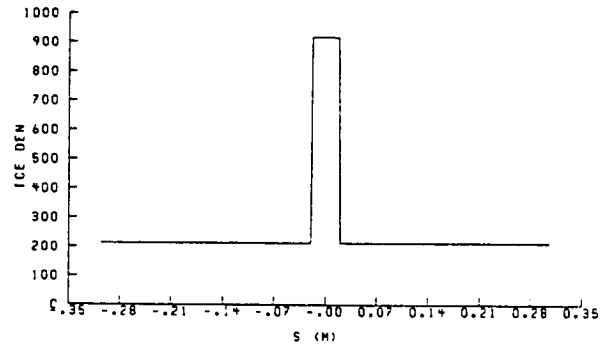
j. Ice density vs. surface location
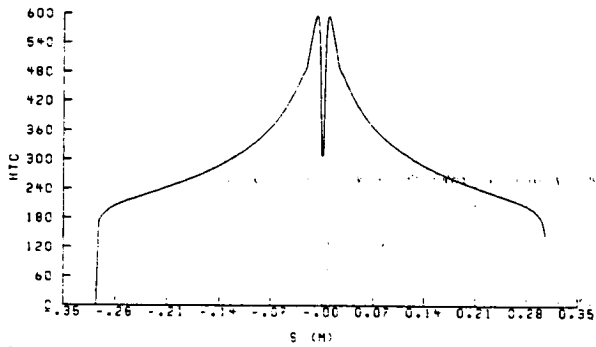
h. Convective heat transfer coefficient
    vs. surface location
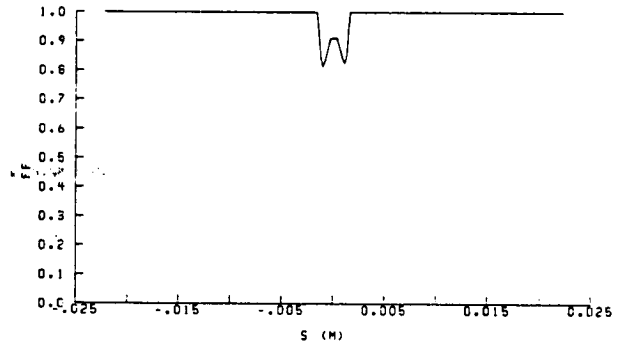
k. Freezing fraction vs. surface location
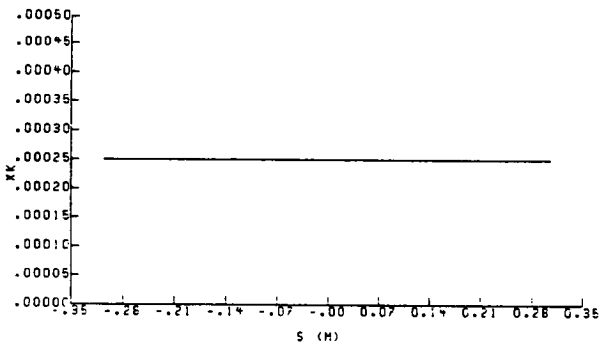
i. Equivalent sand-grain roughness
    height vs. surface location

Figure 7.20: Concluded
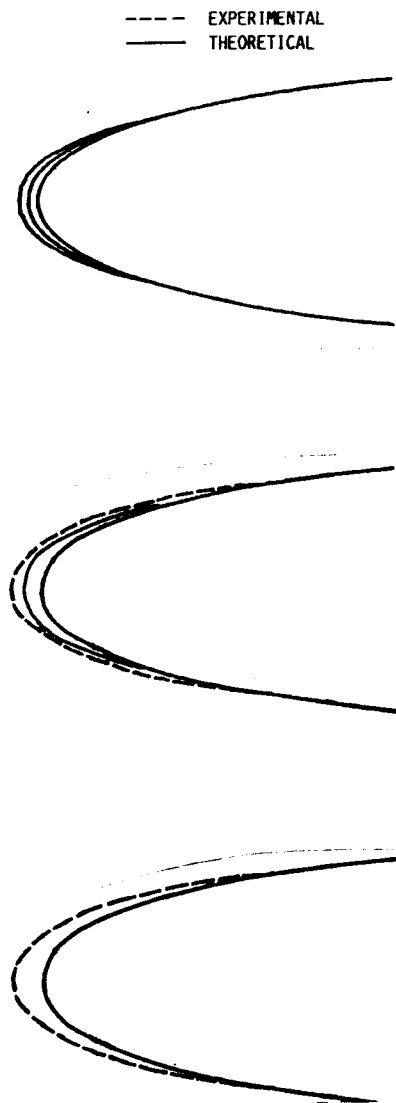
135

Figure 7.21: Comparison of experimental and calculated ice accretion shape for example 3.
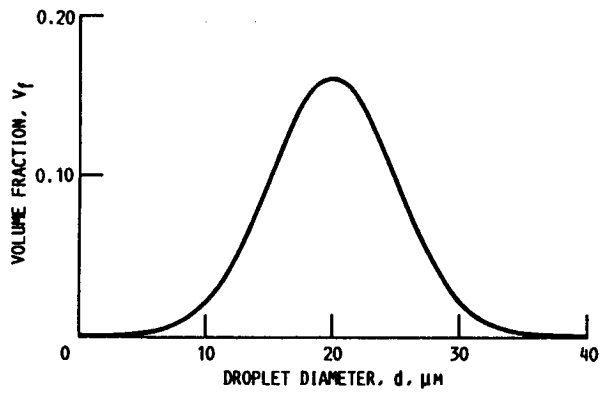
Figure 7.22: Droplet distribution specified for Example 4.
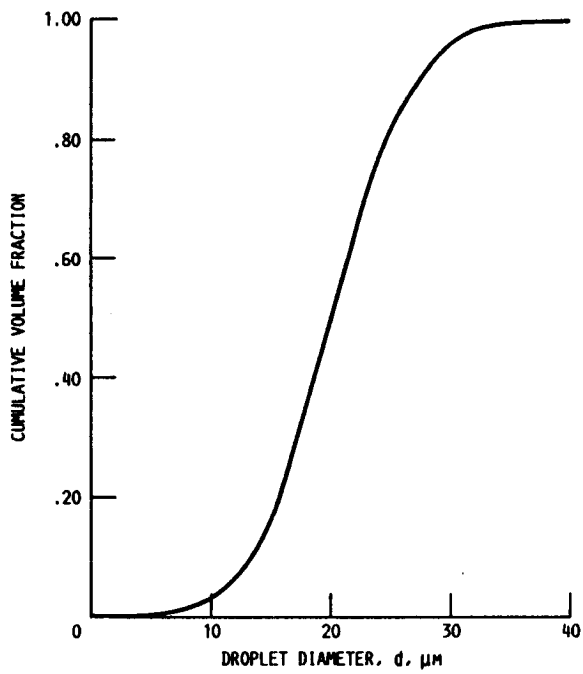
Figure 7.23: Cumulative volume fraction vs. droplet diameter for the droplet distribution specified in Example 4.

137

```
NACA 0012 : EXAMPLE 4
&S24Y
ILIFT= 1
IPARA= 1
IFIRST= 3
ISECHD= 3
IPVOR= 1
INCLT= 0
CLT= 0.0
ICHORD= 0
CCL= 0.0
IND= 1
ISOL= 0
IPRINT= 0
IFLLL= 1
&END
  1.0000000     0.9899999     0.9800000     0.9700000     0.9500000     0.9250000    6 0 3
  0.9000000     0.8750000     0.8500000     0.8250000     0.8000000     0.7750000    6 0 3
  0.7500000     0.7250000     0.7000000     0.6750000     0.6500000     0.6250000    6 0 3
  0.6000000     0.5750000     0.5500000     0.5250000     0.5000000     0.4750000    6 0 3
  0.4500000     0.4250000     0.4000000     0.3750000     0.3500000     0.3250000    6 0 3
  0.3000000     0.2750000     0.2500000     0.2250000     0.2000000     0.1750000    6 0 3
  0.1500000     0.1250000     0.1000000     0.0900000     0.0800000     0.0700000    6 0 3
  0.0600000     0.0500000     0.0450000     0.0400000     0.0350000     0.0300000    6 0 3
  0.0250000     0.0200000     0.0150000     0.0100000     0.0075000     0.0050000    6 0 3
  0.0037500     0.0025000     0.0022500     0.0020000     0.0017500     0.0015000    6 0 3
  0.0012500     0.0010000     0.0008750     0.0007500     0.0006250     0.0005000    6 0 3
  0.0003750     0.0002500     0.0001250     0.0000000     0.0001250     0.0002500    6 0 3
  0.0003750     0.0005000     0.0006250     0.0007500     0.0008750     0.0010000    6 0 3
  0.0012500     0.0015000     0.0017500     0.0020000     0.0022500     0.0025000    6 0 3
  0.0037500     0.0050000     0.0075000     0.0100000     0.0150000     0.0200000    6 0 3
  0.0250000     0.0300000     0.0350000     0.0400000     0.0450000     0.0500000    6 0 3
  0.0600000     0.0700000     0.0800000     0.0900000     0.1000000     0.1250000    6 0 3
  0.1500000     0.1750000     0.2000000     0.2250000     0.2500000     0.2750000    6 0 3
  0.3000000     0.3250000     0.3500000     0.3750000     0.4000000     0.4250000    6 0 3
  0.4500000     0.4750000     0.5000000     0.5250000     0.5500000     0.5750000    6 0 3
  0.6000000     0.6250000     0.6500000     0.6750000     0.7000000     0.7250000    6 0 3
  0.7500000     0.7750000     0.8000000     0.8250000     0.8500000     0.8750000    6 0 3
  0.9000000     0.9250000     0.9500000     0.9700000     0.9800000     0.9899999    6 0 3
  1.0000000     0.0000000     0.0000000     0.0000000     0.0000000     0.0000000    1 1 3
  0.0000000    -0.0018740    -0.0036110    -0.0052390    -0.0082510    -0.0117000    6 0 4
 -0.0149080    -0.0179530    -0.0208880    -0.0237390    -0.0265150    -0.0292210    6 0 4
 -0.0318550    -0.0344110    -0.0368870    -0.0392810    -0.0415850    -0.0437950    6 0 4
 -0.0459040    -0.0479060    -0.0497930    -0.0515600    -0.0531980    -0.0546980    6 0 4
 -0.0560510    -0.0572430    -0.0582620    -0.0590900    -0.0597070    -0.0600940    6 0 4
 -0.0602260    -0.0600760    -0.0596120    -0.0587940    -0.0575700    -0.0558790    6 0 4
 -0.0536360    -0.0507320    -0.0470040    -0.0452280    -0.0432520    -0.0410380    6 0 4
 -0.0385350    -0.0356740    -0.0340820    -0.0323620    -0.0304960    -0.0284620    6 0 4
 -0.0262300    -0.0237260    -0.0207970    -0.0172480    -0.0150780    -0.0123860    6 0 4
 -0.0106990    -0.0086200    -0.0081360    -0.0076230    -0.0070750    -0.0064850    6 0 4
 -0.0058470    -0.0051460    -0.0047660    -0.0043630    -0.0039310    -0.0034620    6 0 4
 -0.0029450    -0.0023560    -0.0016320     0.0000000     0.0016320     0.0023560    6 0 4
  0.0029450     0.0034620     0.0039310     0.0043630     0.0047660     0.0051460    6 0 4
  0.0058470     0.0064850     0.0070750     0.0076230     0.0081360     0.0086200    6 0 4.
  0.0106990     0.0123860     0.0150780     0.0172480     0.0207970     0.0237260    6 0 4
  0.0262300     0.0284620     0.0304960     0.0323620     0.0340820     0.0356740    6 0 4
  0.0385350     0.0410380     0.0432520     0.0452280     0.0470040     0.0507320    6 0 4
  0.0536360     0.0558790     0.0575700     0.0587940     0.0596120     0.0600760    6 0 4
  0.0602260     0.0600940     0.0597070     0.0590900     0.0582620     0.0572430    6 0 4
  0.0560510     0.0546980     0.0531980     0.0515600     0.0497930     0.0479060    6 0 4
  0.0459040     0.0437950     0.0415850     0.0392810     0.0368870     0.0344110    6 0 4
  0.0318550     0.0292210     0.0265150     0.0237390     0.0208880     0.0179530    6 0 4
  0.0149080     0.0117000     0.0082510     0.0052390     0.0036110     0.0018740    6 0 4
  0.0000000     0.0000000     0.0000000     0.0000000     0.0000000     0.0000000    1 1 4
&TRAJ1
GEPS= 0.4999999E-04
DSHIFT= 0.20E-02
VEPS= 0.9999999E-03
LCMB= 0
LCMP= 0
LEQM= 1
LSYM= 0
LYOR= 1
LXOR= 1
NBDY= 1
NEQ= 4
NPL= 15
NSEAR= 50
NSI= 5
TIMSTP= 0.9999999E-03
&END
&TRAJ2
CHORD= 0.30
G= 0.0
PIT= 0.0
PITDOT= 0.0
PRATK= 0.0
XORC= -4.0
XSTOP= 0.50
YOLIM= 0.9999999E-04
YOMAX= 0.50E-01
YOMIN= -0.50E-01
YORC= 0.9999996E-01
&END
&DIST
CFP= 1.042, 4*1.0, 5*0.0
DPD= 4.0, 12.0, 20.0, 28.0, 36.0, 5*0.0
FLWC= 0.0082, 0.2037, 0.5762, 0.2037, 0.0082, 5*0.0
&END
&ICE
VINF= 129.460
LWC= 0.750
TAMB= 260.5498
PAMB= 90748.0
RH= 100.0
DPMM= 20.0
XKINIT= 0.00035
SEGTOL= 1.50
&END
```

Figure 7.24: Input data file for Example 4.

```
VELOCITY (M/S)        129.46
TEMPERATURE (C)       -12.60
PRESSURE (KPA)         90.75
HUMIDITY (%)          100.00
LWC (G/M**3)            0.75
DROP DIAM (MICRON)     20.00
TIME (SEC)             60.00
```
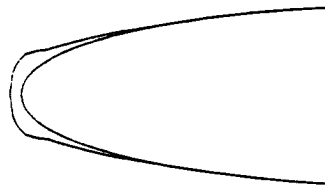
a.   Iced airfoil geometry
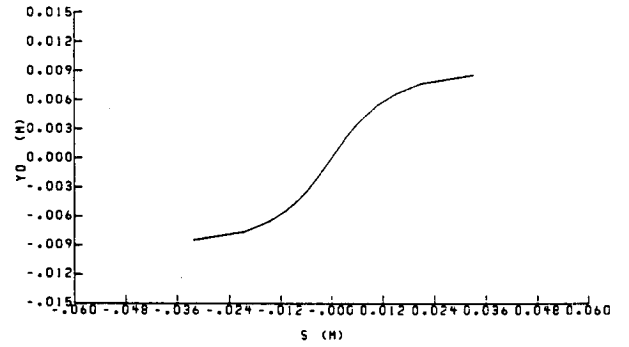
d.   Particle release position vs. surface impact distance, $\bar{d}_m = 20$ microns
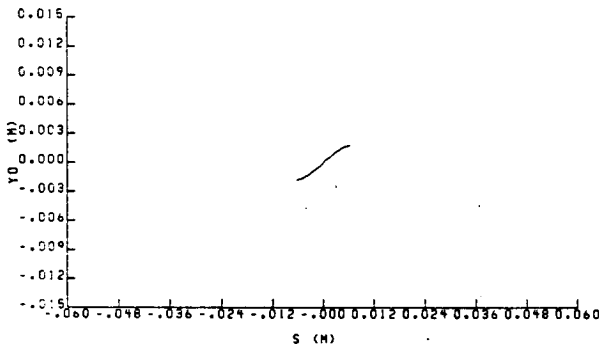
b.   Particle release position vs. surface impact distance, $\bar{d}_m = 4$ microns
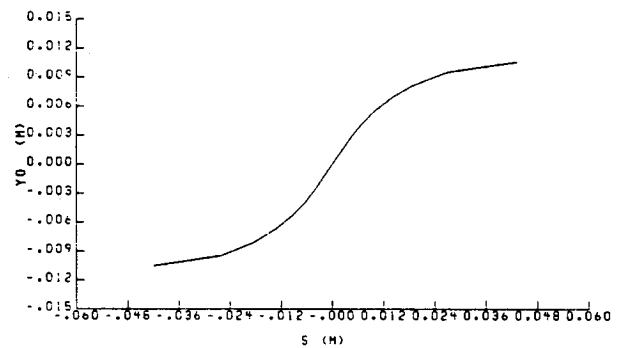
e.   Particle release position vs. surface impact distance, $\bar{d}_m = 28$ microns
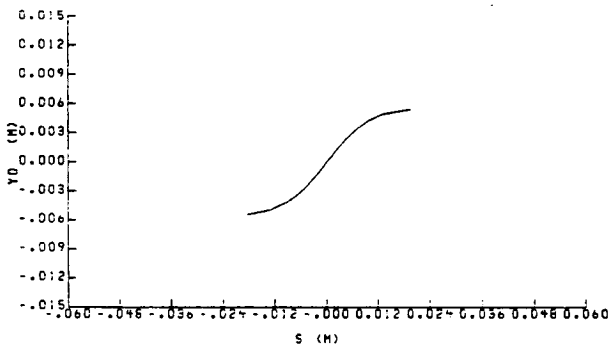
c.   Particle release position vs. surface impact distance, $\bar{d}_m = 12$ microns
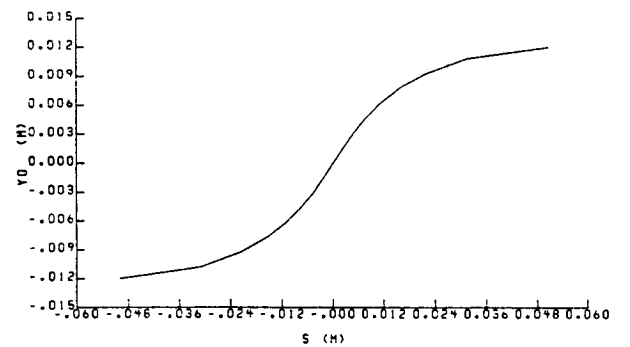
f.   Particle release position vs. surface impact distance, $\bar{d}_m = 36$ microns

Figure 7.25: Icing parameter plots for the first timestep of Example 4.

139

VELOCITY (M/S)	129.46
TEMPERATURE (C)	-12.60
PRESSURE (KPA)	90.75
HUMIDITY (%)	100.00
LWC (G/M**3)	0.75
DROP DIAM (MICRON)	20.00
TIME (SEC)	60.00
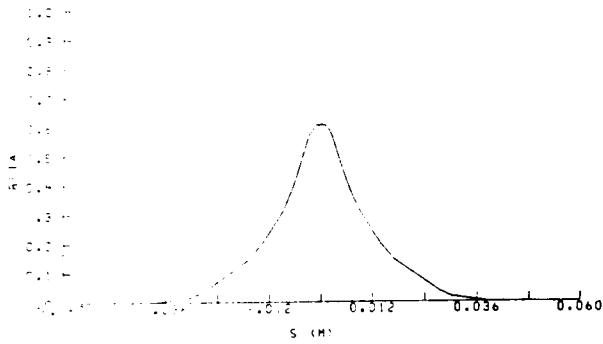
g. Local collection efficiency vs. surface location
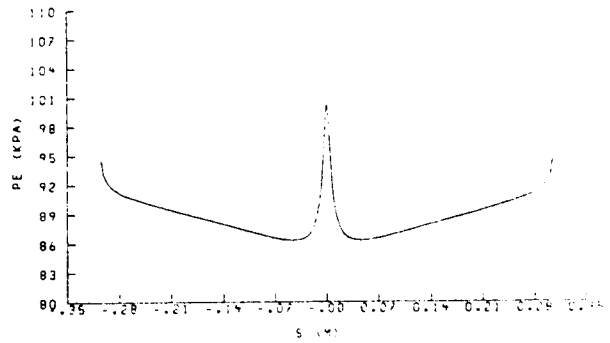
j. Edge pressure vs. surface location
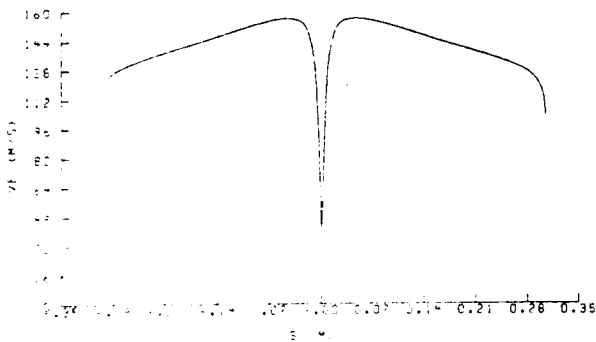
h. Edge velocity vs. surface location
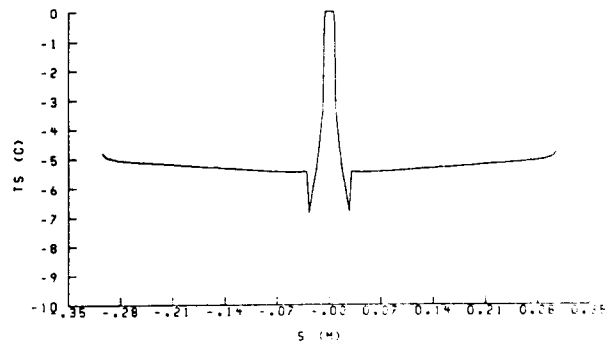
k. Equilibrium surface temperature vs. surface location
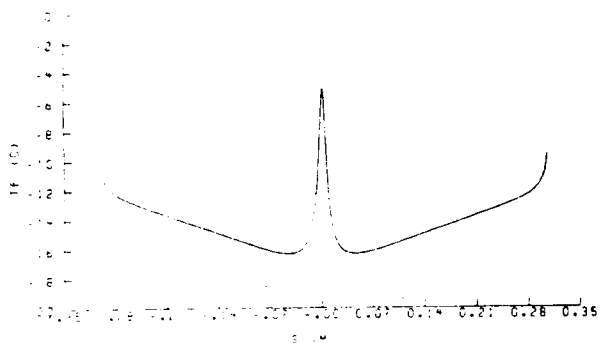
i. Edge temperature vs. surface location
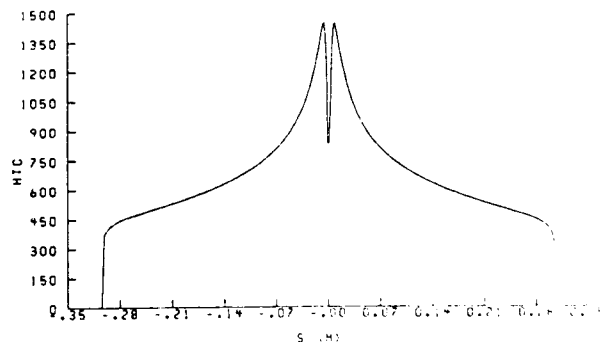
l. Convective heat transfer coefficient vs. surface location

Figure 7.25: Continued.

140

```
VELOCITY (M/S)          129.46
TEMPERATURE (C)         -12.60
PRESSURE (KPA)           90.75
HUMIDITY (%)            100.00
LWC (G/M**3)              0.75
DROP DIAM (MICRON)       20.00
TIME (SEC)               60.00
```
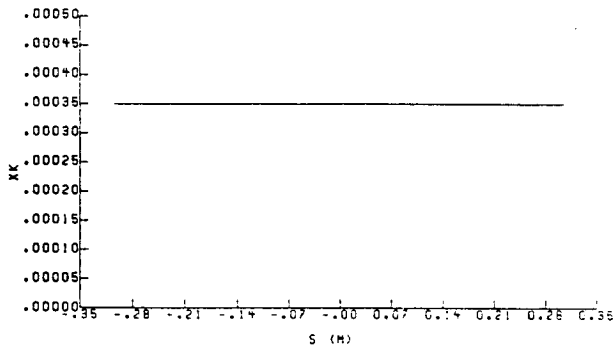
m. Equivalent sand-grain roughness
    height vs. surface location
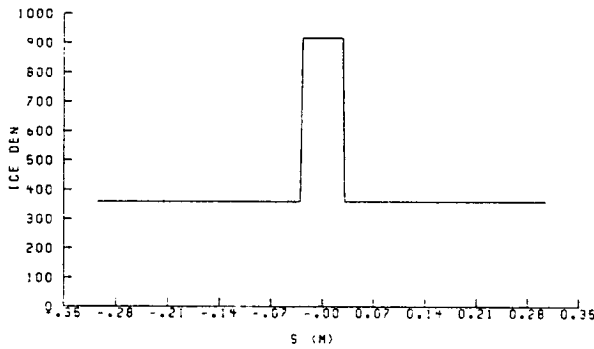
n. Ice density vs. surface location
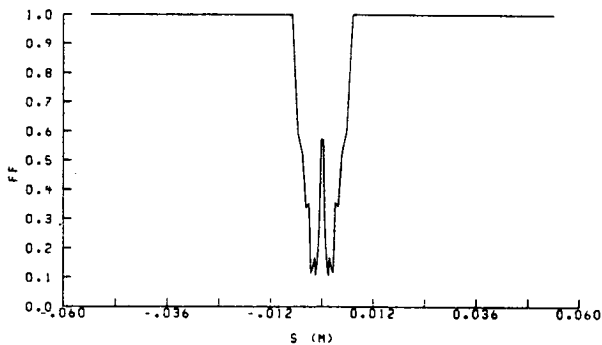
o. Freezing fraction vs. surface location

Figure 7.25: Concluded.

141
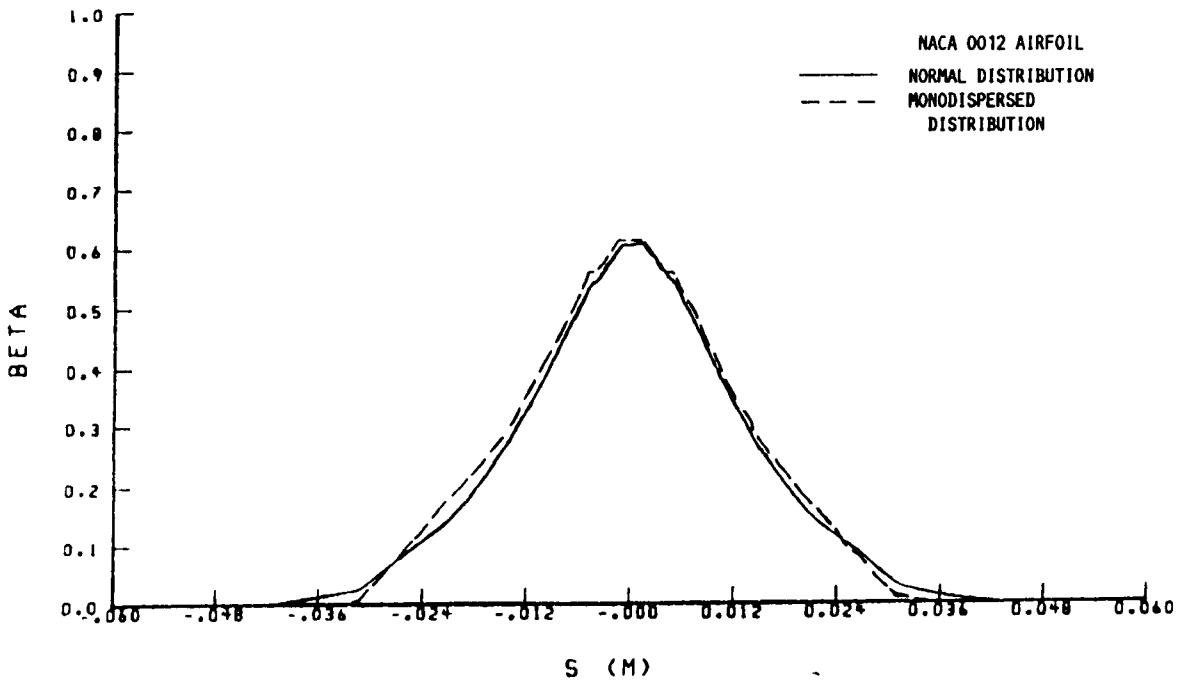
Figure 7.26: Comparison of the calculated local collection efficiency vs. surface distance for a normal and monodispersed droplet distributions with mass median diameters of 20.0 microns.
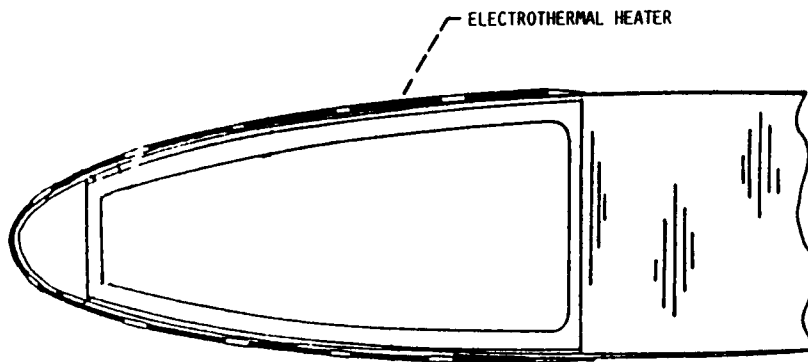
Figure 7.27: Electrothermal heater on a NACA 0012 airfoil modeled in Example 5.

```
NACA 0012 : THERMAL A/I
&S24Y
ILIFT= 1
IPARA= 1
IFIRST= 3
ISECND= 3
IPVOR= 1
INCLT= 0
CLT= 6.0
ICHORD= 0
CCL= 0.0
IND= 1
ISOL= 0
IPPRINT= 0
IFLLL= 1
&END
   1.0000000    0.9899999    0.9800000    0.9700000    0.9500000    0.9250000    6 0 3
   0.9000000    0.8750000    0.8500000    0.8250000    0.8000000    0.7750000    6 0 3
   0.7500000    0.7250000    0.7000000    0.6750000    0.6500000    0.6250000    6 0 3
   0.6000000    0.5750000    0.5500000    0.5250000    0.5000000    0.4750000    6 0 3
   0.4500000    0.4250000    0.4000000    0.3750000    0.3500000    0.3250000    6 0 3
   0.3000000    0.2750000    0.2500000    0.2250000    0.2000000    0.1750000    6 0 3
   0.1500000    0.1250000    0.1000000    0.0900000    0.0800000    0.0700000    6 0 3
   0.0600000    0.0500000    0.0450000    0.0400000    0.0350000    0.0300000    6 0 3
   0.0250000    0.0200000    0.0150000    0.0100000    0.0075000    0.0050000    6 0 3
   0.0037500    0.0025000    0.0022500    0.0020000    0.0017500    0.0015000    6 0 3
   0.0012500    0.0010000    0.0008750    0.0007500    0.0006250    0.0005000    6 0 3
   0.0003750    0.0002500    0.0001250    0.0000000    0.0001250    0.0002500    6 0 3
   0.0003750    0.0005000    0.0006250    0.0007500    0.0008750    0.0010000    6 0 3
   0.0012500    0.0015000    0.0017500    0.0020000    0.0022500    0.0025000    6 0 3
   0.0037500    0.0050000    0.0075000    0.0100000    0.0150000    0.0200000    6 0 3
   0.0250000    0.0300000    0.0350000    0.0400000    0.0450000    0.0500000    6 0 3
   0.0600000    0.0700000    0.0800000    0.0900000    0.1000000    0.1250000    6 0 3
   0.1500000    0.1750000    0.2000000    0.2250000    0.2500000    0.2750000    6 0 3
   0.3000000    0.3250000    0.3500000    0.3750000    0.4000000    0.4250000    6 0 3
   0.4500000    0.4750000    0.5000000    0.5250000    0.5500000    0.5750000    6 0 3
   0.6000000    0.6250000    0.6500000    0.6750000    0.7000000    0.7250000    6 0 3
   0.7500000    0.7750000    0.8000000    0.8250000    0.8500000    0.8750000    6 0 3
   0.9000000    0.9250000    0.9500000    0.9700000    0.9800000    0.9899999    6 0 3
   1.0000000    0.0000000    0.0000000    0.0000000    0.0000000    0.0000000    1 1 3
   0.0000000   -0.0018740   -0.0036110   -0.0052390   -0.0082510   -0.0117000    6 0 4
  -0.0149080   -0.0179530   -0.0208880   -0.0237390   -0.0265150   -0.0292210    6 0 4
  -0.0318550   -0.0344110   -0.0368870   -0.0392810   -0.0415850   -0.0437950    6 0 4
  -0.0459040   -0.0479060   -0.0497930   -0.0515600   -0.0531980   -0.0546980    6 0 4
  -0.0560510   -0.0572430   -0.0582620   -0.0590900   -0.0597070   -0.0600940    6 0 4
  -0.0602260   -0.0600760   -0.0596120   -0.0587940   -0.0575700   -0.0558790    6 0 4
  -0.0536360   -0.0507320   -0.0470040   -0.0452280   -0.0432520   -0.0410380    6 0 4
  -0.0385350   -0.0356740   -0.0340820   -0.0323620   -0.0304960   -0.0284620    6 0 4
  -0.0262300   -0.0237260   -0.0207970   -0.0172480   -0.0150780   -0.0123860    6 0 4
  -0.0106990   -0.0086200   -0.0081360   -0.0076230   -0.0070750   -0.0064850    6 0 4
  -0.0058470   -0.0051460   -0.0047660   -0.0043630   -0.0039310   -0.0034620    6 0 4
  -0.0023450   -0.0023560   -0.0016320    0.0000000    0.0016320    0.0023560    6 0 4
   0.0029450    0.0034620    0.0039310    0.0043630    0.0047660    0.0051460    6 0 4
   0.0058470    0.0064850    0.0070750    0.0076230    0.0081360    0.0086200    6 0 4
   0.0106990    0.0123860    0.0150780    0.0172480    0.0207970    0.0237260    6 0 4
   0.0262300    0.0284620    0.0304960    0.0323620    0.0340820    0.0356740    6 0 4
   0.0385350    0.0410380    0.0432520    0.0452280    0.0470040    0.0507320    6 0 4
   0.0536360    0.0558790    0.0575700    0.0587940    0.0596120    0.0600760    6 0 4
   0.0602260    0.0600940    0.0597070    0.0590900    0.0582620    0.0572430    6 0 4
   0.0560510    0.0546980    0.0531980    0.0515600    0.0497930    0.0479060    6 0 4
   0.0459040    0.0437950    0.0415850    0.0392810    0.0368870    0.0344110    6 0 4
   0.0318550    0.0292210    0.0265150    0.0237390    0.0208880    0.0179530    6 0 4
   0.0149080    0.0117000    0.0082510    0.0052390    0.0036110    0.0018740    6 0 4
   0.0000000    0.0000000    0.0000000    0.0000000    0.0000000    0.0000000    1 1 4
&TRAJ1
GEPS= 0.4999999E-04
DSHIFT= 0.20E-02
VEPS= 0.9999999E-03
LCMB= 0
LCMP= 0
LEQM= 1
LSYM= 0
LYOR= 1
LXOR= 1
NBDY= 1
NEQ= 4
NPL= 15
NSEAR= 50
NSI= 1
TIMSTP= 0.9999999E-03
&END
&TRAJ2
CHORD= 0.30
G= 0.0
PIT= 0.0
PITDOT= 0.0
PRATK= 0.0
XORC= -4.0
XSTOP= 0.50
YOLIM= 0.9999999E-04
YOMAX= 0.50E-01
YOMIN= -0.50E-01
YORC= 0.9999996E-01
&END
&DIST
CFP=1.0, 9*0.0
DPD=20.0, 9*0.0
FLWC=1.00, 9*0.0
&END
&ICE
VINF= 128.408
LWC= 0.500
TAMB= 265.00
PAMB= 90748.0
RH= 100.0
DPMM= 20.0
XKINIT= 0.20E-03
SEGTOL= 1.50
QCOND=34*0.0,71*6000.,395*0.0
&END
```

Figure 7.28: Input data file for Example 5.

VELOCITY (M/S)	128.41
TEMPERATURE (C)	-8.15
PRESSURE (KPA)	90.75
HUMIDITY (%)	100.00
LWC (G/M**3)	0.50
DROP DIAM (MICRON)	20.00
TIME (SEC)	60.00
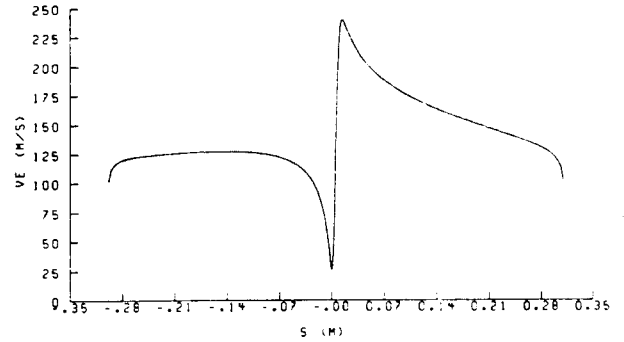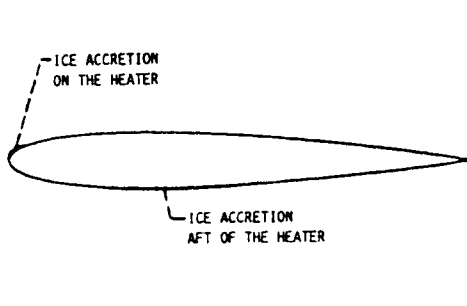
a. Iced airfoil geometry

d. Edge velocity vs. surface location
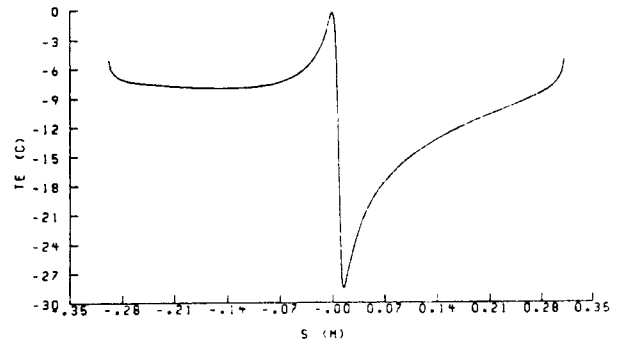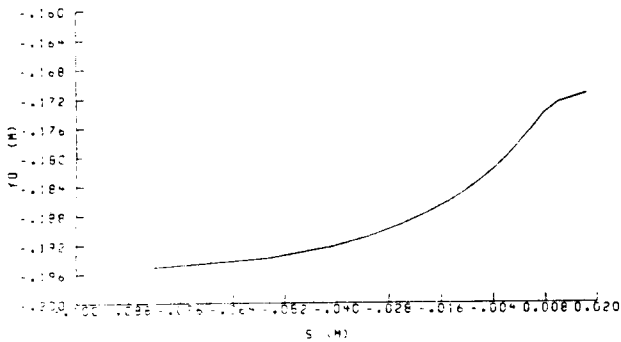
b. Particle release position vs. surface impact distance

e. Edge temperature vs. surface location
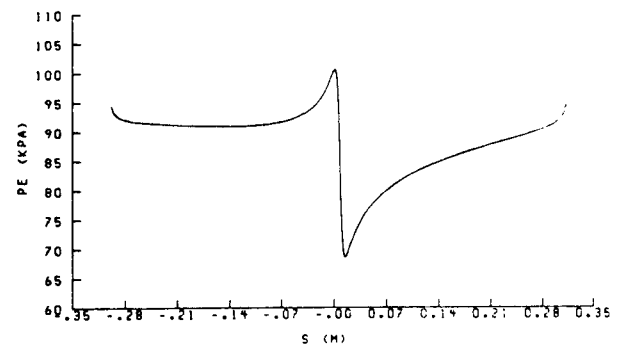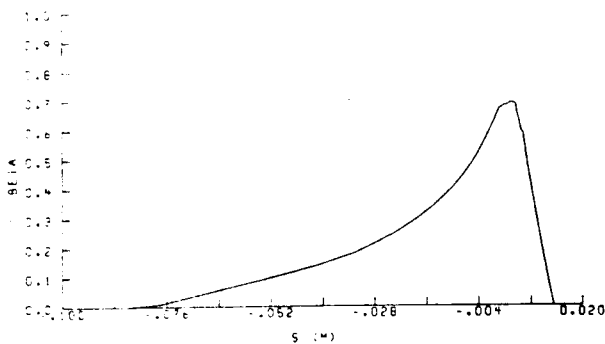
c. Local collection efficiency vs. surface location

f. Edge pressure vs. surface location

Figure 7.29: Icing parameter plots for the first timestep of Example 5.

144

VELOCITY (M/S)	128.41
TEMPERATURE (C)	-8.15
PRESSURE (KPA)	90.75
HUMIDITY (%)	100.00
LWC (G/M**3)	0.50
DROP DIAM (MICRON)	20.00
TIME (SEC)	60.00
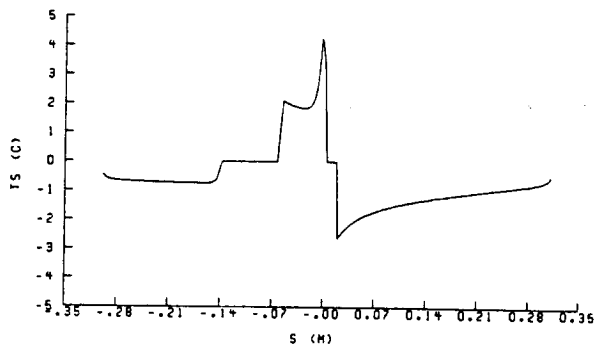
g. Equilibrium surface temperature vs. surface location
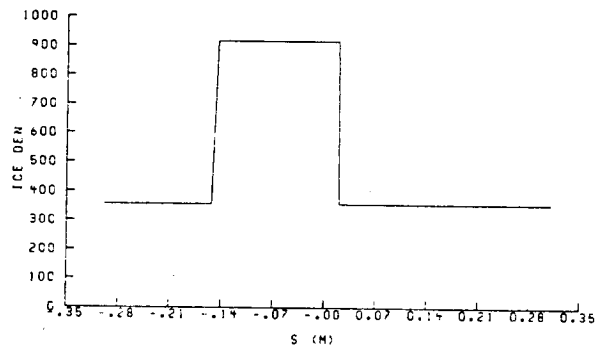
j. Ice density vs. surface location
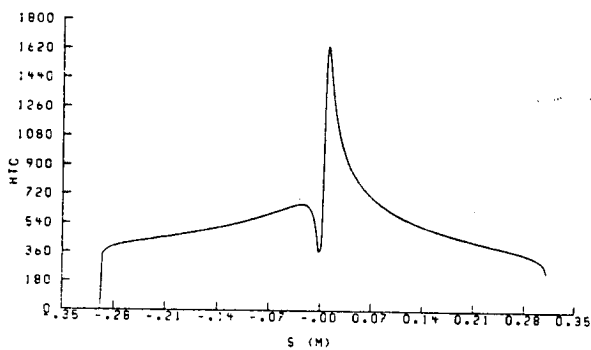
h. Convective heat transfer coefficient vs. surface location
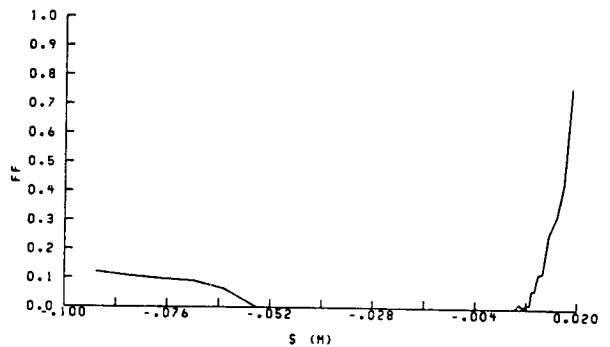
k. Freezing fraction vs. surface location
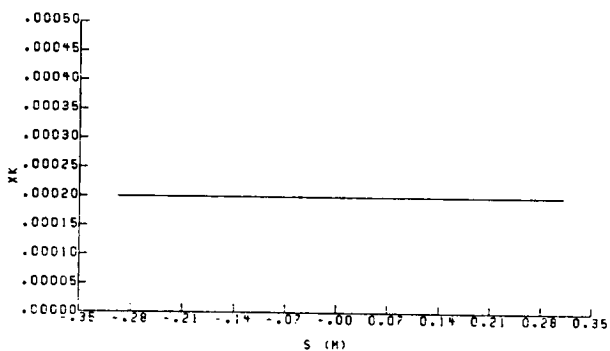
i. Equivalent sand-grain roughness height vs. surface location

Figure 7.29: Concluded.

145

Chapter 8

PROGRAMMING AIDS

This section contains information regarding the coding of LEWICE to aid users who require a more advanced understanding of the program. Descriptions of the subroutines, common blocks, and work files are included, along with flow charts of various sections of the program.

8.1   Descriptions of Subroutines

The subroutines will not be discussed individually in this user's manual. Instead, a description can be found in the program listing in COMMENT statements preceding most subroutines. These descriptions include the purpose of the subroutine, the input and output variables, and additional notes describing special features of the subroutine.

8.2   Diagnostic and Error Messages

In a program as complex as LEWICE, the programmer must provide messages informing the user of any abnormalities in the calculations. The most common error messages are discussed in this section. They are grouped by the program module in which they will occur, i.e., potential flow calculation, particle trajectory calculation, or thermodynamic and ice accretion calculation.

When an error message or unusual situation occurs, the first step should be to check the description of the input parameters found in Section 5.0. The following descriptions of the error messages will assume that this step has already been completed, and will concentrate on how the error may relate to certain aspects of the icing condition or geometry being evaluated.

8.3   Potential Flow Calculations

All of the lines of data input to the potential flow code are identified by a card type number found in the most right-hand column in each line of

data. When the data line is read, this value is checked against the value of the card type that was anticipated. If these numbers do not match, an error message is printed and the program terminated. This error condition is usually caused by having input values in the wrong columns on a line of data.

Another error occurs occasionally when stagnation points are calculated behind (downstream) of the large horns of a glaze ice accretion. The error will usually be characterized by "division by zero" messages. The situation cannot be corrected by forming a pseudo-surface as described in Section 7.2 and Appendix C. However, the case should be re-run with a larger timestep which will make the predicted glaze ice accretion somewhat smoother and may allow the calculations to continues.

Another error condition can occur when multiple stagnation points are calculated which cannot be removed by the formation of a pseudo-surface, and a stagnation point has been manually selected. In this case, there will be at least two locations where the local velocity is 0.0 m/s. When the compressible, dimensional surface velocity is calculated from the incompressible, non-dimensional values (subroutine VEDGE), division by zero errors can again occur. It is best to force the calculations to continue through this error, if possible, because the locations of the error may be downstream of the impingement region and, therefore, will not affect the ice accretion shape. If the calculations cannot be continued, re-run the case with a larger timestep.

8.4 Particle Trajectory Calculations

Most of the errors that occur in the particle trajectory calculations result from inaccuracies in the flow field or errors in input data. Errors caused by improper input parameters will generally be accompained by diagnostic messages, which will be discussed below.

Subroutine RANGE will allow a total of 30 trajectories to be calculated while searching for a trajectory that passes above and below the body. If two such trajectories are not identified, the following message will be printed and the program stopped:

30 Trajectories are calculated in RANGE. Run aborted.

The most probable cause of the error is that the values of Y0MAX and Y0MIN have been input incorrectly. If the values are correct, review the body coordinates that are being used by the program.

A run can be terminated in a similar manner in subroutine IMPLIM. In this case, if the number of trajectories required to identify the upper and lower impingement limits exceed NSEAR, the run is terminated. The value of NSEAR is input by the user through namelist TRAJ1 and is normally set equal to 50. If the limiting value of NSEAR is reached, the value of YOLIM may be unnecessarily small or there may be a problem with the way the program has read or interpreted the body coordinates.

In subroutine COLLEC, the program will be terminated if the value of NPL is greater than 100. The value of NPL is input by the user through namelist TRAJ1, and typical values are between 10 and 20. If this error occurs, verify that the value of NPL is in the proper column in the input file.

Occasionally, errors occur in the flow field near the surface of the body, especially for convoluted glaze ice accretions. In these cases, very large local velocities are calculated which cause exponent overflows or negative arguments in subroutine ABFORM. If these errors occur, try to force the calculations to continue through this error because, if a bad impingement point is calculated as a result of the error, it can removed before calculating the local collection efficiency. Unfortunately, once this error has been encountered in one timestep, it will probably occur in all subsequent timesteps.

8.5 Thermodynamic and Ice Accretion Calculations

If the program completes the flow field and particle trajectory calculations with no errors, there generally will be no additional errors in the thermodynamic calculations. There are temperature limits in the subroutines used to calculate the pressure of water vapor over liquid water and over ice. These calculations are performed in subroutines PVW and PVI, respectively. The temperature ranges, shown below, are sufficient for any anticipated application of the code.

Vapor Pressure over Liquid Water: $223.15 \text{ K} < T < 323.15 \text{ K}$

Vapor Pressure over Ice : $213.15 \text{ K} < T < 273.15 \text{ K}$

8.6 COMMON Blocks and Work Files

In a program of this size, much of the information must be transfered between subroutines through COMMON statements. Table 8.1 lists each COMMON block in the program, the general purpose of the variables in the COMMON block, and the subroutines in which each block is found. No open COMMON statements are used in LEWICE.

In addition to COMMON blocks, much information is passed between subroutines through temporary work files. The work files and the purpose of each are shown in Table 8.2. Many of these files are used in the potential flow calculations (subroutine S24Y), and will not be described in detail because little work was done to modify the potential flow calculations.

8.7 Size of the Code

Because LEWICE combines three complex computer codes into a single computational algorithm, the code requires a substantial amount of computer memory for both the source code and operation. On the IBM 370 computer used at NASA Lewis, the source code itself requires approximately 1400 K of memory. The input file requires only 4 K, but 500 K should be allowed for the output file, especially if a droplet distribution has been specified. Also, a restart file is generated by the program which will be the same size as the input file. The work files used in the code require approximately 150 K of memory. They are erased at the termination of the run and, therefore, could be placed in a temporary work area.

Table 8.1 Common Blocks Used in LEWICE

COMMON Block		Description
LABELS	Contents:	Parameters to be placed on plots
	Variables:	IDR, VINF, LWCKG, TAMB, PAMB, RH,
	Subroutines:	MAIN, BORDER
CNTL	Contents:	Control parameters used in the plotting and particle trajectory routines
	Variable:	LOPT, LEQM, IPLOT, LCMB, LCMP
	Subroutine:	MAIN, TRAJ, IMPLIM, COLLEC, INTIG, RANGE, MODE, READIN, VELCTY, COMB2D
PSEUDO	Contents:	x-coordinates of the pseudo surface that have been generated
	Variables:	IPSURF, XPS
	Subroutines:	MAIN, STAG, VEDGE, PSURF, NEW45, MODE, READIN
ICECOM	Contents:	Variables used in the thermodynamic and ice accretion subroutines
	Variables:	X, Y, SEGLEN, SEGLIN, VE, TE, PE, RA, XK, BETA, TSURF, FFRAC, HTC, RI QCOND, MDOTC, MDOTE, MDOTRI, MDOTTI, MDOTT, DICE, VINF, TAMB, PAMB, RH, DPMM, LWCKG, CPA, CPI, LV, LF, VISC, PI, NPTS, NTHI, NTLOW, ISTAG
	Subroutines:	CNSTS, STAG, PSURF, NWPTS, SEGSEC, ICE, CDYLYR, EBAL, COMPF, COMPT, NWFOIL, OUTPUT, PLOTD

Table 8.1 Continued

COMMON Block		Description
DROP	Contents: Variables: Subroutines:	Droplet distribution data NSI, FLWC, IRS, DPD, EPT PLOTD, TRAJ, EFFICY
BFLAG	Contents: Variables: Subroutines:	**Potential flow data** IDB, INL, IFL, NL, LIFT, IBMF, ISAV1, ISAV2, ISAV3, BTITLE, IBT, IBST, IBTOT, NELTOT, ITRB, INMB, CHORDB, IBD, LIFTOT, IPRB, IFST, ISEC, FTITLE, IPVR S24Y, MAIN1, MAIN3, ASSEMB, ELFORM, FLOWS, MAFORM, PRNTEL, VXYOFF
COMBO	Contents: Variables: Subroutines:	Potential flow data CCL, INCLT, CLT, ALPHA, SUMDS, TLU, IND, ALPHAO, CNU, SMDSWF, MIO S24Y, MAIN1, MAIN3, ASSEMB, COMBO, FLOWS, MAFORM, OFFBOD, VXYOFF
FILEID	Contents: Variables: Subroutines:	Potential flow data IFILE1, IFILE2, IFILE3, IFILE4, IFILE5, IFILE6, IFILE7, IFILE8, IFILE9, IFIL10, IFIL11, IFIL12, IFIL13, IFIL14, IFIL15, IFIL16, IFIL17, IFIL18, IFIL19, IFIL20 S24Y, REWYND, FILRS, MAIN1, MAIN3, SOLVE, ASSEMB, COMBO, ELFORM, FLOWS, MAFORM, VPROFF, VXYOFF
MDATA	Contents: Variables: Subroutines:	Potential flow data ISOL, IOFF, NONU, MBNU, IPRINT, MORE, M S24Y, MAIN1M MAIN3, ASSEMB

Table 8.1 Continued

COMMON Block		Description
ROTAT	Contents: Variables: Subroutines:	Potential flow data NROT, ROTRAD S24Y, ASSEMB, FLOWS, MAFORM
ELDATA	Contents: Variables: Subroutines:	Potential flow data XO, YO, DS, SA, CA, CURV, DL MAIN1, ASSEMB, ELFORM, MAFORM
GCOEFS	Contents: Variables: Subroutines:	Potential flow data CD, CF, CG, CI, WF MAIN1, ASSEMB, ELFORM, MAFORM
COM	Contents: Variables: Subroutines:	Potential flow data IFILL MAIN1, MAIN3, FLOWS, VPROFF, VXYOFF
SPACER	Contents: Variables: Subroutines:	Potential flow data WKAREA SOLVE
SIGMAS	Contents: Variables: Subroutines:	Potential flow data CSIG, CK COMBO, FLOWS, VXOFF
GEOMD	Contents: Variables: Subroutines:	Potential flow data X, Y, XSAVE, YSAVE ELFORM, FLOWS, BTITLE
GCFF	Contents: Variables: Subroutines:	Potential flow data CD, CF, CG, CI, WF FLOWS, VXYOFF

Table 8.1 Continued

COMMON Block		Description
ELDD	Contents:	Potential flow data
	Variables:	X, Y, DS, SA, CA, CURV, DL
	Subroutines:	FLOWS, VXYOFF, READIN, VELCTY
OVER	Contents:	Potential flow data
	Variables:	V1Y, V2Y, V3Y, V4Y, V5Y, V6Y, V3X, V4X, V5X, V6X
	Subroutines:	VPROFF
BODY	Contents:	Coordinates describing the body geometry
	Variables:	NPTS, XSH, YSH, X, Y
	Subroutines:	TRAJ, MODE, READIN, PLTRAJ
BOUND	Contents:	Coordinates of the most forward and aft points of the body geometry and boundaries for the particle trajectory calculations
	Variables:	XFRNT, YFRNT, XREAR, YREAR, XSTOP, YLO, YUP
	Subroutines:	TRAJ, RELEAS, IMPLIM, INTIG, RANGE, MODE, READIN
IMP	Contents:	Particle impingment data for use in the collection efficiency calculation
	Variables:	S, SW, YO, IS
	Subroutines:	TRAJ, IMPLIM, COLLEC, ORDER, INTIG, RANGE, MODE, READIN
INIT	Contents:	Initial conditions for particle release
	Variables:	XIN, YIN, DPM, RL, PITDOT, PIT, VINF, VXP, VYP, AOAR

Table 8.1 Continued

COMMON Block		Description
	Subroutines:	TRAJ, RELEAS, IMPLIM, COLLEC, INTIG, RANGE, DIFFUN, MODE, COMB2D
DIFF	Contents:	Variables used in the particle trajectory equations
	Variables:	Q, AMASS, G, YYI, VISC, CF
	Subroutines:	TRAJ, DIFFUN
STEP	Contents:	Time step and error criteria used in the integration of the particle trajectory equations
	Variables:	TIMSTP, EPS
	Subroutines:	TRAJ, IMPLIM, COLLEC, RANGE
TP15	Contents:	Variables used to calculate the combination solution of velocity
	Variables:	ABCD, ATOTAL, VC15, RSORTC, NX15
	Subroutines:	READIN, COMB2D
NUM	Contents:	Variables used to calculate the flow field velocities
	Variables:	N, M, IND, IBTOT, LIFTOT
	Subroutines:	READIN, VELCTY
GCF	Contents:	Parameters used to calculate the flow field velocities
	Variables:	CD, CF, CG, CI, WF, CSIG, CK, SIG
	Subroutines:	READIN, VELCTY
FLG	Contents:	Parameters used to calculate the flow field velocities
	Subroutines:	READIN, VELCTY

Table 8.1 Continued

COMMON Block		Description
VEX	Contents:	x- and y-components of the flow field velocity
	Subroutines:	VELCTY, COMB2D

Table 8.2 Output and Work Files Used in LEWICE

File Number	Type	Description
1,2,4, 7-18, 21		These are work files used in the potential flow calculations. Since no modifications were made to S24Y, the contents of these files have not been examined in detail.
3	Binary	Unit 3 contains the y_0 vs. s points for each droplet diameter. This file is read in subroutines EFFICY and PLOTD.
5,6	Character	These are the read/write defaults to display information on the screen.
20	Character	This file contains the airfoil coordinates for all timesteps. The file is read in subroutine PLOTD to plot the airfoil.
22	Character	Unit 22 contains the airfoil segment distances used in the collection efficiency calculations.

Table 8.2 Continued

File Number	Type	Description
24	Character	This is an internal input file for subroutine TRAJ. It is created from the input on unit 35. There is no updating of unit 24 for the second or subsequent timesteps.
30	Binary	This is the main working file for the program. It contains the current values of the body coordinates, surface distances, edge velocities, pressures, etc. for each segment.
35	Character	This is the primary input file prepared by the user. It is used to set up all of the other internal input files.
36	Character	This is the restart input file produced by the program after each timestep. It is identical to the input file on unit 35, except that the body coordinates are of the current ice shape. The icing time corresponding to the ice shape coordinates is also included in namelist ICE.
45	Character	This is the internal input file for the potential flow code (S24Y). It is formed from the data input on unit 35.
56	Character	This is the primary output file for LEWICE. It contains the printed output from all portions of the code.

8.8 Execution Times

When an ice shape is predicted, the largest portion of the execution time is spent on the particle trajectory calculations. The CPU time required to run the example cases found in Section 7.0 on the IBM 370 computer are given in Table 8.3. Also indicated are the total number of particle trajectories calculated in each, and the average CPU time per trajectory.

Table 8.3 CPU Time for Examples 1-5

Example Number	CPU Time (sec)	Number of Trajectories Calculated	CPU-sec Trajectory
1	362.52	67	5.41
2	350.80	71	4.90
3	395.01	68	5.81
4	719.30	205	3.51
5	185.50	44	4.22

With these results, the computational time required for a specific icing condition can be estimated if the speed of another type of computer is known compared to an IBM 370.

8.9 Getting LEWICE Operational

When LEWICE is transferred to a system other than that at NASA Lewis, it must first be compiled. A FORTRAN 77 compiler has been used to compile the version used at NASA Lewis. The graphics commands used in LEWICE are from a system that is unique to NASA Lewis and will not be directly applicable to any other system. The name of this graphics package is GRAPH3D, but most of the commands in LEWICE are from GRAPH2D, the predecessor of GRAPH3D. Calls to the graphics package are located in subroutines STAG, PSURF, PLOTD, BORDER, INTIG, PLTRAJ, and EFFICY. The graphics in LEWICE use only the simplest commands, and, therefore, modification of the commands should not be difficult; unfortunately, it will probably be time-consuming.

157

List of References

1. Ackley, S.F. and Templeton, M.K. "Computer Modeling of Atmospheric Ice Accretion." Cold Regions Research and Engineering Laboratory Report 79-4, 1979.

2. Lozowski, E.P., Stallabrass, J.R., and Hearty, P.F. "The Icing of an Unheated Non-Rotating Cylinder in Liquid Water Droplet-Ice Crystal Clouds." National Research Council of Canada Report LTR-LT-96, 1979.

3. Hankey, W.L. and Kirchner, R. "Ice Accretion of Wing Leading Edges." AFFDL-TM-85-FXM, 1979.

4. Cansdale, J.T. and Gent, R.W. "Ice Accretion on Aerofoils in Two-Dimensional Compressible Flow - A Theoretical Model." Royal Aircraft Establishment Technical Report 82128, 1983.

5. MacArthur, C.D., Keller, J.L., and Leurs, J.K. "Mathematical Modeling of Ice Accretion on Aerofoils." AIAA-82-0284, 1982.

6. Olsen, W., Shaw, R., and Newton, J. "Ice Shapes and the Resulting Drag Increase for an NACA 0012 Airfoil." NASA Technical Memorandum 83556, 1984.

7. Tribus, M.V., et al. "Analysis of Heat Transfer Over a Small Cylinder in Icing Conditions on Mount Washington." American Society of Mechanical Engineers Transactions, Vol. 70, 1949, pp. 871-876.

8. Messinger, B.L. "Equilibrium Temperature of an Unheated Icing Surface as a Function of Airspeed." Journal of the Aeronautical Sciences, Vol. 20, No. 1, 1953, pp. 29-42.

9. Olsen, W. "Close-up Movies of the Icing Process on the Leading Edge of an Airfoil." NASA Lewis Research Center Movie C-313, 1985.

10. Hess, J.L. and Smith, A.M.O. "Calculation of Potential Flow About Arbitrary Bodies." Progress in Aeronautical Sciences, 8:1-138, (D. Kuchemann, editor). Elmsford, New York, Pergmon Press, 1967.

11. Harris, C.D. "Two-Dimensional Aerodynamic Characteristics of the NACA 0012 Airfoil in the Langley 8-Foot Transonic Pressure Tunnel." NASA TM 81927, April 1981.

12. Frost, W., Chang, H., Shieh, C., and Kimble, K. "Two- Dimensional Particle Trajectory Computer Program." Interim Report for Contract NAS3-22448, 1982.

13. Chang, H., Frost, W., and Shaw, R.J. "Influence of Multidroplet Size Distribution on Icing Collection Efficiency." AIAA-83-0110, 1983.

14. Hobbs, P.V. Ice Physics. Oxford University Press, Ely House, London, 1974.

15. Carlson, D.J. and Haglund, R.F. "Particle Drag and Heat Transfer in Rocket Nozzles." AIAA Journal, Vol. 2, No. 11, 1964, pp. 1980-1984.

16. Gear, C.W. "The Automatic Integration of Ordinary Differential Equations." Comm. ACM 14, 1971, pp. 176-179.

17. Gear, C.W. "DIFSUB for Solutions of Ordinary Differential Equations." Comm. ACM 14, 1971, pp. 185-190.

18. Macklin, W.C. "The Density and Structure of Ice Formed by Accretion." Quarterly Journal of the Royal Meteorological Society, Vol. 88, 1962, pp. 30-50.

19. Bragg, M.B., Gregorek, G.M., and Shaw, R.J. "An Analytical Approach to Airfoil Icing." AIAA-81-0403, 1981.

20. Gent, R.W., Markiewicz, R.H., and Cansdale, J.T. "Further Studies of Helicopter Rotor Ice Accretion and Protection." Paper No. 54, Eleventh European Rotorcraft Forum, September 1985.

Appendix A

DERIVATION OF THE ICING ENERGY EQUATION

In this appendix, the thermodynamic processes that take place during the formation of an ice accretion are identified and expressed mathematically to form the icing energy equation. This derivation is similar to that presented in Reference A-1, except that the equation is applicable to an arbitrary control volume instead of a control volume situated on the stagnation line.

A.1 Definition of the Control Volume

The control volume to be analyzed is located on the surface of the body and extends from outside the boundary layer to the surface of the body, as shown in Figure A-1. It encloses a distance along the external surface, and, for dimensional completeness, extends one unit length in the spanwise direction (into the page). The lower boundary of the control volume is initially on the surface of the clean geometry, and moves outward with the surface as the ice accretes. Therefore, the control volume is always situated on either the clean or iced surface, and any accumulated ice is considered to leave the control volume through the lower boundary. This definition is important in conduction heat transfer, discussed later in this appendix.

A.2 Mass Balance on an Icing Surface

An evaluation of all mass entering and leaving the control volume is shown in Figure A-2. A mass balance equation can be formed from these terms as shown below.

$$\dot{m}_c + \dot{m}_{r_{in}} - \dot{m}_e - \dot{m}_{r_{out}} = \dot{m}_i \qquad (A-1)$$

At the stagnation point, there will be no water inflow along the surface so therefore, $m_{r_{in}} = 0.0$.

Since the freezing fraction is defined as the proportion of the total mass of liquid entering the control volume that freezes in the control volume, it can be expressed by the following equation:

$$f = \frac{\dot{m}_i}{\dot{m}_c + \dot{m}_{r_{in}}} \qquad (A-2)$$

160

Substituting Equation (A-1) into Equation (A-2), the water flow out of the control volume can be expressed as

$$\dot{m}_{r_{out}} = (1 - f)(\dot{m}_c + \dot{m}_{r_{in}}) - \dot{m}_e \qquad (A-3)$$

A.3 Energy Balance on an Icing Surface

The same control volume concept is used to formulate the energy balance on the icing surface. The First Law of Thermodynamics for a control volume can be expressed as: energy inflow rate = energy outflow rate + energy storage rate.

The modes of energy transfer, illustrated in Figure A-3, are as follows:

Mode of Energy Transfer	Energy Flow Rate
1. Impinging Water	$\dot{m}_c i_{w,T}$
2. Water Flow Into Control Volume	$\dot{m}_{r_{in}} i_{w,sur(i-1)}$
3. Evaporation	$\dot{m}_e i_{v,sur}$
4. Water Flow Out of Control Volume	$\dot{m}_{r_{out}} i_{w,sur(i)}$
5. Ice Accumulation Within Control Volume	$\dot{m}_i i_{i,sur}$
6. Convection	$q_c \Delta s$
7. Conduction through the Skin	$q_k \Delta s$

Using the convention that energy flow into the control volume is positive, the terms can be summed to yield the general form of the energy equation:

$$\dot{m}_c \, i_{w,T} + \dot{m}_{r_{in}} \, i_{w,sur(i-1)} = \dot{m}_e \, i_{v,sur} + \dot{m}_{r_{out}} \, i_{w,sur}$$

$$+ \dot{m}_i \, i_{i,sur} + q_c \, \Delta s + q_k \, \Delta s \qquad (A-4)$$

The evaluation of the terms of the energy equation has been made by various authors, most notably by Sogin (Reference A-2), Lowzowski (Reference A-3), and Cansdale and Gent (Reference A-4). The following sections will evaluate each of the terms of Equation (A-4).

A.4 Impinging Water

Since droplets are essentially brought to rest when they strike an object, it is appropriate to use the stagnation enthalpy defined as

$$i_{w,T} = c_{p_{w,s}} (T_s - 273.15) + \frac{V_\infty^2}{2} \qquad (A-5)$$

The arbitrary reference for zero enthalpy used in this study is water at 273.15 K. Substituting Equation (A-5), the energy flow rate of the impinging water becomes

$$\dot{m}_c\, i_{w,T} = \dot{m}_c'' \left[c_{p_{w,s}}(T_s - 273.15) + \frac{V_\infty^2}{2} \right] \Delta s \qquad (A-6)$$

where

$$\dot{m}_c'' = LWC(V_\infty)\beta \qquad (A-7)$$

A.5 Water Flow Into the Control Volume

The water flowing into the control volume will be at the surface temperature of the preceding control volume. The enthalpy can therefore be expressed as

$$i_{w,sur(i-1)} = c_{p_{w,sur(i-1)}}(T_{sur(i-1)} - 273.15) \qquad (A-8)$$

where (i-1) denotes that the specific heat and temperature are evaluated at the conditions of the proceding control volume. The runback water energy flow rate into the control volume can therefore be expressed as

$$\dot{m}_{r_{in}}\, i_{w,sur(i-1)} = \dot{m}_{r_{in}}\, c_{p_{w,sur(i-1)}} \left(T_{sur(i-1)} - 273.15 \right) \qquad (A-9)$$

A.6 Evaporation

The rate of energy transfer from the surface because of evaporation is given by

$$\dot{m}_e \, i_{v,sur} = \dot{m}_e'' \left[c_{p_w,sur}(T_{sur} - 273.15) + L_v \right] \Delta s \qquad (A-10)$$

where $\dot{m}_e''$ is the evaporative mass transfer flux and L_v is the latent heat of vaporization.

The mass transfer rate is analogous to the convective heat transfer rate and can be written as

$$\dot{m}_e'' = g \, \Delta B \qquad (A-11)$$

where g is the mass transfer coefficient and ΔB is the evaporative driving potential. The mass transfer coefficient, g, can be evaluated using the analogy to heat transfer given by the following equation found in Reference A-5:

$$g = \frac{h_c}{c_{p_a}} \left(\frac{Pr}{Sc} \right)^{.667} \qquad (A-12)$$

In Equation (A-12), Pr is the Prandtl number and Sc is the Schmidt number.

The mass transfer driving potential is analogous to the temperature difference in the convective heat transfer equation. In the case of evaporation, the driving potential is a vapor concentration difference instead of a temperature difference. The equation used in this study is similar to that derived by Sogin (Reference A-2), and given as

$$\Delta B = \frac{P_{v,sur}/T_{sur} - r_h \left(P_e/T_e \right) P_{v,s}/P_s}{\left(1/.622 \right) P_e/T_e - P_{v,sur}/T_{sur}} \qquad (A-13)$$

163

This term accounts for compressibility effects, as does the term derived by Cansdale in Reference A-4.

When the water droplets freeze on impact (f = 1.0), there is no liquid water on the surface to be evaporated; however, water vapor can still leave the surface through sublimation. In this case, Equations (A-10), (A-11), (A-12), and (A-13) are still used to determine the rate of energy transfer from the surface, except that the latent heat of sublimation, L_s, is used in Equation (A-10) instead of the latent heat of vaporization, L_v.

A.7 Water Flow Out of the Control Volume

The water flowing out of the control volume will be at the surface temperature of the control volume, allowing the enthalpy to be expressed as

$$i_{w,sur(i)} = c_{P_w,sur(i)} - (T_{sur(i)} - 273.15) \qquad (A-14)$$

where (i) denotes that the specific heat is to be evaluated at the surface temperature of the control volume being analyzed. Using Equation (A-3), the runback water energy flow rate can be expressed as

$$\dot{m}_{r_{out}} i_{w,sur(i)} = \left[(1-f)(\dot{m}_c + \dot{m}_{r_{in}}) - \dot{m}_e \right] c_{P_w,sur(i)} (T_{sur(i)} - 273.15) \qquad (A-15)$$

A.8 Ice Accumulation Leaving the Control Volume

As previously discussed, the control volume remains on the surface of the geometry as the ice accumulates within the control volume.

From the definition of the freezing fraction, Equation (A-2), the freezing rate is

$$\dot{m}_i = f (\dot{m}_c + \dot{m}_{r_{in}}) \qquad (A-16)$$

The enthalpy of ice referenced to water at 273.15 K is

$$i_{i,sur} = c_{P_i,sur} (T_{sur} - 273.15) - L_f \qquad (A-17)$$

Combining Equations (A-16) and (A-17), the rate of energy leaving the control volume in the accumulated ice can be expressed as

$$\dot{m}_i \, i_{i,sur} = f \, (\dot{m}_c + \dot{m}_{r_{in}}) \left[c_{p_{i,sur}}(T_{sur} - 273.15) - L_f \right] \qquad (A-18)$$

A.9 Net Convective Heat Flux

The local value of the aerodynamically induced heat flow to or from the outer boundary of the control volume is determined by the convective cooling and kinetic heating of the surface. The net convective heat flow can therefore be defined by the following equation:

$$q_c \, \Delta s = h_c \, (T_{sur} - T_{aw}) \, \Delta s \qquad (A-19)$$

In this equation, T_{sur} is the surface temperature and T_{aw} is the adiabatic wall temperature. The adiabatic wall temperature is given by

$$T_{aw} = T_e + r_c \, \frac{V_e^2}{2 \, c_{p_a}} \qquad (A-20)$$

where T_e and V_e are the temperature and velocity at the edge of the boundary layer, respectively, and r_c is the recovery factor. The local temperature is calculated from the pressure coefficients calculated by the potential flow code using the isentropic relationships. Substituting Equation (A-20) into Equation (A-19), the expression for the convective heat flow rate becomes

$$q_c \, \Delta s = h_c \, (T_{sur} - T_e - \frac{r_c \, V_e^2}{2 \, c_{p_a}}) \, \Delta s \qquad (A-21)$$

The heat transfer coefficient is calculated using the integral boundary method described in Appendix B.

A.10 Conduction From the Airfoil Surface

When the cloud is first encountered, a temperature difference will exist between the wetted surface and the inner structure of the airfoil. Prior to

entering the cloud, this inner structure is assumed to be at an equilibrium temperature. The evaluation of the resulting conductive heat flow rate is dependent on knowing the thermal conductivity and detailed geometry of the inner structure of the airfoil.

After a layer of ice forms on an unheated surface, the temperature of the skin should again reach an equilibrium temperature. Since ice is an insulator, any heat transfer through the skin will not affect the growth of the ice accretion at the air/ice interface.

In a thermal deicing system, an ice layer is allowed to form and heat is then applied at the ice/skin interface. The effect of this heat is to melt the ice attached directly to the surface, thereby allowing the ice to shed due to the aerodynamic forces acting on the ice accretion. Currently, LEWICE is not capable of analyzing this deicing phenomenon because a thermal analysis would be required not only at the air/ice interface but also at the ice/surface interface. A complete description of the current capability to model a thermal deicing system is given in Reference A-6.

A thermal anti-icing system differs from a deicing system in that sufficient heat is applied to prevent any ice from forming. The formulation of the icing energy equation in LEWICE should be applied to thermal anti-icing systems only to determine the minimum heating requirements to keep ice from forming on the surface. The heat flux from the skin is specified as a function of s and is assumed to be from the inner control volume boundary. On the first timestep, this boundary is the uniced surface. If the heat input is not sufficient to keep ice from forming, the heat input on the second timestep would be assumed to come from the iced surface and incorrectly neglects the thermal conductivity of ice and the effect of the varying ice thickness on the surface. An example of the application of the code to a thermal anti-icing system is discussed in Section 7.5.

The energy terms can now be summed to form the complete energy balance for an icing surface used in LEWICE. This equation is as follows:

$$\dot{m}_c \left[c_{p_{w,s}}(T_s - 273.15) + \frac{V_\infty^2}{2} \right] +$$

$$\dot{m}_{r_{in}} \left[c_{p_{w,sur(i-1)}} (T_{sur(i-1)} - 273.15) \right] + q_k \, \Delta s =$$

$$\dot{m}_e \left[c_{p_{w,sur}}(Tsur - 273.15) + L_v \right] +$$

$$\left[(1 - f)(\dot{m}_c + \dot{m}_{r_{in}}) - \dot{m}_e \right] c_{p_{w,sur}}(T_{sur} - 273.15) +$$

$$f(\dot{m}_c - \dot{m}_{r_{in}}) \left[c_{p_{i,sur}}(T_{sur} - 273.15) - L_f \right] +$$

$$h_c \left[T_{sur} - T_e - \frac{r_c V_e^2}{2 c_{p_a}} \right] \Delta s \qquad\qquad (A - 22)$$

The solution of Equation (A-22) is presented in Section 4.3.2.

List of References

1. Ruff, G.A. "Analysis and Verification of the Icing Scaling Equations." AEDC-TR-85-30 Vol. 1 (Revised), 1985.

2. Sogin, H.H. "A Design Manual for Thermal Anti-Icing Systems." Wright Air Development Center (WADC) Technical Report 54-313, 1954.

3. Lozowski, E.P., Stallabrass, J.R., and Hearty, P.F. "The Icing of an Unheated Non-Rotating Cylinder in Liquid Water Droplet-Ice Crystal Clouds." National Research Council of Canada (NRC) Report LTR-LT-96, 1979.

4. Cansdale, J.T. and Gent, R.W. "Ice Accretion on Aerofoils in Two-Dimensional Compressible Flow - A Theoretical Model." Royal Aircraft Establishment Technical Report 82128, 1983.

5. Kreith, F. Principles of Heat Transfer. Harper & Row, Publishers, Inc., New York, 1973.

6. Leffel, K.L. "A Numerical and Experimental Investigation of Electrothermal Aircraft Deicing." NASA CR 175024, 1986.
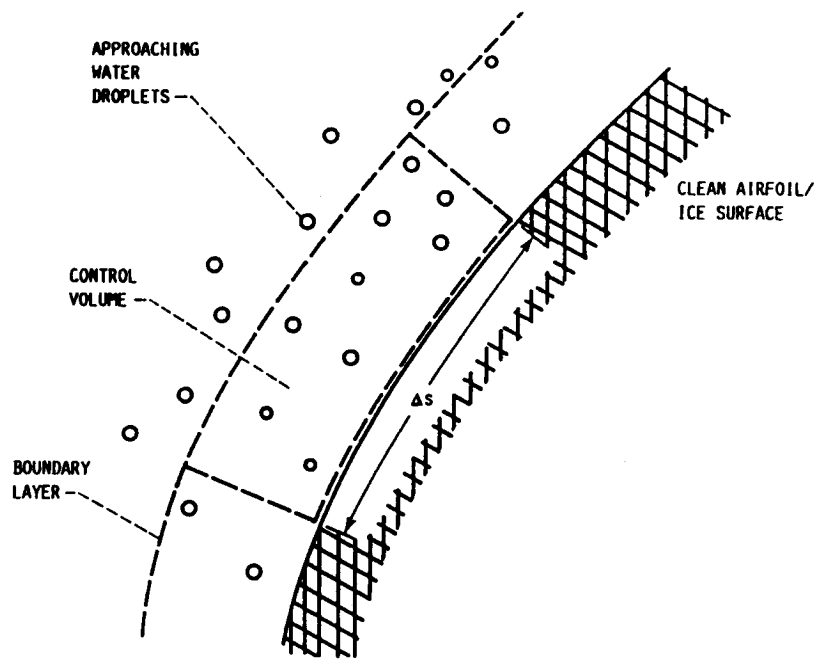
Figure A-1: Identification of a control volume.

1. IMPINGING WATER $\dot{m}_c$

2. EVAPORATION $\dot{m}_e$

3. WATER FLOW OUT OF CV $\dot{m}_{r_{OUT}}$

4. WATER FLOW INTO CV $\dot{m}_{r_{IN}}$

5. ICE ACCUMULATION $\dot{m}_i$
   LEAVING THE CV
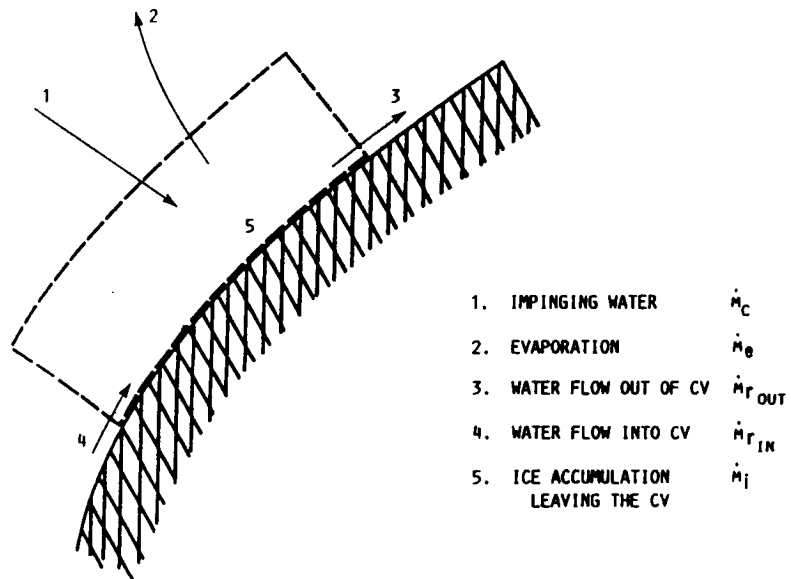
Figure A-2: Mass balance for a control volume.

1.	IMPINGING WATER	$\dot{m}_c i_{w,T}$
2.	EVAPORATION	$\dot{m}_e i_{v,SUR}$
3.	WATER FLOW OUT OF CV	$\dot{m}_{r_{OUT}} i_{w,SUR}$
4.	WATER FLOW INTO CV	$\dot{m}_{r_{IN}} i_{w,SUR}$
5.	ICE ACCUMLATION LEAVING THE CV	$\dot{m}_i i_{i,SUR}$
6.	CONVECTION	$q_c \Delta s$
7.	CONDUCTION	$q_K \Delta s$

$$\dot{m}_c i_{w,T} + \dot{m}_{r_{IN}} i_{w,SUR} + q_K \Delta s = \dot{m}_e i_{v,SUR} + \dot{m}_{r_{OUT}} i_{w,SUR} + \dot{m}_i i_{i,SUR} + q_c \Delta s$$
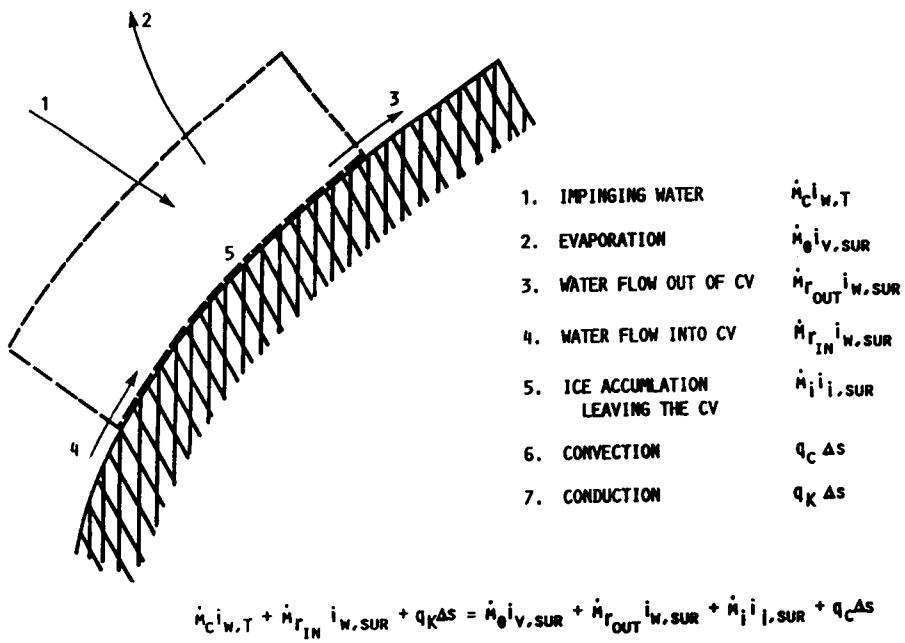
Figure A-3: Energy balance for a control volume.

APPENDIX B

INTEGRAL BOUNDARY LAYER METHOD ON AN ICED SURFACE

As described in the text, the evaluation of the boundary layer characteristics using a complete Navier-Stokes solver would be too time-consuming to be practical in an interactive program such as LEWICE. An integral boundary layer solution was therefore developed to account for surface roughness and variable velocity in the calculation of the convective heat transfer coefficient. The original algorithm was developed by UDRI, but was modified in the current version of LEWICE.

B.1 Characterization of the Ice Surface Roughness

The integral boundary layer method to be applied in LEWICE is required not only to determine the convective heat transfer coefficient on the iced surface in the laminar and turbulent regions, but also to determine the location of the transition from laminar to turbulent flow (transition point). The transition to turbulent flow is caused primarily by the surface roughness of the iced surface which acts to trip the boundary layer from laminar to turbulent flow. Also, once turbulent, the surface roughness elements enhance the convective heat transfer coefficient by 1) increasing the skin friction coefficient and 2) increasing the effective surface area from which heat transfer takes place.

A representative surface of an actual ice accretion is shown in profile in Figure B-1. The size and shape of the surface roughness elements found on typical ice accretions are functions of the atmospheric and meteorological conditions at which the ice is formed. Unfortunately, there is insufficient data to characterize the size and shape of the surface roughness as a function of those conditions. Also, the complex roughness patterns found on typical glaze ice accretions are beyond the analysis capability of an integral boundary layer method. Therefore, an alternate method to characterize the surface roughness is required.

Analysis of rough surfaces has been performed by numerous investigators, one of the earliest and most well-known being Nikuradse (Reference B-1). These experiments dealt primarily with turbulent flow in pipes that

were artificially roughened with uniform grains of sand. Schlichting (Reference B-2) introduced the concept of equivalent sand-grain roughness as a means of characterizing other types of roughness elements by referring to the equivalent net effect produced by Nikuradse's experiments. In this application, the irregular roughness elements of an iced surface are represented by a value of equivalent sand-grain roughness height, k_s, as shown in Figure B-2. This value is specified by the user and is constant during the calculation of a given icing condition. The value of k_s should be changed as a function of the atmospheric and meteorological parameters of the icing condition using the guidelines discussed in the text.

B.2 Calculation of the Boundary Layer Characteristics

Determination of the Transition Location

The evaluation of the boundary layer is begun at the stagnation point (s = 0.0). The calculations are initiated by determining the location of the transition for laminar to turbulent flow, i.e., the transition point. The criteria for transition, developed by Von Doenhoff (Reference B-3), assumes that the flow will become turbulent when the local roughness Reynolds number is greater than 600. The empirical criteria, based on data obtained using sand-grain type roughness elements, are therefore given by the following equation

$$R_{e_k} = \frac{V_k \, k_s}{\nu} \geq 600 \qquad (B-1)$$

where k_s is the equivalent sand-grain roughness height representing the actual ice surface roughness. The velocity at $y = k_s$, designated V_k, (Figure B-2) must be determined to evaluate the local roughness Reynolds number. The following is the method used to determine V_k, found in Equation (B-1).

Assume that the laminar velocity profile can be represented by a 4th order polynomial of the form

$$\frac{V(y)}{V_e} = a_o + a_1\left(\frac{y}{\delta}\right) + a_2\left(\frac{y}{\delta}\right)^2 + a_3\left(\frac{y}{\delta}\right)^3 + a_4\left(\frac{y}{\delta}\right)^4 \qquad (B-2)$$

where δ is the boundary layer thickness, and V_e and y are defined in Figure B-2. This assumption is known as the Pohlhausen approximation (Reference B-4, pp. 310-311). By applying the following boundary conditions at $y = 0$:

$$\nu \frac{\partial^2 V}{\partial y^2} = \frac{1}{\rho} \frac{\partial \rho}{\partial s} = -V_e \frac{dV_e}{d_e} \qquad (B-3a)$$

$$\lim_{y \to \infty} \frac{\partial^n V}{\partial y^n} = 0 \qquad n = 1, 2, 3, \dots \qquad (B-3b)$$

it can be shown that the expression for V/V_e resulting from Equation (B-2) is

$$\frac{V(y)}{V_e} = \left[2(y/\delta) - 2(y/\delta)^3 + 2(y/\delta)^4\right] + 1/6 \, \Lambda \, (y/\delta) \, (1 - y/\delta)^3 \qquad (B-4)$$

where

$$\Lambda = \delta^2/\nu \, \frac{dV_e}{ds} \qquad (B-5)$$

If we let $y = k_s$ in Equation (B-4), the velocity at $y = k_s$ can be written as follows:

$$\frac{V_k}{V_e} = \left[2(k_s/\delta) - 2(k_s/\delta)^3 + (k_s/\delta)^4\right] + 1/6 \, \Lambda \, (k_s/\delta)(1 - k_s/\delta)^3 \qquad (B-6)$$

To apply this equation, the boundary layer thickness, δ, must be evaluated.

The laminar momentum thickness, θ_l, is defined in Reference B-4, p. 244, as

$$\theta_l = \int_0^\delta \frac{V}{V_e} \left(1 - \frac{V}{V_e}\right) dy \qquad (B-7)$$

173

Substituting Equation (B-4) into Equation (B-7) and integrating from $y = 0$ to $y = \delta$, it can be shown that δ is related to the laminar momentum thickness by the following approximation:

$$\delta \approx 8.5 \, \theta_l \qquad\qquad (B-8)$$

From the integral momentum equation, the laminar momentum thickness can be evaluated using Thwaites formula (Reference B-4, p. 315) which is given by the following equation:

$$\theta_l^2 = \frac{.45\nu}{V_e^6} \int_o^s V_e^5 d_s \qquad\qquad (B-9)$$

If it is assumed that the velocity at the edge of the boundary layer, V_e, is the surface velocity calculated by the potential flow equations, Equation (B-9) can be numerically evaluated to determine θ_l for each segment on the body. Equations (B-6) and (B-8) can then be applied to determine V_k as a function of s, and, therefore, Equation (B-1) can be evaluated along the surface to determine whether the flow has transitioned from laminar to turbulent flow.

Laminar Convective Heat Transfer Coefficient

If the boundary layer is found to be laminar at a surface distance, s, the convective heat transfer coefficient for flow over a constant temperature body of arbitrary shape is calculated using an equation developed by Smith and Spaulding and described in Reference B-4, pp. 327-329. This equation is given as

$$h_l(s) = .296 \, \frac{\lambda}{\sqrt{\nu}} \left[V_e^{-2.88} \int_0^s V_e^{1.88} ds \right]^{-1/2} \qquad\qquad (B-10)$$

where λ is the thermal conductivity of air.

Turbulent Convective Heat Transfer Coefficient

174

If, upon evaluating Equation (B-1), it is found that the boundary layer is turbulent, Equations (B-7)-(B-10) are not applicable, and an alternate method to determine the convective heat transfer coefficient must be developed. Using a technique outlined in Reference B-5, an overall Stanton number can be developed using the thermal and momentum laws of the wall for fully rough flow. This equation is given in Reference B-5, p. 132 as

$$St = \frac{c_f/2}{Pr_t + \sqrt{c_f/2}\,(1/St_k)} \qquad (B-11)$$

The terms of this equation that must be evaluated are the skin friction coefficient, c_f, and the roughness Stanton number, St_k. The experimental data for air (Reference B-6) suggest that the turbulent Prandtl number, Pr_t, is approximately constant and equal to 0.9.

Assuming for now that the values of c_f and St_k are known, the turbulent heat transfer coefficient is calculated using Equation (B-11) and the definition of the Stanton number. Therefore,

$$h_t(s) = St\rho V_e c_p = \left[\frac{c_f/2}{Pr_t + \sqrt{c_f/2}(1/St_k)}\right]\rho V_e c_p \qquad (B-12)$$

The expressions for the skin friction coefficient and the roughness Stanton number are now developed.

Skin Friction Coefficient

If the boundary layer has been found to be turbulent, i.e., the roughness Reynolds number is greater than 600.0, the surface can be considered to be fully rough (Reference B-5, p. 186). A basic characteristic of the fully rough surface is that the skin friction coefficient, c_f, is independent of the Reynolds number. In this region, the pressure drag on individual roughness elements dominates and viscosity is no longer a significant variable. With this assumption, an expression for the skin friction coefficient can be developed from the momentum law of the wall for fully rough flow (Reference B-5, pp. 186-188) as follows

$$\frac{c_f}{2} = \left[\frac{.41}{ln(\frac{864.0\theta_t}{k_s} + 2.568)}\right]^2 \qquad (B-13)$$

where θ_t is the turbulent momentum thickness and k_s is the equivalent sand-grain roughness height. (This equation was derived in a manner similar to Equation 10-45 in Reference B-5 except that Equation 10-43 was not simplified.)

The turbulent momentum thickness is evaluated using the momentum integral equation in a manner similar to that for the laminar momentum thickness. The equation for θ_t is given in Reference B-5, p. 175 as

$$\theta_t(s) = \left[\frac{.0156}{V_e^{4.11}} \int_o^s V_e^{3.86} \, ds\right]^{.8} \qquad (B-14)$$

Since the turbulent boundary layer is proceeded by a laminar boundary layer, the numerical integration of Equation (B-14) is begun at $s = s_{tr}$ instead of $s = 0.0$. The laminar momentum thickness already existing at $s = s_{tr}$ must then be added. Equation (B-14) can therefore be written as

$$\theta_t(s) = \left[\frac{.0156}{V_e^{4.11}} \int_{S_{tr}}^s V_e^{3.86} ds\right]^{.8} + \theta_l(s_{tr}) \qquad (B-15)$$

where θ_l is evaluated using Equation (B-9) and V_e is the surface velocity calculated by the potential flow code.

Roughness Stanton Number

The roughness Stanton number is developed from the thermal law of the wall for fully rough flow, and is given in Reference B-5, p. 231 by an equation of the form

$$St_k = C\left(\frac{V_r k_s}{\nu}\right)^{-.2} Pr^{-.44} \qquad (B-16)$$

176

where V_r is the shear velocity. In Equation (B-16), C is a constant that must be determined from experimental data and is a function of the type of roughness. Data for a rough surface composed of closely-packed spheres yields a value of C = 1.0 (Reference B-6). Setting the Prandtl number, Pr, equal to 0.72 and substituting the values for C and Pr into Equation (B-16), the expression for St_k becomes

$$St_k = 1.16\left(\frac{V_r k_s}{\nu}\right)^{-.2} \qquad (B-17)$$

The shear velocity, u_r, is evaluated using the equation from Reference B-5, p. 187.

$$\frac{V_r}{V_e} = \sqrt{c_f/2} \qquad (B-18)$$

In this equation, c_f is determined from Equation (B-13).

B.3 Method of Solution

To correctly apply the equations previously discussed, the integration procedure should be identified. As discussed in the text, the geometry is represented by a set of Cartesian coordinates (nodes) connected by straight line segments, as shown in Figure B-3. The stagnation point is designated s = 0.0, and will always fall on a nodel 1 point. The s values used in the integration correspond to the midpoint of each of the body segments. The calculation of the boundary layer characteristics is begun by evaluating Equations (B-6), (B-8), and (B-9) for s = 0.0 to s = s_1. The transition criteria, Equation (B-1), is then applied, and, if the flow is found to be turbulent at this point, it is assumed to be turbulent at each segment downstream. Equations (B-13), (B-15), (B-17), (B-18), (B-11), and (B-12) are applied to calculate h_c if the boundary layer is turbulent. If the flow is laminar, Equation B-10 is used to calculate h_c and the turbulence criteria is checked at the next segment. This procedure is then repeated for the lower surface.

B.4 Comparison with Experimental Data

The results of the integral boundary layer method described in the previous sections have been compared to experimental convective heat transfer data collected by Achenbach (Reference B-7). The current method was also compared to an integral boundary layer method developed by Makkonen (Reference B-8).

An excellent discussion of the analytical method developed by Makkonen and the comparisons to experimental data can be found in Reference B-8. The work by Makkonen also includes a discussion about the applicability of an integral boundary layer method to the calculation of convective heat transfer characteristics over an ice accretion shape. Therefore, a description of the experimental data and detailed analysis of the results will not be presented in this appendix. Instead, the results of the integral boundary layer method described in this appendix will only be compared to the results in Reference B-8 and the general trends identified.

The experimental measurements were made on a 15-cm diameter cylinder roughened with grains of sand at various Reynolds numbers. The roughness element height, k, is 0.9 mm and the equivalent sand grain roughness height, k_s, is 1.35 mm. The method developed by Makkonen uses both the maximum probable roughness height and the equivalent sand grain roughness height. The method described in this appendix uses only the equivalent sand grain roughness. Figure B-4 shows a comparison of the analytical results of LEWICE (with $k_s = 1.35$ mm) and Makkonen to the experimental results. At a Reynolds number of 4.8×10^4, the method of LEWICE shows a transition at an angle of approximately 50°, while no transition is predicted by Makkonen's results or in the experimental data. Similar transition locations and location of the maximum heat transfer coefficient are predicted by both analytical methods for Reynold's numbers of 2.8×10^5 and 8.8×10^5. However, the magnitude of the maximum heat transfer coefficient is over-predicted by the method used in LEWICE.

Since the current method uses only a single roughness parameter, there is some question whether the maximum probable roughness or the equivalent sand grain roughness height should be used in comparisons with experimental data. A comparison of the analytical and experimental results with $k_s = 0.9$ mm in LEWICE is shown in Figure B-5. These results compare

178

more favorably with the method of Makkonen and with experimental data than those in Figure B-4, but still over-predict the maximum value of the convective heat transfer coefficient.

Measurements of convective heat transfer have also been made on simulated wooden ice accretion shapes roughened with grains of sand (Reference B-9). Figures B-6a, b, c, and d show the comparisons of the values calculated by LEWICE with experimental data for 2, 5, and 15 min glaze ice accretions. In these cases, the maximum probable roughness height of 0.00033 m was used in the calculations. These results show that the predicted values of h_c generally compare well with experiment in the leading edge region where much of the accretion process will take place.

Appendix B

List of References

1. Nikuradse, J., Forsh. Arb. Ing.-Wes. No. 361, 1933.

2. Schlichting, H., Ing. Arch.. Vol. 7, 1936, pp. 1-34.

3. Von Doenhoff, A.E. and Horton, E.A. "Low-Speed Experimental Investigation of the Effect of Sandpaper Type of Roughness on Boundary-Layer Transition." NACA TN 3858, 1956.

4. White, F.M., <u>Viscous Fluid Flow</u>. McGraw-Hill, Inc, 1974.

5. Kays, W.M. and Crawford, M.E., <u>Convective Heat and Mass Transfer</u>. 2nd Edition, MacGraw-Hill Book Company, New York, 1980.

6. Pimenta, M.M., Moffat, R.J., and Kays, W.M. Report No. HMT-21, Department of Mechanical Engineering, Stanford University, May 1975.

7. Achenbach, E. "The Effect of Surface Roughness on the Heat Transfer from a Circular Cylinder to the Cross Flow of Air." "International Journal of Heat and Mass Transfer.", Vol. 20, 1977, pp. 359-369.

8. Makkonen, L. "Heat Transfer and Icing of a Rough Cylinder." "Cold Regions Science and Technology." Vol. 10, 1985, pp. 105-116.

9. Van Fossen, G.J., Simnoneau, R.J., Olsen, W.A., and Shaw, R.J. "Heat Transfer Distributions Around Nominal Ice Accretion Shapes Formed on a Cylinder in the NASA Lewis Icing Research Tunnel." NASA TM 83557, January 1984.
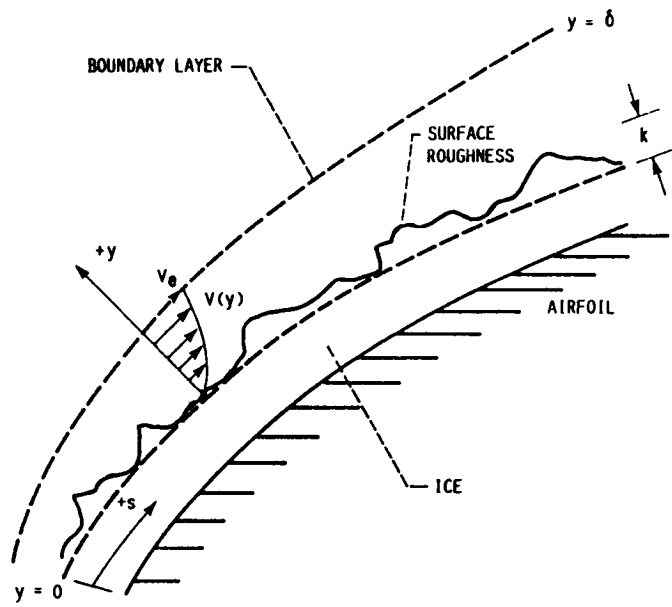
Figure B-1: Identification of the boundary layer terms used
in the integral boundary layer method.
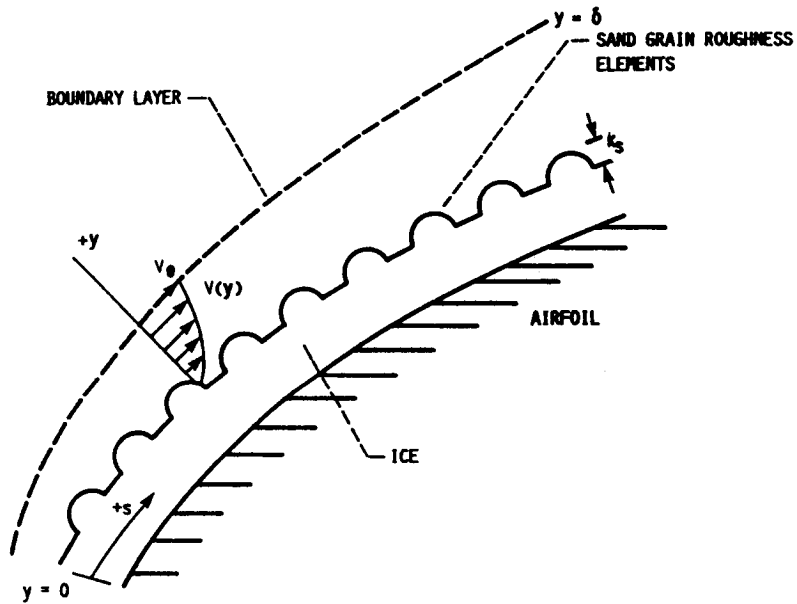
Figure B-2: Identification of the computational surface being
evaluated by the integral boundary layer method.
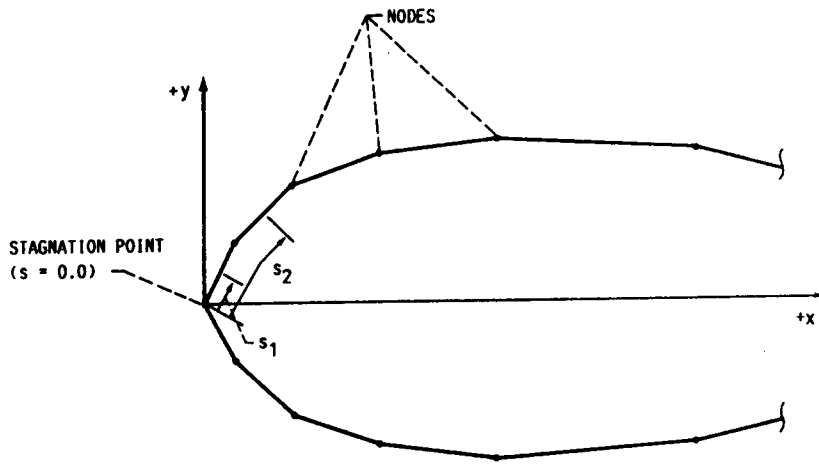
Figure B-3: Analytical representation of a typical geometry.
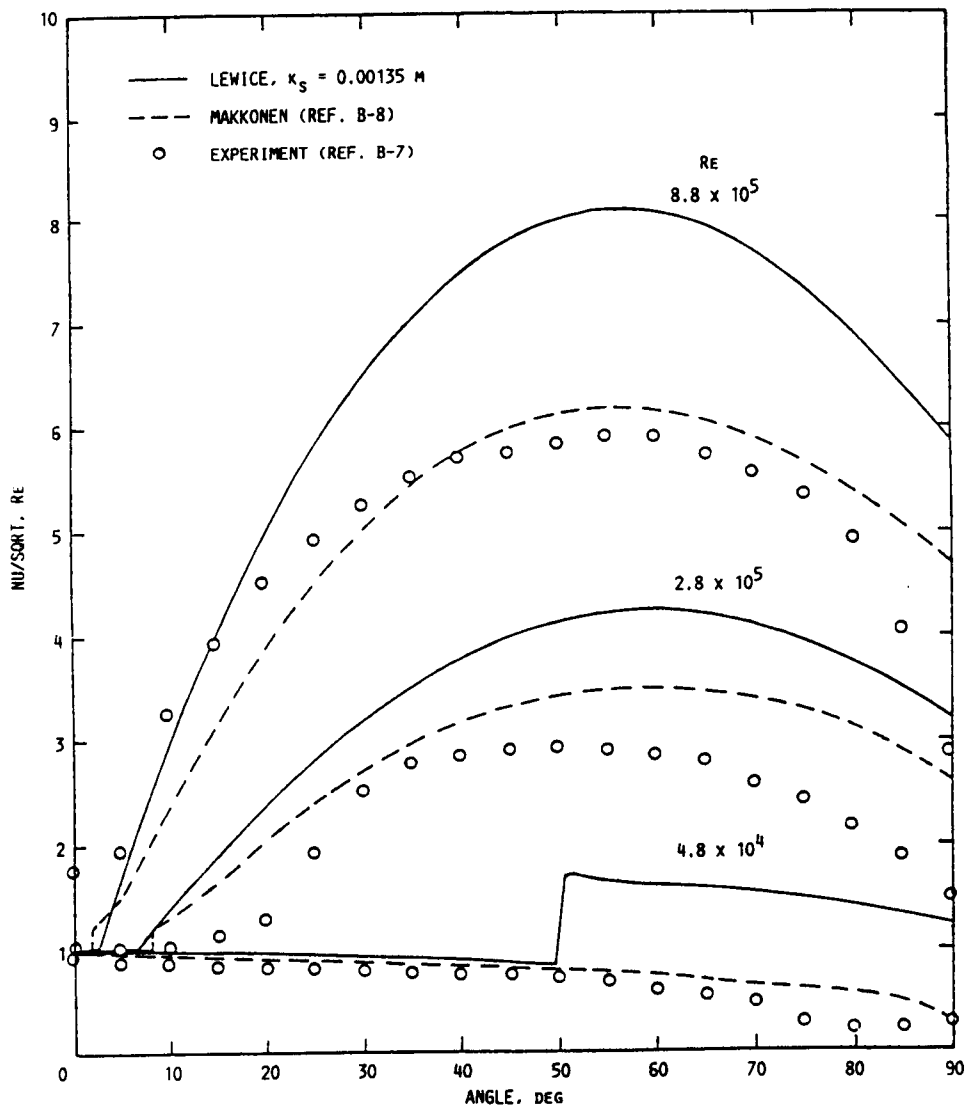
Figure B-4: Comparison of caluclated and experimental corrective heat transfer characteristics, LEWICE $k_s = 0.00135m$.

182
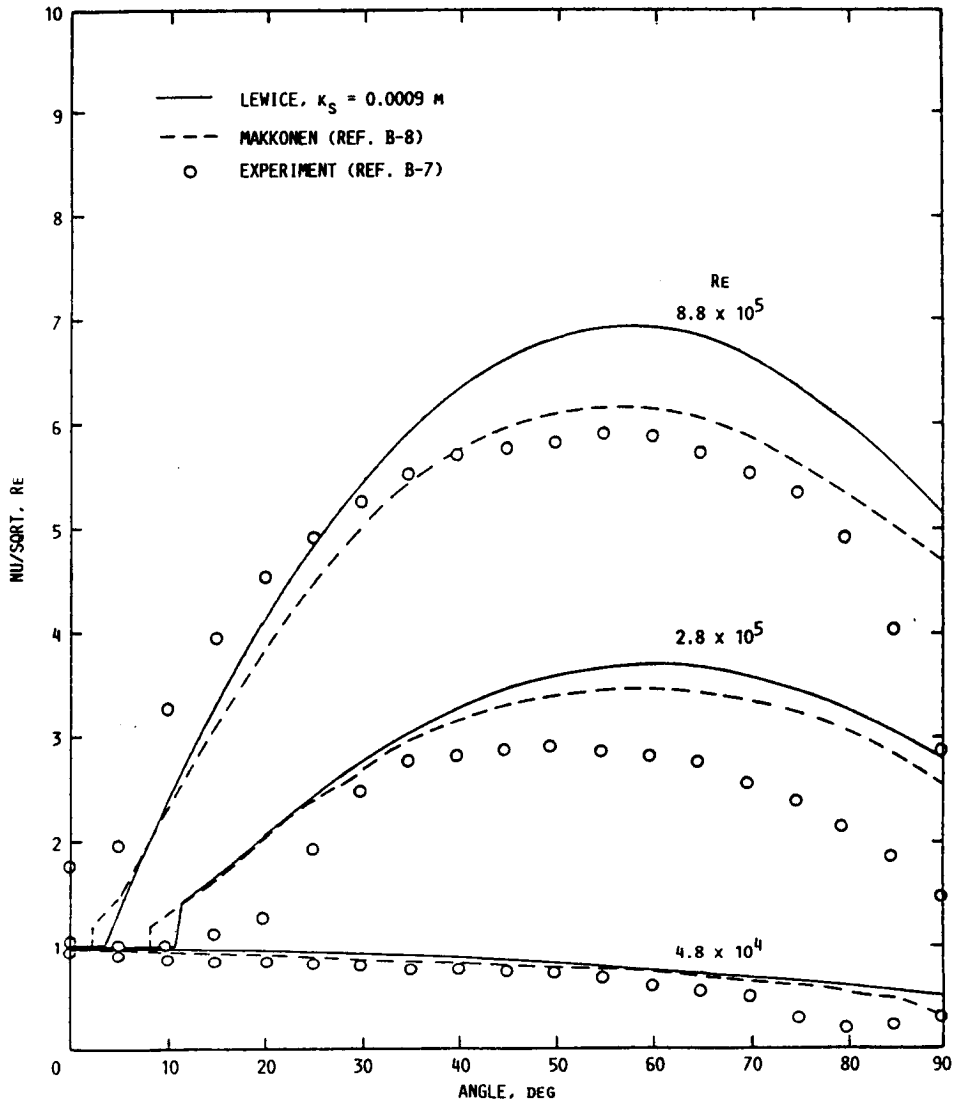
Figure B-5: Comparison of calculated and experimental corrective heat transfer characteristics, LEWICE $k_s = 0.0009m$.
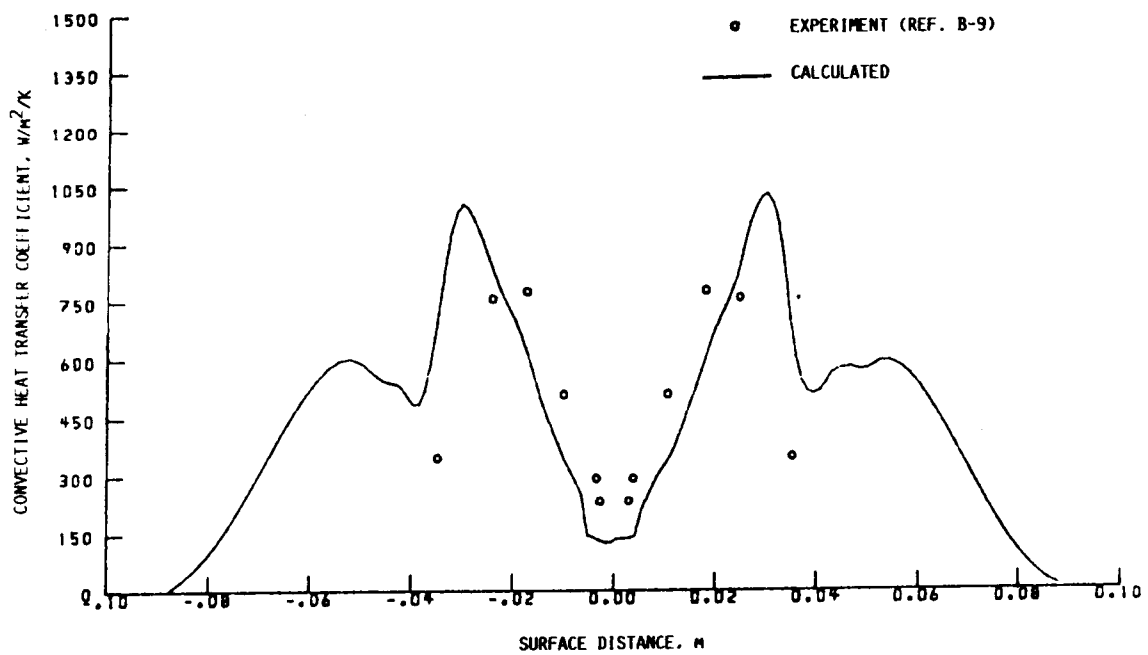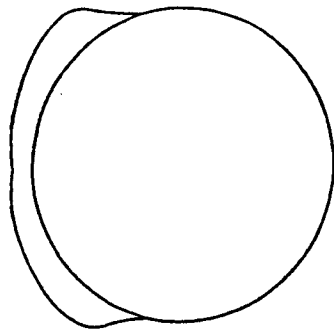
a. Two minute glaze ice shape.
Figure B-6: Comparison of calculated and experimental heat
transfer coefficients on simulated glaze and rime ice shapes.
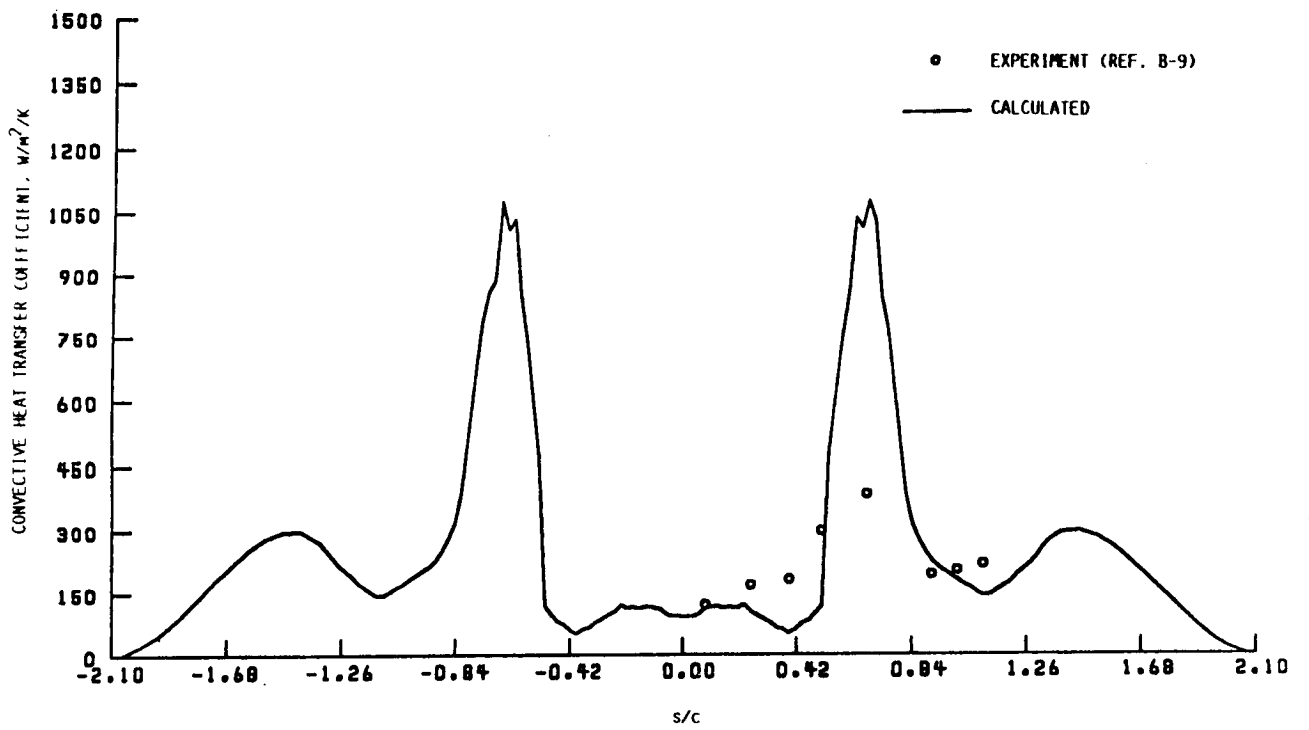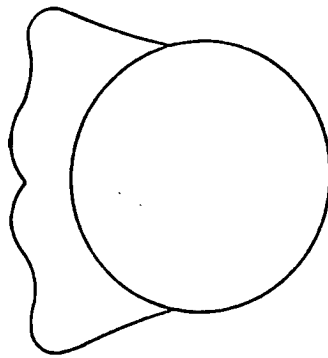
b. Five min glaze ice shape.
Figure B-6: continued
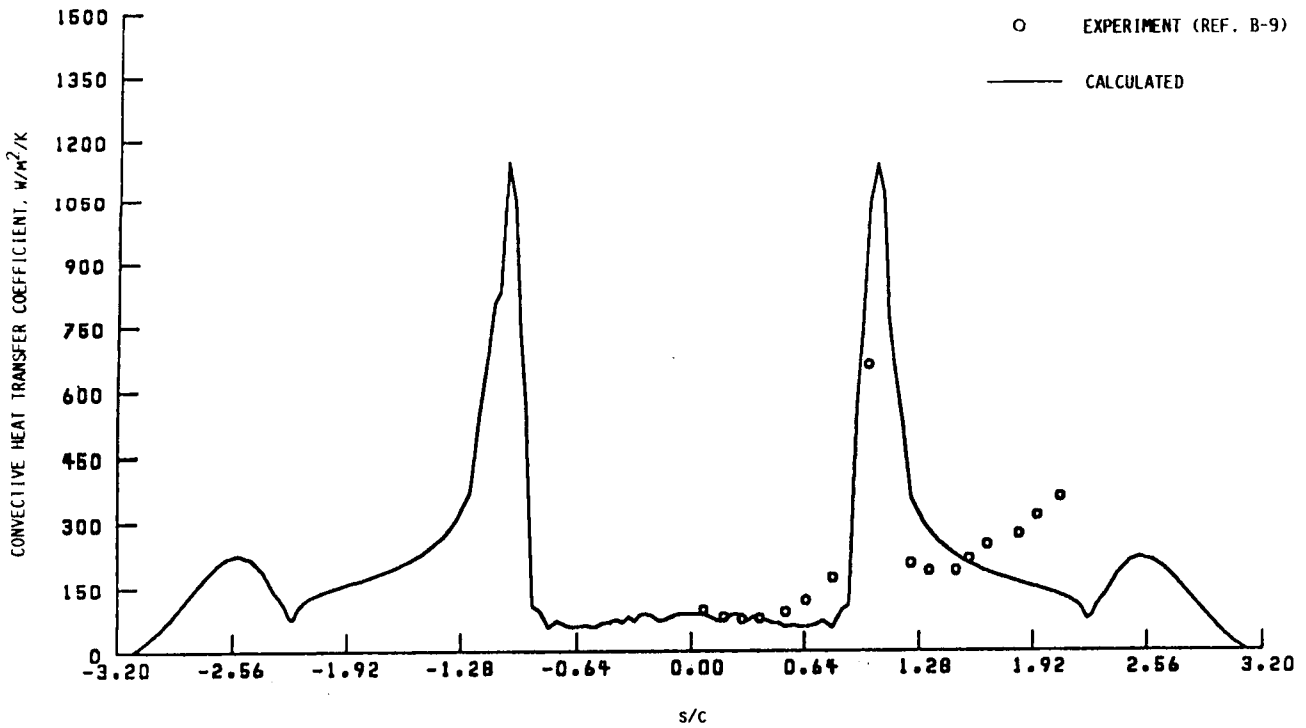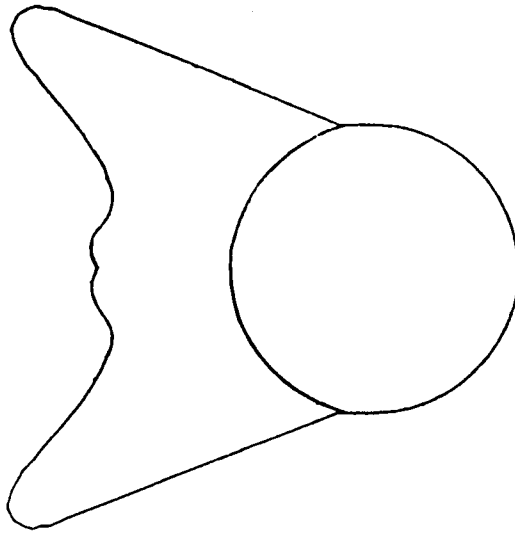
c. Fifteen min glaze ice shape.
Figure B-6: continued

186
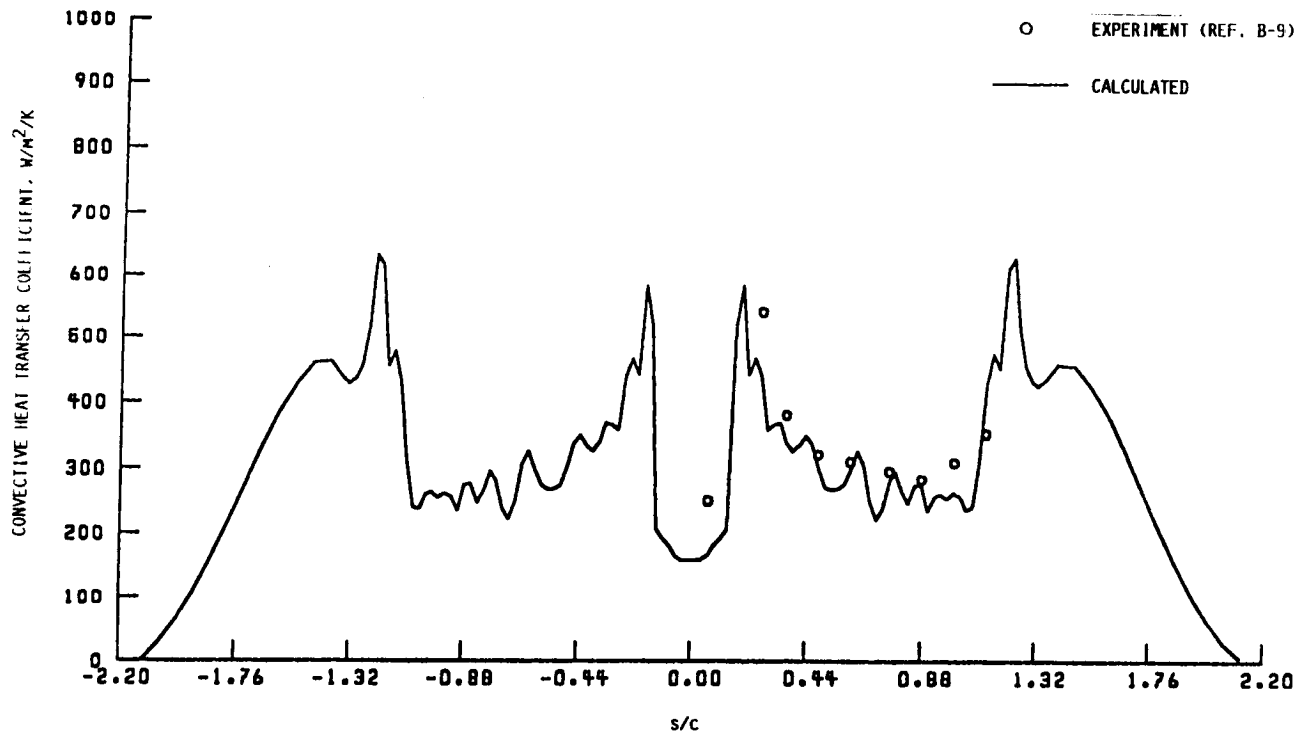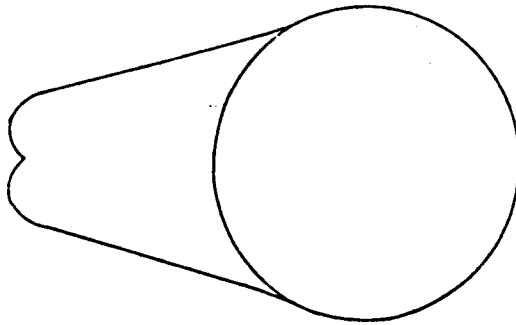
d. Fifteen min rime ice shape.
Figure B-6: Concluded

187

C3

APPENDIX C
FLOW FIELD CORRECTIONS

As discussed in the text, there are two types of flow field corrections that are applied in LEWICE to allow more accurate particle trajectory calculations. The first correction is made to avoid errors that occur in the flow field close to the surface because the geometry is represented by discrete points connected by line segments instead of a smooth curve. These are called discretization errors. The second correction is made to avoid errors caused by convoluted ice shapes. Both of these corrections are performed by producing an imaginary or pseudo-surface which is used in the calculations instead of the actual ice surface. The corrections are described in the following sections.

C.1 Correction for Discretization Errors Near the Body

The potential flow computer program used in this study has a relatively large discretization error very close to the body. As shown in Figure C-1, taken from Reference C-1, the longitudinal and vertical velocities around the leading edge of the Joukowski airfoil are very irregular close to the airfoil but become smoother as $\Delta\xi$ is increased. (In Figure C-1, $\Delta\xi$ is equivalent to the DSHIFT parameter in LEWICE). The velocity is computed for different constant values of separation distance from the body, as illustrated in the insert. Note the large peaks or oscillations in the flow field velocity near the surface.

Figure C-2 illustrates the trajectories of three different particles released at very small separation distances, y_0, upstream of the body. Note that the upper particle turns near the nose and flows backward, reverses direction again, and flows around the body. The initial intermediate positioned particle trajectory crosses the lower particle trajectory near the body. It approaches very close to the surface somewhat downstream of the nose, and then departs off into the free-stream without impinging on the body. Finally, the lower particle trajectory impinges on the body. These erratic trajectories are caused by the strong perturbations in the flow field near the body.

To overcome the effect of the discretization error near the body, an artificial impingement surface is generated by the computer program. This

188

surface is achieved by displacing the surface of the body a small increment DSHIFT in the upstream x direction. To generate the pseudo-impingement surface, the x-coordinates are increased by the quantity DSHIFT times the cosine of the segment angle while the y-coordinates remain constant. The resulting pseudo-impingement surface is displaced outward into the freestream as shown in Figure C-3. The value of DSHIFT is input by the user in namelist TRAJ1. Commonly used values between .2 to .6 percent of the chord length encompass the major area of uncertainty in the flow field.

The pseudo-impingement surface is used only for particle impingement calculations and does not influence the potential flow calculations. The pseudo-impingement surface is discarded once the particle trajectory calculations are completed and is not present when a new ice surface is formed.

C.2 Correction for Multiple Calculated Stagnation Points

Glaze ice accretions are often characterized by the formation of two horns, as shown in Figure C-4a. The calculation of the flow field around these typical glaze ice shapes produces undesirable results such as multiple calculated stagnation points (surface velocity = 0.0). An example of such a calculation is shown in Figure C-4b. When more than one stagnation point is calculated, errors occur in the particle trajectory and thermodynamic portions of the code, causing an abnormal termination. Since the Douglas potential flow solution is the most feasible method for use in this code, a method to obtain a sufficiently accurate flow field solution is required when this situation occurs.

Before the development of computer codes capable of applying the Navier-Stokes equations to the calculation of flow characteristics in recirculation zones, the potential flow codes available had a problem similar to that in this application. One solution was to replace the boundary of the separation/reattachment zone with a pseudo-surface, as shown in Figure C-5. A similar approach is used in this application to smooth the groove found at the stagnation point of many ice accretions.

Determination of the Locations of Stagnation Points

The location of the stagnation point(s) is determined in subroutine STAG by checking the non-dimensional edge velocities calculated by S24Y

189

(VT) for a change in sign. These velocities will be negative on the lower surface and positive on the upper surface. The velocity on each segment is checked, and the number of each segment at which the sign of VT changes is stored as a stagnation point. If more than one sign reversal is found, it is assumed that the flow field is inaccurate, and the user will be given the option of selecting one of the calculated stagnation points to use in the remaining calculations, or to form a pseudo-surface over the calculated stagnation points.

The algorithm to form the pseudo-surface is located in subroutine PSURF. The computer prompts and responses used to form the surface can be found in Example 2 of Chapter 7. The purpose of the remainder of this appendix is to demonstrate the accuracy of this method by comparing experimental data to surface velocity profiles calculated using a pseudo-surface. The geometries used for these comparisons are simulated 2- and 5-min glaze ice accretions and a 15-min rime ice accretion. These ice shapes are made of wood and simulate actual ice accretions formed on a cylinder. The surface velocity measurements were obtained from surface pressure data for each of the geometries.

Recall that Figure C-4a shows a 5-min glaze ice accretion for which two stagnation points were calculated. The corresponding calculated surface velocity profile is shown in Figure C-4b. A pseudo-surface, shown in Figure C-6a, was placed over the glaze accretion, and the resulting calculated surface velocity compared to experimental data. Note that the calculated velocity profile now has only one stagnation point, and that the calculated and experimental velocities compare very well near the stagnation point. Additional applications of the pseudo-surface technique are shown in Figures C-6b and c. In all cases, the presence of the pseudo-surface produced smoother velocity profiles which more closely matched experimental results.

This method, while capable of improving the accuracy of the flow field solution, is an approximation to the true solution and must be treated as such. For example, Figures C-7a and b show a 15-min glaze ice accretion and the corresponding calculated surface velocity. In this case, ten stagnation points were calculated. A pseudo-surface, shown in Figure C-8a, was placed over the glaze ice accretion, and the calculations were repeated. As shown in Figure C-8b, the calculated velocity profile is much smoother than that for the actual ice shape, and the velocity in the groove is slightly

over-predicted. While this solution would allow the calculation of the ice accretion to continue, it illustrates that the pseudo-surface technique can produce a very rough approximation to the actual flow field.

Appendix C
List of References

1. Frost, W., Chong, H., Shieh, C., and Kimble, K. "Two-Dimensional Particle Trajectory Computer Program." Interim Report for Contract NAS3-2244B, 1982.
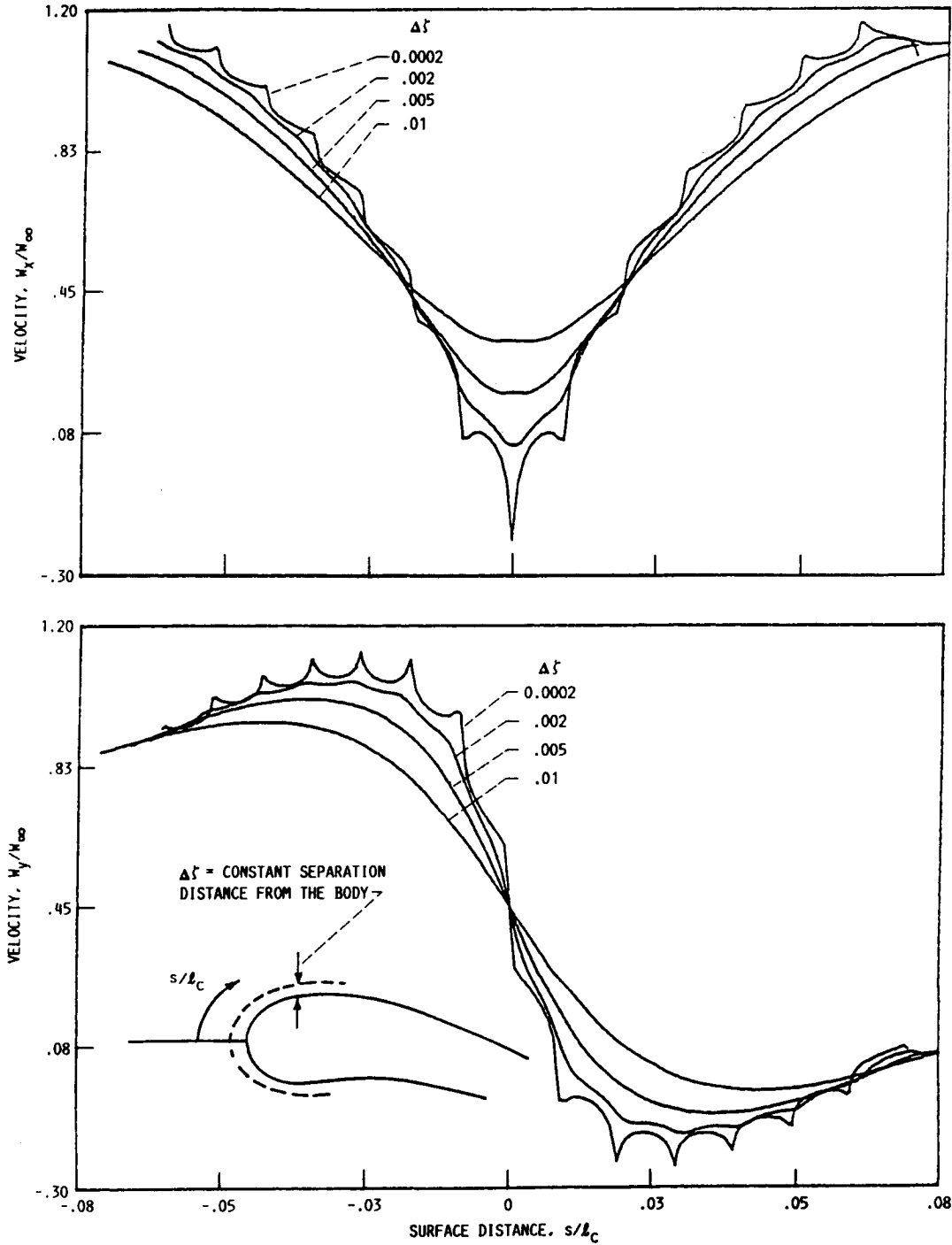
C-1: Discretization error in the flow field near the nose of the Joukowski airfoil.
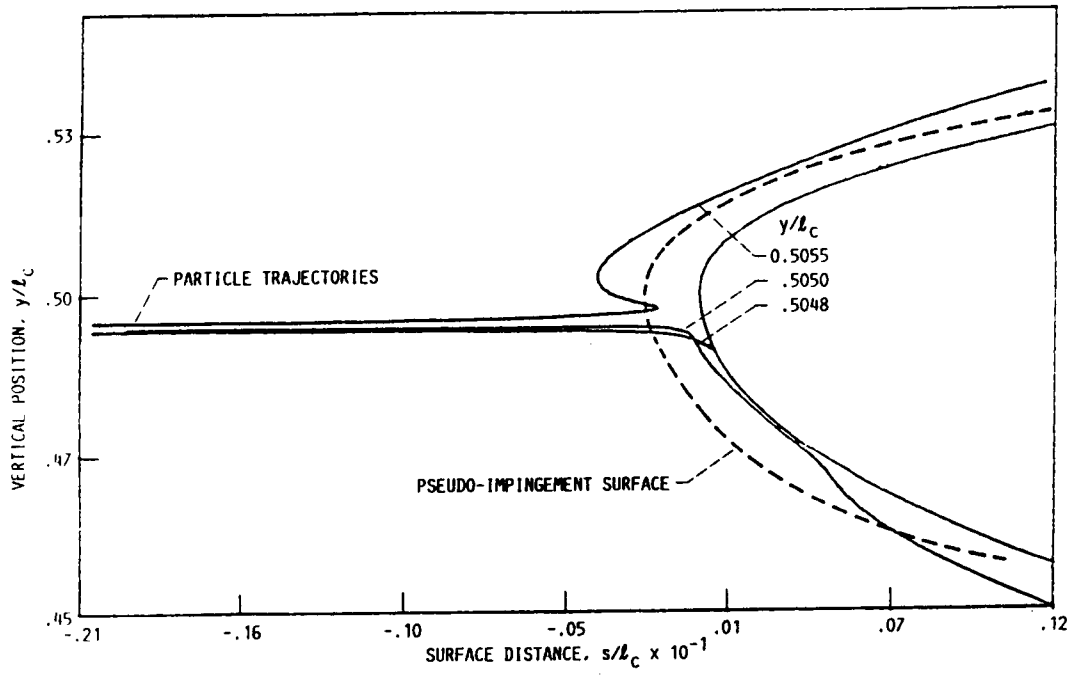
C-2: Discretization error in the flow field near the nose of the upper body of a two-dimensional inlet.
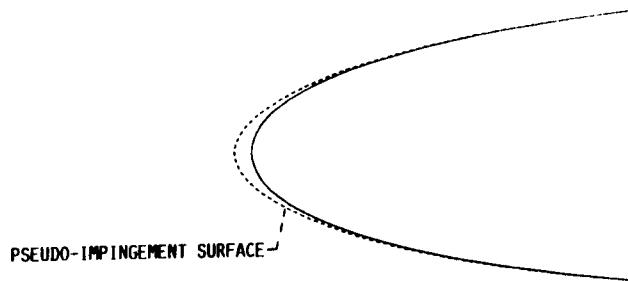
C-3: Illustration of the pseudo-impingement surface.
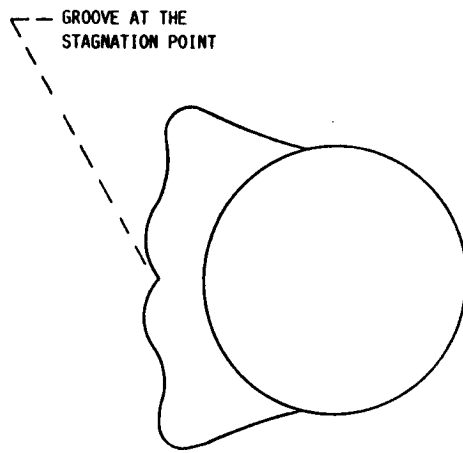
(a) FIVE MINUTE GLAZE ICE ACCRETION WITH GLAZE HORNS.
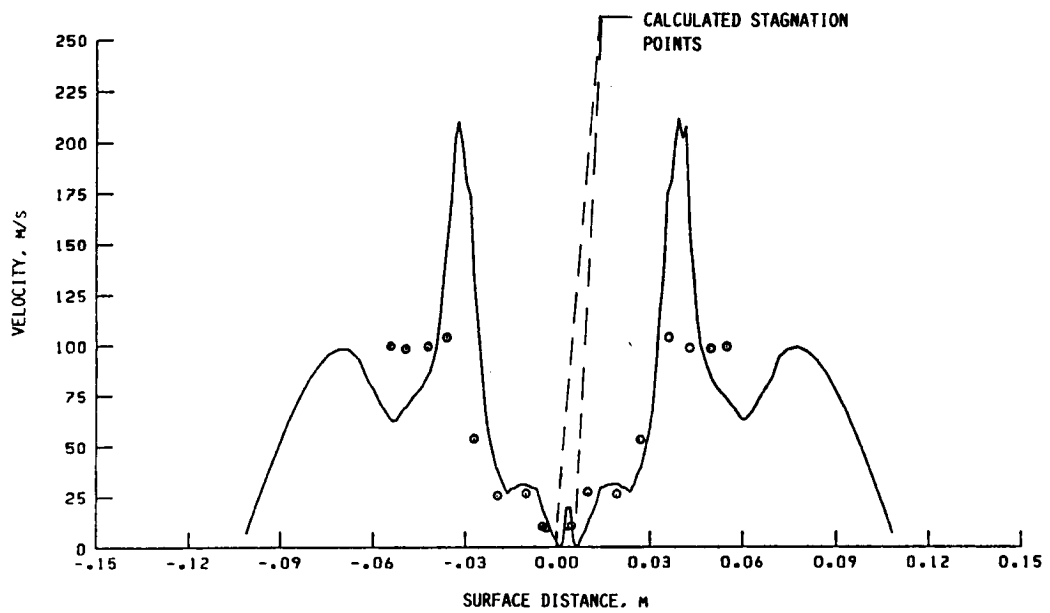
(b) MULTIPLE CALCULATED STAGNATION POINTS FOR A 5 MINUTE GLAZE ICE SHAPE.

C-4: Simulated five min glaze ice accretion on a cylinder and the corresponding calculated surface velocity profile.
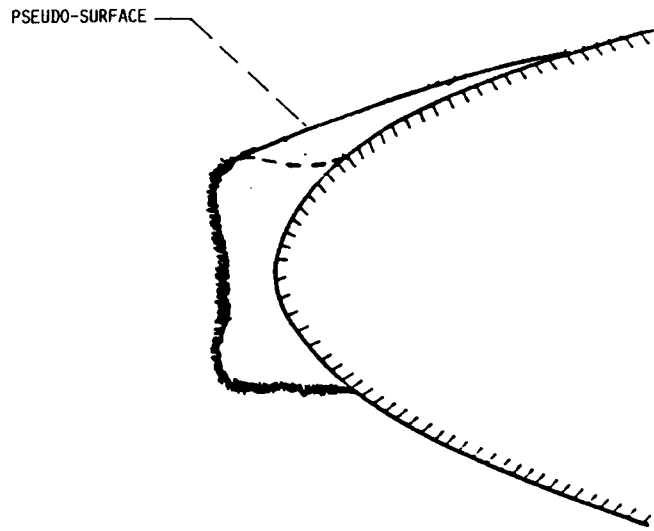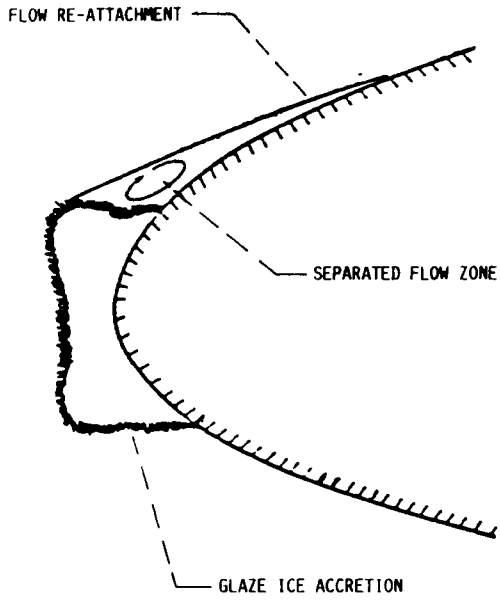
C-5: Example of the application of the pseudo-surface technique on a recirculation zone.
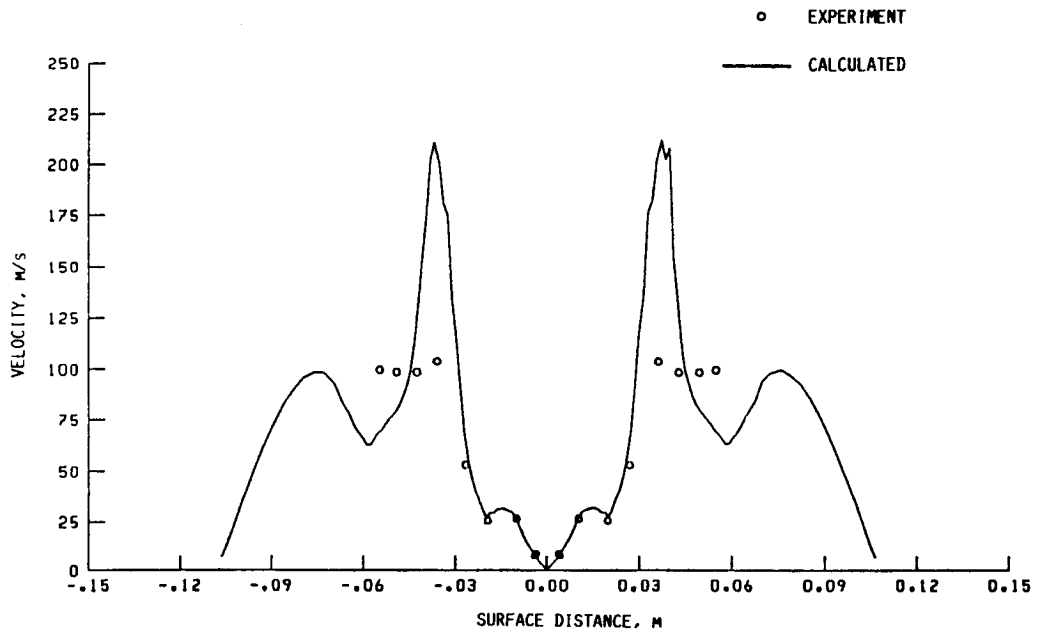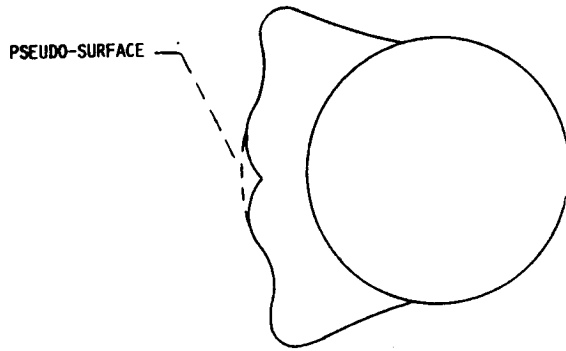
a. Simulated five min glaze ice shape

C-6: Comparison of experimental surface velocities on simulated ice shapes
to those callculated for the ice shape with pseudo-surface.
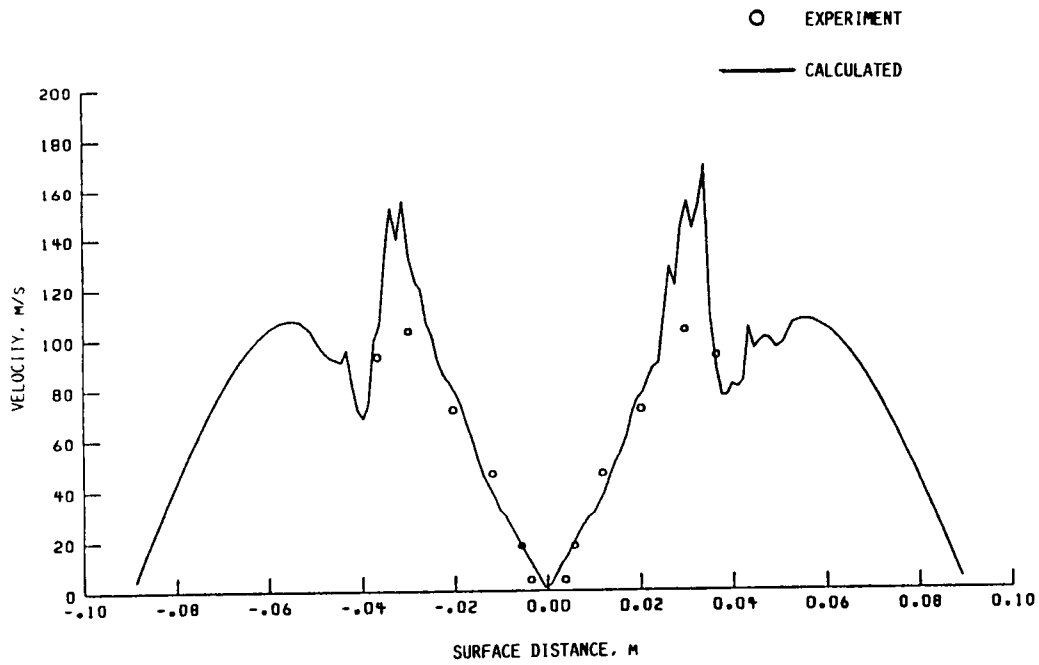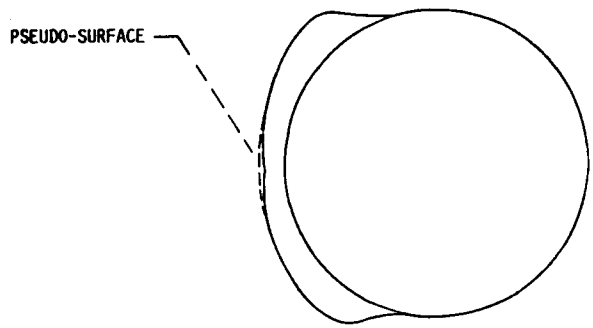
b. Simulated two min glaze ice shape
C-6: continued

PSEUDO-SURFACE — —

EXPERIMENT
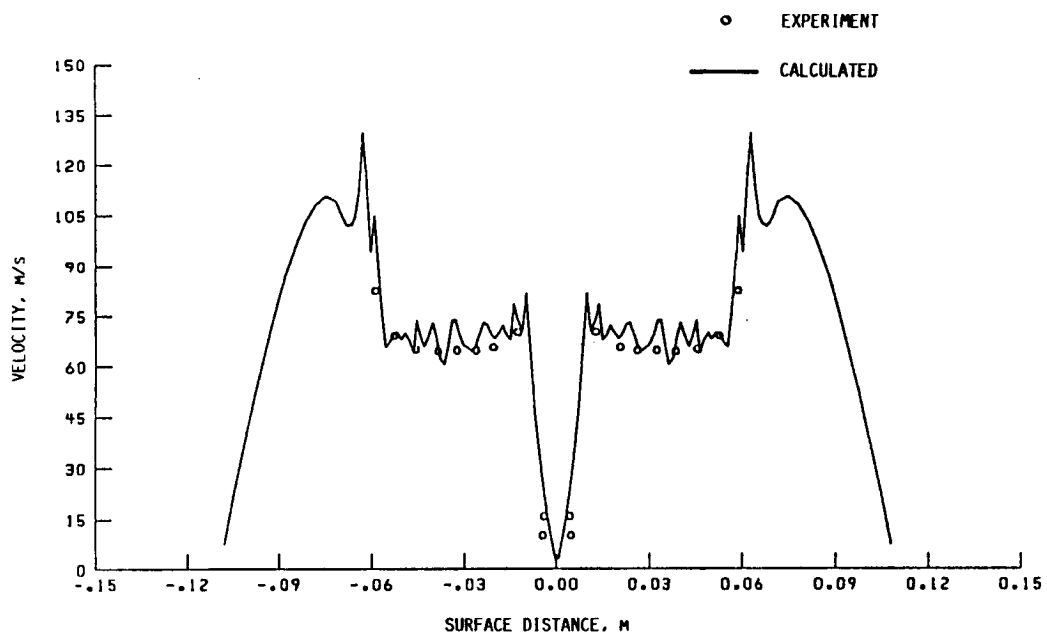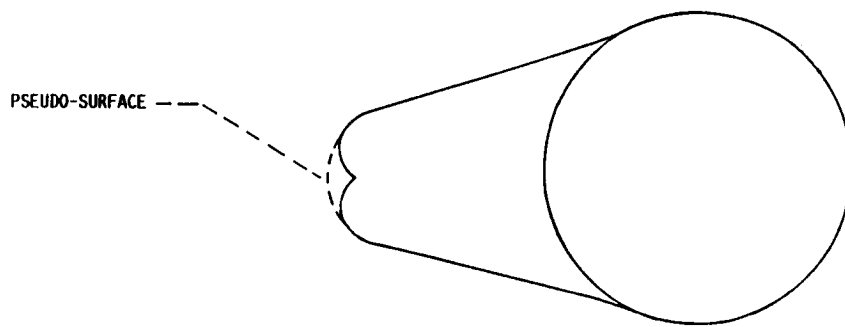
CALCULATED

c. Simulated fifteen min rime ice shape
C-6: Concluded

199
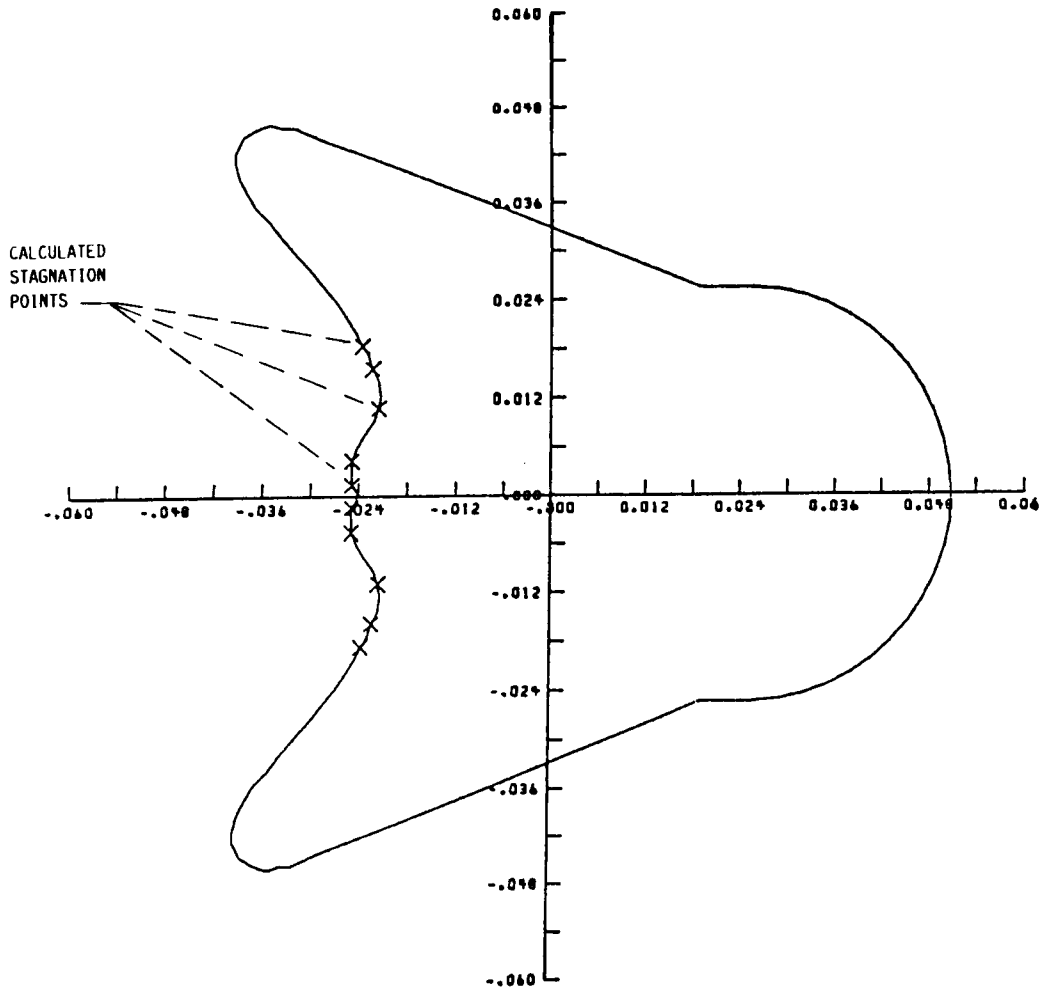
a. Locations of the multiple calculated stagnation points
C-7: Simulated fifteen min glaze ice accretion on a cylinder.
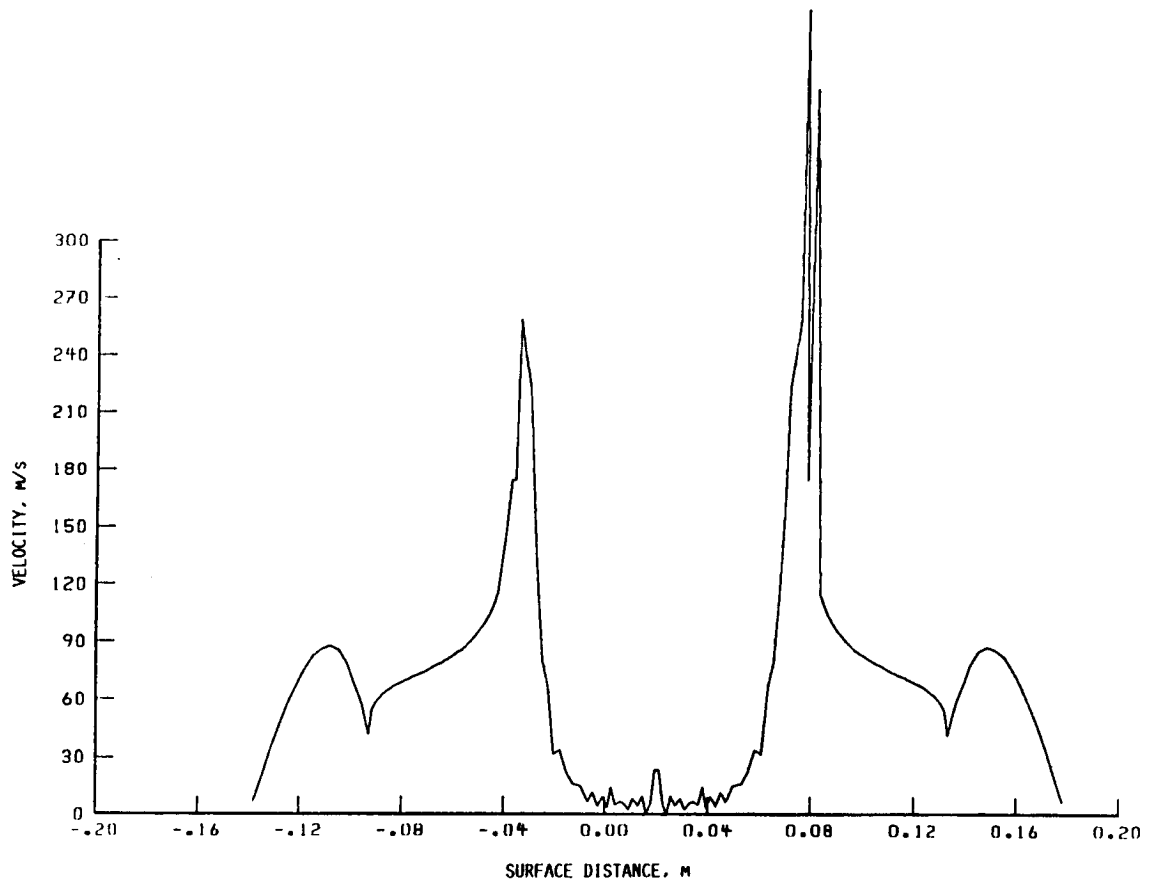
b. Calculated surface velocity over the ice shape
C-7: Concluded.
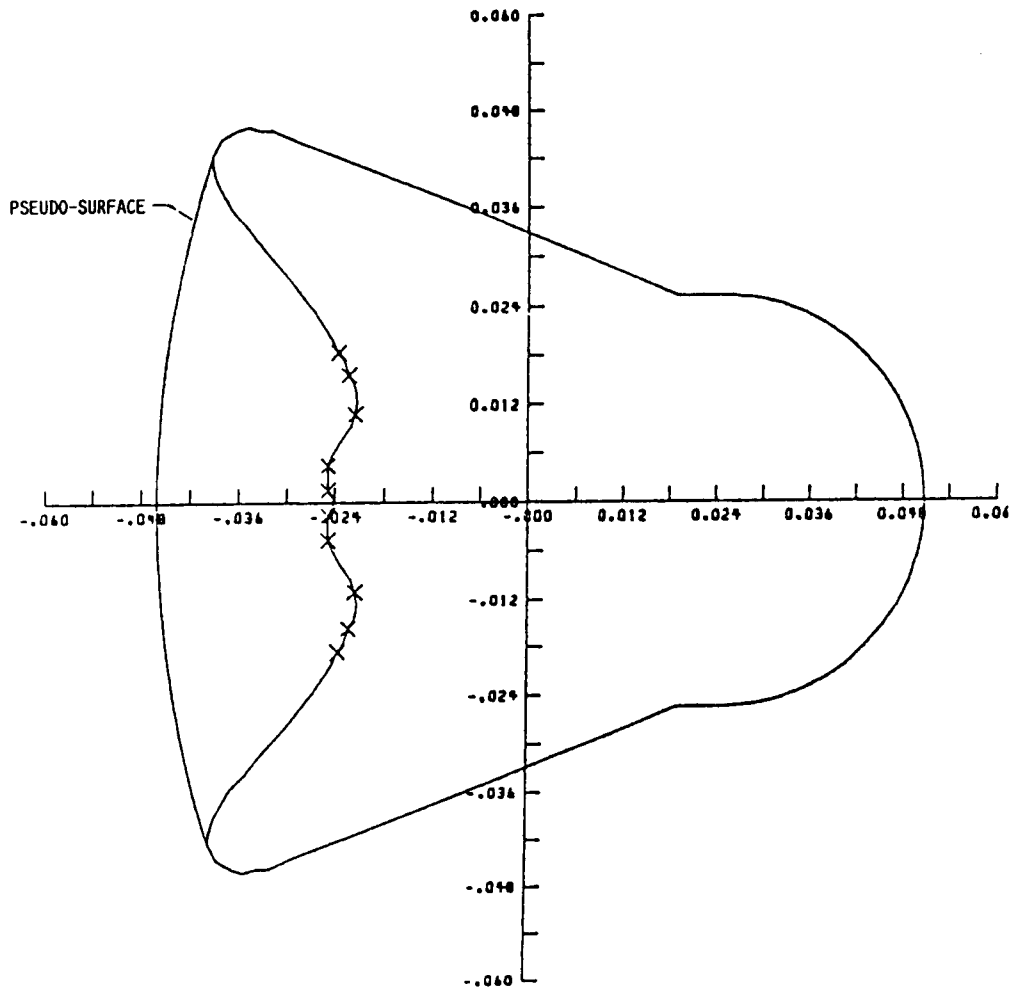
C-8a: Application of the pseudo-surface technique on a simulated
fifteen min glaze ice accretion.
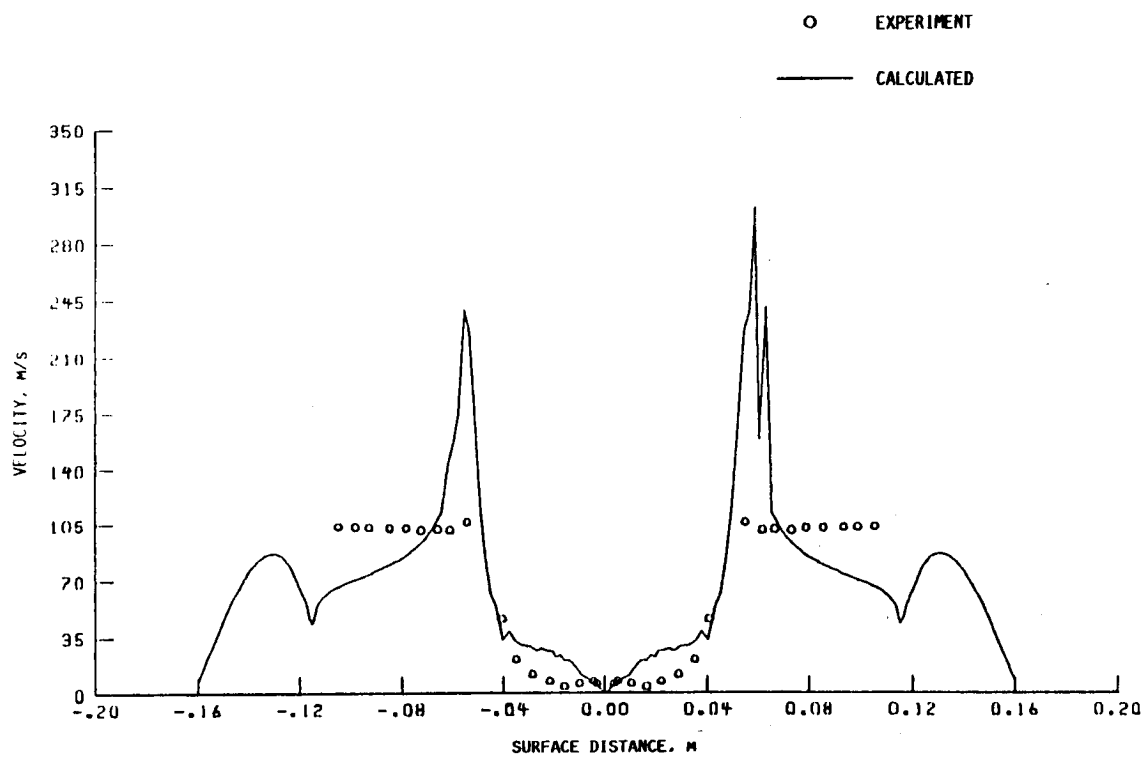
C-8b: Calculated surface velocity over ice shape with pseudo-surface.

APPENDIX D

COMPLETE INPUT TO THE POTENTIAL FLOW CODE (S24Y)

As noted in Section 5.1, the input to the potential flow code was simplified for use in LEWICE. Many of the generalities in S24Y are not applicable to LEWICE, and, therefore, are set to default values in the program (SUBROUTINE SETUP). SUBROUTINE SETUP reads the simplified input from unit 35, and, after assigning the default values, writes to unit 45 in the proper S24Y input format. Since the original input to the code is still used, it is necessary to define all of variables used in this input file. The following is the description of the S24Y input file written to unit 45.

D.1 Potential Flow Code Input Cards

Card 01   Program Control Card
(3(I1,2X), 1X, 7A4, 5X, 9(I1, 2X), 1X, I1)

Column	Code	Format	Description
01	ID		Body Number
04	ISV		Flag to control the saving of the geometry for future use by the 2-D program = 0 Do not save data = 1 Save the input geometry data for future use
07	ILIFT		Lift Control Flag = 0 This is not a lifting body = 1 This is a lifting body
11-38	TTITLE		Body Description

44	IPARA	Element Geometry Flag
		= 0 Linear Elements
		= 1 Parabolic Elements

47	IFIRST	First-order Terms Flag
		= 0 No first-order terms
		= 1 First derivative term
		= 2 Curvature term
		= 3 Both first-order terms

50	ISECND	Second-order terms flag
		= 0 No second-order terms
		= 1 Second derivative term
		= 2 Curvature squared term
		= 3 Both second-order terms

53	ITR	Geometry transformation card
		= 0 Transformation card will not be input
		= 1 Geometry transformation card will be input
		= 2 Ellipse generation. Ellipse generation card will be input. Transformation card will not be input.
		= 3 Ellipse generation. Ellipse generation card will be input. Transformation card will be input.

56	INORM	Geometry Normalization Card
		= 0 Geometry will not be normalized
		= 1 All of the geometry data (x and y) will be divided by the chord length before use by the potential flow program

| 59 | IBOD | Body Disposition Flag |

This flag together with the IDOLD parameter controls the sequence of the potential flow analysis part of the program. With the use of these two flags and the ISV parameter, it is possible to perform a variety of multi-element problems with a minimum of input data. For normal useage when all of the geometry data are input, only the IBOD = 1 and = 2 are used.

= 1 New geometry is being used. The storage of geometry data for the potential flow solution will start with this body.

= 2 New geometry is being input, but this is not the first body. This body will be added to the sequence of body data already input.

= 3 New geometry is being input, but it is to be added to an old sequence of data.

= 4 All previously saved geometry will be used

= 5 The geometry for this body will be selected from the previously saved data (body IDOLD will be selected). This selected body will be added to the current string of bodies.

= 6 Previously saved geometry data will be used with the body number indicated by the IDOLD parameter removed from the solution

62	IDOLD	Old Body ID Number This parameter is used in conjunction with the IBOD parameter in selecting which previously saved shape is to be retrieved as the present body
65	IPVOR	Vorticity Distribution Flag = 0 Use constant vorticity between the body elements = 1 Use a variable vorticity distribution

68	LAST	Last Body Flag
		= 0 This is not the last body.
		    After this body is input, the
		    program will return to read another
		    Body Title and Control Card for the
		    next body.
		= 1 This is the last body.

72	ITYPE	Card Type Flag = 1

X-Coordinate Cards (6F12.7, 2X, I1, 1X, I1, 1X, I1)

Column	Code	Format	Description
1-12	X(1)	6F12.7	x-coordinates of the body geometry.
13-24	X(2)		Up to six points may be on each card
25-36	X(3)		depending upon how the INO flag is set.
37-48	X(4)		
49-60	X(5)		
61-72	X(6)		
75	INO	I1	Number of data points on the card

77	ISTAT	I1	Last Card Flag = 0 This is not the last x-coordinate card. More cards will follow. = 1 This is the last x-coordinate card.
79	ITYPE	I1	Card Type Flag = 3

Y-Coordinate Cards (6F12.7, 2X, I1, 1X, I1, 1X, I1)

Column	Code	Format	Description
1-12	Y(1)	6F12.7	y-coordinates of the body geometry.
13-24	Y(2)		Up to six points may be input on
25-36	Y(3)		each card depending upon how the
37-48	Y(4)		INO flag is set.
49-60	Y(5)		
61-72	Y(6)		
75	INO	I1	Number of data points on the card (Maximum of six)
77	ISTAT	I1	Last Card Flag = 0 This is not the last y-coordinate card. More cards will follow. =1 This is the last y-coordinate card
79	ITYPE	I1	Card Type Flag =4

Flow Title Card (15A4, 11X, I1)

Column	Code	Format	Description
1-60	FTITLE	15A4	Title
72	ITYPE	I1	Card Type Flag = 8

Flow Control Card
(I1,4X,F10.5,2X,I1,2X,F10.5,5(4X.I1),9X,I1,3X,I1,I2,I1)

Column	Code	Format	Description
1	INCLT	I1	c_l, α Flag = 0 Airfoil angle of attack, α, is input.
6-15	CLT	F10.5	= 1 Total lift coefficient, C_e, is Value of the angle of attack or lift coefficient depending on how the INCLT flag was set
18	ICHORD	I1	Reference Length Flag = 0 The reference length used to calculate C_e is set = 1.0 = 1 The reference length used to calculate C_e will be input as CCL
21-30	CCL	F10.5	The input value for the reference length used in calculating C_e (generally the airfoil chord)
35	IND	I1	Individual Solution Flag S24Y is capable of calculating the potential flow about up to 6 bodies

and then superimpose the results of each. The possible values of IND are as follows:

= 0 Edge velocities are not calculated for each body

= 1 Edge velocities are calculated for each body

In LEWICE, only one body is input and the edge velocities are always required. Therefore, IND = 1.

| 40 | ISOL | I1 | Matrix Solution Method Control Flag |

= 0 Use routine SOLVIT for the matrix solution (used when a very large number of points have been input)

= 1 Use routine QUASI for the matrix solution

= 2 Use routine MIS1 for the matrix solution. The maximum number of geometry points = 101. If the number of points is greater than 101, the program will automatically shift to use SOLVIT.

| 45 | IOFF | I1 | Off-body Calculation Flag |

= 0 Off-body points will not be calculated

= 1 Off-body points will be calculated

| 50 | NONU | I1 | Non-uniform Flow Flag |

= 0 Non-uniform flow is not input

= 0 Non-uniform flow will be input. The number of flows input = NONU (maximum of six). When this option is used, the program sets ISOL = 1.

55	NBNU	I1	The number of bodies for which the non-uniform flows are input
65	IPRINT	I1	Print/punch Flag = 0 Normal output = 2 Print the individual matrices = 7 Punch the output on cards
70	MORE	I1	Last Case Flag = 0 This is the last case = 1 This is not the last case Another set of Flow Title and Flow Control cards (and any non-uniform or off-body cards) will be expected after this case is completed
70-71	IFILL	I2	Parabolic Integration Flag S24Y calculates the forces and moments acting on the body using both a trapezoidal and parabolic integration of the calculated coefficient. The results of the trapezoidal calculations are always output. The value of IFILL determines whether the parabolic results are printed.
72	ITYPE	I1	Card Type Flag = 9

Off-Body Title and Control Card
(11, 9X, 7A4, 12X, 2(2X, I1), 2(5X, I1), 2X, I2)

Column	Code	Format	Description
1	ID	I1	Identification number for this group of off-body points. Off-body points are read in groups of up to 100. There is no limit on the number of groups.
11-38	TITLE	7A4	Title or description for this group of off-body points
53	ITR	I1	Coordinate Transformation Flag See the ITR parameter on the Body Title and Control Card
56	INORM	I1	Coordinate Normalization Flag = 0 Off-body coordinates will not be normalized = 1 Normalize the coordinates by the input chord or by the chord for the body with ID = IDOLD
62	IDOLD	I1	Body Selection Flag for Normalizing Off-body Points = 0 Use the input chord to normalize the off-body points = 0 Use the chord for body with ID = IDOLD to normalize the off-body points
68	LAST	I1	Off-body Group Termination Flag = 0 Another group of off-body points will follow this group = 1 This is the last group of off-body points

71-72	ITYPE	I2	Card Type Flag = 21

Off-Body X-Coordinate Cards (6F12.7, 2X, I1, 1X, I1, 1X, I1)

Column	Code	Format	Description
1-12	X(1)	6F12.7	x-coordinates of the off-body
13-24	X(2)		points. Up to six points may be
25-36	X(3)		input on each card depending upon
37-48	X(4)		how the INO flag is set.
61-72	X(6)		
75	INO	I1	Number of data points on the card

77	ISTAT	I1	Last Card Flag
			= 0 This is not the last
			    x-coordinate card. More cards
			    will follow.
			= 1 This is the last x-coordinate
			    card

79	ITYPE	I1	Card Type Flag = 3

Off Body Y-Coordinate Cards (6F12.7, 2X, I1, 1X, I1, 1X, I1)

Column	Code	Format	Description
1-12	Y(1)	6F12.7	y-coordinates of the off-body
13-24	Y(2)		points. Up to six points may be
25-36	Y(3)		input on each card depending upon
37-48	Y(4)		how the INO flag is set.
49-60	Y(5)		
61-72	Y(6)		
75	INO	I1	Number of data points on the card

77	ISTAT	I1	Last Card Flag = 0 This is not the last y-coordinate card. More cards will follow.
			= 1 This is the last y-coordinate card
79	ITYPE	I1	Card Type Flag = 4

D.2 Sample Input

The input to the S24Y code using the formats described in the previous section is written to unit 45 in subroutine SETUP. An example of the S24Y input file on unit 45 is shown in Figure D-1. For normal operation of LEWICE, this file should not have to be examined or modified.

```
 1  0  1   NACA    0012                               1   3   3   0   0   1   0   1   1    1
    1.0000000    0.9899999    0.9800000    0.9700000    0.9500000    0.9250000    6  0  3
    0.9000000    0.8750000    0.8500000    0.8250000    0.8000000    0.7750000    6  0  3
    0.7500000    0.7250000    0.7000000    0.6750000    0.6500000    0.6250000    6  0  3
    0.6000000    0.5750000    0.5500000    0.5250000    0.5000000    0.4750000    6  0  3
    0.4500000    0.4250000    0.4000000    0.3750000    0.3500000    0.3250000    6  0  3
    0.3000000    0.2750000    0.2500000    0.2250000    0.2000000    0.1750000    6  0  3
    0.1500000    0.1250000    0.1000000    0.0900000    0.0800000    0.0700000    6  0  3
    0.0600000    0.0500000    0.0450000    0.0400000    0.0350000    0.0300000    6  0  3
    0.0250000    0.0200000    0.0150000    0.0100000    0.0075000    0.0050000    6  0  3
    0.0037500    0.0025000    0.0022500    0.0020000    0.0017500    0.0015000    6  0  3
    0.0012500    0.0010000    0.0008750    0.0006250    0.0005000    6  0  3
    0.0003750    0.0002500    0.0001250    0.0000000    0.0001250    0.0002500    6  0  3
    0.0003750    0.0005000    0.0006250    0.0007500    0.0008750    0.0010000    6  0  3
    0.0012500    0.0015000    0.0017500    0.0020000    0.0022500    0.0025000    6  0  3
    0.0037500    0.0050000    0.0075000    0.0100000    0.0150000    0.0200000    6  0  3
    0.0250000    0.0300000    0.0350000    0.0400000    0.0450000    0.0500000    6  0  3
    0.0600000    0.0700000    0.0800000    0.0900000    0.1000000    0.1250000    6  0  3
    0.1500000    0.1750000    0.2000000    0.2250000    0.2500000    0.2750000    6  0  3
    0.3000000    0.3250000    0.3500000    0.3750000    0.4000000    0.4250000    6  0  3
    0.4500000    0.4750000    0.5000000    0.5250000    0.5500000    0.5750000    6  0  3
    0.6000000    0.6250000    0.6500000    0.6750000    0.7000000    0.7250000    6  0  3
    0.7500000    0.7750000    0.8000000    0.8250000    0.8500000    0.8750000    6  0  3
    0.9000000    0.9250000    0.9500000    0.9700000    0.9800000    0.9899999    6  0  3
    1.0000000    0.0000000    0.0000000    0.0000000    0.0000000    0.0000000    1  1  3
    0.0000000   -0.0018740   -0.0036110   -0.0052390   -0.0082510   -0.0117000    6  0  4
   -0.0149080   -0.0179530   -0.0208880   -0.0237390   -0.0265150   -0.0292210    6  0  4
   -0.0318550   -0.0344110   -0.0368870   -0.0392810   -0.0415850   -0.0437950    6  0  4
   -0.0459040   -0.0479060   -0.0497930   -0.0515600   -0.0531980   -0.0546980    6  0  4
   -0.0560510   -0.0572430   -0.0582620   -0.0590900   -0.0597070   -0.0600940    6  0  4
   -0.0602260   -0.0600760   -0.0596120   -0.0587940   -0.0575700   -0.0558790    6  0  4
   -0.0536360   -0.0507320   -0.0470040   -0.0452280   -0.0432520   -0.0410380    6  0  4
   -0.0385350   -0.0356740   -0.0340820   -0.0323620   -0.0304960   -0.0284620    6  0  4
   -0.0262300   -0.0237260   -0.0207970   -0.0172480   -0.0150780   -0.0123860    6  0  4
   -0.0106990   -0.0086200   -0.0081360   -0.0076230   -0.0070750   -0.0064850    6  0  4
   -0.0058470   -0.0051460   -0.0047660   -0.0043630   -0.0039310   -0.0034620    6  0  4
   -0.0029450   -0.0023560   -0.0016320    0.0000000    0.0016320    0.0023560    6  0  4
    0.0029450    0.0034620    0.0039310    0.0043630    0.0047660    0.0051460    6  0  4
    0.0058470    0.0064850    0.0070750    0.0076230    0.0081360    0.0086200    6  0  4
    0.0106990    0.0123860    0.0150780    0.0172480    0.0207970    0.0237260    6  0  4
    0.0262300    0.0284620    0.0304960    0.0323620    0.0340820    0.0356740    6  0  4
    0.0385350    0.0410380    0.0432520    0.0452280    0.0470040    0.0507320    6  0  4
    0.0536360    0.0558790    0.0575700    0.0587940    0.0596120    0.0600760    6  0  4
    0.0602260    0.0600940    0.0597070    0.0590900    0.0582620    0.0572430    6  0  4
    0.0560510    0.0546980    0.0531980    0.0515600    0.0497930    0.0479060    6  0  4
    0.0459040    0.0437950    0.0415850    0.0392810    0.0368870    0.0344110    6  0  4
    0.0318550    0.0292210    0.0265150    0.0237390    0.0208880    0.0179530    6  0  4
    0.0149080    0.0117000    0.0082510    0.0052390    0.0036110    0.0018740    6  0  4
    0.0000000    0.0000000    0.0000000    0.0000000    0.0000000    0.0000000    1  1  4
NACA    0012                                                                       8
0       4.00000    0      0.00000     1     0    1     0    0          0    0 19
1        NACA    0012                                      0   0     0     1   1
   -0.0200000   -0.0200000    0.0000000    0.0000000    0.0000000    0.0000000    2  1  3
    1.0000000    0.5000000    0.0000000    0.0000000    0.0000000    0.0000000    2  1  4
```

D-1: Input to S24y written to unit 45.

215

APPENDIX E

CALCULATION OF THE LOCAL EDGE VELOCITIES

Another pseudo-surface, related to the one created for particle impingement calculations, is created to determine non-dimensional edge velocities. This pseudo-surface is formed by moving each point on the body a distance DSHIFT along the outward normal to the surface. The resulting pseudo-surface is shown in Figure E-1. The non-dimensional edge velocities that were originally computed in subroutine FLOWS on the "true" surface are recalculated in subroutine READIN on the pseudo-surface. (This recalculation step can be omitted with only a small change to subroutine READIN.) The purpose of creating a pseudo-surface is to shift the surface outward into a region where the velocity profile is smoother, thus avoiding numerical problems that may occur when velocities must be computed on an irregular ice surface. This method will produce higher stagnation velocities but will affect the ice shape only in a relatively small region of the airfoil unless a value of DSHIFT larger than recommended in this manual is used.

The non-dimensional edge velocities that are recalculated on the pseudo-surface are the ones used in the evaluation of the thermodynamic characteristics of the ice surface. These non-dimensional velocities, V'_e, are given by the equation

$$V'_e = \frac{V_e}{V_\infty} \qquad (E-1)$$

The values of V'_e are initially written to unit 30 in subroutine READIN and then read in subroutine VEDGE, where they are used to calculate the dimensional local edge velocities. The boundary layer edge velocities, V_e, temperature, T_e, and pressure, P_e, are calculated from V'_e using the isentropic equations with the Karman-Tsien compressibility correction. These parametes are assigned the following variable names in the computer code:

Local static pressure, (P_e) PE(I)
Local static temperature, (T_e) TE(I)

Local dimensional velocity, (V_e) VE(I)   (compressible)

Local non-dimensional velocity, (V_e') VT(I)   (incompressible)

Each of the parameters are arrays with (I) denoting the segment number. This appendix describes the equations used to calculate these flow properties.

The free stream mach number, total temperature, and total pressure are first calculated using the following isentropic equations:

$$M_\infty = \frac{V_\infty}{20.05\sqrt{T_s}} \qquad (E-2)$$

$$T_T = T_s(1 + \frac{M_\infty^2}{5}) \qquad (E-3)$$

$$P_T = P_s(1 + \frac{M_\infty^2}{5})^{3.5} \qquad (E-4)$$

An incompressible pressure coefficient is calculated from the non-dimensional edge velocities using the following equation:

$$c_{P_{inc}} = 1 - (V_e')^2 \qquad (E-5)$$

This incompressible pressure distribution around the body is then corrected for compressibility using the Karman-Tsien compressibility correction given by the following equation:

$$c_{p_c} = (1 - M_\infty^2)^{1/2} + \left[\frac{c_{p_{inc}}}{2} \frac{M_\infty^2}{1. + (1 - M_\infty^2)^{1/2}} \right] \qquad (E-6)$$

The local pressure is calculated using this corrected pressure coefficient and the following equation:

$$P_e = P_s \left(1 + \frac{\gamma}{2} c_{p_e} M_\infty^2\right) \qquad (E-7)$$

where P_s is the free stream static pressure. If a local static pressure is calculated to be greater than the total pressure, the local static pressure is set equal to the total pressure.

The local mach number is calculated using the following isentropic relationship between the local static and total pressures:

$$M_e = \left[\left(\left(\frac{P_T}{P_e}\right)^{1/3.5} - 1\right)5\right]^{1/2} \qquad (E-8)$$

The local static temperature is determined using the following isentropic relation:

$$T_e = T_T \left(1 + \frac{M_e^2}{5}\right)^{-1} \qquad (E-9)$$

The dimensional local edge velocity is then calculated using the isentropic equation for the speed of sound in air and the local Mach number, e.g.,

$$V_e = M_e (20.05\sqrt{T_e}) \qquad (E-10)$$

The values of VE, TE, and PE for each body segment are then written to unit 30.
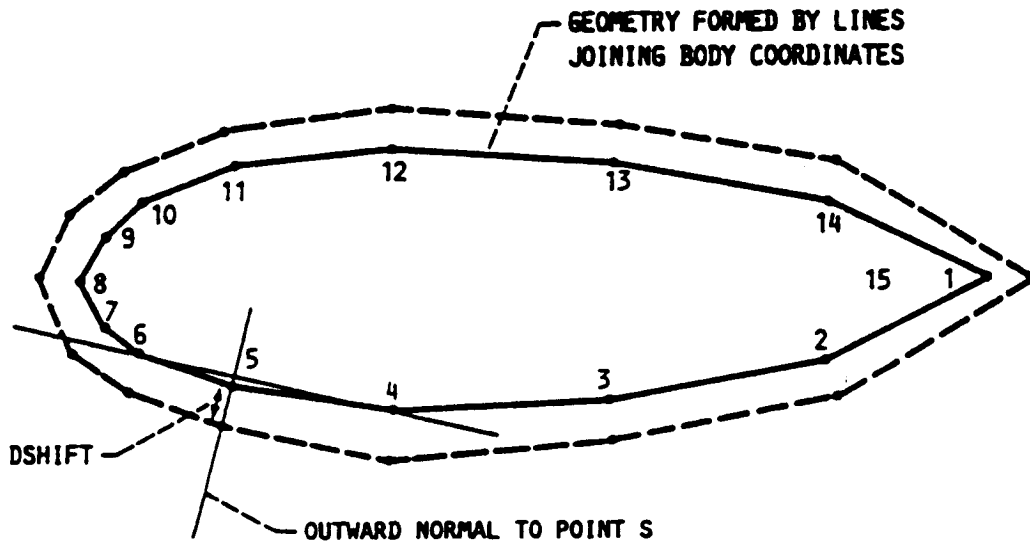
E-1: Illustration of the pseudo-surface.

APPENDIX F

EMPIRICAL RELATIONSHIP FOR THE EQUIVALENT SAND GRAIN ROUGHNESS HEIGHT

As discussed in Section 5.2, the size, shape, and type of ice accretion that is formed is dependent upon the convective heat transfer rate from the ice surface. The integral boundary layer method, described in Appendix B, requires that a surface roughness height be specified to identify transition to turbulent flow and evaluate the convective heat transfer characteristics of the rough surface.

Increasing the size of the roughness elements will increase the calculated convective heat transfer coefficient. Therefore, a calculated ice shape can change quite drastically when various values of roughness element height are specified. Figure F-1 shows the effect of varying the input value of the sand grain roughness height, k_s, on the calculated ice accretion shape. When the value of k_s is smaller, the amount of heat removed from the surface by convection is reduced. Therefore, the surface temperature is not lowered sufficiently to allow all of the ice to freeze on impact and a glaze accretion is formed. Incrementally increasing k_s increases the convective heat transfer, thereby increasing the fraction of impinging water that freezes on contact. As a result, the accretions begin to take on more characteristics of rime ice. At some value of k_s, sufficient heat will be removed to freeze all of the water on impact, and a complete rime ice accretion is formed.

Empirical correlations that can be used to evaluate the effect of roughness exist in the literature (Reference F-1 and F-2). Unfortunately, these correlations are usually applicable only for a specific, well-defined type of roughness element. None of these correlations are directly applicable to the irregular surface roughness elements found on typical ice accretions. Furthermore, the size and shape of the roughness elements on an ice surface are dependent on the conditions at which the ice was formed. They can vary with the icing condition, surface location, and, since the ice shape changes with time, the icing time. While the effect of each of these parameters on the formation of the surface roughness elements is very complex, all analytical ice accretion prediction methods must address the problem because of the strong influence on the calculated ice accretion shape shown in Figure F-1.

It has become standard practice in current ice accretion prediction methods to develop an empirical correlation for either the surface element roughness height (Reference F-3) or the convective heat transfer coefficient (Reference F-4). These correlations are developed by first predicting the ice shapes for a set of experimental ice shapes by changing the convective heat transfer coefficient (or roughness element height) to determine the value that yields the best agreement with experiment. Unfortunately, the correlation will depend on the computational algorithm and may not be directly applicable to any other analytical ice accretion prediction method. Since the timestepping procedure applied in LEWICE is unique among analytical ice accretion prediction methods, an empirical correlation relating the surface roughness height to the icing condition had to be developed.

The experimental data used to develop this correlation was obtained by Gent (Reference F-5). This data set, shown in Figures F-2, -3, and -4, show the effect of velocity, LWC, and static temperature on the shape of the ice accretion formed. Also shown in the figures are the ice accretion shapes, calculated by LEWICE, that best compare with the experimental shape and the corresponding value of k_s. The accretion shown in Figure F-3a for LWC $=0.5g/m^3$ was used as a baseline condition for the correlation. Therefore, all values of k_s were divided by the value of k_s for this case and plotted as a function of either velocity, LWC, or static temperature. The resulting data points, normalized by the airfoil chord of 0.3m are shown in Figures F-5, -6, and -7, respectively.

A correlation relating the sand grain roughness height to the icing parameter was formed by fitting the data on each of these plots with a least squares linear or quadratic curve fit. The curve calculated from each correlation is also shown in Figures F-5, -6, and -7. The equations are as follows:

Velocity

$$\frac{k_s/c}{k_s/c)_{base}} = 0.4286 + 0.0044139(V_\infty) \qquad (F-1)$$

Liquid Water Content

$$\frac{k_s/c}{k_s/c)_{base}} = 0.5714 + 0.2457(LWC) + 1.2571(LWC)^2 \qquad (F-2)$$

Static Temperature

$$\frac{k_s/c}{k_s/c)_{base}} = 46.8384\left(\frac{T_s}{1000}\right) - 11.2037 \qquad (F-3)$$

In all of these equations, $k_s/c)_{base}$, the baseline value, is 0.00117. The velocity, LWC, and static temperature are input into the equations in m/sec, g/m^3, and K, respectively. By relating them to a baseline value, the correlations calculate a multiplying factor accounting for the effect of velocity, LWC, and static temperature. The value of sand-grain roughness height to be input is calculated using the following equation:

$$k_s = \left[\frac{k_s/c}{k_s/c)_{base}}\right]_{V\infty} \left[\frac{k_s/c}{k_s/c)_{base}}\right]_{LWC} \left[\frac{k_s/c}{k_s/c)_{base}}\right]_{T_s} k_s/c)_{base} \ c \qquad (F-4)$$

The use of these equations is best illustrated by a numerical example. Suppose that the ice shape for the following icing condition is to be determined.

Airfoil Chord	=	0.3m
Velocity	=	75.0 m/s
Static Temperature	=	255.0 K_s
LWC	=	0.5 g/m

The multiplying factors calculated from Equations (F-1), (F-2), and (F-3) are 0.7596, 1.0085, and 0.7401, respectively. Substituting these values into Equation (F-4), the final factor to be multiplied by the baseline value and the airfoil chord is 0.5670. Therefore, for a baseline value of 0.00117 and chord of 0.3 m, the sand-grain roughness to be input into the code is 0.000199 m.

As previously noted, these three correlations were developed to account for the effect of velocity, LWC, and static temperature on the surface roughness elements formed on an ice accretion. These three icing parameters were selected because of their obvious influence on the type of ice formed, and because a complete and consistent set of experimental data existed from which to form a correlation. The effects of droplet diameter, body geometry, static pressure, etc. have not been included. Also inherent in the baseline value of sand-grain roughness height are any characteristics unique to the facility in which the experimental ice accretion shapes were formed. These can include levels of free-stream turbulence, LWC and droplet diameter calibrations, and possibly even the droplet size distribution produced by the spray nozzle. Comparisons with experimental ice accretion shapes have indicated that the baseline value of $k_s/c)_{base} = 0.00117$ yields good results for the facility of Reference F-1 and the NASA Lewis Icing Research Tunnel (IRT) but would not be expected to be appropriate for all icing facilities and applications. A value for flight test data has not been determined but is expected to be less than 0.00117, primarily because of the lower level of free-stream turbulence encountered in flight.

The surface roughness, while known to be a function of icing time and surface location, is currently specified to be constant for the entire icing time. Sufficient experimental data does not exist to produce meaningful correlations relating these parameters to the roughness element height.

APPENDIX F

List of References

1. Kays, W.M. and Crawford, M.E. <u>Convective Heat and Mass Transfer</u>. 2nd Edition, MacGraw-Hill Book Company, New York, 1980.

2. White, F.M. <u>Viscous Fluid Flow</u>. MacGraw-Hill Book Company, New York, 1974.

3. Kirchner, R.D. "Aircraft Icing Roughness Features and Its Effect on the Icing Process." AIAA-83-0111, January 1983.

4. Cansdale, J.T. and Gent, R.W. "Ice Accretion on Aerofoils in Two-Dimensional Compressible Flow - A Theoretical Model." Royal Aircraft Establishment Technical Report 82128, January 1983.

5. Gent, R.W., Markiewicz, R.H., and Cansdale, J.T. "Further Studies of Helicopter Rotor Ice Accretion and Protection." Paper No. 54, Eleventh European Rotorcraft Forum, September 1985.

RIME FEATHERS

EXPERIMENT (IRT)

$K_S = 0.001$ M

$K_S = 0.0005$ M

$K_S = 0.004$ M

$K_S = 0.002$ M

VELOCITY (M/S)	93.88
TEMPERATURE (C)	-14.37
PRESSURE (KPA)	93.61
HUMIDITY (%)	100.00
LWC (G/M**3)	0.96
DROP DIAM (MICRONS)	37.50
TIME (SEC)	225.00
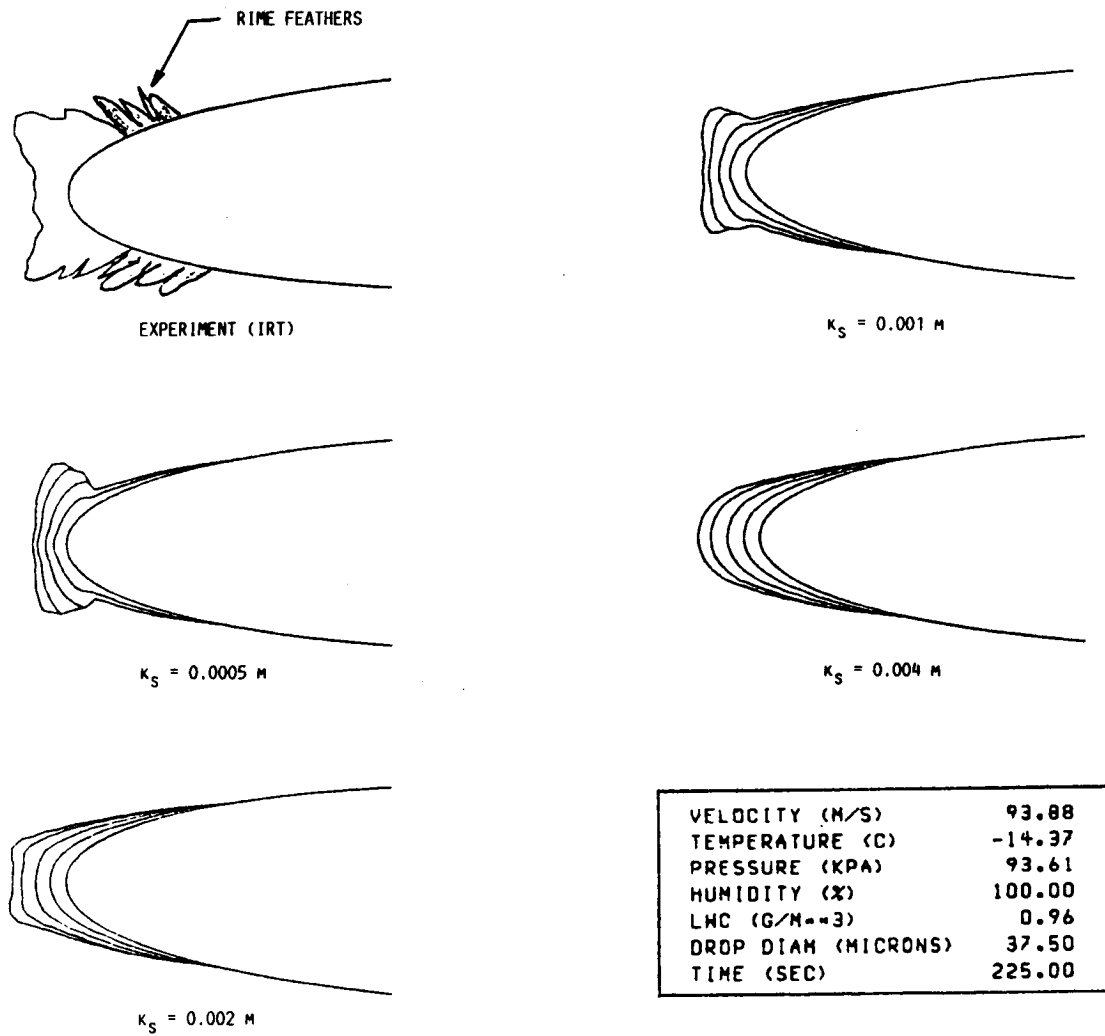
F-1: Effect of varying the equivalent sand-grain roughness on the ice accretion calculated for a mixed icing condition on a NACA 0012 airfoil section at 0.0 deg angle of attack.
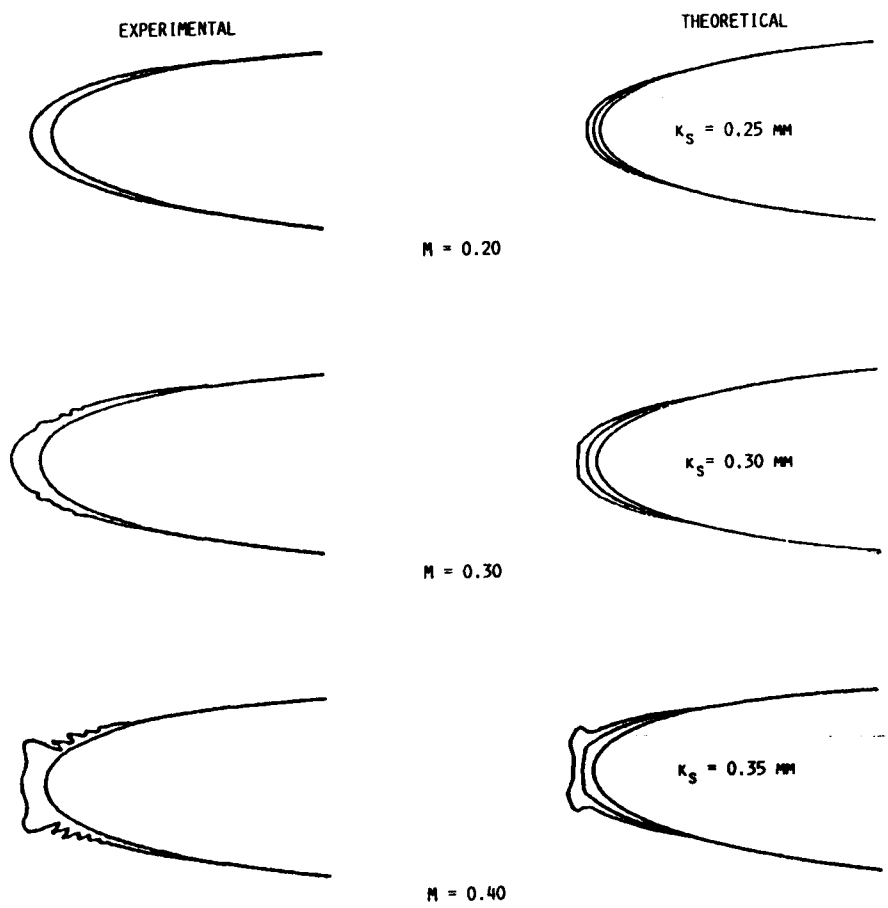
K_S = 0.25 MM

M = 0.20

K_S= 0.30 MM

M = 0.30

K_S = 0.35 MM

M = 0.40

TEMPERATURE (C)	-12.60
PRESSURE (KPA)	90.75
HUMIDITY (X)	100.00
LWC (G/M**3)	0.50
DROP DIAM (MICRONS)	20.00
TIME (SEC)	120.00

F-2: Effect of velocity on ice accretion shape.

EXPERIMENTAL

THEORETICAL

$K_S = 0.20$ MM

LWC = 0.25 g/m^3

$K_S = 0.35$ MM

LWC = 0.50 g/m^3

$K_S = 0.6$ MM

LWC = 0.75 g/m^3

$K_S = 0.85$ MM

LWC = 1.00 g/m^3

VELOCITY (M/S)	129.00
TEMPERATURE (C)	-12.60
PRESSURE (KPA)	90.76
HUMIDITY (%)	100.00
DROP DIAM (MICRONS)	20.00
TIME (SEC)	120.00

a. Angle of attack = 0.0°

F-3: Effect of LWC on ice accretion shape.

227

EXPERIMENTAL   THEORETICAL

LWC = 0.25 g/m^3

LWC = 0.50 g/m^3

LWC = 0.75 g/m^3

LWC = 1.00 g/m^3
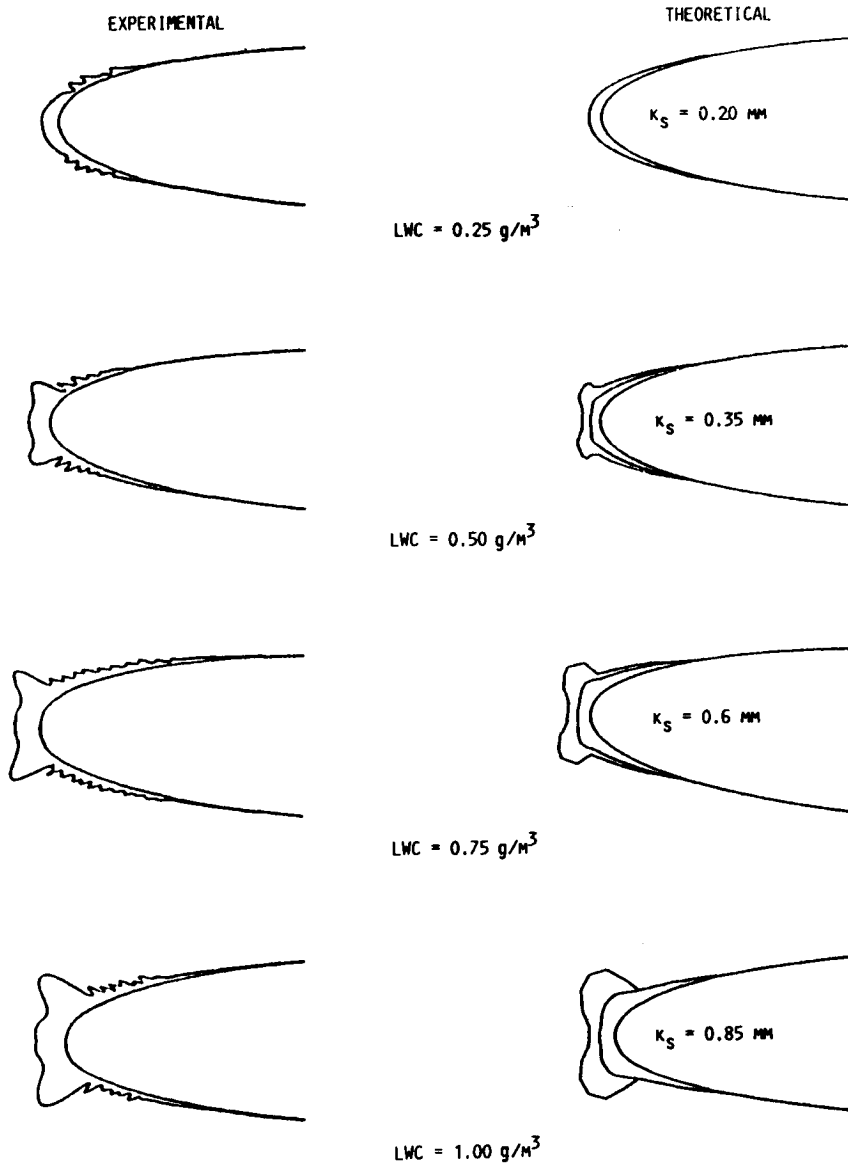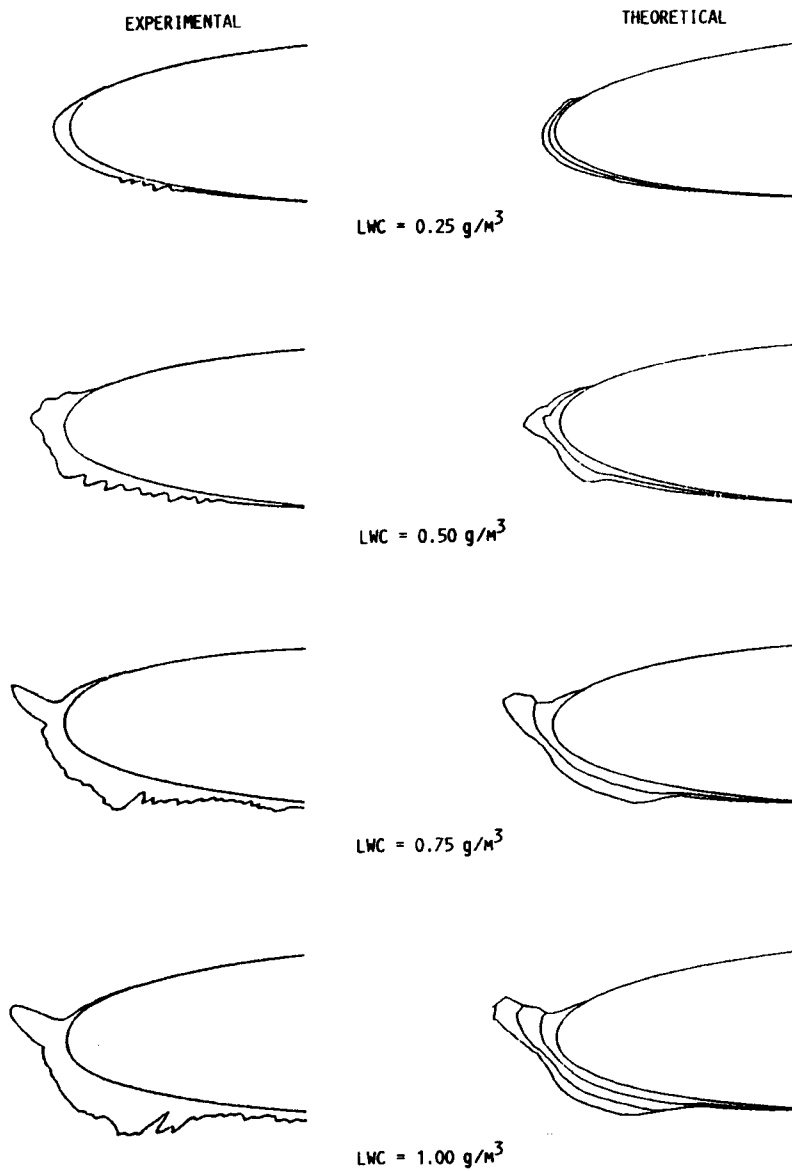
VELOCITY (M/S)	129.00
TEMPERATURE (C)	-12.60
PRESSURE (KPA)	90.76
HUMIDITY (X)	100.00
DROP DIAM (MICRONS)	20.00
TIME (SEC)	120.00

b. Angle of attack = 4.0°
F-3: Concluded.

EXPERIMENTAL   THEORETICAL

K_s = 0.43 MM

T_s = -8.0 C

K_s = 0.35 MM

T_s = -12.6 C

K_s = 0.28 MM

T_s = -16.8 C

K_s = 0.18 MM

T_s = -22.9 C
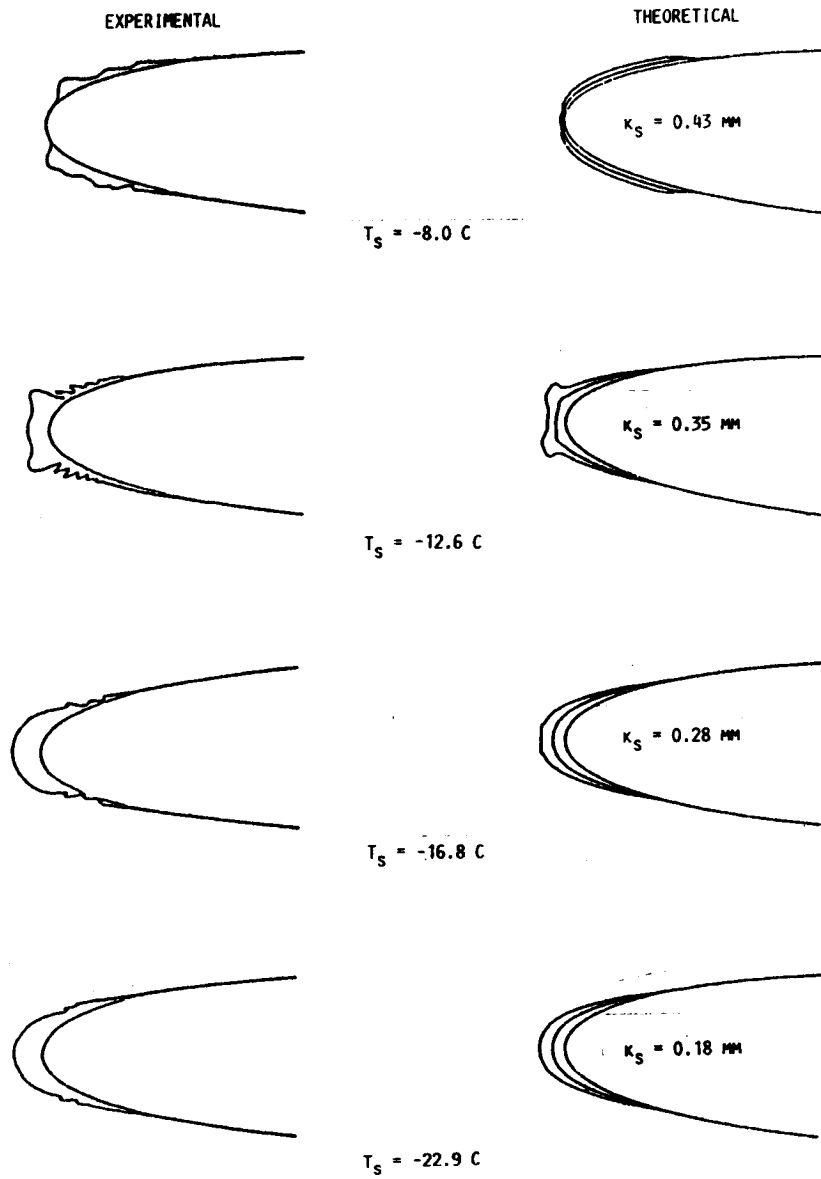
VELOCITY (M/S)	131.00
PRESSURE (KPA)	90.75
HUMIDITY (X)	100.00
LWC (G/M**3)	0.50
DROP DIAM (MICRONS)	20.00
TIME (SEC)	120.00

F-4: Effect of static temperature on ice accretion shape.
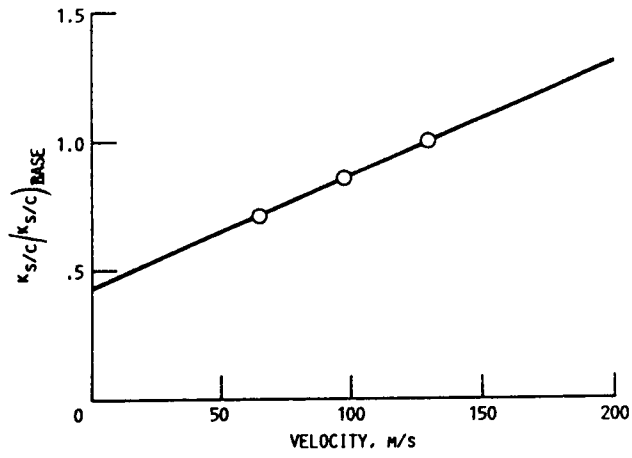
F-5: Emperical relationship for equivalent sand-grain roughness as a function of velocity.
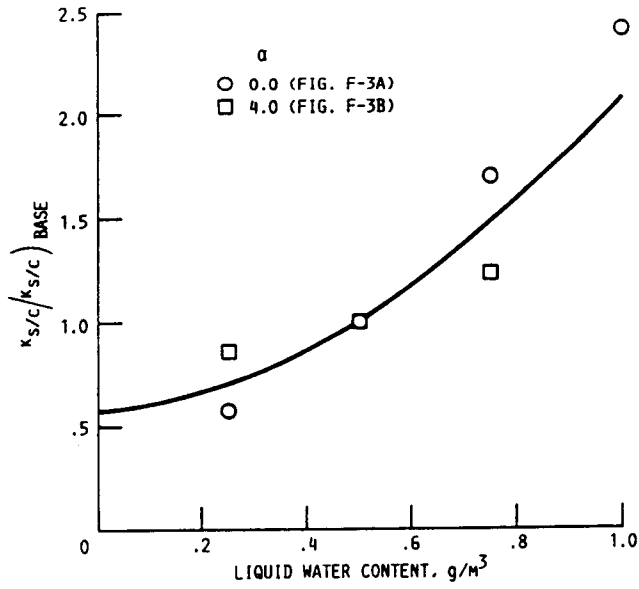
F-6: Emperical relationship for equivalent sand-grain roughness as a function of LWC.
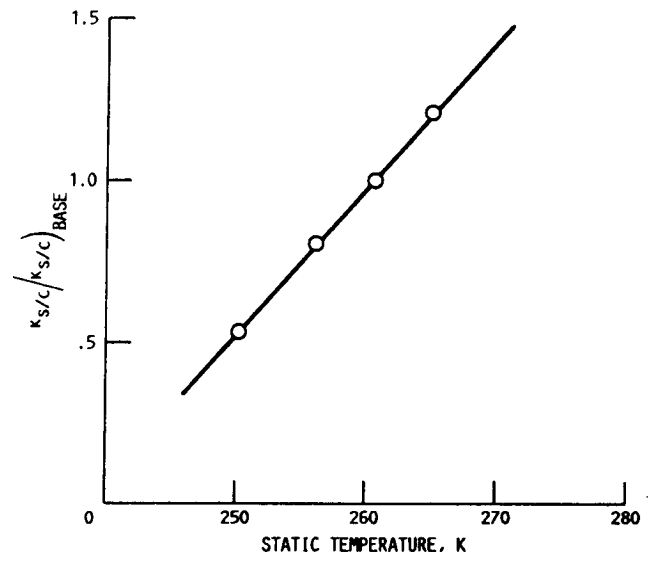
F-7: Emperical relationship for equivalent sand-grain roughness
as a function of static temperature.

NASA
National Aeronautics and
Space Administration

Report Documentation Page

1. Report No. NASA CR-185129	2. Government Accession No.	3. Recipient's Catalog No.
4. Title and Subtitle Users Manual for the NASA Lewis Ice Accretion Prediction Code (LEWICE)		5. Report Date May 1990
		6. Performing Organization Code
7. Author(s) Gary A. Ruff and Brian M. Berkowitz		8. Performing Organization Report No. None
		10. Work Unit No. 505-68-11
9. Performing Organization Name and Address Sverdrup Technology, Inc. Lewis Research Center Group 2001 Aerospace Parkway Brook Park, Ohio 44142		11. Contract or Grant No. NAS3-25266
		13. Type of Report and Period Covered Contractor Report Final
12. Sponsoring Agency Name and Address National Aeronautics and Space Administration Lewis Research Center Cleveland, Ohio 44135-3191		14. Sponsoring Agency Code

15. Supplementary Notes

Project Manager, J.J. Reinmann, Propulsion Systems Division, NASA Lewis Research Center.

16. Abstract

LEWICE is an ice accretion prediction code that applies a time-stepping procedure to calculate the shape of an ice accretion. The potential flow field is calculated in LEWICE using the Douglas Hess-Smith 2-D panel code (S24Y). This potential flow field is then used to calculate the trajectories of particles and the impingement points on the body. These calculations are performed to determine the distribution of liquid water impinging on the body, which then serves as input to the icing thermodynamic code. The icing thermodynamic model is based on the work of Messinger, but contains several major modifications and improvements. This model is used to calculate the ice growth rate at each point on the surface of the geometry. By specifying an icing time increment, the ice growth rate can be interpreted as an ice thickness which is added to the body, resulting in the generation of new coordinates. This procedure is repeated, beginning with the potential flow calculations, until the desired icing time is reached. The operation of LEWICE is illustrated through the use of five examples. These examples are representative of the types of applications expected for LEWICE. All input and output is discussed, along with many of the diagnostic messages contained in the code. Several error conditions that may occur in the code for certain icing conditions are identified, and a course of action is recommended. LEWICE has been used to calculate a variety of ice shapes, but should still be considered a research code. The code should be exercised further to identify any shortcomings and inadequacies. Any modifications identified as a result of these cases, or of additional experimental results, should be incorporated into the model. Using it as a test bed for improvements to the ice accretion model is one important application of LEWICE.

17. Key Words (Suggested by Author(s)) Aircraft icing Ice accretion modeling Heat transfer	18. Distribution Statement Unclassified – Unlimited Subject Category 01		
19. Security Classif. (of this report) Unclassified	20. Security Classif. (of this page) Unclassified	21. No. of pages 233	22. Price* A10